Efficacy of Targeting the PI3 Kinase and mTOR Pathways as a Treatment Modality for Multiple Myeloma

Zhen Ying Gan

Myeloma Research Laboratory
Bone and Cancer Laboratories
Department of Haematology
SA Pathology

&

Department of Health Sciences
School of Pharmacy and Medical Sciences
The University of South Australia

A thesis submitted to the University of South Australia
for the degree of Masters of Science
December 2014

Table of Contents

Abstract..... i

Declaration..... ii

Acknowledgement..... iv

Abbreviations..... vi

Publications..... ix

Introduction..... 1

1.1. Overview..... 2

1.2 Multiple Myeloma..... 3

1.2.1 General Description..... 3

1.2.2 Epidemiology..... 3

1.2.3 Variants of Multiple Myeloma..... 6

1.2.4. Clinical Features and Diagnosis of Multiple Myeloma..... 9

1.3. PI3k and mTOR pathway..... 14

1.3.1. Phosphotidylinositol„kinase (PI3k) Pathway..... 14

1.3.2. Mechanistic Target of Rapamycin (mTOR) Pathway..... 18

1.3.3. DEP-domain-containing mTOR-interacting protein (DEPTOR)..... 19

1.3.4. PI3k and mTOR pathways in Multiple Myeloma..... 22

1.4. Bone..... 25

1.4.1. Bone Remodelling..... 25

1.4.2. Osteoblast..... 28

1.4.2.1. Osteoblastic Signalling Pathways..... 28

1.4.3. Osteoclast..... 31

1.4.3.1. Transcription Factors and Cytokines Involved in Osteoclastogenesis..... 31

1.4.4. Mechanisms Underlying Myeloma-Induced Bone Loss..... 34

1.4.5. PI3k/mTOR pathway in osteoblasts and osteoclasts..... 36

1.5. Treatment for Myeloma and Myeloma-induced Bone Loss..... 38

1.5.1. Treatment for Myeloma..... 38

1.5.2. Treatment for Myeloma-induced Bone Loss..... 39

1.5.3. Novel anti-myeloma agents with bone promoting properties..... 40

1.6. Summary and Project Aims..... 49

Reference..... 50

Materials and Methods..... 65

2.1 List of Reagents..... 66

2.2 Solutions, Buffers and Media for Cell Culture..... 68

2.2.1 Additives for Tissue Culture Medium (abbreviated to Adds)..... 68
2.2.2 Ascorbate-2-Phosphate, 10mM (abbreviated to Asc)..... 68
2.2.3 α-Modified Eagle•s Medium (α-MEM) for Murine Bone Marrow Stromal Cell (mBMSC) Culture (c-αMEM)..... 69
2.2.4 α-MEM For Murine Mineralisation (m-αMEM)..... 69
2.2.5 α-MEM For Murine Bone Marrow Monocyte (mBM) Culture (o-αMEM)..... 69
2.2.6 Blocking Buffer (for Flow Analysis)..... 69
2.2.7 Calcium Standards..... 69
2.2.8 Dexamethasone, 10-5M Stock Solution..... 70
2.2.9 DMEM for RAW264.7 Cell Culture (c-DMEM)..... 70
2.2.10 DNA Standards..... 70
2.2.11 HHF Wash Buffer..... 70
2.2.12 Iscove's Modified Dulbecco's Medium (IMDM) for Murine Myeloma Cell Culture (c-IMDM). 70
2.2.13 NVP-BEZ235 (BEZ235) For Tissue Culture..... 70
2.2.14 NVP-BKM120 (BKM120) For Tissue Culture..... 71
2.2.15 Proteinase K, 10mg/mL Stock Solution..... 71
2.2.16 Potassium phosphate, 400mM Stock Solution..... 71
2.2.17 Roswell Park Memorial Institute Medium (RPMI-1640) for Human Myeloma Cell Culture (c-RPMI)..... 71
2.2.18 rhM-CSF, 25µg/mL Stock Solution..... 71
2.2.19 rhPDGF-BB, 10µg/mL Stock Solution..... 72
2.2.20 rhRANKL, 500µg/mL Stock Solution..... 72
2.2.21 Serum-free a-MEM (sf-aMEM)..... 72
2.2.22 Serum-free DMEM (sf-DMEM)..... 72
2.2.23 Trypsin, 0.05%..... 72
2.3 Stains, Buffers and Solutions for Histology and Immunohistochemistry..... 72
2.3.1 3,3'-Diamino Benzidine Tetrahydrochloride Hydrate (DAB) Working Solution..... 72
2.3.2 Acetate-Tartrate Buffer..... 73
2.3.3 Acid Alcohol..... 73
2.3.4 Citrate/Acetone/Formaldehyde Fixative..... 73
2.3.5 Decalcification Solution..... 73
2.3.6 Eosin..... 73
2.3.7 Fast Garnet TRAP Stain..... 73
2.3.8 Gelatin/Chromic Potassium Sulphate Solution..... 74
2.3.9 Mayer's Haematoloxylin..... 74
2.3.10 Methyl green, 0.5mg/mL..... 74

2.3.11 Naphthol AS-BI Phosphate, 0.39mg/mL..... 74
2.3.12 Pararosaniline, 40mg/mL Stock Solution..... 74
2.3.13 Pararosaniline TRAP Stain..... 74
2.3.14 Silver Nitrate, 1% (w/v)..... 75
2.3.15 Silver Nitrate, 5% (w/v)..... 75
2.3.16 Saline Sodium Citrate Buffer (SSC Buffer)..... 75
2.3.17 Spreading Solution..... 75
2.3.18 Sodium Bicarbonate, 1% (w/v)..... 75
2.3.19 Sodium Carbonate, 5% (w/v)..... 75
2.3.20 Sodium Phosphate/Citrate Buffer..... 76
2.3.21 Tris Buffer..... 76
2.3.22 Terminal Deoxynucleotidyl Transferase Buffer (TdT Buffer)..... 76
2.3.23 Toluidine Blue Stain, 2% (w/v)..... 76
2.3.24 TUNEL Reaction Solution..... 76
2.4 Cell Culture Techniques..... 76
2.4.1 Cell Lines and Standard Culture Conditions..... 76
2.4.2 Trypsinisation of Adherent Cell Lines..... 78
2.4.3 Cell Counts and Viability Staining..... 78
2.4.4 Cryopreservation and Storage of Cells..... 78
2.4.5 Thawing of Cryopreserved Cells..... 78
2.4.6 Establishment of mBM Cultures (Isolation of Osteoclast Precursor)..... 79
2.4.7 Establishment of mBMSC Cultures..... 79
2.5 Osteoclastogenesis Assays..... 80
2.5.1 mBM Osteoclast Formation and Activity Assays..... 80
2.5.2 RAW264.7 Osteoclastogenesis Assays..... 80
2.5.3 TRAP Stain..... 80
2.5.4 von Kossa Silver Stain..... 81
2.6 Osteoblastogenesis Assay..... 81
2.6.1 Murine Mineralisation Assay..... 81
2.6.2 Mineral Quantitation..... 82
2.6.3 Pico Green DNA Assay..... 82
2.7 WST-1 Assay..... 82
2.8 Cell Apoptosis Analysis by Immunofluorescence Staining: FOXO3a..... 83
2.9 Cell Apoptosis Analysis by Flow Cytometry: Annexin-V (AnnV) and 7-AAD..... 84

2.10 Cell Cycle Arrest Analysis by Flow Cytometry: Propidium Iodide (PI)..... 84
2.11 In Vivo Mouse Studies..... 85
2.11.1 Animals..... 85
2.11.2 Experimental Design..... 85
2.11.3 In vivo Bioluminescence Scanning..... 86
2.11.4 BEZ235 and BKM120 Preparation for Oral Gavage..... 86
2.12 Micro-CT (µ-CT)..... 87
2.13 Histology..... 87
2.13.1 Methacrylate Embedding..... 87
2.13.2 Paraffin Embedding..... 88
2.13.3 TRAP Stain..... 88
2.13.4 Toluidine Blue Stain..... 89
2.13.5 von Kossa Stain..... 89
2.14 Serum Paraprotein Analysis..... 89
2.15 Serum Bone Marker Analyses - Total Procollagen Type 1 N-terminal Propeptide (P1NP) and Tartrate Resistant Acid Phosphatase (TRAP) 5b..... 89
2.16 Immunohistochemistry Staining..... 90
2.16.1 Terminal deoxynucleotidyl transferase dUTP nick end labelling (TUNEL) Staining..... 90
2.17 Western Blotting Reagents..... 90
2.17.1 Blocking Solution..... 90
2.17.2 Lysis Buffer..... 90
2.17.3 10% Polyacrylamide Gel (Separating Gel)..... 91
2.17.4 15% Polyacrylamide Gel (Separating Gel)..... 91
2.17.5 Reducing Loading Buffer, 4x..... 91
2.17.6 Stacking Gel..... 91
2.17.7 Running Buffer, 10x..... 91
2.17.8 Tris-Buffered Saline (TBS), 10x..... 92
2.17.9 0.1% Tween/TBS (TBS-Tween)..... 92
2.17.10 TBS-Tween with 10% BSA..... 92
2.17.11 Transfer Buffer..... 92
2.18 Western Blotting..... 92
2.18.1 Preparation of Cell Lysates..... 92
2.18.2 RCDC Protein Estimation..... 93
2.18.3 Preparation of Samples for SDS-PAGE..... 93
2.18.4 SDS-PAGE Gel Preparation..... 94

2.18.5 Loading and Running of SDS-PAGE Gels..... 94
2.18.6 Transfer of Protein to Polyvinylidene Difluoride (PVDF) Membranes..... 94
2.18.7 Protein Detection..... 95
2.19 Statistical Analyses..... 96
Reference..... 97
The Effect of BEZ235 and BKM120 on MM cells in vitro..... 98
3.1 Introduction..... 99
3.2 Results..... 100
3.2.1 The effect of BEZ235 and BKM120 on human and murine MM cell lines in vitro..... 100
3.2.1.1 The effect of BEZ235 and BKM120 on the PI3K and mTOR signalling pathways..... 100
3.2.1.2 The effect of BEZ235 and BKM120 on Deptor expression in human and murine MM cells. 101
3.2.1.3 The effect of BEZ235 and BKM120 on cell proliferation in human and murine MM cells. 101
3.2.1.4 The effect of PIK75 on cell proliferation in human and murine MM cells..... 114
3.2.2 The effect of BEZ235 and BKM120 on apoptosis in human and murine MM cell lines in vitro. 114
3.2.2.1 The effect of BEZ235 and BKM120 on Cyclin D1 expression, Caspase-3 and Caspase-9 phosphorylation in MM cell lines in vitro..... 114
3.2.2.2 The effect of BEZ235 and BKM120 on MM cell apoptosis in vitro..... 128
3.2.2.3 The effect of BEZ235 and BKM120 in inducing oxidative stress in MM cell lines in vitro. 141
3.2.2.4 The effect of BEZ235 and BKM120 on cell cycle in MM cell lines in vitro..... 150
3.3 Discussion..... 163
Reference..... 178
The Effect of BEZ235 and BKM120 on MM and MM-induced Bone Loss..... 183
4.1 Introduction..... 184
4.2 Results..... 185
4.2.1 The effect of BEZ235 tumour progression and osteolytic bone disease in vivo..... 187
4.2.1.1 BEZ235 slows tumour progression down in vivo..... 187
4.2.1.2 BEZ235 decreases serum paraprotein levels and has no effect on animal weight..... 187
4.2.1.3 BEZ235 reduces the number of osteolytic lesions..... 190
4.2.1.4 BEZ235 increases bone volume density and trabecular number..... 190
4.2.1.5 BEZ235 increases serum P1NP levels decreases TRAcP5 levels..... 195
4.2.1.6 BEZ235 reduces osteoclast numbers and induces MM cell apoptosis in vivo..... 195
4.2.2 The effect of BKM120 on MM cells and bone in vivo..... 202
4.2.2.1 BKM120 inhibits tumour progression in vivo..... 202
4.2.2.2 BKM120 decreases serum paraprotein levels and has no effect animal weight..... 209
4.2.2.3 BKM120 reduces the number of osteolytic lesions perforating the tibiae cortices..... 209

4.2.2.4 BKM120 increases bone density, trabecular bone surface to bone volume ratio and trabecular number..... 214

4.2.2.5 BKM120 increases serum P1NP levels decreases serum TRAcP5 levels..... 214

4.2.2.6 BKM120 reduces osteoclast numbers and induces MM cell apoptosis in vivo..... 214

4.3 Discussion..... 221

Reference..... 228

The Role of the PI3k and mTOR pathways on Osteoblasts and Osteoclasts..... 236

5.1 Introduction..... 237

5.2 Results..... 239

5.2.1 The effect of BEZ235 and BKM120 on osteoblastogenesis in vitro..... 239

5.2.1.1 BEZ235 and BKM120 inhibit the PI3k and mTOR pathways in mBMSCs..... 239

5.2.1.2 BEZ235 and BKM120 inhibit mBMSC proliferation..... 244

5.2.1.3 BEZ235 and BKM120 do not induce apoptosis in mBMSCs..... 247

5.2.1.4 BEZ235 and BKM120 stimulate the osteogenic differentiation of mBMSCs in vitro..... 247

5.2.2 The effect of BEZ235 and BKM120 on osteoclastogenesis in vitro..... 254

5.2.2.1 BEZ235 and BKM120 inhibit osteoclastogenesis and osteoclast activity in mBM cells in vitro..... 254

5.2.2.2 BEZ235 and BKM120 inhibit the phosphorylation of Akt but not p70S6K in RAW264.7 cells..... 263

5.2.2.3 BEZ235 and BKM120 inhibit RAW264.7 cell proliferation..... 268

5.2.2.4 BEZ235 and BKM120 do not induce apoptosis in RAW264.7 cells..... 268

5.2.2.5 BEZ235 and BKM120 inhibit osteoclastogenesis and osteoclast activity in RAW264.7 cells in vitro..... 275

5.3 Discussion..... 275

Reference..... 288

Discussion..... 294

6.1 Summary and General Discussion..... 295

6.2 Future Directions..... 298

Reference..... 300

Abstract

Multiple myeloma (MM) is an incurable haematological malignancy characterised by the uncontrolled proliferation of clonal plasma cells within the bone marrow (BM). MM patients present with osteolytic bone lesions throughout the axial and apendicular skeleton, pathological fractures, spinal cord compression, hypercalcaemia, renal failure and immunosuppression. Approximately 10-15% of MM patients have been shown to have chromosomal translocations involving the phosphatidylinositol 3-kinase (PI3k) and mammalian target of rapamycin (mTOR) pathways. The PI3k and mTOR pathways mediate cellular proliferation, growth and survival. In MM, these pathways promote uncontrolled plasma cell proliferation, cell survival and protection against apoptosis. The PI3k and mTOR pathways have also been shown to be important in osteoblast and osteoclast formation and function.

In this study, we have examined the efficacy of two novel inhibitors of the PI3K/mTOR pathway: NVP-BEZ235 (BEZ235), a dual PI3k and mTOR inhibitor, and NVP-BKM120 (BKM120), a PI3k-specific inhibitor. Both of these drugs have been shown to effectively inhibit growth of a number of tumour cell lines. Unlike other haematological malignancies, MM is associated with pathological bone disease. In view of the importance of the PI3k and mTOR pathways in bone biology, we also investigated the effects of BEZ235 and BKM120 as potential treatments for MM-induced bone loss. *In vitro* studies outlined in this thesis demonstrate that BEZ235 and BKM120 inhibit plasma cell proliferation and induce oxidative stress in plasma cells, but do not induce apoptosis. Furthermore, both BEZ235 and BKM120 induce osteogenic differentiation in murine MSCs and inhibit osteoclast formation of murine BM monocytes.

The C57BL6/KaLwRij mouse model of myeloma was used to assess the effects of BEZ235 and BKM120 on tumour growth and osteolytic bone disease *in vivo*. We found that BEZ235 and BKM120 significantly reduced tumour growth and serum paraprotein levels *in vivo*. Importantly, both BEZ235- and BKM120-treated animals also showed a significant decrease in the number of osteolytic lesions of the cortical bone surface.

Overall, the findings of this study demonstrate that the single PI3k inhibitor, BKM120, is as effective as the dual PI3k/mTOR inhibitor, BEZ235, in inhibiting MM tumour growth and osteoclast formation and bone resorption *in vitro*. Furthermore, both

BEZ235 and BKM120 induce osteogenic differentiation and mineralised matrix formation of MSC *in vitro* and reduce osteolytic bone loss *in vivo*. These studies suggest that inhibition of the PI3k/mTOR pathways may serve as an effective approach to treat myeloma and myeloma-associated bone disease.

Declaration

I certify that this work contains no material which has been accepted for the award of any other degree or diploma in any university of other tertiary institution and, to the best of my knowledge and belief, contains no material previously published or written by another person, except where due reference has been made in the text. I give consent to the copy of my thesis, when deposited at the University Library, being made available for loan and photocopying, subject to the provisions of the Copyright Act 1968. I also give permission for the digital version of my thesis to be made available on the web, via the University's digital research repository, the Library catalogue and also through web search engines, unless permission has been granted by the University to restrict access for a period of time.

Signed

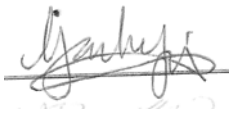

Zhen Ying Gan

Acknowledgement

Firstly, I would like to thank my supervisors Professor Andrew Zannettino and Dr Sally Martin. I am very grateful to the both of you for your tremendous guidance and help throughout this journey. Without your honest feedback, wisdom and believing in me, I would not have made it to the end successfully. Thank you for showing me the way to not only grow professionally as a researcher with high standards but also help me grow personally.

I would also like to thank my fellow colleagues in the Bone and Cancer Reserach Laboratory who have one way or another played a part in helping me succeed. Chee Man Cheong, Sarah Hemming, Romana Panagopoulos, Mary Matthews, Dr Peter Diamond, Dr Kate Vandyke, Dr Sharon Williams, Kris Mrozik, Sharon Paton, Sandra Isenmann, Dr Stephen Fitter, Jenny Drew, Vicki Wilczek, Dr Jim Cakouros, Dr Duncan Hewett, Dr Jacqueline Noll, Dr Kim Hynes, Thao Nguyen, Dr Danijela Menicanin, Dr Tony Camberari, Jimin Xiong and Kate Pilkington; thank you for your guidance and friendship which I greatly treasure. Kate Vandyke, thank you for guiding me in my histological and μCT analyses. Danijela, our sectioning guru, thank you being patient with me and showing me how to use the microtome. Pete and Sharon Williams, thanks you teaching me how to handle those aggressive KaLwRij mice and showing me how to carry out tail vein injections and cardiac punctures. Thanks to the SA Pathology Animal Care Facility staff for looking after my animals.

To all my friends, thank you for walking with me and sticking with me through thick and thin throughout this journey. Being with you guys kept me sane and made this journey easier. A big thank you to my best friends Sabrina and Michelle, I appreciate our 3-way Skype and being there for me during the toughest times. To Krystle, Jin, Chern and Say Ying, thank you for our hang out sessions and listening to my non-stop complains.

A huge thanks to my parents for supporting, advising and encouraging me in everything I do. I am so grateful to the both of you for sending me over to Australia to further my education and having faith in me when I am so far away from the both of you. To my brother Kenneth, thank you for your constant prayers and support throughout this journey.

Last but not least, to Linus – thank you. Thank you for always being there for me and the sacrifices made. I am eternally grateful for your constant love, patience, support and encouragement. I am thankful to you for sticking with me during this journey and our long distance relationship. I know it has not been easy for you being so far away. Without you, I would not have completed this education.

ABBREVIATIONS

µ-CT	micro-CT
α-MEM	α-modified Eagle's medium
µg/ µl/ µm/ µM	microgram/ microlitre/ micrometre/ micromolar
5TGM1-SFG	murine 5TGM1-SFG myeloma cell line
Adds	additives for tissue culture medium
Akt	serine/threonine kinase
ALP	alkaline phosphatise
AnnV	annexin-V
ANOVA	analysis of variance
Asc	ascorbate-2-phosphate
ATCC	American Type Culture Collection
BAD	Bcl-2-associated death promoter
BM	bone marrow
BMP	bone morphogenetic protein
BLI	bioluminescence imaging
B.Pm	bone perimeter
BS	bone surface
BSA	bovine serum albumin
BV	bone volume
c-α-MEM	α-MEM for murine bone marrow stromal cell culture
c-DMEM	DMEM for RAW264.7 cell culture
c-IMDM	IMDM for murine myeloma cell culture
c-RPMI	RPMI-1640 for human myeloma cell culture
DAB	3,3'-Diamino benzidine tetrahydrochloride hydrate
DEPTOR	DEP-domain-containing mTOR-interacting protein
DMEM	Dulbecco's modified Eagle's medium
DMSO	dimethyl sulphoxide
EDTA	ethylenediaminetetraacetic acid
ELISA	enzyme-linked immunosorbent assay
FCS	foetal calf serum
FGFR3	fibroblast growth factor receptor 3
FOXO	transcription factors of the Forkhead family
GFP	green fluorescent protein
GSK	glycogen synthase kinase
HBSS	Hanks' buffered saline solution
HCl	hydrochloric acid
HEPES	N-2-hydroxyethylpiperazine-N'-2-ethanesulfonic acid
IC_{50}	inhibitory concentration, 50%
IKK	inhibitors of NFκB
IL	interleukin
IMDM	Iscove's Modified Dulbecco's Medium

IP	intraperitoneally
ISS	International Staging System
kDa	kilodalton
m-αMEM	α-MEM for murine mineralisation
mBM	murine bone marrow monocyte
mBMSC	murine bone marrow stromal cell
M-CSF	macrophage colony stimulating factor
mg/ mL/ mm/ mM	milligram/ millilitre/ millimetre/ millimolar
MGUS	monoclonal gammopathy of undetermined significance
MM	multiple myeloma
mTOR	mammalian target of rapamycin
mTORC1	raptor-mTOR complex
mTORC2	rictor-mTOR complex
NBF	neutral buffered formalin
NF-κB	nuclear factor of κ light polypeptide gene enhancer in B-cells
N.Oc	number of osteoclasts
o-αMEM	α-MEM for murine bone marrow monocyte culture
OC	osteoclast
OCN	osteocalcin
Oc.S	osteoclast surface
OPN	osteopontin
P1NP	pro-collagen type I amino-terminal propeptide
p70S6K	70kDa ribosomal protein S6 Kinase 1
PBS	phosphate buffered saline
PDGF	platelet-derived growth factor
PDGFR	platelet-derived growth factor receptor
PEG	polyethylene glycol
PI	propidium iodide
PI3K	phosphoinositide-3-kinase
PIP^3	phosphatidylinositol-3,4,5-trisphosphate
PIP^2	phosphatidylinositol 4,5-bisphosphate
PKC	protein kinase C
PTEN	phosphatase and tensin homolog deleted on chromosome 10
PVDF	polyvinylidene difluoride
RANK	receptor activator of nuclear factor κB
RANKL	receptor activator of nuclear factor κB ligand
runx2	runt-related transcription factor 2
rh	recombinant human
RPMI	Roswell Park Institute Medium
SDS	sodium dodecyl sulphate
SDS-PAGE	sodium dodecyl sulphate polyacrylamide gel electrophoresis
Ser^{473}	non-catalytic domain of Akt
SEM	standard error of the mean

sf-α-MEM	serum-free α-modified Eagle's medium
sf-DMEM	serum-free Dulbecco's modified Eagle's medium
SMI	structure model index
SSC	saline sodium citrate
Std Dev	standard deviation
Tb.N	trabecular number
Tb.Pf	trabecular pattern factor
TBS	Tris-buffered saline
Tb.Sp	trabecular spacing
TBS-Tween	Tris-buffered saline with 1% Tween 20
Tb.Th	trabecular thickness
TdT	terminal deoxynucleotidyl transferase
TGF-β	transforming growth factor-β
Thr^{308}	catalytic domain of Akt
TEMED	N,N,N,N-tetramethylethylenediamine
TKR	tyrosine kinase-linked receptors
TRAP	tartrate-resistant acid phosphatase 5
TUNEL	terminal deoxynucleotidyl transferase dUTP nick end labeling
TV	total volume
Wnt	wingless-type mouse mammary tumour virus integration
WST-1	4-[3-(4-iodophenyl)-2-(4-nitrophenyl)-2H-5-tetrazolio]-1,3-benzene disulphonate

Publications

Scientific Manuscripts

1. **Gan Z.Y.**, Fitter S., Vandyke K., To L.B., Zannettino A.C., Martin S.K. (2014). The effect of the dual PI3k and mTOR inhibitor BEZ235on tumour growth and osteolytic bone disease in multiple myeloma. *Eur J Haematol doi: 10.1111/ejh.12436*.

Conference Proceedings

1. S. Fitter, S. Martin, **Z.Y. Gan**, J. Drew, S. Gronthos, P. Sheperd, A. Zannettino. BEZ235, a Dual Pan Class I PI3 Kinase and mTOR Inhibitor Promotes Osteogenic Differentiation of Human Mesenchymal Stromal Cells. *HAA Annual Scientific Meeting*, Adelaide, Australia, October 2009.

2. S. Fitter, S. Martin, **Z.Y. Gan**, J. Drew, S. Gronthos, P. Sheperd, A. Zannettino. BEZ235, a Dual Pan Class I PI3 Kinase and mTOR Inhibitor Promotes Osteogenic Differentiation of Human Mesenchymal Stromal Cells. *Australian and New Zealand Orthopaedic Research Society*, Adelaide, Australia, October 2009.

3. S. Fitter, S. Martin, **Z.Y. Gan**, J. Drew, S. Gronthos, P. Sheperd, A. Zannettino. BEZ235, a Dual Pan Class I PI3 Kinase and mTOR Inhibitor Promotes Osteogenic Differentiation of Human Mesenchymal Stromal Cells. *Centre for Stemcell Research*, Adelaide, Australia, November 2010.

Chapter 1

Introduction

1.1. Overview

Multiple myeloma (MM) is an incurable haematological malignancy characterised by the uncontrolled proliferation of monoclonal plasma cells in the bone marrow (BM)[1]. Depending on the severity of the disease at diagnosis, patients with MM have a median survival of approximately 5 years with conventional therapy[2; 3].

The survival and proliferation of MM plasma cells within the BM is facilitated by both autocrine stimuli and paracrine interactions with other cells within the BM microenvironment, such as endothelial cells, stromal cells and osteoclasts[4; 5]. In particular, growth factors such as interleukin-6 (IL-6) contribute to MM cell survival and proliferation by activating signalling pathways such as the phosphotidylinositol-3-kinase (PI3k)/Akt pathway and mechanistic Target of Rapamycin (mTOR)[4; 5].

The PI3k and mTOR pathways are vital in maintaining cell growth, proliferation and survival. A number of studies have identified several genetic mutations within these pathways in MM patients. Chromosomal translocations such as 11q13, 4p16.3, 16q32 and 6p25 which are associated with upregulation of the PI3k and mTOR pathways have been identified in 10-15% of MM patients while mutations of the RAS oncogenes, small GTPases which are able to trigger the activity of the PI3k pathway, are found in 30-50% of MM patients at diagnosis and 81% of patients at disease relapse[6; 7; 8; 9; 10; 11; 12; 13; 14; 15; 16]. These mutations contribute to the uncontrolled proliferation and resistance towards apoptosis[17; 18].

In addition to their role in maintaining MM cell survival and proliferation, several studies have also shown that the PI3k and mTOR pathways are important regulators of bone formation and resorption. Studies from our laboratory and those of others have demonstrated that inhibition of the PI3k and mTOR pathways stimulates osteogenesis, thus increasing bone formation[19; 20; 21; 22], and inhibits osteoclast formation and bone resorption[23; 24]. Notably, a number of the critical osteoclast stimulating factors implicated in MM-associated bone loss, including macrophage-colony stimulating factor (M-CSF), tumour necrosis factor alpha (TNF-α) and receptor activator of nuclear factor-κB ligand (RANKL)[21; 23; 25] mediate their actions, in part, via the mTOR pathway[26; 27; 28].

In light of the importance the PI3k and mTOR pathways on MM cell survival and proliferation and their roles in bone biology, the research outlined in this thesis was conducted to examine the efficacy of the two newly-developed drugs, the PI3K inhibitor, BKM120, and the dual PI3K and mTOR inhibitor, BEZ235, in targeting MM PCs and promoting bone formation. The following introduction represents an overview of the literature regarding (i) MM biology, (ii) the role of PI3k and mTOR pathways in MM and (iii) the role of PI3k and mTOR pathways in osteoblast and osteoclast formation and function.

1.2. *Multiple Myeloma*

1.2.1. *General Description*

Ranging from Monoclonal Gammopathy of Undetermined Significance (MGUS), smouldering or indolent myeloma, to active MM; MM is characterised by the homing malignant monoclonal plasma cells from secondary lymphoid organs to the bone marrow (BM)[1] (Figure 1.1). A majority of MM patients present with increased plasma cell number, renal failure and immunosuppression along with debilitating osteolytic bone lesions of the axial and apendicular skeleton which lead to pathological fractures, spinal cord compression and hypercalcaemia of malignancy[29]. The prognosis and response to treatment differs greatly between MM patients depending on the severity of the disease and the patients' age. To date, the survival of MM patients undergoing conventional therapy ranges between 6 months to 10 years, with a median of 5 years[2; 3]. With treatment for MM improving over the years, the 5 year survival rate has increased from 26.3% (1982-1987) to 43.4% (2006-2010)[30].

While the mechanisms of MM development remain to be elucidated, environmental and genetic factors are involved. Genetic predispositions and chromosomal mutations have been identified in the development of MM[31; 32]. Environmental factors such as radiation and chemical exposure have been shown to contribute to disease development[33].

1.2.2. Epidemiology

MM is the second most common haematological malignancy after non-Hodgkin's lymphoma and accounts for about 15% of all haematological cancers[29; 30]. MM affects

Figure 1.1. Myeloma Plasma Cells Bone marrow smear taken from a MM patient showing abnormal plasma cells[34]

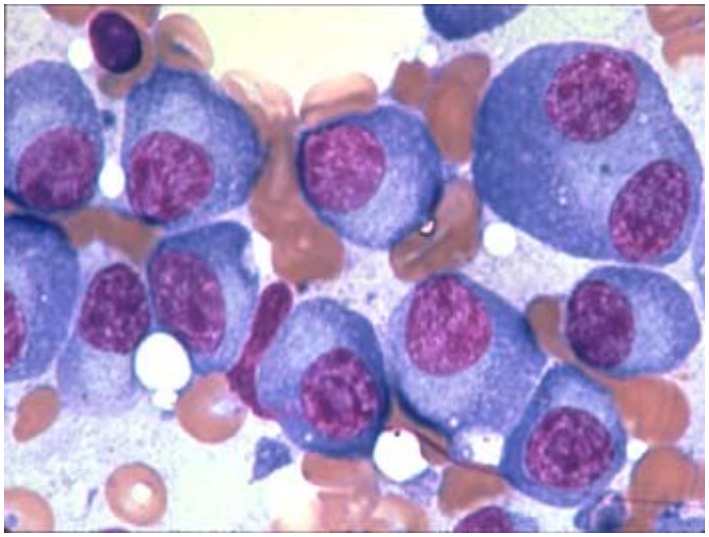

mostly the elderly with a median age of 69 years in men and 71 years in women[35]. In Australia, 78% of newly diagnosed MM patients are over the age of 60[30]. The incidences of MM vary according to ethnicity and geography and ranges between 1 MM patient per 100,000 people in China to 6.4 MM patients per 100,000 people per year in Western countries[29]. In Australia, about 6.1 patients per 100,000 people are diagnosed each year[30]. The number of African Americans diagnosed with MM each year is 2-times higher than Caucasians, with more men than women diagnosed [29; 30]. As diagnostic and therapeutic techniques have improved over the years, the number of Australian patients being diagnosed with MM increased by 36% in 2009 when compared to 1982[30].

1.2.3. *Variants of Multiple Myeloma*

MGUS is a stable premalignant plasma cell condition that derives from B-cell proliferation, which produces paraprotein similar to MM[36]. MGUS affects about 3% of adults over the age of 50 years and 5% of those over the age of 70 years[37]. MGUS patients are not affected by the debilitating symptoms of MM and can remain undiagnosed for many years. Each year, 0.5-3% MGUS patients progress to MM, while 75% do not progress for at least 20 years[38].

Indolent MM or smouldering MM which accounts for 1% of all MM cases, is an asymptomatic form of MM. Indolent MM patients do not require treatment even though they exhibit all the diagnostic features of MM as the MM cells in their bone marrow are either static or they progress very slowly[1]. Although possessing diagnostic features of MM, these patients do not suffer from any organ failure[1]. Patients progressing from indolent MM to active MM develop one or more of the following features; osteolytic bone lesions, anaemia, renal impairment and immunosuppression (Table 1.1). Patients with indolent MM are monitored closely so that treatment can begin immediately once the progression to active MM takes place. In some patients, MM cells develop tumours outside of the bone in places such as blood, skin and pleural fluid[32]. This extramedullary state of MM is the most aggressive form of plasma cell malignancy and when it is in the blood, it is called plasma cell leukaemia[32].

Table 1.1. Clinical Variants of Multiple Myeloma

Clinical Variant	Definition
Monoclonal Gammopathy of Undertermined Significance (MGUS)	<10% plasma cells in the bone marrow with the presence of paraprotein. No presence of MM related symptoms.
Indolent or Smouldering Myeloma	10-30% plasma cells in the bone marrow with high levels of paraprotein. No presence of MM related symptoms.
Multiple Myeloma	> 30% plasma cells in the bone marrow. Presence of osteolytic lesions, hypercalcaemia, renal impairment, anaemia and immunosuppression.
Plasma Cell Leukaemia	Similar to Multiple Myeloma. However, $>2x10^9$/litre of plasma cells have entered the peripheral blood or is >20% of the differential white blood cell count.

1.2.4. *Clinical Features and Diagnosis of Multiple Myeloma*

The increased proliferation of MM plasma cells results in an increase in paraprotein production, and is associated withanaemia, renal impairment and immunosuppression. Bence-Jones protein, a free light chain immunoglobulin that is produced by the MM plasma cells and released into the urine, is found in approximately 75% of MM patients at diagnosis and is the main cause of renal impairment in these patients[1]. Approximately 70 to 80% of MM patients exhibit osteolytic lesions, intractable bone pain, pathological fractures and spinal cord compression which can cause nerve compression caused by this debilitating disease[1; 39; 40]. Osteolytic lesions are found throughout the apendicular and axial skeleton. These lesions formed as a result of increased bone resorbing osteoclastic activity. Notably, these osteolytic lesions rarely heal, even after complete remission is achieved[39]. The increase in osteoclast activity leads to hypercalcaemia (elevated serum calcium levels) as a result of loss of calcium from the skeleton, which leads to renal impairment.

Another clinical feature seen in MM patients is an increase in angiogenesis within the bone marrow[41; 42]. The increase in angiogenesis not only provides oxygen and nutrient supply to facilitate MM cell growth, but also facilitates tumour cell migration and proliferation[43].

Developed in 1975, the Durie and Salmon staging system (Table 1.2) divides MM into three stages based on clinical parameters such as serum paraprotein level, serum calcium level, osteolytic lesions and the percentage of MM plasma cells in the BM[44]. Historically, MM was diagnosed when a patient presented with more than 10% of BM plasma cells, more than 3g/dL paraprotein in the blood or urine and evidence of osteolytic bone lesions [44].

The Durie and Salmon staging system was superseded in 2005 by the International Staging System (ISS) for MM (Table 1.3). The ISS was developed by pooling data from 10,750 MM patients at diagnosis and evaluating numerous potential prognostic factors[45]. The ISS classifies patients based on 2 blood parameters, beta-2-microglobulin (β2M) and serum albumin, which were found to have the greatest prognostic power in MM patients[45].

Table 1.2 The Durie and Salmon Staging System for Multiple Myeloma[44]

Stage	Criteria	Measured myeloma cell mass (cells x $10^{12}/m^2$)
I	All of the following: •Haemoglobin value >10g/100mL •Serum calcium value normal or ≤12mg/100mL •Normal bone structure (scale 0) or solitary bone plasmacytoma only on X-ray •Low M-component production rates Ig G value <5g/100mL Ig A value <3g/100mL Urine light chain M-component on electrophoresis <4g/24hours	<0.6 (low cell mass)
II	Fitting neither stage I nor stage III	0.6-1.2 (intermediate cell mass)
III	One or more of the following: •Haemoglobin value <8.5mg.100mL •Serum calcium value >12mg/100mL •Advanced lytic bone lesions (Scale 3) •High M-component production rates Ig G value >7g/100mL Ig A value >5g/100mL Urine light chain M-component on electrophoresis >12g/24hours	> 1.2 (high cell mass)
Subclassfication	A – Relatively normal renal function with serum creatinine velue of <2.0mg/100mL B – Abnormal renal function with serum creatinine value of ≥2.0mg/100mL	

Table 1.3 International Staging System for Multiple Myeloma[45]

Stage	Criteria	Median Survival (Months)
I	• Serum β2-microglobulin <3.5mg/L • Serum albumin ≥3.5g/100mL	62
II	Neither Stage I or III*	44
III	Serum β2-microglobulin ≥5.5mg/L	29

* There are 2 categories for stage II:
• Serum β2-microglobulin <3.5mg/L but serum albumin <3.5g/mL
• Serum β2-microglobulin 3.5 to <5.5mg/l irrespective of the serum albumin level.

Besides the Durie and Salmon and ISS systems for stratifying MM, conventional karyotyping has emerged as a relevant prognostic tool[46]. Studies based on large numbers of MM patients have identified karyotypic abnormalities in 30-50% of MM patients including translocations, hyper- and hypo-diploid karyotypes which are associated with poor outcomes. Karyotyping has shown that approximately 30% of MM patients exhibit chromosomal gain of 1q, 3q, 9q, 11, and 15q and deletion of chromosome 13q[32].Hallek and colleagues reported that karyotypic mutations are also evident in MGUS patients and progress throughout the entire course of the disease[46]. They also reported that the incidence of trisomy for at least one chromosome was 43% and 53% in two groups of MGUS patients[46].

1.3. *PI3k and mTOR pathway*

1.3.1. *Phosphotidylinositol—kinase (PI3k) Pathway*

The PI3k pathway is fundamental in maintaining cell growth, proliferation and survival. Aberrant loss or gain of the downstream effectors of the PI3k pathway has been linked to a variety of diseases such as diabetes, autoimmune diseases and cancer[47; 48]. The mammalian PI3 kinases are the only members of the PI3 kinase-related kinases family (comprising 8 members) that have an endogenous lipid substrate. Based on their isoform and substrate specificities, the PI3 kinases can be divided into three major classes, I (comprises two subgroups termed class Ia and Ib), II and III[47; 49; 50]. Class Ia PI3k are heterodimeric lipid kinases comprising a regulatory adaptor, p85 and a catalytic subunit, p110[50; 51]. p85 regulates various cellular proteins from transmembrane tyrosine kinase-linked receptors (TKR) and intracellular proteins such as protein kinase C (PKC), SHP1, Ras oncogene and hormonal receptors to provide an integration point for the activation of p110 and its downstream molecules[47; 50]. The p110 catalytic subunit of Class Ia PI3k comprises 3 isoforms (p110α, p110β and p110δ) while the p110 catalytic subunit of Class Ib PI3k consist of 110γ. p110α and p110β are ubiquitously expressed in various tissues, while p110δ and p110γ are largely restricted to the immune system[51].

The activated p110 catalytic subunit phosphorylates phosphatidylinositol 4,5-bisphosphate (PIP_2) to phosphatidylinositol-3,4,5-trisphosphate (PIP_3), which acts as a second messenger by translocating signalling molecules with pleckstrin homolog (PH) regions such as serine/threonine kinase (Akt) and phosphoinositide-dependent kinase 1

(PDK-1) to the plasma membrane[47; 51]. Phosphorylation of PIP_2 to PIP_3 is required to activate Akt, which is a key regulator in various cellular responses. Phosphatase and tensin homolog deleted on chromosome 10 (PTEN), a lipid phosphatase, can reverse the activation of PIP_2 to PIP_3 to regulate PI3k activity[51; 52].

Class II PI3k are monomeric enzymes consisting of 3 mammalian class II isoforms. PI3K-C2α and PI3K-C2β are ubiquitously expressed whereas PI3K-C2γ is liver specific[50]. Class III PI3k are heterodimeric enzymes comprising an adaptor, p150 and a 100kDa catalytic subunit, Vps34[50]. Class III PI3k are thought to be central to vesicle trafficking and lack a Ras-binding domain[50]. Class III PI3k has also been implicated in activating autophagy[50].

Akt, also known as protein kinase B (PKB), exists in three isoforms namely Akt1, Akt2 and Akt3[47; 50]. Akt has been shown to play crucial roles in cancer. Akt2 regulates cancer cell motility and invasion and Akt3 is over-expressed in hormone-insensitive breast and prostate cancers to maintain cancer cell survival[50; 53]. Total knockout of Akt1 is embryonically lethal, while Akt2 and Akt3 null mice with one functioning Akt1 allele has been demonstrated to be viable even though their glucose homeostasis is impaired[50; 54].

Phosphorylation of Akt is a complex process, and occurs on several residues such as Threonine 308 (Thr^{308}) and Serine 473 (Ser^{473}) within the molecule. Phosphorylation within the catalytic domain of Akt at Thr^{308} by PDK-1 leads to the activation of numerous signalling molecules such as GSK3, Caspase-9, Bcl-2-associated death promoter (BAD) protein, transcription factors of the Forkhead (FOXO) family, inhibitors of NFκB (IKK), mechanistic target of rapamycin (mTOR), p27 Kip1 and eukaryotic translation initiation factor 4E binding proteins (4E-BPs) to activate essential cellular effects of growth, proliferation, survival, and motility (Figure 1.2)[47; 48; 49; 55; 56; 57]. Phosphorylation of Akt also occurs at Ser^{473} within the carboxyl-terminal hydrophobic motif of Akt by PKCβII[50; 58].

Figure 1.2. The PI3k pathway. The PI3k consists of p85, a regulatory adaptor and p110, a catalytic subunit. p85 activates p110 through TKR, PKC, SHP1, Ras oncogenes and hormonal receptors. PDK-1 is activated by the phosphorylation of PIP_2 to PIP_3 by activated p110. Akt is phosphorylated by PDK-1 at Thr^{308} or by mTORC2 at Ser^{473} to activate FOXO, p27 and mTOR and inhibit GSK, BAD and IKK which are essential for cellular growth, proliferation survival and motility.

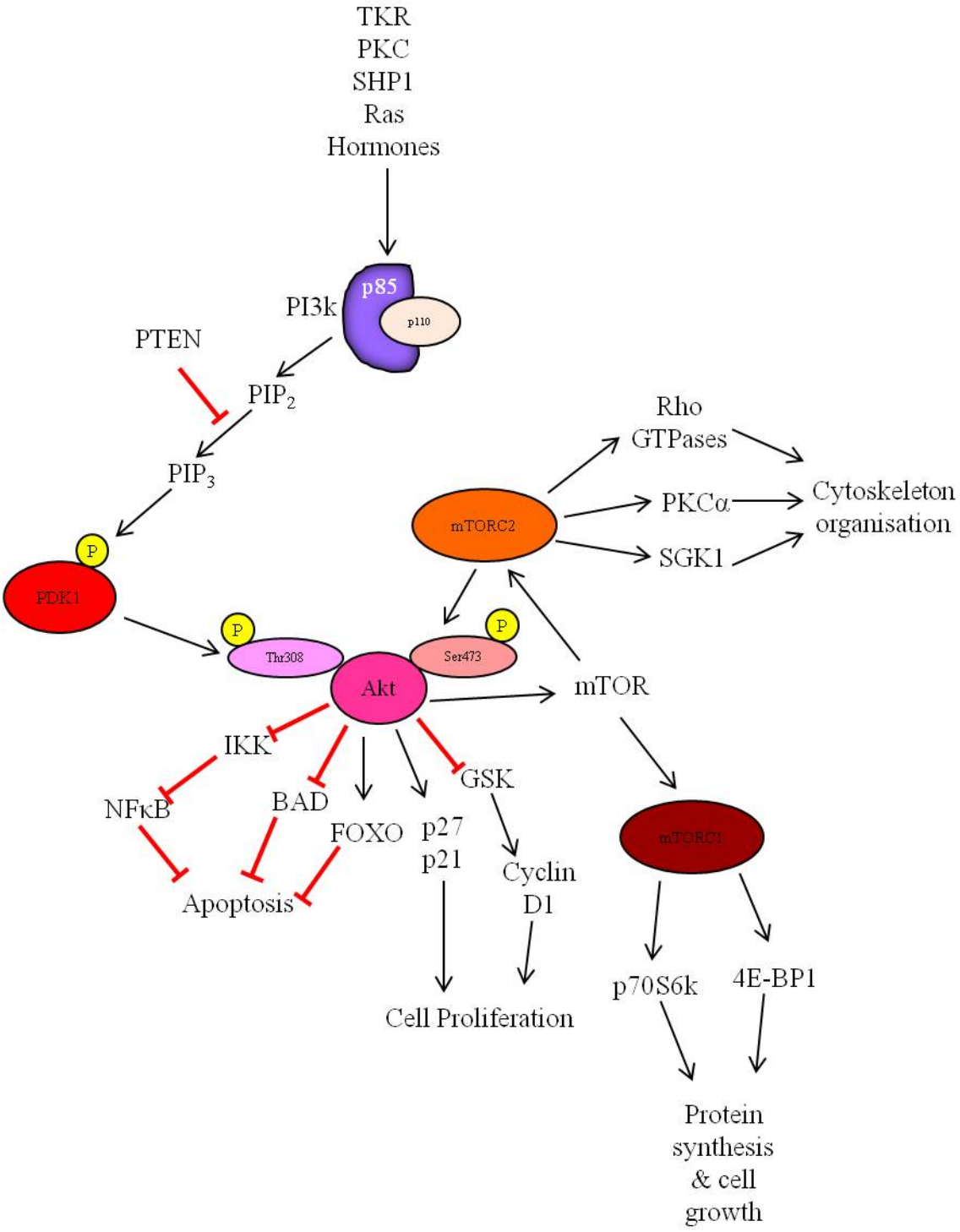
TKR
PKC
SHP1
Ras
Hormones
PI3k
p85
p110
PTEN
PIP2
PIP3
Rho
GTPases
PKCα
SGK1
Cytoskeleton
organisation
mTORC2
P
PDK1
P
Thr308
P
Ser473
Akt
mTOR
IKK
NFκB
BAD
FOXO
p27
p21
GSK
Cyclin
D1
mTORC1
Apoptosis
Cell Proliferation
p70S6k
4E-BP1
Protein
synthesis
& cell
growth

Akt promotes cell survival by inhibiting the activation of apoptotic mediators such as Caspase-9, FOXO and BAD protein as well as preventing the degradation of NFκB[48; 50]. Akt inhibits FOXO-mediated transcription of genes associated with apoptosis by inhibiting FOXO transcription factors from being translocated from the cytoplasm to the nucleus via the cystolic phosphoserine-binding protein, 14-3-3[59]. BAD is also inhibited by Akt via the 14-3-3 protein thus prevents cell apoptosis. Akt drives cell proliferation by inhibiting the phosphorylation of glycogen synthase kinase (GSK) which allows the activation of Cyclin D1[60]. Akt also negatively regulates the cyclin-dependent kinase inhibitors, $p27^{KIP1}$ and $p21^{CIP1/WAF1}$, thus allowing cellular proliferation[61; 62].

The activity of Akt is regulated by several effectors including PTEN, PDK-1 and mTORC2[47; 49]. As mentioned, PDK-1 is essential for the activation of Akt by PI3k while PTEN negatively regulates Akt by dephosphorylating PIP_3 to PIP_2[47; 51; 52]. mTORC2, a downstream effector of the PI3k/Akt pathway, is a positive regulator of Akt activity through Ser[47347; 63]. Dysregulations of the PI3k/Akt pathway by these factors are often implicated in cancers such as breast, lung, pancreatic and ovarian cancers[55; 64;].

1.3.2. *Mechanistic Target of Rapamycin (mTOR) Pathway*

The TOR protein is responsible for cellular growth by regulating DNA transcription, translation, protein degradation and ribosomal biogenesis[67]. The TOR proteins, Tor1 and Tor2, were first identified in *Saccharomyces cerevisiae* with a molecular weight of 280kDa[67; 68; 69]. The two highly conserved TOR orthologues have also been found in human, rat and mouse, sharing about 95% identity at the amino acid level, all with a molecular weight of 289kDa[67; 68; 69]. The mTOR proteins have a C-terminal region with high homology to the catalytic domain of PI3k and belong to the PIKK family[67; 68].

mTOR forms two multiprotein complexes: the rapamycin-sensitive mTOR-GβL-raptor complex (mTORC1) and the rapamycin-insensitive mTOR, GβL and rictor complex (mTORC2). mTORC1 is responsible for synthesising cell cycle regulatory proteins while mTORC2 regulates cytoskeletal organisation in mammalian cells[67; 68; 69; 70].

mTORC1 regulates cell growth by phosphorylating ribosomal protein S6 Kinase 1 (p70S6K) and 4E-BP1, [67; 68; 69]. Akt activates mTORC1 by inhibiting tuberous sclerosis

complexes (TSC1/TSC2) and Ras homolog enriched in brain (Rheb), leading to the phosphorylation of 4E-BP1 and p70S6K from eIF4E to promote cell growth and protein synthesis[48; 67; 68; 69; 71]. Studies have shown that Raptor maintains mTOR protein activity, in that overexpression of Raptor promotes mTOR kinase activity whereas knock down of Raptor decreases mTOR expression *in vitro*[72; 73]. Raptor knock down also decreases p70S6k phosphorylation and cell size. Notably, the reduction in cell size is similar to what is observed in studies examining knock down of mTOR suggesting close functional relationship between mTOR and Raptor[72]. Hara and colleagues suggested that Raptor serves as a scaffolding protein to bridge mTOR and its substrates, p70S6k and 4E-BP1[73]. A study by Kim *et al* showed that inhibition of this interaction by Rapamycin interrupts mTOR function[72].

Another major component of mTORC1 is GβL. GβL is an essential binding protein of mTORC1. Knock down GβL reduces Raptor binding affinity to mTOR, while overexpression of GβL stabilises the interaction between mTOR and Raptor and enhances mTOR activity[74]. GβL has also been suggested to mediate cellular signals from nutrients to modulate the formation of the mTOR-Raptor complex[74].

mTORC2 controls cytoskeleton organisation by activating downstream Rho GTPases and PKCα[70]. Activation of these downstream effectors indirectly phosphorylates p27 through serum- and glucocorticoid-inducible kinase 1 (SGK1) as well as Akt[63]. Whilst rapamycin predominantly inhibits mTORC1 and has little effect on mTORC2, prolonged rapamycin treatment can, in some instances, affect the assembly of mTORC2[75]. Nonetheless, both complexes function together to modulate cellular proliferation and growth (Figure 1.3).

1.3.3. *DEP-domain-containing mTOR-interacting protein (DEPTOR)*

DEPTOR is a novel binding partner of mTOR[76]. DEPTOR contains two dishevelled-egl-10-pleckstrin (DEP) domains whose functions, to date, are unknown. DEPTOR contains a PDZ domain through which DEPTOR binds to mTOR[76]. Studies have shown that depletion of DEPTOR activates both mTORC1 and mTORC2 signalling

Figure 1.3. The mTOR pathway. The mTOR pathway consists of mTOR-raptor (mTORC1) and mTOR-rictor (mTORC2). Akt activates mTORC1 by inhibiting TSC1/TSC2 which then inhibits Rheb. mTORC1 is responsible for protein synthesis and cell proliferation through the activation of p70S6k and 4E-BP. mTORC2. mTORC2 also activates Rho GTPases, PKCα and SGK1 to stimulate cytoskeleton organisation and Akt for protein synthesis and cell growth.

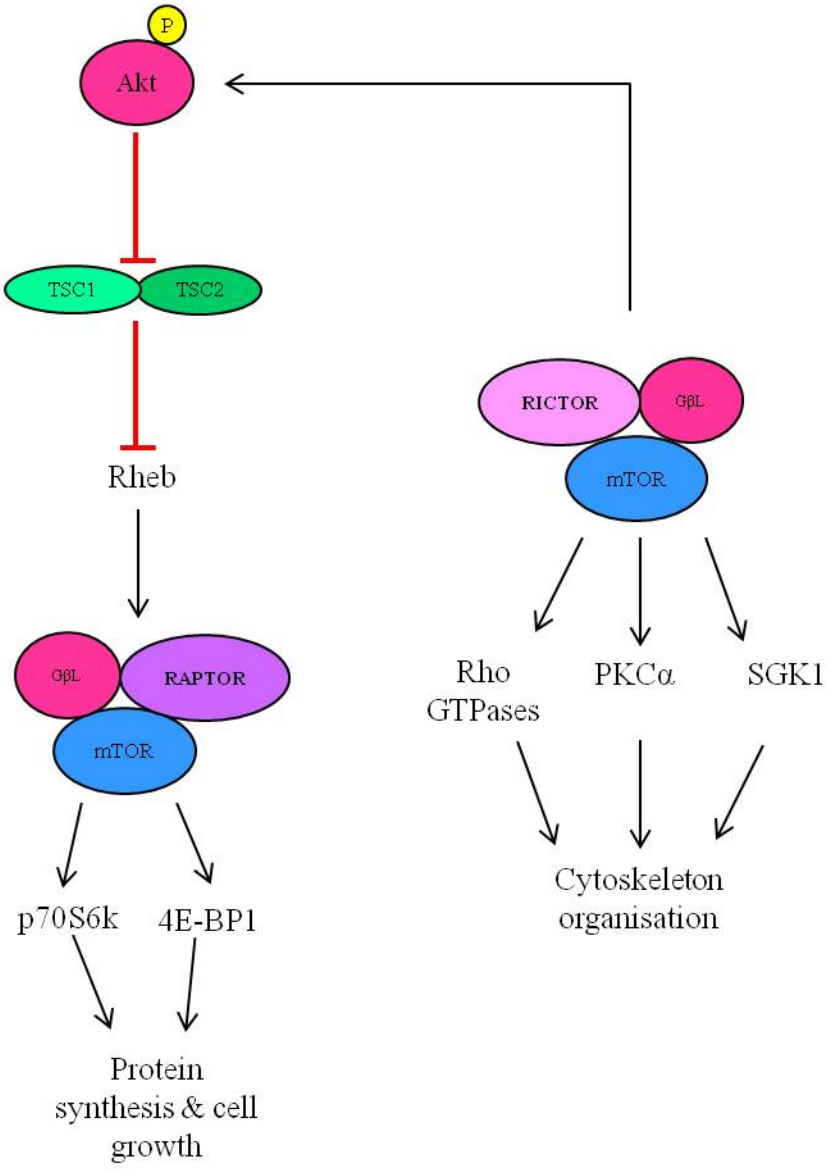
P
Akt
TSC1
TSC2
Rheb
GβL
RAPTOR
mTOR
p70S6k
4E-BP1
Protein
synthesis & cell
growth
RICTOR
GβL
mTOR
Rho
GTPases
PKCα
SGK1
Cytoskeleton
organisation

suggesting that DEPTOR inhibits both mTORC1 and mTORC2 (Figure 1.4)[76]. In MM cells, suppression of DEPTOR inhibits cell proliferation[76]. However, overexpression of DEPTOR also activates Akt signalling and therefore activates mTORC2, largely due to the S6k-dependent negative feedback loop activating Akt through the PI3k pathway[76].

1.3.4. *PI3k and mTOR pathways in Multiple Myeloma*

MM cells rely heavily on the PI3k and mTOR pathways for their survival, growth and proliferation. Numerous studies have identified genetic mutations in these pathways that enable the MM cells to continually proliferate and avoid undergoing apoptosis. As described in Section 1.2.4, karyotyping is able to identify chromosomal translocations in MM patients. Chromosomal translocations at 4p16.3 associated with fibroblast growth factor receptor 3 (FGFR3) and 16q32 associated c-MAF have been implicated in 10% and 15% of MM patients respectively[7; 8; 9; 12; 32]. Both FGFR3 and c-MAF are upstream effectors of the PI3k pathway. Chromosomal translocation at 11q13 which is associated with Cyclin D1, a cell cycle regulator and downstream of the PI3k pathway was observed in 20-25% of MM patients[11; 32]. A complex secondary translocation of c-MYC, which is downstream of the PI3k pathway and associated with enhanced proliferation, has also been observed in late progression of MM[32]. Deltion or mutation of PTEN has been linked to uncontrolled cell proliferation and inhibition of apoptosis in solid tumours and MM[77; 78; 79; 80]. In addition, mutations of the RAS oncogenes have been reported in 30-50% of MM patients and has been identified in 81% of relapsed MM patients[13; 14; 15]. The RAS oncogene, small GTPases which able to trigger the activity of the PI3k pathway, have been shown to be mutated at different clinical stages of MM but are more prevalent in relapsed patients[13; 14; 15]. p53, a tumour suppressor gene which stimulates PTEN and TSC2 to inhibit the downstream effects of the PI3k and mTOR pathways respectively, has also been identified to be mutated in MM cells[14].

Recently, over-expression of DEPTOR in MM patients has been shown to hyperactivate Akt and promotes cell survival[76]. The over-expression of DEPTOR is not only found in MM but also in breast cancer, prostate cancer, chronic myeloid leukaemia and lung cancer[81]. The overexpression of DEPTOR has been linked to poor prognosis and earlier recurrence in MM and thyroid carcinoma[81].

Figure 1.4. The interaction of DEPTOR between mTORC1 and mTORC2. DEPTOR is a novel binding partner of mTOR, comprising two disheveled-egl-10-pleckstrin domains. DEPTOR inhibits both mTORC1 and mTORC2 thus inhibiting their downstream effectors which maintains protein synthesis and cell growth through mTORC1 and cytoskeleton organisation through mTORC2.

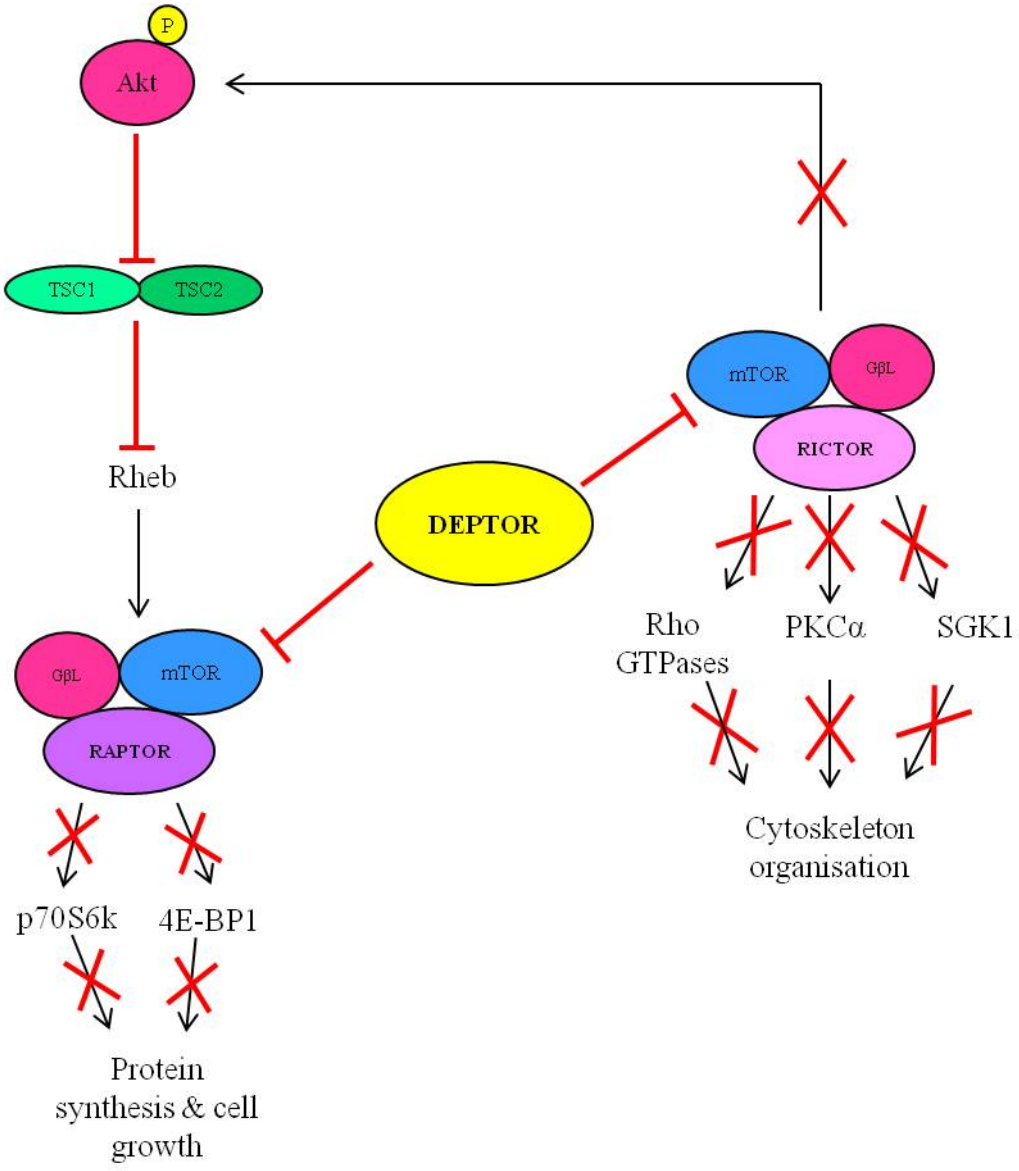
P
Akt
TSC1
TSC2
Rheb
GβL
mTOR
RAPTOR
p70S6k
4E-BP1
Protein synthesis & cell growth
DEPTOR
mTOR
GβL
RICTOR
Rho GTPases
PKCα
SGK1
Cytoskeleton organisation

A number of studies have examined the importance of these pathways in the survival and proliferation of MM cells. When the human OPM2 and RPMI-8226 MM cell lines were cultured with PI3k inhibitors such as LY294002 and Wortmannin, inhibition of cell proliferation, and induction of cell apoptosis and cell cycle arrest were observed[5; 82; 83]. Akt, the downstream target of PI3k, and its downstream effectors such as Caspase-9, GSK-3β, Bad and FKHR were also inhibited when the MM cells were cultured with these inhibitors[5; 82; 83]. As a single agent, the mTOR inhibitor Rapamycin is ineffective in inducing MM cell apoptosis however, when combined with conventional drugs such CC-5013 (lenalidomide; Revlimid), an immunomodulatory analogue of thalidomide, and dexamethasone, it induces MM cell apoptosis.[84; 85].

1.4. *Bone*

1.4.1. *Bone Remodelling*

A well-maintained skeleton is required to support the human body. Bone is constantly being resorbed by bone-resorbing osteoclasts and new bone is replaced by bone-forming osteoblasts. Under normal circumstances, this process is tightly regulated, with osteoblast activity balanced with osteoclast activity to maintain te structural and mineral integrity of the bone.

Bone remodelling takes place in 4 stages[86]. The *resorption phase* occurs when osteocytes recognise a fracture or damage in bone surface and recruit osteoclasts to degrade and resorb the bone. The *reversal phase* takes place when growth factors and proteins released by osteoblast precursors stimulate the differentiation and proliferation of osteoblasts on the resorbed bone surface. During this phase, the osteoblasts actively synthesise bone matrix and secrete collagenous and non-collagenous proteins. In the *formation phase*, osteoblasts lay down a layer of non-mineralised matrix, known as osteoid, which is mineralised by the secretion of hydroxyapatite at the site of resorption[87]. Finally, osteoblasts are then enclosed by the matrix and converted into osteocytes during the *resting phase* until a new cycle begins (Figure 1.5).

The crosstalk between osteoblasts and osteoclasts ensures that there is a balanced activity. Osteoblasts secrete macrophage colony stimulating factor (M-CSF), receptor activator of nuclear factor-κB ligand (RANKL) and osteoprotegrin (OPG), which are

Figure 1.5. Bone Remodelling. Upon detecting a fracture or damage on the bone surface, osteoclasts are recruited to degrade and resorb the bone. This *resorption phase* is followed by the *reversal phase* when growth factors and proteins are released by osteoblast precursors to stimulate the differentiation and activation of osteoblasts on the resorbed bone surface. The mature osteoblasts synthesise a bone matrix and lay down non-mineralised matrix, known as osteoid, at the site of resorpion during the *formation phase*. Finally the osteoblasts are enclosed by the matrix an converted into osteocytes during the *resting phase*.

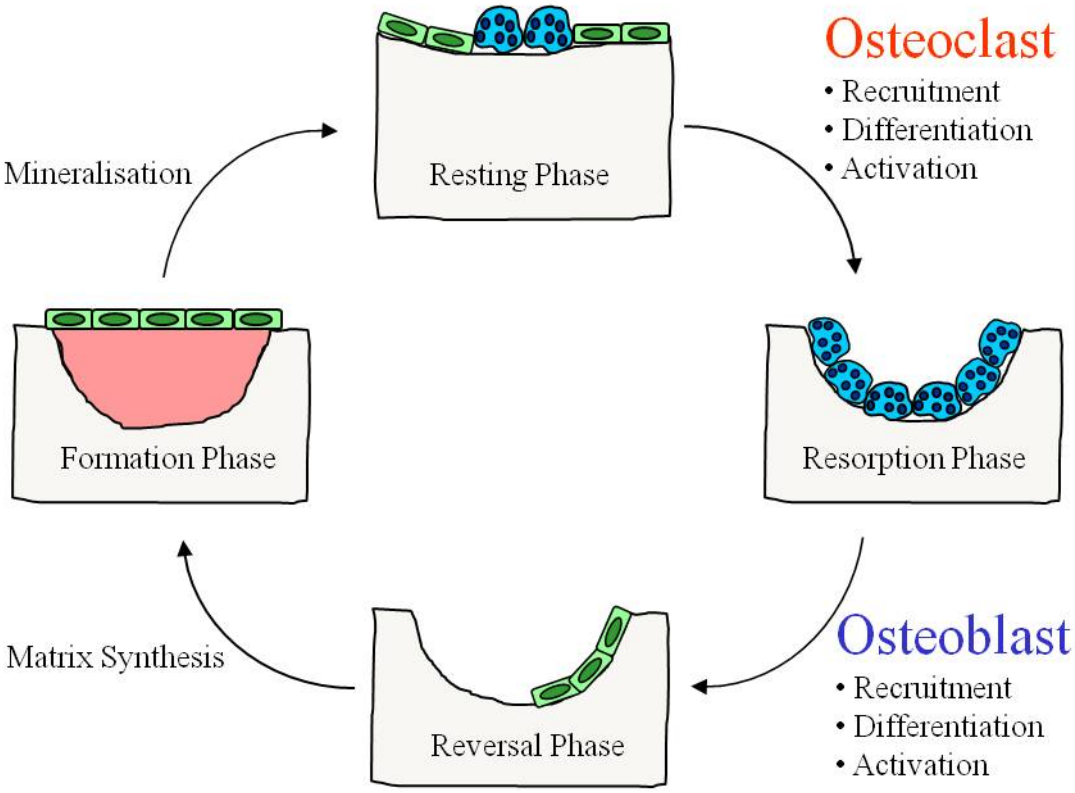
Osteoclast
• Recruitment
• Differentiation
• Activation
Resting Phase
Resorption Phase
Osteoblast
• Recruitment
• Differentiation
• Activation
Reversal Phase
Matrix Synthesis
Formation Phase
Mineralisation

essential regulators for osteoclast formation and activity[88; 89]. Similarly osteoblast activation is reliant on osteoclast-mediated release of factors such as transforming growth factor-β (TGF-β) that are sequestered in the bone matrix[90].

1.4.2. *Osteoblast*

Osteoblasts are mature, non-proliferative cuboidal cells that are derived from pluripotent mesenchymal stem cells which also give rise to adipocytes, myoblasts, fibroblasts and chondroblasts[91]. In addition to their pivotal role in extracellular matrix production and matrix mineralisation, osteoblasts are important in calcium homeostasis whereby they control the release of calcium from the bone into the bloodstream[92].

1.4.2.1. *Osteoblastic Signalling Pathways*

Runx2, also known as Cbaf1, is an osteogenic transcription factor and one of the earliest marker to drive MSCs toward the osteoblastic lineage (Figure 1.6)[93; 94; 95]. Runx2 upregulates osteoblastic gene expressions such as type I collagen, osteocalcin and bone sialoprotein[95]. Studies have shown that Runx2 knockout mice have skeletal deformities due to defective osteoblastic differentiation[93; 94]. Osterix is a key regulator of osteoblastic formation, which is downstream of Runx2. Osterix is the final transcription factor that drives MSCs towards the osteoblastic lineage. Nakashima and colleagues showed that Osterix knockout mice lack mature osteoblasts and endochondral and intramembranous ossification is absent[96]. BMPs, members of the TGF-β superfamily, are potent stimulators of osteoblastic differentiation[97]. BMPs activate Runx2 and Osterix to promote osteoblastic differentiation[98; 99; 100].

Wnt signalling is critical for promoting osteoblastogenesis, inhibit chondrogenesis differentiation and maintain bone formation[101]. Wnt binds to β-Catenin to stimulate genes involved in osteoblastic differentiation[102]. Studies showed that the Wnt/β-Catenin interaction is detrimental for osteoblastic differentiation and bone formation *in vivo* in mice conditional knockout studies[101; 103; 104]. Mutations in Wnt genes have been shown to be associated with abnormal bone phenotypes in humans. Mutations have been shown in the Wnt co-receptor, LDL receptor-related protein 5 (LRP5). Loss of LRP5 function has been shown to be related to Osteoporosis Pseudo-Glioma syndrome, a low bone mass disease while increased LRP5 function is involved in autosomal high

Figure 1.6. Osteoblast formation. The PI3k and mTOR pathways stimulate transcription factors such as Runx2 and Osterix to drive mesenchymal stem cell differentiation towards the osteoblastic lineage. Osteoblast maturation is stimulated by ALP, OPN and OCN production, while Sclerostin, a Wnt inhibitor, inhibits the commitment of the mesenchymal stem cells towards the osteoblastic lineage.

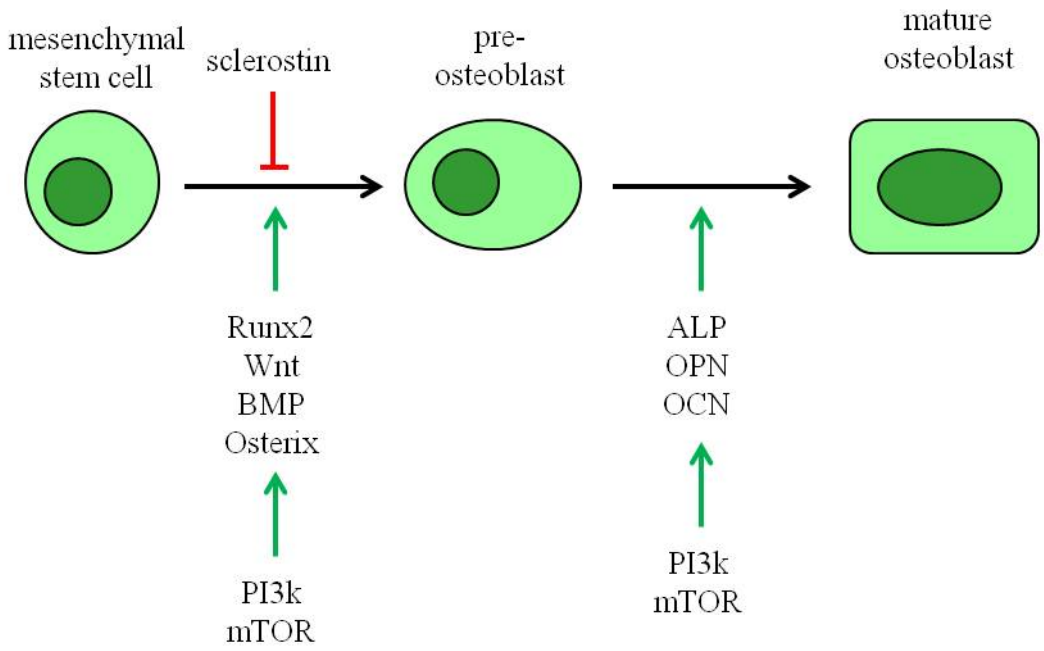
mesenchymal
stem cell
sclerostin
pre-
osteoblast
mature
osteoblast
Runx2
Wnt
BMP
Osterix
PI3k
mTOR
ALP
OPN
OCN
PI3k
mTOR

bone mass phenotype[105; 106; 107]. Mutations in the SOST gene which encodes the Wnt inhibitor, Sclerostin, has been shown to be associated with diseases of osteosclerosis (high bone mass) such as Sclerosteosis and Van Buchem disease[108; 109; 110].

1.4.3. *Osteoclast*

Osteoclasts are large, multinucleated cells that originate from the monocyte/macrophage family[111; 112; 113]. They resorb bone, thereby facilitating the laying down of new bone by osteoblasts. A multi-step process is required to activate mature osteoclasts. A "clear site" is formed following recognition of and binding to matrix proteins, cell polarisation and actin ring formation[114]. The "clear site" creates an enclosed area between the osteoclast and bone surface to allow the formation of an environment suitable for resorption to occur[90; 114]. Following adhesion of the osteoclast to the bone surface, the osteoclast spreads and transport protons and proteases to the osteoclast surface next to the bone to form a ruffled membrane[90; 114]. This allows mineralised bone to be solubilised and degraded by cathepsin-K, a osteoclast derived lysosomal enzyme[90; 114].

1.4.3.1. *Transcription Factors and Cytokines Involved in Osteoclastogenesis*

The B-cell transcription factor, PU.1, is required for early commitment of the monocyte/macrophage haematopoeitic stem cells towards osteoclastogenesis[115]. PU.1 induces the expression of the Fms gene, CSF1R, giving rise to osteoclast precursors[115]. Fms is then activated by M-CSF to stimulate osteoclast cell proliferation and survival, and up-regulate receptor activator of nuclear factor-κB (RANK) expression[115; 116]. These pre-osteoclasts are then driven by M-CSF and RANKL and through the activation of the nuclear factor for activated T cells (NFAT) c1 to become multinucleated osteoclasts (Figure 1.7)[116].

RANK, expressed on the surface of mature osteoclasts and osteoclast precursors, and its ligand, RANKL, which is expressed on MSCs and osteoblasts, are needed for osteoclast activation and survival, a process that is tightly regulated by osteoblast-osteoclast interaction[88; 89]. The interaction between RANK and RANKL is crucial as studies using RANKL deficient mice demonstrated severely dense bones in these animals due to the absence of mature osteoclasts[117; 118]. Several cytokines such as

Figure 1.7. Osteoclast formation. The transcription factor, PU.1, drives monocyte/macrophage haematopoeitic stem cells towards the osteoclast lineage. PU.1 also induces the expression of Fms which is activated by M-CSF to promote osteoclast proliferation and survival. Activation of M-CSF and RANKL stimulates osteoclast maturation by fusing osteoclast precursors to become activated multinucleated osteoclasts. RANKL and cathepsin-K are genes activated by RANK for osteoclast activity while OPG, secreted by osteoblasts, inhibits RANK-RANKL interaction to prevent osteoclastogenesis.

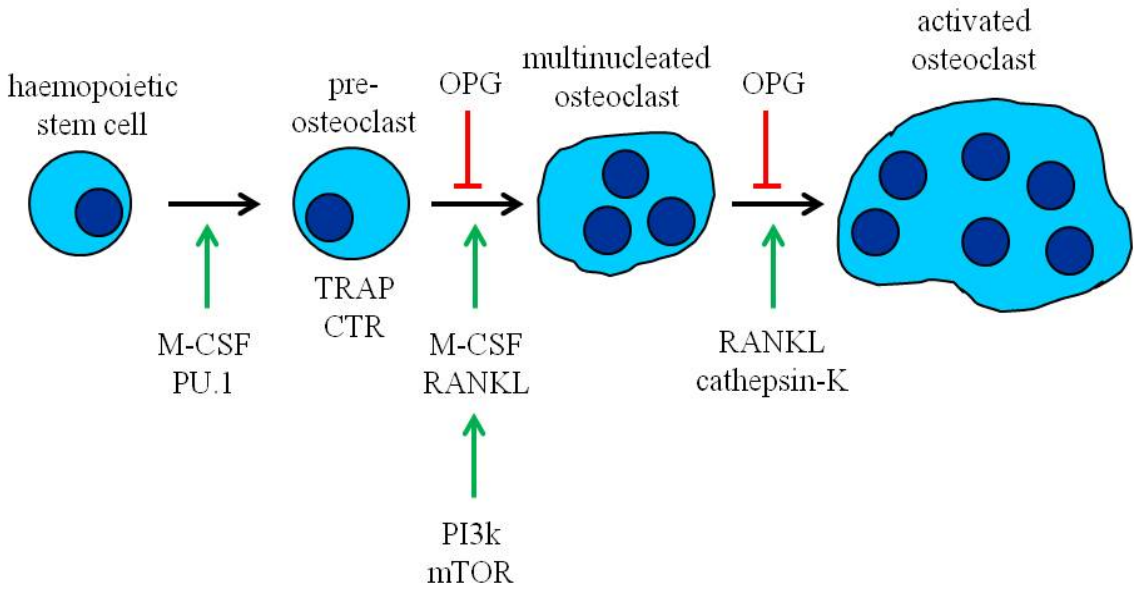
haemopoietic
stem cell
M-CSF
PU.1
pre-
osteoclast
TRAP
CTR
OPG
M-CSF
RANKL
PI3k
mTOR
multinucleated
osteoclast
OPG
RANKL
cathepsin-K
activated
osteoclast

PTHrP, TNFα, IL-1β, IL-11, thyroid hormone, 1,25-(OH)2, vitamin D and prostaglandin E2 are involved in RANK/RANKL interaction[119; 120].

Tumour necrosis factors (TNFs), particularly TNF-α, plays an important role in RANKL-mediated osteoclast formation [121; 122]. Moreover, Interleukin-1 (IL-1), produced by osteoblasts and osteoclasts, binds directly to pre-osteoclasts to stimulate the fusion of pre-osteoclasts leading to mature osteoclast formation[119; 120]. TGF-β, present in the bone matrix, is released and activated by both osteoblasts and osteoclasts to stimulate both bone formation and bone resorption[123]. Mackie and Trechsel demonstrated that administration of TGF-β stimulates osteogenesis in healthy BALB/c mice[124]. This was supported by *in vitro* studies showing that TGF-β enhanced osteoprogenitor cell proliferation and differentiation[125]. In osteoclastogenesis, TGF-β has been shown to stimulate osteoclast differentiation from haematopoietic cells in the absence of osteoblasts by acting on macrophage-like osteoclast precursors[126]. In contrast, TGF-β has been reported to suppress RANKL expression[126] and stimulate OPG production *in vitro*[127]. These studies suggest that the activity of TGF-β on osteogenesis and osteoclastogenesis depend on the number of osteoblasts and osteoclasts present in order to maintain a balanced osteoblast:osteoclast ratio.

OPG is produced by osteoblasts and binds to RANKL to inhibit the interaction of RANK and RANKL, thus inhibiting osteoclast formation and activity [88; 89]. OPG is crucial in bone remodelling as it regulates osteoclastogenesis to prevent uncontrolled bone resorption[88]. The balance between OPG and RANKL is crucial as deregulation of this balance can result in abnormal bone turnover and increased or decrease in bone mass[88; 128]. Hence, the OPG/RANKL ratio in the bone microenvironment determines whether osteoclastogenesis or osteopetrosis occurs.

1.4.4. *Mechanisms Underlying Myeloma-Induced Bone Loss*

Present in 70-80% of MM patients, bone destruction is one of the most debilitating and predominant clinical feature of MM[1; 39; 40]. It is caused by increased osteoclastic resorption in response to factors produced by the MM cells, or the bone marrow microenvironment in response to the tumour cells. The MM cells produce factors such as IL-1, IL-6, GM-CSF, M-CSF, TNF-α, Lymphotoxin, and RANKL to stimulate osteoclast formation and osteoclastic bone resorption[39; 40]. Interactions between the MM cells and the MSCs within the bone marrow microenvironment induce an increase in

IL-6, a potent MM growth/survival factor, production that contribute to the stimulation of bone degradation [39; 40]. IL-6 is also produced by osteoclasts which enhances both osteoclast formation and its bone resorbing capacity[40]. In addition to IL-6, IL-1, TNF-α, Lymphotoxin and M-CSF are produced by the MM cells to sustain high levels of osteoclastic formation and activity[40].

Macrophage inflammatory protein-1α (MIP-1α), secreted by most MM cells, has been shown to be a major mediator of osteoclastic bone destruction in MM[129; 130]. MIP-1α directly stimulates osteoclast precursors to differentiate into bone resorbing osteoclasts[129; 130]. The role of MIP-1α in maintaining osteoclastogenesis and the interaction between osteoclasts and MM cells was demonstrated when osteoclasts were shown to be protect MM cell from Doxorubicin-induced apoptosis [131]. This was also confirmed in studies using MM murine models that showed a significant decrease in bone destruction and tumour burden when MIP-1α was inhibited[129; 130].

Previous studies from our laboratory showed that the chemokine, stromal-derived factor-1α (SDF-1α) play a role in the increased osteoclastic activity in MM[132]. This study showed that MM cells produce significant levels of SDF-1α protein and increased plasma level of SDF-1α were observed in MM patients when compared to age matched normal controls[132]. Importantly, a significant increase in the number and size of resorption pits formed when SDF-1α-positive MM cells were cultured on dentine slices under osteoclastogenic conditions[132]. The increase in osteoclastogenesis in response to SDF-1α was related to the increase in the expression of osteoclast activation genes such as RANKL, RANK, TRAP and Cathepsin K[132].

The inhibition of osteoblast formation and function in MM is not fully understood and a number of theories have been proposed for this. The inhibition of Runx2, a transcription factor critical for osteoblastic formation[93; 94; 95], has been suggested as one of the mechanisms of osteoblast inhibition in MM[133]. Studies have shown that the inhibition of Runx2 activity by MM cells is mediated by cell-to-cell contact via VLA-4 (present on MM cells)-VCAM-1 (present on osteoblast progenitors) interaction[134]. This interaction was shown when the human MM cell line, JJN3, which expresses high levels of VLA-4, was implanted into NOD-SCID mice. These mice develop osteolytic lesions and marker osteoblastopenia with significant reduction of bone formation[135]. Furthermore, inhibition of osteoblast precursors and osteoblast differentiation markers

such as alkaline phosphatase, osteocalcin and collagen I was observed when human MM cells were cocultured with osteoprogenitor cells[134].

Another proposed mechanism for the inhibition of osteoblast formation and function is via MM cell-mediated inhibition of Wnt signalling in osteoblasts. As described in Section 1.4.2.1, Wnt signalling is critical for promoting osteoblastogenesis and maintaining bone formation[101]. Dickkopf-1 (DKK-1), a inhibitor of Wnt which blocks early osteoblast formation[136], has been reported to be overexpressed by MM cells. A study by Tian *et al* showed that CD138+ MM cells overexpress DKK-1 when compared to plasma cells from MGUS patients and normal plasma cells[137]. Furthermore, Tian *et al* showed a correlation between high levels of DKK-1 serum levels and the presence of bone leasions in MM patients[137].

IL-3, produced by T-cells in bone marrow microenvironment[138], has been reported to inhibit osteoblastogenesis by inhibiting basal- and BMP-2 stimulated osteoblast formation in MM patients[139]. IL-3 plasma levels were increased by 70% in MM patients when compared to healthy controls or MGUS patients[140]. *In vitro* studies showed that bone marrow plasma from MM patients with high levels of IL-3 inhibited osteoblast formation in human cultures[139]. This inhibitory effect was further enhanced when TNF-α was included in the culture[139]. Furthermore, IL-3 was also shown to be involved in osteoclast activation in MM[141]. These findings suggest that IL-3 plays a dual role in the bone-destruction in MM by both stimulating osteoclastic function while at the same time inhibiting osteoblastic function.

1.4.5. *PI3k/mTOR pathway in osteoblasts and osteoclasts*

The role of the PI3k and mTOR pathways has not been fully understood in regulating osteoblast and osteoclast formation and function. Several studies have demonstrated the importance of the PI3k pathway in bone development. Defects are also seen in bone development in Akt1 or Akt1/Akt2 knockout mice, while an increase in bone density was observed in PTEN knockout mice[142]. Furthermore, when healthy C57BL/6 mice were administered 10mg/kg PIK75 (p110α inhibitor) once daily for 34 days, a significant decrease in bone volume density (BV/TV), bone volume (BV) and strength of the femurs were observed[142]. Using the PI3k inhibitor LY294002, Vinals demonstrated an increase in BMP-2 expression, an early marker of osteoblast

differentiation, and late-stage markers such as alkaline phosphatase and osteocalcin in response to PI3K inhibition[143].

In studies using Rapamycin, an mTOR inhibitor, Ogawa *et al* showed an increase in ALP activity and osteopontin and osteocalcin mRNA expression in rat osteosarcoma cells[20]. Interestingly however, a number of studies have demonstrated the opposite. A study by Isomoto *et al* showed that when rat BMSCs were cultured with Rapamycin, the drugs treatment inhibited osteogenic differentiation where a decrease in ALP activity was observed after 2 weeks and low calcium and osteocalcin levels after 4 weeks of treatment[144]. Singha *et al* also showed that inhibiting the mTOR pathway reduced osteocalcin, bone sialoprotein and Osterix mRNA levels and the ability of mBMSCs to mineralise under osteogenic conditions[145]. These contradicting findings could be due to the cell types and treatment conditions used. Besides that, Rapamycin inhibits mTORC1 and to a much lesser extent, mTORC2, and ultimately activates the PI3k pathway through several feedback loops such as the S6k-PI3k-Ras pathway or the insulin-like growth factor-1 receptor signalling pathway[146; 147].

The PI3k pathway has been shown to induce osteoclastic differentiation, activation and survival by transducing signals from RANKL and M-CSF[21; 25]. RANKL and M-CSF, both expressed by osteoblasts, have been shown to promote osteoclast survival by activating Akt[24; 148]. Kawamura and colleagues demonstrated that Akt1 is necessary for the function of osteoclasts, as impairment of Akt1 down-regulates RANKL expression on osteoblasts and leads to a reduction in bone resorption *in vitro*[24]. Bradley and colleagues showed that M-CSF activates the PI3k pathway in osteoclasts[148], which inhibits the survival of RANKL-dependent osteoclasts[21; 25; 149; 150]. Inhibition of PTEN has been shown to inhibit RANKL- and Osteopontin-activated pathways thus inhibiting osteoclast differentiation, survival and migration in RAW264.7 osteoclast precursor cells[149].

The mTOR pathway is also involved in osteoclast formation, survival and bone resorption[23]. By inhibiting the mTOR pathway with Rapamycin, Mogi *et al* showed an inhibition of osteoprotegerin, an inhibitor of RANKL, thus promoting the formation and proliferation of osteoclasts when murine ST2 stromal cells were cultured under osteoclastogenic conditions with Rapamycin (Figure 1.6)[151].

1.5. *Treatment for Myeloma and Myeloma-induced Bone Loss*

1.5.1. Treatment for Myeloma

Response to therapy is measured by a number of response criteria. These include the percentage reduction in serum paraprotein, urinary light chain excretion and the reduction of MM-related symptoms following treatment[154]. In 2007, the International Myeloma Working Group (IMWG), developed uniform response criteria and included the addition of free light chain response for patients without measureable disease[155]. These standardised criteria ensure that clinical trials are stringently evaluated and enable response rates to therapy to be compared between studies[155].

Over the past decade, the treatment options for MM have improved considerably owing to the development of new compounds, such as the immune-modulatory drug, thalidomide and the proteasome inhibitor, bortezomib[152]. Thalidomide alone, has a 65-75% response rate in newly diagnosed patients[153] and a 25-35% response rate in relapsed patients[152]. To further increase the response rate to treatment, drug combinations involving an alkylating agent such as cyclophosphamide, an immuno-modulatory drug such as thalidomide or lenalidomide and a glucocorticosteriod such as prednisone and dexamethasone have been used. Two-drug combinations, such as lenalidomide-dexamethasone and bortezomib-dexamethasone have been shown to have a 70% and 80% response rate respectively[153]. Bortezomib-dexamethasone treatment is commonly used in patients with high-risk MM and those presenting with acute renal failure[153]. While bortezomib-dexamethasone treatment is effective, this treatment approach is associated with the risk of neurotoxicity which can occur abruptly[153]. Nevertheless, the risk of neurotoxicity can be significantly reduced by reducing the dose of bortezomib without a significant loss of efficacy[153].

Patients undergoing 3-drug combinations have shown better response rates compared to those being treated with 2-drug combinations. In newly diagnosed patients, bortezomib-thalidomide-dexamethasone and bortezomib-lenalidomide-dexamethasone have resulted in response rates of up to 95% and 100%, respectively[153; 156]. Importantly, the bortezomib-lenalidomide-dexamethasone combination has been shown to be effective in 61% of relapsed patients[156]. In elderly patients, or those patients who are ineligible for high dose chemotherapy, the combination of melphalan-prednisone with bortezomib or lenalidomide has shown improved response rates and overall survival[153; 156].

Following induction chemotherapy, patients who display good performance status may be eligible for an autologous stem-cell transplant. These patients undergo high dose melphalan treatment (200mg/m^2) as a conditioning regime and subsequently transplanted with autologous mobilised peripheral blood haematopoietic stem cells. This form of treatment has been shown to prolong median survival rates by approximately 12 months[153].

1.5.2. Treatment for Myeloma-induced Bone Loss

Bisphosphonates are primarily used to treat bone loss disorders including MM, cancer-associated bone metastases and osteoporosis[157]. Bisphosphonates possess high affinity for hydroxyapatite and act by inhibiting osteoclast function and promoting osteoclast cell death[158; 159]. Although this therapy assists in preventing further osteoclastic activity, bisphosphonates do not possess pro-osteoblastic properties. Notably, high dose bisphosphonate therapy has been associated with the development of osteonecrosis of the jaw (ONJ) at incidences of 1.5% to 7.7% following 4-12 and 37-48 months respectively[157; 158; 159; 160].

The efficacy of anti-RANKL and PTH therapies to treat cancer-induced bone loss is currently being evaluated in clinical trials. Denosumab, an anti-RANKL agent, has been trialled in post-menopausal women with osteoporosis, cancer patients with bone metastases and patients with rheumatoid arthritis[161; 162; 163]. In post-menopausal women, Denosumab was able to increase bone mineral density in the lumbar spine and hips after receiving 30mg every 3 months or 60mg every 6 months subcutaneously for 12 months[164]. Denosumab was also shown to delay or prevent bone osteolysis in patients with breast cancer with bone metastases and was well tolerated after 120mg subcutaneous administration was performed every 4 weeks for a period of 34 months[165]. Although ONJ was not observed in McClung's study[164], 2% of patients suffered with ONJ in breast cancer patients in Stopeck's study[165].

To date, a pre-clinical study examining the efficacy of PTH in inhibiting MM-induced osteolysis has shown promising results[166]. In this study, bone formation, indicated by an increase in bone volume and trabecular thickness, was observed in SCID-rab mice xenografted with either the BN myeloma cell line or primary myeloma cells from MM patients following the administration of 80µg/kg PTH 1-34, corresponding to the active N-terminal composition of the 84 amino acid long human parathyroid hormone, once

daily for 8-12 weeks or until control mice reached high tumour burden[166]. This study also showed that PTH 1-34 inhibited MM disease progression[166].

1.5.3. Novel anti-myeloma agents with bone promoting properties

Previous studies have shown that both PI3K and mTOR negatively regulate osteogenesis, with inhibition of these pathways strongly promoting mineralised matrix production *in vitro*[20; 22; 167]. However, while broad-spectrum PI3K inhibitors such as LY294002 and Wortmannin have provided the necessary proof-of-concept data *in vitro*, they are associated with significant cellular toxicity *in vivo* and are therefore unsuitable for clinical use. A number of candidate compounds, including the dual pan-class I PI3k and mTOR inhibitor, NVP-BEZ235 (Figure 1.8) and the PI3k inhibitor, NVP-BKM120 (Figure 1.9) (Norvartis Pharma, Basel, Switzerland), are currently undergoing Phase I/IIb clinical evaluation for the treatment of solid tumours and have shown promising preliminary results. These compounds were structurally designed as orally-bioavailable drugs with anti-tumour activity. BEZ235 functions by competitively inhibiting ATP binding to the ATP-binding pocket of the PI3k and mTOR kinase (Figure 1.10)[168], while BKM120 shows specificity for only PI3k (Figure 1.11)[169].

BEZ235 has been shown to be effective in treating a number of malignancies in pre-clinical animal models. Studies have shown that BEZ235 demonstrated anti-tumour activity in lung cancer cell lines[170; 171; 172; 173], breast cancer cell lines[174; 175], pancreatic cancer cell lines[176; 177], gastrointestinal cancer cell lines[178] and haematological malignancies such as lymphoma[179; 180; 181] and Waldenstrom macroglobulinemia[182] in xenograft animal models. The PI3k inhibitor, BKM120, has also shown promising results as a treatment for cancers. Recent studies showed that BKM120 is effective in inhibiting tumour cell proliferation in colon colorectal carcinoma cell lines[169], pancreatic cancer cell lines[178], breast cancer cell lines[183; 184; 185], glioma cell lines[186] and haematological disorders such as lymphoma[181] and B-chronic lympholytic leukaemia[187], both *in vitro* and *in vivo* xenograft models.

Recently, studies from our laboratory showed that BEZ235 induces osteogenesis *in vitro* with an increase in mineralisation observed when human MSCs were cultured with increasing doses of BEZ235 under osteogenic conditions[19]. This increase in mineralisation was associated with a significant increase in Runx2, osteocalcin and alkaline phosphatase expression[19]. Furthermore, our laboratory also showed that

Figure 1.8. BEZ235 chemical structure. BEZ235 is a pan Class I dual PI3k/mTOR inhibitor that is currently undergoing Phase I/II clinical trial. The molecular weight for BEZ235 is 469.55.

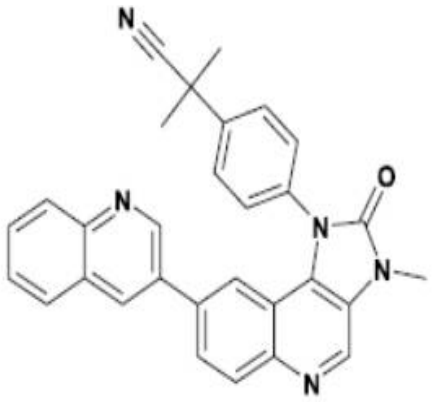
N
O
N
N
N
N

Figure 1.9. BKM120 chemical structure. BKM120 is a pan Class I PI3k inhibitor with a molecular weight of 410.9 undergoing Phase I/II clinical trials for solid tumours.

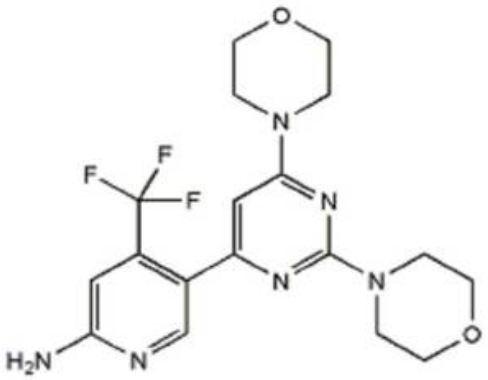
O
N
F
F
F
N
N
N
O
H_2N
N

Figure 1.10. BEZ235 inhibition of the PI3k and mTOR pathways. The downstream effector of PI3k, Akt is inhibited when BEZ235 binds to PI3k. This inhibits cell proliferation, cell growth and protein synthesis. BEZ235 also binds to mTOR raptor and rictor causing the inhibition of p70S6k, 4E-BP1, Rho GTPases, PKCα and SGK1. The inhibition of these downstream effectors causes the inhibition of protein synthesis, cell growth and cytoskeleton organisation.

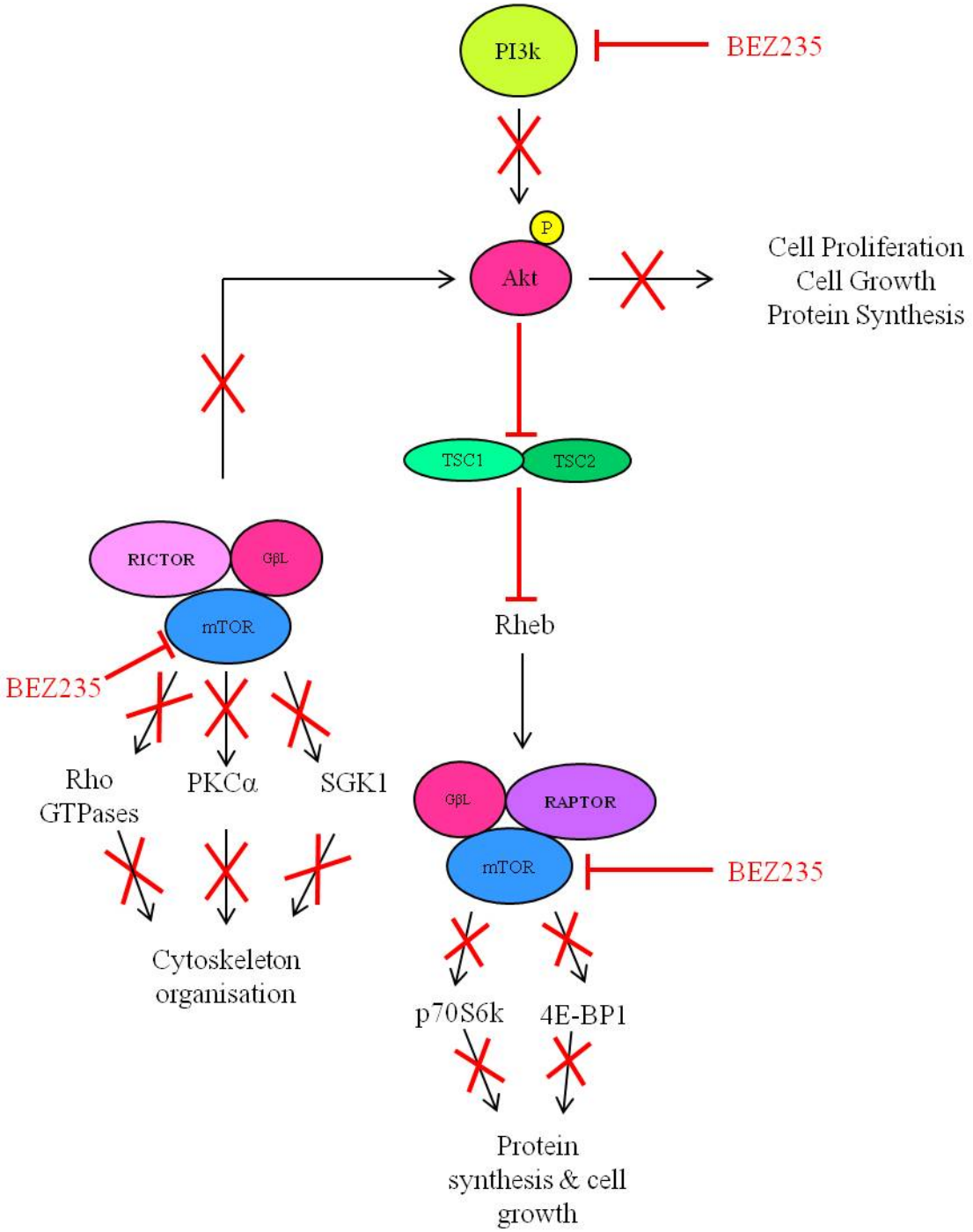
PI3k
BEZ235
P
Akt
Cell Proliferation
Cell Growth
Protein Synthesis
TSC1
TSC2
RICTOR
GβL
mTOR
BEZ235
Rho
GTPases
PKCα
SGK1
Cytoskeleton
organisation
Rheb
GβL
RAPTOR
mTOR
BEZ235
p70S6k
4E-BP1
Protein
synthesis & cell
growth

Figure 1.11. BKM120 inhibition of the PI3k pathway. BKM120 inhibit Akt by binding to PI3k. This inhibits cell proliferation, cell growth and protein synthesis.

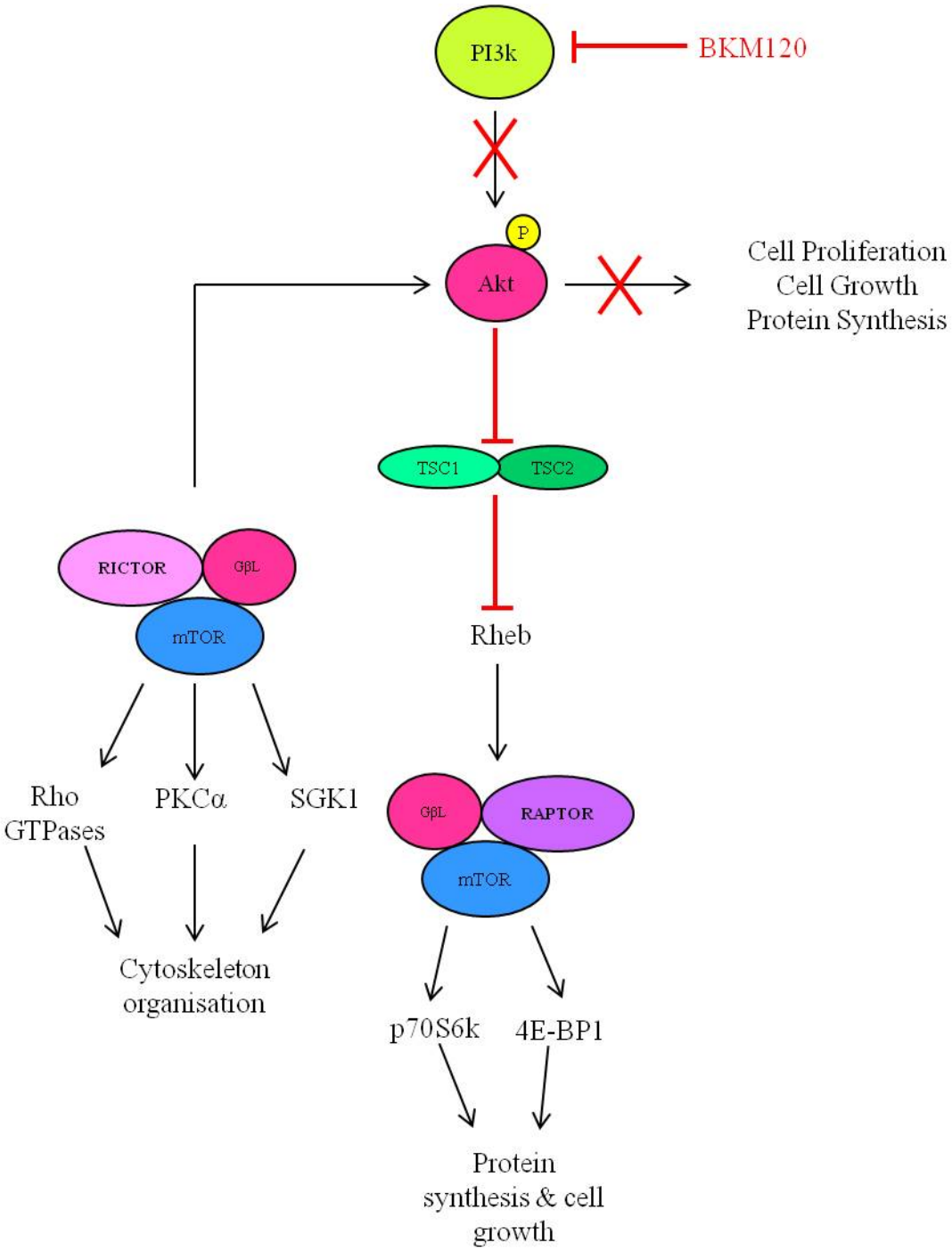
PI3k
BKM120
P
Akt
Cell Proliferation
Cell Growth
Protein Synthesis
TSC1
TSC2
RICTOR
GβL
mTOR
Rheb
Rho
GTPases
PKCα
SGK1
GβL
RAPTOR
mTOR
Cytoskeleton
organisation
p70S6k
4E-BP1
Protein
synthesis & cell
growth

BEZ235 increased bone formation *in vitro* in BEZ235-treated organotypic murine calvarial cultures.

1.6. *Summary and Project Aims*

MM is an incurable haematological malignancy caused by the uncontrolled proliferation of malignant plasma cells[1]. Growth factors such as interleukin-6 (IL-6) also contribute to MM cell survival and proliferation by phosphorylating the PI3k/Akt pathway[4; 5]. Studies have identified several genetic mutations along the PI3k and mTOR pathways

in MM cells which contribute to the uncontrolled proliferation of these cells and their resistance towards apoptosis[6; 7; 8; 9; 10; 11; 12; 13; 14; 15].

The PI3k and mTOR pathways have been implicated in controlling bone formation and resorption. Studies from our laboratory and those of others have shown that inhibiting the PI3k and mTOR pathways stimulate osteogenesis thus increasing bone formation[19; 20; 21; 22]. Furthermore, inhibition of these pathways has also been shown to inhibit osteoclast formation and function[23; 24]. In view of these findings, we hypothesise that the inhibition of the PI3k and mTOR pathways by BEZ235 and/or BKM120 will inhibit MM cell proliferation, inhibit osteoclastogenesis and induce osteogenesis.

The studies outlined in this thesis were designed to address the following aims:

1. To investigate the effects of BEZ235 and BKM120 on MM cell proliferation *in vitro*.
2. To investigate the effects of BEZ235 and BKM120 on MM tumour growth and bone remodelling *in vivo*.
3. To investigate the effects of BEZ235 and BKM120 on osteoblast and osteoclast formation and function *in vitro*.

Reference:

1. Grogan, T. M., Muller-Hermelink, H. K., Van Camp, B., Harris, N. L. & Kyle, R. A. (2001). Plasma Cell Neoplasms: Mature B-cell Neoplasms. In: Jaffe ES HN, Stein H and Vardiman JW, ed. World Health Organisation Classification of Tumours: Pathology and Genetics of Tumours of Haematopoietic and Lymphoid Tissues. *Lyon: IARC Press*, 142-156.
2. Kumar, S. K., Lee, J. H., Lahuerta, J. J., Morgan, G., Richardson, P. G., Crowley, J., Haessler, J., Feather, J., Hoering, A., Moreau, P., LeLeu, X., Hulin, C., Klein, S. K., Sonneveld, P., Siegel, D., Blade, J., Goldschmidt, H., Jagannath, S., Miguel, J. S., Orlowski, R., Palumbo, A., Sezer, O., Rajkumar, S. V. & Durie, B. G. (2012). Risk of progression and survival in multiple myeloma relapsing after therapy with IMiDs and bortezomib: a multicenter international myeloma working group study. *Leukemia : official journal of the Leukemia Society of America, Leukemia Research Fund, U.K* **26**, 149-57.
3. Morgan, G. J., Gregory, W. M., Davies, F. E., Bell, S. E., Szubert, A. J., Brown, J. M., Coy, N. N., Cook, G., Russell, N. H., Rudin, C., Roddie, H., Drayson, M. T., Owen, R. G., Ross, F. M., Jackson, G. H. & Child, J. A. (2012). The role of maintenance thalidomide therapy in multiple myeloma: MRC Myeloma IX results and meta-analysis. *Blood* **119**, 7-15.
4. Hideshima, T., Mitsiades, C., Tonon, G., Richardson, P. G. & Anderson, K. C. (2007). Understanding multiple myeloma pathogenesis in the bone marrow to identify new therapeutic targets. *Nature reviews. Cancer* **7**, 585-98.
5. Hideshima, T., Bergsagel, P. L., Kuehl, W. M. & Anderson, K. C. (2004). Advances in biology of multiple myeloma: clinical applications. *Blood* **104**, 607-18.
6. Malgeri, U., Baldini, L., Perfetti, V., Fabris, S., Vignarelli, M. C., Colombo, G., Lotti, V., Compasso, S., Bogni, S., Lombardi, L., Maiolo, A. T. & Neri, A. (2000). Detection of t(4;14)(p16.3;q32) chromosomal translocation in multiple myeloma by reverse transcription-polymerase chain reaction analysis of IGH-MMSET fusion transcripts. *Cancer research* **60**, 4058-61.
7. Chesi, M., Nardini, E., Brents, L. A., Schrock, E., Ried, T., Kuehl, W. M. & Bergsagel, P. L. (1997). Frequent translocation t(4;14)(p16.3;q32.3) in multiple myeloma is associated with increased expression and activating mutations of fibroblast growth factor receptor 3. *Nature genetics* **16**, 260-4.
8. Chesi, M., Nardini, E., Lim, R. S., Smith, K. D., Kuehl, W. M. & Bergsagel, P. L. (1998). The t(4;14) translocation in myeloma dysregulates both FGFR3 and a novel gene, MMSET, resulting in IgH/MMSET hybrid transcripts. *Blood* **92**, 3025-34.
9. Ronchetti, D., Greco, A., Compasso, S., Colombo, G., Dell'Era, P., Otsuki, T., Lombardi, L. & Neri, A. (2001). Deregulated FGFR3 mutants in multiple myeloma cell lines with t(4;14): comparative analysis of Y373C, K650E and the novel G384D mutations. *Oncogene* **20**, 3553-62.
10. Lauring, J., Abukhdeir, A. M., Konishi, H., Garay, J. P., Gustin, J. P., Wang, Q., Arceci, R. J., Matsui, W. & Park, B. H. (2008). The multiple myeloma associated MMSET gene contributes to cellular adhesion, clonogenic growth, and tumorigenicity. *Blood* **111**, 856-64.
11. Soverini, S., Cavo, M., Cellini, C., Terragna, C., Zamagni, E., Ruggeri, D., Testoni, N., Tosi, P., De Vivo, A., Amabile, M., Grafone, T., Ottaviani, E., Giannini, B., Cangini, D., Bonifazi, F., Neri, A., Fabris, S., Tura, S., Baccarani, M. & Martinelli, G. (2003). Cyclin D1 overexpression is a favorable prognostic variable for newly diagnosed multiple myeloma patients treated with high-dose chemotherapy and single or double autologous transplantation. *Blood* **102**, 1588-94.

12. Santra, M., Zhan, F., Tian, E., Barlogie, B. & Shaughnessy, J., Jr. (2003). A subset of multiple myeloma harboring the t(4;14)(p16;q32) translocation lacks FGFR3 expression but maintains an IGH/MMSET fusion transcript. *Blood* **101**, 2374-6.
13. Neri, A., Murphy, J. P., Cro, L., Ferrero, D., Tarella, C., Baldini, L. & Dalla-Favera, R. (1989). Ras oncogene mutation in multiple myeloma. *The Journal of experimental medicine* **170**, 1715-25.
14. Neri, A., Baldini, L., Trecca, D., Cro, L., Polli, E. & Maiolo, A. T. (1993). p53 gene mutations in multiple myeloma are associated with advanced forms of malignancy. *Blood* **81**, 128-35.
15. Bezieau, S., Devilder, M. C., Avet-Loiseau, H., Mellerin, M. P., Puthier, D., Pennarun, E., Rapp, M. J., Harousseau, J. L., Moisan, J. P. & Bataille, R. (2001). High incidence of N and K-Ras activating mutations in multiple myeloma and primary plasma cell leukemia at diagnosis. *Human mutation* **18**, 212-24.
16. Castellano, E. & Downward, J. (2011). RAS Interaction with PI3K: More Than Just Another Effector Pathway. *Genes & cancer* **2**, 261-74.
17. Igney, F. H. & Krammer, P. H. (2002). Death and anti-death: tumour resistance to apoptosis. *Nature reviews. Cancer* **2**, 277-88.
18. Wee, S., Jagani, Z., Xiang, K. X., Loo, A., Dorsch, M., Yao, Y. M., Sellers, W. R., Lengauer, C. & Stegmeier, F. (2009). PI3K pathway activation mediates resistance to MEK inhibitors in KRAS mutant cancers. *Cancer research* **69**, 4286-93.
19. Martin, S. K., Fitter, S., Bong, L. F., Drew, J. J., Gronthos, S., Shepherd, P. R. & Zannettino, A. C. (2010). NVP-BEZ235, a dual pan class I PI3 kinase and mTOR inhibitor, promotes osteogenic differentiation in human mesenchymal stromal cells. *Journal of bone and mineral research : the official journal of the American Society for Bone and Mineral Research* **25**, 2126-37.
20. Ogawa, T., Tokuda, M., Tomizawa, K., Matsui, H., Itano, T., Konishi, R., Nagahata, S. & Hatase, O. (1998). Osteoblastic differentiation is enhanced by rapamycin in rat osteoblast-like osteosarcoma (ROS 17/2.8) cells. *Biochemical and biophysical research communications* **249**, 226-30.
21. Lee, S. E., Woo, K. M., Kim, S. Y., Kim, H. M., Kwack, K., Lee, Z. H. & Kim, H. H. (2002). The phosphatidylinositol 3-kinase, p38, and extracellular signal-regulated kinase pathways are involved in osteoclast differentiation. *Bone* **30**, 71-7.
22. Kratchmarova, I., Blagoev, B., Haack-Sorensen, M., Kassem, M. & Mann, M. (2005). Mechanism of divergent growth factor effects in mesenchymal stem cell differentiation. *Science* **308**, 1472-7.
23. Glantschnig, H., Fisher, J. E., Wesolowski, G., Rodan, G. A. & Reszka, A. A. (2003). M-CSF, TNFalpha and RANK ligand promote osteoclast survival by signaling through mTOR/S6 kinase. *Cell death and differentiation* **10**, 1165-77.
24. Kawamura, N., Kugimiya, F., Oshima, Y., Ohba, S., Ikeda, T., Saito, T., Shinoda, Y., Kawasaki, Y., Ogata, N., Hoshi, K., Akiyama, T., Chen, W. S., Hay, N., Tobe, K., Kadowaki, T., Azuma, Y., Tanaka, S., Nakamura, K., Chung, U. I. & Kawaguchi, H. (2007). Akt1 in osteoblasts and osteoclasts controls bone remodeling. *PloS one* **2**, e1058.
25. Gingery, A., Bradley, E., Shaw, A. & Oursler, M. J. (2003). Phosphatidylinositol 3-kinase coordinately activates the MEK/ERK and AKT/NFkappaB pathways to maintain osteoclast survival. *Journal of cellular biochemistry* **89**, 165-79.
26. Pearse, R. N., Sordillo, E. M., Yaccoby, S., Wong, B. R., Liau, D. F., Colman, N., Michaeli, J., Epstein, J. & Choi, Y. (2001). Multiple myeloma disrupts the TRANCE/ osteoprotegerin cytokine axis to trigger bone destruction and promote tumor

progression. *Proceedings of the National Academy of Sciences of the United States of America* **98**, 11581-6.
27. Croucher, P. I., Shipman, C. M., Lippitt, J., Perry, M., Asosingh, K., Hijzen, A., Brabbs, A. C., van Beek, E. J., Holen, I., Skerry, T. M., Dunstan, C. R., Russell, G. R., Van Camp, B. & Vanderkerken, K. (2001). Osteoprotegerin inhibits the development of osteolytic bone disease in multiple myeloma. *Blood* **98**, 3534-40.
28. Farrugia, A. N., Atkins, G. J., To, L. B., Pan, B., Horvath, N., Kostakis, P., Findlay, D. M., Bardy, P. & Zannettino, A. C. (2003). Receptor activator of nuclear factor-kappaB ligand expression by human myeloma cells mediates osteoclast formation in vitro and correlates with bone destruction in vivo. *Cancer research* **63**, 5438-45.
29. MMRF. (2013). Multiple Myeloma: A Disease Overview (ed. Patient Handbook).
30. AIHW. (2012). Cancer in Australia: An Overview.
31. Bergsagel, P. L., Chesi, M., Nardini, E., Brents, L. A., Kirby, S. L. & Kuehl, W. M. (1996). Promiscuous translocations into immunoglobulin heavy chain switch regions in multiple myeloma. *Proceedings of the National Academy of Sciences of the United States of America* **93**, 13931-6.
32. Kuehl, W. M. & Bergsagel, P. L. (2002). Multiple myeloma: evolving genetic events and host interactions. *Nature reviews. Cancer* **2**, 175-87.
33. Cuzick, J. & De Stavola, B. (1988). Multiple myeloma--a case-control study. *British journal of cancer* **57**, 516-20.
34. Gertz, M. A. G., P. R. (2004). Multiple Myeloma and Related Plasma Cel Disorders. 53-110.
35. Howlader, N., Noone, A. M., Krapcho, M., Garshell, J., Neyman, N., Altekruse, S. F., Kosary, C. L., Yu, M., Ruhl, J., Tatalovich, Z., Cho, H., Mariotto, A., Lewis, D. R., Chen, H. S., Feuer, E. J. & Cronin, K. A. (2013). SEER Cancer Statistics Review, 1975-2010.
36. Fonseca, R., Barlogie, B., Bataille, R., Bastard, C., Bergsagel, P. L., Chesi, M., Davies, F. E., Drach, J., Greipp, P. R., Kirsch, I. R., Kuehl, W. M., Hernandez, J. M., Minvielle, S., Pilarski, L. M., Shaughnessy, J. D., Jr., Stewart, A. K. & Avet-Loiseau, H. (2004). Genetics and cytogenetics of multiple myeloma: a workshop report. *Cancer research* **64**, 1546-58.
37. Kyle, R. A., Therneau, T. M., Rajkumar, S. V., Larson, D. R., Plevak, M. F., Offord, J. R., Dispenzieri, A., Katzmann, J. A. & Melton, L. J., 3rd. (2006). Prevalence of monoclonal gammopathy of undetermined significance. *The New England journal of medicine* **354**, 1362-9.
38. Kyle, R. A., Therneau, T. M., Rajkumar, S. V., Offord, J. R., Larson, D. R., Plevak, M. F. & Melton, L. J., 3rd. (2002). A long-term study of prognosis in monoclonal gammopathy of undetermined significance. *The New England journal of medicine* **346**, 564-9.
39. Callander, N. S. & Roodman, G. D. (2001). Myeloma bone disease. *Seminars in hematology* **38**, 276-85.
40. Roodman, G. D. (2003). Mechanisms of bone resorption in myeloma. *Journal of musculoskeletal & neuronal interactions* **3**, 271-2; discussion 292-4.
41. Munshi, N. C. & Wilson, C. (2001). Increased bone marrow microvessel density in newly diagnosed multiple myeloma carries a poor prognosis. *Seminars in oncology* **28**, 565-9.
42. Pruneri, G., Ponzoni, M., Ferreri, A. J., Decarli, N., Tresoldi, M., Raggi, F., Baldessari, C., Freschi, M., Baldini, L., Goldaniga, M., Neri, A., Carboni, N., Bertolini, F. & Viale, G. (2002). Microvessel density, a surrogate marker of

angiogenesis, is significantly related to survival in multiple myeloma patients. *British journal of haematology* **118**, 817-20.
43. Moehler, T. M., Hawighorst, H., Neben, K., Egerer, G., Hillengass, J., Max, R., Benner, A., Ho, A. D., van Kaick, G. & Goldschmidt, H. (2001). Bone marrow microcirculation analysis in multiple myeloma by contrast-enhanced dynamic magnetic resonance imaging. *International journal of cancer. Journal international du cancer* **93**, 862-8.
44. Durie, B. G. & Salmon, S. E. (1975). A clinical staging system for multiple myeloma. Correlation of measured myeloma cell mass with presenting clinical features, response to treatment, and survival. *Cancer* **36**, 842-54.
45. Greipp, P. R., San Miguel, J., Durie, B. G., Crowley, J. J., Barlogie, B., Blade, J., Boccadoro, M., Child, J. A., Avet-Loiseau, H., Kyle, R. A., Lahuerta, J. J., Ludwig, H., Morgan, G., Powles, R., Shimizu, K., Shustik, C., Sonneveld, P., Tosi, P., Turesson, I. & Westin, J. (2005). International staging system for multiple myeloma. *Journal of clinical oncology : official journal of the American Society of Clinical Oncology* **23**, 3412-20.
46. Hallek, M., Bergsagel, P. L. & Anderson, K. C. (1998). Multiple myeloma: increasing evidence for a multistep transformation process. *Blood* **91**, 3-21.
47. West, K. A., Castillo, S. S. & Dennis, P. A. (2002). Activation of the PI3K/Akt pathway and chemotherapeutic resistance. *Drug resistance updates : reviews and commentaries in antimicrobial and anticancer chemotherapy* **5**, 234-48.
48. Manning, B. D. & Cantley, L. C. (2007). AKT/PKB signaling: navigating downstream. *Cell* **129**, 1261-74.
49. Paez, J. & Sellers, W. R. (2003). PI3K/PTEN/AKT pathway. A critical mediator of oncogenic signaling. *Cancer treatment and research* **115**, 145-67.
50. Hennessy, B. T., Smith, D. L., Ram, P. T., Lu, Y. & Mills, G. B. (2005). Exploiting the PI3K/AKT pathway for cancer drug discovery. *Nature reviews. Drug discovery* **4**, 988-1004.
51. Utermark, T., Rao, T., Cheng, H., Wang, Q., Lee, S. H., Wang, Z. C., Iglehart, J. D., Roberts, T. M., Muller, W. J. & Zhao, J. J. (2012). The p110alpha and p110beta isoforms of PI3K play divergent roles in mammary gland development and tumorigenesis. *Genes & development* **26**, 1573-86.
52. Parsons, R. (2004). Human cancer, PTEN and the PI-3 kinase pathway. *Seminars in cell & developmental biology* **15**, 171-6.
53. Nakatani, K., Thompson, D. A., Barthel, A., Sakaue, H., Liu, W., Weigel, R. J. & Roth, R. A. (1999). Up-regulation of Akt3 in estrogen receptor-deficient breast cancers and androgen-independent prostate cancer lines. *The Journal of biological chemistry* **274**, 21528-32.
54. Dummler, B., Tschopp, O., Hynx, D., Yang, Z. Z., Dirnhofer, S. & Hemmings, B. A. (2006). Life with a single isoform of Akt: mice lacking Akt2 and Akt3 are viable but display impaired glucose homeostasis and growth deficiencies. *Molecular and cellular biology* **26**, 8042-51.
55. Dancey, J. E. (2004). Molecular targeting: PI3 kinase pathway. *Annals of oncology : official journal of the European Society for Medical Oncology / ESMO* **15 Suppl 4**, iv233-9.
56. LoPiccolo, J., Granville, C. A., Gills, J. J. & Dennis, P. A. (2007). Targeting Akt in cancer therapy. *Anti-cancer drugs* **18**, 861-74.
57. Alessi, D. R., Andjelkovic, M., Caudwell, B., Cron, P., Morrice, N., Cohen, P. & Hemmings, B. A. (1996). Mechanism of activation of protein kinase B by insulin and IGF-1. *The EMBO journal* **15**, 6541-51.

58. Kawakami, Y., Nishimoto, H., Kitaura, J., Maeda-Yamamoto, M., Kato, R. M., Littman, D. R., Leitges, M., Rawlings, D. J. & Kawakami, T. (2004). Protein kinase C betaII regulates Akt phosphorylation on Ser-473 in a cell type- and stimulus-specific fashion. *The Journal of biological chemistry* **279**, 47720-5.
59. Burgering, B. M. & Medema, R. H. (2003). Decisions on life and death: FOXO Forkhead transcription factors are in command when PKB/Akt is off duty. *Journal of leukocyte biology* **73**, 689-701.
60. Diehl, J. A., Cheng, M., Roussel, M. F. & Sherr, C. J. (1998). Glycogen synthase kinase-3beta regulates cyclin D1 proteolysis and subcellular localization. *Genes & development* **12**, 3499-511.
61. Zhou, B. P., Liao, Y., Xia, W., Spohn, B., Lee, M. H. & Hung, M. C. (2001). Cytoplasmic localization of p21Cip1/WAF1 by Akt-induced phosphorylation in HER-2/neu-overexpressing cells. *Nature cell biology* **3**, 245-52.
62. Medema, R. H., Kops, G. J., Bos, J. L. & Burgering, B. M. (2000). AFX-like Forkhead transcription factors mediate cell-cycle regulation by Ras and PKB through p27kip1. *Nature* **404**, 782-7.
63. Sarbassov, D. D., Guertin, D. A., Ali, S. M. & Sabatini, D. M. (2005). Phosphorylation and regulation of Akt/PKB by the rictor-mTOR complex. *Science* **307**, 1098-101.
64. Denlinger, C. E., Rundall, B. K. & Jones, D. R. (2005). Inhibition of phosphatidylinositol 3-kinase/Akt and histone deacetylase activity induces apoptosis in non-small cell lung cancer in vitro and in vivo. *The Journal of thoracic and cardiovascular surgery* **130**, 1422-9.
65. Hu, L., Zaloudek, C., Mills, G. B., Gray, J. & Jaffe, R. B. (2000). In vivo and in vitro ovarian carcinoma growth inhibition by a phosphatidylinositol 3-kinase inhibitor (LY294002). *Clinical cancer research : an official journal of the American Association for Cancer Research* **6**, 880-6.
66. Ng, S. S., Tsao, M. S., Nicklee, T. & Hedley, D. W. (2001). Wortmannin inhibits pkb/akt phosphorylation and promotes gemcitabine antitumor activity in orthotopic human pancreatic cancer xenografts in immunodeficient mice. *Clinical cancer research : an official journal of the American Association for Cancer Research* **7**, 3269-75.
67. Inoki, K., Ouyang, H., Li, Y. & Guan, K. L. (2005). Signaling by target of rapamycin proteins in cell growth control. *Microbiology and molecular biology reviews : MMBR* **69**, 79-100.
68. Raught, B., Gingras, A. C. & Sonenberg, N. (2001). The target of rapamycin (TOR) proteins. *Proceedings of the National Academy of Sciences of the United States of America* **98**, 7037-44.
69. Bjornsti, M. A. & Houghton, P. J. (2004). The TOR pathway: a target for cancer therapy. *Nature reviews. Cancer* **4**, 335-48.
70. Sarbassov, D. D., Ali, S. M., Kim, D. H., Guertin, D. A., Latek, R. R., Erdjument-Bromage, H., Tempst, P. & Sabatini, D. M. (2004). Rictor, a novel binding partner of mTOR, defines a rapamycin-insensitive and raptor-independent pathway that regulates the cytoskeleton. *Current biology : CB* **14**, 1296-302.
71. Hara, K., Yonezawa, K., Weng, Q. P., Kozlowski, M. T., Belham, C. & Avruch, J. (1998). Amino acid sufficiency and mTOR regulate p70 S6 kinase and eIF-4E BP1 through a common effector mechanism. *The Journal of biological chemistry* **273**, 14484-94.
72. Kim, D. H., Sarbassov, D. D., Ali, S. M., King, J. E., Latek, R. R., Erdjument-Bromage, H., Tempst, P. & Sabatini, D. M. (2002). mTOR interacts with raptor to

form a nutrient-sensitive complex that signals to the cell growth machinery. *Cell* **110**, 163-75.
73. Hara, K., Maruki, Y., Long, X., Yoshino, K., Oshiro, N., Hidayat, S., Tokunaga, C., Avruch, J. & Yonezawa, K. (2002). Raptor, a binding partner of target of rapamycin (TOR), mediates TOR action. *Cell* **110**, 177-89.
74. Kim, D. H., Sarbassov, D. D., Ali, S. M., Latek, R. R., Guntur, K. V., Erdjument-Bromage, H., Tempst, P. & Sabatini, D. M. (2003). GbetaL, a positive regulator of the rapamycin-sensitive pathway required for the nutrient-sensitive interaction between raptor and mTOR. *Molecular cell* **11**, 895-904.
75. Sarbassov, D. D., Ali, S. M., Sengupta, S., Sheen, J. H., Hsu, P. P., Bagley, A. F., Markhard, A. L. & Sabatini, D. M. (2006). Prolonged rapamycin treatment inhibits mTORC2 assembly and Akt/PKB. *Molecular cell* **22**, 159-68.
76. Peterson, T. R., Laplante, M., Thoreen, C. C., Sancak, Y., Kang, S. A., Kuehl, W. M., Gray, N. S. & Sabatini, D. M. (2009). DEPTOR is an mTOR inhibitor frequently overexpressed in multiple myeloma cells and required for their survival. *Cell* **137**, 873-86.
77. Chang, H., Qi, X. Y., Claudio, J., Zhuang, L., Patterson, B. & Stewart, A. K. (2006). Analysis of PTEN deletions and mutations in multiple myeloma. *Leukemia research* **30**, 262-5.
78. Shi, Y., Gera, J., Hu, L., Hsu, J. H., Bookstein, R., Li, W. & Lichtenstein, A. (2002). Enhanced sensitivity of multiple myeloma cells containing PTEN mutations to CCI-779. *Cancer research* **62**, 5027-34.
79. Hyun, T., Yam, A., Pece, S., Xie, X., Zhang, J., Miki, T., Gutkind, J. S. & Li, W. (2000). Loss of PTEN expression leading to high Akt activation in human multiple myelomas. *Blood* **96**, 3560-8.
80. Zhang, J., Choi, Y., Mavromatis, B., Lichtenstein, A. & Li, W. (2003). Preferential killing of PTEN-null myelomas by PI3K inhibitors through Akt pathway. *Oncogene* **22**, 6289-95.
81. Wang, Z., Zhong, J., Inuzuka, H., Gao, D., Shaik, S., Sarkar, F. H. & Wei, W. (2012). An evolving role for DEPTOR in tumor development and progression. *Neoplasia* **14**, 368-75.
82. Pene, F., Claessens, Y. E., Muller, O., Viguie, F., Mayeux, P., Dreyfus, F., Lacombe, C. & Bouscary, D. (2002). Role of the phosphatidylinositol 3-kinase/Akt and mTOR/P70S6-kinase pathways in the proliferation and apoptosis in multiple myeloma. *Oncogene* **21**, 6587-97.
83. Mitsiades, C. S., Mitsiades, N., Poulaki, V., Schlossman, R., Akiyama, M., Chauhan, D., Hideshima, T., Treon, S. P., Munshi, N. C., Richardson, P. G. & Anderson, K. C. (2002). Activation of NF-kappaB and upregulation of intracellular anti-apoptotic proteins via the IGF-1/Akt signaling in human multiple myeloma cells: therapeutic implications. *Oncogene* **21**, 5673-83.
84. Stromberg, T., Dimberg, A., Hammarberg, A., Carlson, K., Osterborg, A., Nilsson, K. & Jernberg-Wiklund, H. (2004). Rapamycin sensitizes multiple myeloma cells to apoptosis induced by dexamethasone. *Blood* **103**, 3138-47.
85. Raje, N., Kumar, S., Hideshima, T., Ishitsuka, K., Chauhan, D., Mitsiades, C., Podar, K., Le Gouill, S., Richardson, P., Munshi, N. C., Stirling, D. I., Antin, J. H. & Anderson, K. C. (2004). Combination of the mTOR inhibitor rapamycin and CC-5013 has synergistic activity in multiple myeloma. *Blood* **104**, 4188-93.
86. Michaud, L. B. & Goodin, S. (2006). Cancer-treatment-induced bone loss, part 1. *American journal of health-system pharmacy : AJHP : official journal of the American Society of Health-System Pharmacists* **63**, 419-30.

87. Anderson, H. C. (2003). Matrix vesicles and calcification. *Current rheumatology reports* **5**, 222-6.
88. Lacey, D. L., Timms, E., Tan, H. L., Kelley, M. J., Dunstan, C. R., Burgess, T., Elliott, R., Colombero, A., Elliott, G., Scully, S., Hsu, H., Sullivan, J., Hawkins, N., Davy, E., Capparelli, C., Eli, A., Qian, Y. X., Kaufman, S., Sarosi, I., Shalhoub, V., Senaldi, G., Guo, J., Delaney, J. & Boyle, W. J. (1998). Osteoprotegerin ligand is a cytokine that regulates osteoclast differentiation and activation. *Cell* **93**, 165-76.
89. Yasuda, H., Shima, N., Nakagawa, N., Yamaguchi, K., Kinosaki, M., Mochizuki, S., Tomoyasu, A., Yano, K., Goto, M., Murakami, A., Tsuda, E., Morinaga, T., Higashio, K., Udagawa, N., Takahashi, N. & Suda, T. (1998). Osteoclast differentiation factor is a ligand for osteoprotegerin/osteoclastogenesis-inhibitory factor and is identical to TRANCE/RANKL. *Proceedings of the National Academy of Sciences of the United States of America* **95**, 3597-602.
90. Zaidi, M. (2007). Skeletal remodeling in health and disease. *Nature medicine* **13**, 791-801.
91. Pittenger, M. F., Mackay, A. M., Beck, S. C., Jaiswal, R. K., Douglas, R., Mosca, J. D., Moorman, M. A., Simonetti, D. W., Craig, S. & Marshak, D. R. (1999). Multilineage potential of adult human mesenchymal stem cells. *Science* **284**, 143-7.
92. Nakashima, K. & de Crombrugghe, B. (2003). Transcriptional mechanisms in osteoblast differentiation and bone formation. *Trends in genetics : TIG* **19**, 458-66.
93. Otto, F., Thornell, A. P., Crompton, T., Denzel, A., Gilmour, K. C., Rosewell, I. R., Stamp, G. W., Beddington, R. S., Mundlos, S., Olsen, B. R., Selby, P. B. & Owen, M. J. (1997). Cbfa1, a candidate gene for cleidocranial dysplasia syndrome, is essential for osteoblast differentiation and bone development. *Cell* **89**, 765-71.
94. Komori, T., Yagi, H., Nomura, S., Yamaguchi, A., Sasaki, K., Deguchi, K., Shimizu, Y., Bronson, R. T., Gao, Y. H., Inada, M., Sato, M., Okamoto, R., Kitamura, Y., Yoshiki, S. & Kishimoto, T. (1997). Targeted disruption of Cbfa1 results in a complete lack of bone formation owing to maturational arrest of osteoblasts. *Cell* **89**, 755-64.
95. Ducy, P., Zhang, R., Geoffroy, V., Ridall, A. L. & Karsenty, G. (1997). Osf2/Cbfa1: a transcriptional activator of osteoblast differentiation. *Cell* **89**, 747-54.
96. Nakashima, K., Zhou, X., Kunkel, G., Zhang, Z., Deng, J. M., Behringer, R. R. & de Crombrugghe, B. (2002). The novel zinc finger-containing transcription factor osterix is required for osteoblast differentiation and bone formation. *Cell* **108**, 17-29.
97. Yamaguchi, A., Ishizuya, T., Kintou, N., Wada, Y., Katagiri, T., Wozney, J. M., Rosen, V. & Yoshiki, S. (1996). Effects of BMP-2, BMP-4, and BMP-6 on osteoblastic differentiation of bone marrow-derived stromal cell lines, ST2 and MC3T3-G2/PA6. *Biochemical and biophysical research communications* **220**, 366-71.
98. Lee, K. S., Kim, H. J., Li, Q. L., Chi, X. Z., Ueta, C., Komori, T., Wozney, J. M., Kim, E. G., Choi, J. Y., Ryoo, H. M. & Bae, S. C. (2000). Runx2 is a common target of transforming growth factor beta1 and bone morphogenetic protein 2, and cooperation between Runx2 and Smad5 induces osteoblast-specific gene expression in the pluripotent mesenchymal precursor cell line C2C12. *Molecular and cellular biology* **20**, 8783-92.
99. Lee, M. H., Kim, Y. J., Kim, H. J., Park, H. D., Kang, A. R., Kyung, H. M., Sung, J. H., Wozney, J. M. & Ryoo, H. M. (2003). BMP-2-induced Runx2 expression is mediated by Dlx5, and TGF-beta 1 opposes the BMP-2-induced osteoblast differentiation by suppression of Dlx5 expression. *The Journal of biological chemistry* **278**, 34387-94.

100. Lee, M. H., Kwon, T. G., Park, H. S., Wozney, J. M. & Ryoo, H. M. (2003). BMP-2-induced Osterix expression is mediated by Dlx5 but is independent of Runx2. *Biochemical and biophysical research communications* **309**, 689-94.
101. Day, T. F., Guo, X., Garrett-Beal, L. & Yang, Y. (2005). Wnt/beta-catenin signaling in mesenchymal progenitors controls osteoblast and chondrocyte differentiation during vertebrate skeletogenesis. *Developmental cell* **8**, 739-50.
102. Brault, V., Moore, R., Kutsch, S., Ishibashi, M., Rowitch, D. H., McMahon, A. P., Sommer, L., Boussadia, O. & Kemler, R. (2001). Inactivation of the beta-catenin gene by Wnt1-Cre-mediated deletion results in dramatic brain malformation and failure of craniofacial development. *Development* **128**, 1253-64.
103. Hu, H., Hilton, M. J., Tu, X., Yu, K., Ornitz, D. M. & Long, F. (2005). Sequential roles of Hedgehog and Wnt signaling in osteoblast development. *Development* **132**, 49-60.
104. Hill, T. P., Spater, D., Taketo, M. M., Birchmeier, W. & Hartmann, C. (2005). Canonical Wnt/beta-catenin signaling prevents osteoblasts from differentiating into chondrocytes. *Developmental cell* **8**, 727-38.
105. Gong, Y., Slee, R. B., Fukai, N., Rawadi, G., Roman-Roman, S., Reginato, A. M., Wang, H., Cundy, T., Glorieux, F. H., Lev, D., Zacharin, M., Oexle, K., Marcelino, J., Suwairi, W., Heeger, S., Sabatakos, G., Apte, S., Adkins, W. N., Allgrove, J., Arslan-Kirchner, M., Batch, J. A., Beighton, P., Black, G. C., Boles, R. G., Boon, L. M., Borrone, C., Brunner, H. G., Carle, G. F., Dallapiccola, B., De Paepe, A., Floege, B., Halfhide, M. L., Hall, B., Hennekam, R. C., Hirose, T., Jans, A., Juppner, H., Kim, C. A., Keppler-Noreuil, K., Kohlschuetter, A., LaCombe, D., Lambert, M., Lemyre, E., Letteboer, T., Peltonen, L., Ramesar, R. S., Romanengo, M., Somer, H., Steichen-Gersdorf, E., Steinmann, B., Sullivan, B., Superti-Furga, A., Swoboda, W., van den Boogaard, M. J., Van Hul, W., Vikkula, M., Votruba, M., Zabel, B., Garcia, T., Baron, R., Olsen, B. R. & Warman, M. L. (2001). LDL receptor-related protein 5 (LRP5) affects bone accrual and eye development. *Cell* **107**, 513-23.
106. Boyden, L. M., Mao, J., Belsky, J., Mitzner, L., Farhi, A., Mitnick, M. A., Wu, D., Insogna, K. & Lifton, R. P. (2002). High bone density due to a mutation in LDL-receptor-related protein 5. *The New England journal of medicine* **346**, 1513-21.
107. Little, R. D., Carulli, J. P., Del Mastro, R. G., Dupuis, J., Osborne, M., Folz, C., Manning, S. P., Swain, P. M., Zhao, S. C., Eustace, B., Lappe, M. M., Spitzer, L., Zweier, S., Braunschweiger, K., Benchekroun, Y., Hu, X., Adair, R., Chee, L., FitzGerald, M. G., Tulig, C., Caruso, A., Tzellas, N., Bawa, A., Franklin, B., McGuire, S., Nogues, X., Gong, G., Allen, K. M., Anisowicz, A., Morales, A. J., Lomedico, P. T., Recker, S. M., Van Eerdewegh, P., Recker, R. R. & Johnson, M. L. (2002). A mutation in the LDL receptor-related protein 5 gene results in the autosomal dominant high-bone-mass trait. *American journal of human genetics* **70**, 11-9.
108. Balemans, W., Ebeling, M., Patel, N., Van Hul, E., Olson, P., Dioszegi, M., Lacza, C., Wuyts, W., Van Den Ende, J., Willems, P., Paes-Alves, A. F., Hill, S., Bueno, M., Ramos, F. J., Tacconi, P., Dikkers, F. G., Stratakis, C., Lindpaintner, K., Vickery, B., Foernzler, D. & Van Hul, W. (2001). Increased bone density in sclerosteosis is due to the deficiency of a novel secreted protein (SOST). *Human molecular genetics* **10**, 537-43.
109. Staehling-Hampton, K., Proll, S., Paeper, B. W., Zhao, L., Charmley, P., Brown, A., Gardner, J. C., Galas, D., Schatzman, R. C., Beighton, P., Papapoulos, S., Hamersma, H. & Brunkow, M. E. (2002). A 52-kb deletion in the SOST-MEOX1 intergenic

region on 17q12-q21 is associated with van Buchem disease in the Dutch population. *American journal of medical genetics* **110**, 144-52.
110. Balemans, W., Patel, N., Ebeling, M., Van Hul, E., Wuyts, W., Lacza, C., Dioszegi, M., Dikkers, F. G., Hildering, P., Willems, P. J., Verheij, J. B., Lindpaintner, K., Vickery, B., Foernzler, D. & Van Hul, W. (2002). Identification of a 52 kb deletion downstream of the SOST gene in patients with van Buchem disease. *Journal of medical genetics* **39**, 91-7.
111. Fischman, D. A. & Hay, E. D. (1962). Origin of osteoclasts from mononuclear leucocytes in regenerating newt limbs. *The Anatomical record* **143**, 329-37.
112. Tinkler, S. M., Linder, J. E., Williams, D. M. & Johnson, N. W. (1981). Formation of osteoclasts from blood monocytes during 1 alpha-OH Vit D-stimulated bone resorption in mice. *Journal of anatomy* **133**, 389-96.
113. Scheven, B. A., Visser, J. W. & Nijweide, P. J. (1986). In vitro osteoclast generation from different bone marrow fractions, including a highly enriched haematopoietic stem cell population. *Nature* **321**, 79-81.
114. Nordahl, J., Andersson, G. & Reinholt, F. P. (1998). Chondroclasts and osteoclasts in bones of young rats: comparison of ultrastructural and functional features. *Calcified tissue international* **63**, 401-8.
115. Dai, X. M., Ryan, G. R., Hapel, A. J., Dominguez, M. G., Russell, R. G., Kapp, S., Sylvestre, V. & Stanley, E. R. (2002). Targeted disruption of the mouse colony-stimulating factor 1 receptor gene results in osteopetrosis, mononuclear phagocyte deficiency, increased primitive progenitor cell frequencies, and reproductive defects. *Blood* **99**, 111-20.
116. Suda, T., Takahashi, N., Udagawa, N., Jimi, E., Gillespie, M. T. & Martin, T. J. (1999). Modulation of osteoclast differentiation and function by the new members of the tumor necrosis factor receptor and ligand families. *Endocrine reviews* **20**, 345-57.
117. Dougall, W. C., Glaccum, M., Charrier, K., Rohrbach, K., Brasel, K., De Smedt, T., Daro, E., Smith, J., Tometsko, M. E., Maliszewski, C. R., Armstrong, A., Shen, V., Bain, S., Cosman, D., Anderson, D., Morrissey, P. J., Peschon, J. J. & Schuh, J. (1999). RANK is essential for osteoclast and lymph node development. *Genes & development* **13**, 2412-24.
118. Kong, Y. Y., Boyle, W. J. & Penninger, J. M. (1999). Osteoprotegerin ligand: a common link between osteoclastogenesis, lymph node formation and lymphocyte development. *Immunology and cell biology* **77**, 188-93.
119. Matsuo, K. & Irie, N. (2008). Osteoclast-osteoblast communication. *Archives of biochemistry and biophysics* **473**, 201-9.
120. Roux, S. & Orcel, P. (2000). Bone loss. Factors that regulate osteoclast differentiation: an update. *Arthritis research* **2**, 451-456.
121. Blair, H. C., Robinson, L. J. & Zaidi, M. (2005). Osteoclast signalling pathways. *Biochemical and biophysical research communications* **328**, 728-38.
122. Feng, X. (2005). Regulatory roles and molecular signaling of TNF family members in osteoclasts. *Gene* **350**, 1-13.
123. Fuller, K., Lean, J. M., Bayley, K. E., Wani, M. R. & Chambers, T. J. (2000). A role for TGFbeta(1) in osteoclast differentiation and survival. *Journal of cell science* **113 (Pt 13)**, 2445-53.
124. Mackie, E. J. & Trechsel, U. (1990). Stimulation of bone formation in vivo by transforming growth factor-beta: remodeling of woven bone and lack of inhibition by indomethacin. *Bone* **11**, 295-300.
125. Bonewald, L. F. & Dallas, S. L. (1994). Role of active and latent transforming growth factor beta in bone formation. *Journal of cellular biochemistry* **55**, 350-7.

126. Quinn, J. M., Itoh, K., Udagawa, N., Hausler, K., Yasuda, H., Shima, N., Mizuno, A., Higashio, K., Takahashi, N., Suda, T., Martin, T. J. & Gillespie, M. T. (2001). Transforming growth factor beta affects osteoclast differentiation via direct and indirect actions. *Journal of bone and mineral research : the official journal of the American Society for Bone and Mineral Research* **16**, 1787-94.
127. Takai, H., Kanematsu, M., Yano, K., Tsuda, E., Higashio, K., Ikeda, K., Watanabe, K. & Yamada, Y. (1998). Transforming growth factor-beta stimulates the production of osteoprotegerin/osteoclastogenesis inhibitory factor by bone marrow stromal cells. *The Journal of biological chemistry* **273**, 27091-6.
128. Bucay, N., Sarosi, I., Dunstan, C. R., Morony, S., Tarpley, J., Capparelli, C., Scully, S., Tan, H. L., Xu, W., Lacey, D. L., Boyle, W. J. & Simonet, W. S. (1998). osteoprotegerin-deficient mice develop early onset osteoporosis and arterial calcification. *Genes & development* **12**, 1260-8.
129. Choi, S. J., Cruz, J. C., Craig, F., Chung, H., Devlin, R. D., Roodman, G. D. & Alsina, M. (2000). Macrophage inflammatory protein 1-alpha is a potential osteoclast stimulatory factor in multiple myeloma. *Blood* **96**, 671-5.
130. Han, J. H., Choi, S. J., Kurihara, N., Koide, M., Oba, Y. & Roodman, G. D. (2001). Macrophage inflammatory protein-1alpha is an osteoclastogenic factor in myeloma that is independent of receptor activator of nuclear factor kappaB ligand. *Blood* **97**, 3349-53.
131. Abe, M., Hiura, K., Wilde, J., Shioyasono, A., Moriyama, K., Hashimoto, T., Kido, S., Oshima, T., Shibata, H., Ozaki, S., Inoue, D. & Matsumoto, T. (2004). Osteoclasts enhance myeloma cell growth and survival via cell-cell contact: a vicious cycle between bone destruction and myeloma expansion. *Blood* **104**, 2484-91.
132. Zannettino, A. C., Farrugia, A. N., Kortesidis, A., Manavis, J., To, L. B., Martin, S. K., Diamond, P., Tamamura, H., Lapidot, T., Fujii, N. & Gronthos, S. (2005). Elevated serum levels of stromal-derived factor-1alpha are associated with increased osteoclast activity and osteolytic bone disease in multiple myeloma patients. *Cancer research* **65**, 1700-9.
133. Giuliani, N., Colla, S., Morandi, F., Lazzaretti, M., Sala, R., Bonomini, S., Grano, M., Colucci, S., Svaldi, M. & Rizzoli, V. (2005). Myeloma cells block RUNX2/CBFA1 activity in human bone marrow osteoblast progenitors and inhibit osteoblast formation and differentiation. *Blood* **106**, 2472-83.
134. Giuliani, N., Rizzoli, V. & Roodman, G. D. (2006). Multiple myeloma bone disease: Pathophysiology of osteoblast inhibition. *Blood* **108**, 3992-6.
135. Hjorth-Hansen, H., Seifert, M. F., Borset, M., Aarset, H., Ostlie, A., Sundan, A. & Waage, A. (1999). Marked osteoblastopenia and reduced bone formation in a model of multiple myeloma bone disease in severe combined immunodeficiency mice. *Journal of bone and mineral research : the official journal of the American Society for Bone and Mineral Research* **14**, 256-63.
136. Westendorf, J. J., Kahler, R. A. & Schroeder, T. M. (2004). Wnt signaling in osteoblasts and bone diseases. *Gene* **341**, 19-39.
137. Tian, E., Zhan, F., Walker, R., Rasmussen, E., Ma, Y., Barlogie, B. & Shaughnessy, J. D., Jr. (2003). The role of the Wnt-signaling antagonist DKK1 in the development of osteolytic lesions in multiple myeloma. *The New England journal of medicine* **349**, 2483-94.
138. Giuliani, N., Morandi, F., Tagliaferri, S., Colla, S., Bonomini, S., Sammarelli, G. & Rizzoli, V. (2006). Interleukin-3 (IL-3) is overexpressed by T lymphocytes in multiple myeloma patients. *Blood* **107**, 841-2.

139. Ehrlich, L. A., Chung, H. Y., Ghobrial, I., Choi, S. J., Morandi, F., Colla, S., Rizzoli, V., Roodman, G. D. & Giuliani, N. (2005). IL-3 is a potential inhibitor of osteoblast differentiation in multiple myeloma. *Blood* **106**, 1407-14.
140. Lee, J. W., Chung, H. Y., Ehrlich, L. A., Jelinek, D. F., Callander, N. S., Roodman, G. D. & Choi, S. J. (2004). IL-3 expression by myeloma cells increases both osteoclast formation and growth of myeloma cells. *Blood* **103**, 2308-15.
141. Siegfried, E., Chou, T. B. & Perrimon, N. (1992). wingless signaling acts through zeste-white 3, the Drosophila homolog of glycogen synthase kinase-3, to regulate engrailed and establish cell fate. *Cell* **71**, 1167-79.
142. Smith, G. C., Ong, W. K., Costa, J. L., Watson, M., Cornish, J., Grey, A., Gamble, G. D., Dickinson, M., Leung, S., Rewcastle, G. W., Han, W. & Shepherd, P. R. (2013). Extended treatment with selective PI 3-kinase and mTOR inhibitors has effects on metabolism, growth, behaviour and bone strength. *The FEBS journal*.
143. Vinals, F., Lopez-Rovira, T., Rosa, J. L. & Ventura, F. (2002). Inhibition of PI3K/p70 S6K and p38 MAPK cascades increases osteoblastic differentiation induced by BMP-2. *FEBS letters* **510**, 99-104.
144. Isomoto, S., Hattori, K., Ohgushi, H., Nakajima, H., Tanaka, Y. & Takakura, Y. (2007). Rapamycin as an inhibitor of osteogenic differentiation in bone marrow-derived mesenchymal stem cells. *Journal of orthopaedic science : official journal of the Japanese Orthopaedic Association* **12**, 83-8.
145. Singha, U. K., Jiang, Y., Yu, S., Luo, M., Lu, Y., Zhang, J. & Xiao, G. (2008). Rapamycin inhibits osteoblast proliferation and differentiation in MC3T3-E1 cells and primary mouse bone marrow stromal cells. *Journal of cellular biochemistry* **103**, 434-46.
146. Carracedo, A., Ma, L., Teruya-Feldstein, J., Rojo, F., Salmena, L., Alimonti, A., Egia, A., Sasaki, A. T., Thomas, G., Kozma, S. C., Papa, A., Nardella, C., Cantley, L. C., Baselga, J. & Pandolfi, P. P. (2008). Inhibition of mTORC1 leads to MAPK pathway activation through a PI3K-dependent feedback loop in human cancer. *The Journal of clinical investigation* **118**, 3065-74.
147. Tamburini, J., Chapuis, N., Bardet, V., Park, S., Sujobert, P., Willems, L., Ifrah, N., Dreyfus, F., Mayeux, P., Lacombe, C. & Bouscary, D. (2008). Mammalian target of rapamycin (mTOR) inhibition activates phosphatidylinositol 3-kinase/Akt by up-regulating insulin-like growth factor-1 receptor signaling in acute myeloid leukemia: rationale for therapeutic inhibition of both pathways. *Blood* **111**, 379-82.
148. Bradley, E. W., Ruan, M. M., Vrable, A. & Oursler, M. J. (2008). Pathway crosstalk between Ras/Raf and PI3K in promotion of M-CSF-induced MEK/ERK-mediated osteoclast survival. *Journal of cellular biochemistry* **104**, 1439-51.
149. Sugatani, T., Alvarez, U. & Hruska, K. A. (2003). PTEN regulates RANKL- and osteopontin-stimulated signal transduction during osteoclast differentiation and cell motility. *The Journal of biological chemistry* **278**, 5001-8.
150. Sugatani, T. & Hruska, K. A. (2005). Akt1/Akt2 and mammalian target of rapamycin/Bim play critical roles in osteoclast differentiation and survival, respectively, whereas Akt is dispensable for cell survival in isolated osteoclast precursors. *The Journal of biological chemistry* **280**, 3583-9.
151. Mogi, M. & Kondo, A. (2009). Down-regulation of mTOR leads to up-regulation of osteoprotegerin in bone marrow cells. *Biochemical and biophysical research communications* **384**, 82-6.
152. Kyle, R. A. & Rajkumar, S. V. (2004). Multiple myeloma. *The New England journal of medicine* **351**, 1860-73.

153. Rajkumar, S. V. (2011). Treatment of multiple myeloma. *Nature reviews. Clinical oncology* **8**, 479-91.
154. Blade, J., Samson, D., Reece, D., Apperley, J., Bjorkstrand, B., Gahrton, G., Gertz, M., Giralt, S., Jagannath, S. & Vesole, D. (1998). Criteria for evaluating disease response and progression in patients with multiple myeloma treated by high-dose therapy and haemopoietic stem cell transplantation. Myeloma Subcommittee of the EBMT. European Group for Blood and Marrow Transplant. *British journal of haematology* **102**, 1115-23.
155. Rajkumar, S. V., Harousseau, J. L., Durie, B., Anderson, K. C., Dimopoulos, M., Kyle, R., Blade, J., Richardson, P., Orlowski, R., Siegel, D., Jagannath, S., Facon, T., Avet-Loiseau, H., Lonial, S., Palumbo, A., Zonder, J., Ludwig, H., Vesole, D., Sezer, O., Munshi, N. C. & San Miguel, J. (2011). Consensus recommendations for the uniform reporting of clinical trials: report of the International Myeloma Workshop Consensus Panel 1. *Blood* **117**, 4691-5.
156. Mahindra, A., Laubach, J., Raje, N., Munshi, N., Richardson, P. G. & Anderson, K. (2012). Latest advances and current challenges in the treatment of multiple myeloma. *Nature reviews. Clinical oncology* **9**, 135-43.
157. Russell, R. G., Xia, Z., Dunford, J. E., Oppermann, U., Kwaasi, A., Hulley, P. A., Kavanagh, K. L., Triffitt, J. T., Lundy, M. W., Phipps, R. J., Barnett, B. L., Coxon, F. P., Rogers, M. J., Watts, N. B. & Ebetino, F. H. (2007). Bisphosphonates: an update on mechanisms of action and how these relate to clinical efficacy. *Annals of the New York Academy of Sciences* **1117**, 209-57.
158. Barni, S., Mandala, M., Cazzaniga, M., Cabiddu, M. & Cremonesi, M. (2006). Bisphosphonates and metastatic bone disease. *Annals of oncology : official journal of the European Society for Medical Oncology / ESMO* **17 Suppl 2**, ii91-95.
159. Lipton, A. (2006). Future treatment of bone metastases *Clinical cancer research : an official journal of the American Association for Cancer Research* **12**, 6305s-6308s.
160. Mehrotra, B. & Ruggiero, S. (2006). Bisphosphonate complications including osteonecrosis of the jaw. *Hematology / the Education Program of the American Society of Hematology. American Society of Hematology. Education Program*, 356-60, 515.
161. Taylor, K. H., Middlefell, L. S. & Mizen, K. D. (2010). Osteonecrosis of the jaws induced by anti-RANK ligand therapy. *The British journal of oral & maxillofacial surgery* **48**, 221-3.
162. Kyrgidis, A. & Toulis, K. A. (2011). Denosumab-related osteonecrosis of the jaws. *Osteoporosis international : a journal established as result of cooperation between the European Foundation for Osteoporosis and the National Osteoporosis Foundation of the USA* **22**, 369-70.
163. Anandarajah, A. P. & Schwarz, E. M. (2006). Anti-RANKL therapy for inflammatory bone disorders: Mechanisms and potential clinical applications. *Journal of cellular biochemistry* **97**, 226-32.
164. McClung, M. R., Lewiecki, E. M., Cohen, S. B., Bolognese, M. A., Woodson, G. C., Moffett, A. H., Peacock, M., Miller, P. D., Lederman, S. N., Chesnut, C. H., Lain, D., Kivitz, A. J., Holloway, D. L., Zhang, C., Peterson, M. C. & Bekker, P. J. (2006). Denosumab in postmenopausal women with low bone mineral density. *The New England journal of medicine* **354**, 821-31.
165. Stopeck, A. T., Lipton, A., Body, J. J., Steger, G. G., Tonkin, K., de Boer, R. H., Lichinitser, M., Fujiwara, Y., Yardley, D. A., Viniegra, M., Fan, M., Jiang, Q., Dansey, R., Jun, S. & Braun, A. (2010). Denosumab compared with zoledronic acid for the treatment of bone metastases in patients with advanced breast cancer: a

randomized, double-blind study. *Journal of clinical oncology : official journal of the American Society of Clinical Oncology* **28**, 5132-9.

166. Pennisi, A., Ling, W., Li, X., Khan, S., Wang, Y., Barlogie, B., Shaughnessy, J. D., Jr. & Yaccoby, S. (2010). Consequences of daily administered parathyroid hormone on myeloma growth, bone disease, and molecular profiling of whole myelomatous bone. *PloS one* **5**, e15233.
167. Fitter, S., Dewar, A. L., Kostakis, P., To, L. B., Hughes, T. P., Roberts, M. M., Lynch, K., Vernon-Roberts, B. & Zannettino, A. C. (2008). Long-term imatinib therapy promotes bone formation in CML patients. *Blood* **111**, 2538-47.
168. Maira, S. M., Stauffer, F., Brueggen, J., Furet, P., Schnell, C., Fritsch, C., Brachmann, S., Chene, P., De Pover, A., Schoemaker, K., Fabbro, D., Gabriel, D., Simonen, M., Murphy, L., Finan, P., Sellers, W. & Garcia-Echeverria, C. (2008). Identification and characterization of NVP-BEZ235, a new orally available dual phosphatidylinositol 3-kinase/mammalian target of rapamycin inhibitor with potent in vivo antitumor activity. *Molecular cancer therapeutics* **7**, 1851-63.
169. Maira, S. M., Pecchi, S., Huang, A., Burger, M., Knapp, M., Sterker, D., Schnell, C., Guthy, D., Nagel, T., Wiesmann, M., Brachmann, S., Fritsch, C., Dorsch, M., Chene, P., Shoemaker, K., De Pover, A., Menezes, D., Martiny-Baron, G., Fabbro, D., Wilson, C. J., Schlegel, R., Hofmann, F., Garcia-Echeverria, C., Sellers, W. R. & Voliva, C. F. (2012). Identification and characterization of NVP-BKM120, an orally available pan-class I PI3-kinase inhibitor. *Molecular cancer therapeutics* **11**, 317-28.
170. Engelman, J. A., Chen, L., Tan, X., Crosby, K., Guimaraes, A. R., Upadhyay, R., Maira, M., McNamara, K., Perera, S. A., Song, Y., Chirieac, L. R., Kaur, R., Lightbown, A., Simendinger, J., Li, T., Padera, R. F., Garcia-Echeverria, C., Weissleder, R., Mahmood, U., Cantley, L. C. & Wong, K. K. (2008). Effective use of PI3K and MEK inhibitors to treat mutant Kras G12D and PIK3CA H1047R murine lung cancers. *Nature medicine* **14**, 1351-6.
171. Konstantinidou, G., Bey, E. A., Rabellino, A., Schuster, K., Maira, M. S., Gazdar, A. F., Amici, A., Boothman, D. A. & Scaglioni, P. P. (2009). Dual phosphoinositide 3-kinase/mammalian target of rapamycin blockade is an effective radiosensitizing strategy for the treatment of non-small cell lung cancer harboring K-RAS mutations. *Cancer research* **69**, 7644-52.
172. Xu, C. X., Li, Y., Yue, P., Owonikoko, T. K., Ramalingam, S. S., Khuri, F. R. & Sun, S. Y. (2011). The combination of RAD001 and NVP-BEZ235 exerts synergistic anticancer activity against non-small cell lung cancer in vitro and in vivo. *PloS one* **6**, e20899.
173. Herrera, V. A., Zeindl-Eberhart, E., Jung, A., Huber, R. M. & Bergner, A. (2011). The dual PI3K/mTOR inhibitor BEZ235 is effective in lung cancer cell lines. *Anticancer research* **31**, 849-54.
174. Brachmann, S. M., Hofmann, I., Schnell, C., Fritsch, C., Wee, S., Lane, H., Wang, S., Garcia-Echeverria, C. & Maira, S. M. (2009). Specific apoptosis induction by the dual PI3K/mTor inhibitor NVP-BEZ235 in HER2 amplified and PIK3CA mutant breast cancer cells. *Proceedings of the National Academy of Sciences of the United States of America* **106**, 22299-304.
175. Serra, V., Markman, B., Scaltriti, M., Eichhorn, P. J., Valero, V., Guzman, M., Botero, M. L., Llonch, E., Atzori, F., Di Cosimo, S., Maira, M., Garcia-Echeverria, C., Parra, J. L., Arribas, J. & Baselga, J. (2008). NVP-BEZ235, a dual PI3K/mTOR inhibitor, prevents PI3K signaling and inhibits the growth of cancer cells with activating PI3K mutations. *Cancer research* **68**, 8022-30.

176. Cao, P., Maira, S. M., Garcia-Echeverria, C. & Hedley, D. W. (2009). Activity of a novel, dual PI3-kinase/mTor inhibitor NVP-BEZ235 against primary human pancreatic cancers grown as orthotopic xenografts. *British journal of cancer* **100**, 1267-76.
177. Awasthi, N., Yen, P. L., Schwarz, M. A. & Schwarz, R. E. (2012). The efficacy of a novel, dual PI3K/mTOR inhibitor NVP-BEZ235 to enhance chemotherapy and antiangiogenic response in pancreatic cancer. *Journal of cellular biochemistry* **113**, 784-91.
178. Mueller, A., Bachmann, E., Linnig, M., Khillimberger, K., Schimanski, C. C., Galle, P. R. & Moehler, M. (2012). Selective PI3K inhibition by BKM120 and BEZ235 alone or in combination with chemotherapy in wild-type and mutated human gastrointestinal cancer cell lines. *Cancer chemotherapy and pharmacology* **69**, 1601-15.
179. Zang, C., Eucker, J., Liu, H., Coordes, A., Lenarz, M., Possinger, K. & Scholz, C. W. (2013). Inhibition of pan-class I PI3 kinase by NVP-BKM120 effectively blocks proliferation and induces cell death in diffuse large B cell lymphoma. *Leukemia & lymphoma*.
180. Bhatt, A. P., Bhende, P. M., Sin, S. H., Roy, D., Dittmer, D. P. & Damania, B. (2010). Dual inhibition of PI3K and mTOR inhibits autocrine and paracrine proliferative loops in PI3K/Akt/mTOR-addicted lymphomas. *Blood* **115**, 4455-63.
181. Kim, A., Park, S., Lee, J. E., Jang, W. S., Lee, S. J., Kang, H. J. & Lee, S. S. (2012). The dual PI3K and mTOR inhibitor NVP-BEZ235 exhibits anti-proliferative activity and overcomes bortezomib resistance in mantle cell lymphoma cells. *Leukemia research* **36**, 912-20.
182. Roccaro, A. M., Sacco, A., Husu, E. N., Pitsillides, C., Vesole, S., Azab, A. K., Azab, F., Melhem, M., Ngo, H. T., Quang, P., Maiso, P., Runnels, J., Liang, M. C., Wong, K. K., Lin, C. & Ghobrial, I. M. (2010). Dual targeting of the PI3K/Akt/mTOR pathway as an antitumor strategy in Waldenstrom macroglobulinemia. *Blood* **115**, 559-69.
183. Sanchez, C. G., Ma, C. X., Crowder, R. J., Guintoli, T., Phommaly, C., Gao, F., Lin, L. & Ellis, M. J. (2011). Preclinical modeling of combined phosphatidylinositol-3-kinase inhibition with endocrine therapy for estrogen receptor-positive breast cancer. *Breast cancer research : BCR* **13**, R21.
184. Juvekar, A., Burga, L. N., Hu, H., Lunsford, E. P., Ibrahim, Y. H., Balmana, J., Rajendran, A., Papa, A., Spencer, K., Lyssiotis, C. A., Nardella, C., Pandolfi, P. P., Baselga, J., Scully, R., Asara, J. M., Cantley, L. C. & Wulf, G. M. (2012). Combining a PI3K inhibitor with a PARP inhibitor provides an effective therapy for BRCA1-related breast cancer. *Cancer discovery* **2**, 1048-63.
185. Ibrahim, Y. H., Garcia-Garcia, C., Serra, V., He, L., Torres-Lockhart, K., Prat, A., Anton, P., Cozar, P., Guzman, M., Grueso, J., Rodriguez, O., Calvo, M. T., Aura, C., Diez, O., Rubio, I. T., Perez, J., Rodon, J., Cortes, J., Ellisen, L. W., Scaltriti, M. & Baselga, J. (2012). PI3K inhibition impairs BRCA1/2 expression and sensitizes BRCA-proficient triple-negative breast cancer to PARP inhibition. *Cancer discovery* **2**, 1036-47.
186. Koul, D., Fu, J., Shen, R., LaFortune, T. A., Wang, S., Tiao, N., Kim, Y. W., Liu, J. L., Ramnarian, D., Yuan, Y., Garcia-Echevrria, C., Maira, S. M. & Yung, W. K. (2012). Antitumor activity of NVP-BKM120--a selective pan class I PI3 kinase inhibitor showed differential forms of cell death based on p53 status of glioma cells. *Clinical cancer research : an official journal of the American Association for Cancer Research* **18**, 184-95.

187. Amrein, L., Shawi, M., Grenier, J., Aloyz, R. & Panasci, L. (2013). The phosphatidylinositol-3 kinase I inhibitor BKM120 induces cell death in B-chronic lymphocytic leukemia cells in vitro. *International journal of cancer. Journal international du cancer* **133**, 247-52.

Chapter 2

Materials and Methods

2.1 List of Reagents

Table 2.1 Common Reagents and Suppliers		
Reagent	**Supplier**	**Catalogue number**
0.85% Saline	Media Production Unit, IMVS	N/A
2-Ethylene glycol monoethyl ether	Merck, Kilsyth, VIC	8.00857.2500
α-Modified Eagle's medium (α-MEM)	SAFC Biosciences, Lenexa, USA	51415C
Acetate solution	Sigma-Aldrich	386-3
Acetic acid	Merck	6.10001.2500
Acetone	Ajax Finechem, Taren Point, NSW	6-2.5L
Acrylamide (30% bis solution)	BioRad, Gladesville, NSW	161-0148
Alizarin red	Sigma-Aldrich	A5533
BioRad RCDC Protein Assay	BioRad Laboratories	500-0120
Bovine serum albumin (BSA) powder (Fraction V)	JRH Bioscience, Lenexa, USA	85040-1K
Calcium chloride	Sigma-Aldrich	C1016
Citric acid, powder	Sigma-Aldrich	C1909
Citric acid solution	Sigma-Aldrich	91-S
D-Luciferin K+ (in vivo bioluminescence)	Xenogen	XR-1001
DePeX mounting medium	Merck	361254A
Dimethyl sulphoxide (DMSO)	Ajax Finechem	225-2.5L
Dulbecco's modified Eagle's medium (DMEM)	SAFC	51441C
Eosin Y	Merck	1.15935.0025
Fast garnet GBC salt	Sigma-Aldrich	387-2
Foetal calf serum (FCS)	SAFC	12003C
Haematoxylin	ProSciTech, Thuringowa Central, QLD	C1071
Hanks' buffered saline solution (HBSS)	SAFC BioSciences	55021C
HEPES (1M)	SAFC BioSciences	59205C
Iscove's Modified Dulbecco's Medium (IMDM)	SAFC BioSciences	I3390
L-ascorbate-2-phosphate	Wako Pure Chemical Industries, Osaka, Japan	013-12061
L-glutamine, 200mM	SAFC BioSciences	59202C

Table 2.1, continued: Common Reagents and Suppliers		
Reagent	**Supplier**	**Catalogue number**
Membrane blocking agent	GE Healthcare, Little Chalfont, UK	RPN2125V
Methanol	Chem Supply	MA004-P
Methyl green	Sigma-Aldrich	M8884
Methylmethacrylate	Merck	8.00590.1000
Naphthol AS-BI phosphoric acid solution	Sigma-Aldrich	387-1
Naphthol AS-BI phosphate	Sigma-Aldrich	N1225
Neutral buffered formalin (NBF, 10%)	Fronine Laboratory Supplies, Riverstone, NSW	JJ01810
N,N-dimethylformamide	Sigma-Aldrich	D8654
N,N,N,N-tetramethylethylenediamine (TEMED)	MP Biomedicals, Seven Hills, NSW	194019
Paraformaldehyde	Merck	296474L
Pararosaniline hydrochloride	Sigma-Aldrich	P3750
Penicillin 5000 U/mL, streptomycin 5mg/ml	Sigma-Aldrich	P4458
Perkadox 16	AkzoNobel, Tullamarine, VIC	1552-11-3
Phloxine B	Sigma-Aldrich	P2579
Phosphate buffered saline (PBS), 20x	Media Production Unit, IMVS	N/A
PBS, calcium and magnesium-free	Sigma-Aldrich	D5652
Polyethylene glycol 300 (PEG 300)	Sigma-Aldrich	81162
Protease inhibitor tablets, EDTA-free	Roche, Basel, Switzerland	4693159001
Proteinase K	Invitrogen (New York, USA)	25530-015
Recombinant human M-CSF (rhM-CSF)	PeproTech (Rocky Hill, USA)	PT300-25-100
Recombinant human PDGF-BB (rhPDGF-BB)	PeproTech	PT100-14B-10
Recombinant human RANKL (rhRANKL)	PeproTech	PT310-10-100
Roswell Park Institute Medium (RPMI-1640)	SAFC BioSciences	51501C
Salmon sperm DNA	Sigma-Aldrich	31149
Silver nitrate	Rhone Poulenc Chemicals, Clayton South, VIC	SL810
Sodium acetate trihydrate	Sigma-Aldrich	236500
Sodium bicarbonate	McKenzie's, Altona, VIC	N/A
Sodium carbonate	Merck	10240

Table 2.1, continued: Common Reagents and Suppliers		
Reagent	**Supplier**	**Catalogue number**
Sodium chloride	Sigma-Aldrich	S9625
Sodium dodecyl sulphate (SDS)	Merck	444464T
Sodium fluoride	Sigma-Aldrich	S7920
Sodium hydroxide, pellets	Merck	567530
Sodium hypochlorite (12.5% w/v)	ACE Chemical Company	F386
Sodium-L-tartrate	Sigma-Aldrich	228729
Sodium nitrite solution	Sigma-Aldrich	91-4
Sodium pyruvate	Sigma-Aldrich	P5280
Sodium thiosulfate	Sigma-Aldrich	S7143
Sodium vanadate	Sigma-Aldrich	450243
Tartrate solution	Sigma-Aldrich	387-3
Toluidine blue	Sigma-Aldrich	T3260
Trypsin-EDTA (0.5%)	Gibco	15400-054
Trypan Blue	Sigma-Aldirch	T-8154
Tween-20	Sigma-Aldrich	P9416
WST-1	Roche, Basel, Switzerland	11644807601
Xylene	Ajax Finechem	577-102

2.2 Solutions, Buffers and Media for Cell Culture

2.2.1 Additives for Tissue Culture Medium (abbreviated to Adds)

L-glutamine (200mM; 100mL), sodium pyruvate (100mM; 100mL), penicillin/streptomycin (5000U/mL and 5mg/mL, respectively; 100mL) and HEPES (1M; 150mL) were thawed in a 37°C water bath, mixed thoroughly, filtered and 22.5mL aliquots were stored at -20°C until use.

2.2.2 Ascorbate-2-Phosphate, 10mM (abbreviated to Asc)

L-ascorbate-2-phosphate (289mg) was dissolved in 100mL HBSS, filter-sterilised using a 0.2μm syringe filter and 5mL aliquots were stored at -20°C until use.

2.2.3 α-Modified Eagle's Medium (α-MEM) for Murine Bone Marrow Stromal Cell (mBMSC) Culture (c-αMEM)

α-MEM was supplemented with 20% (v/v) FCS, Adds (Section 2.2.1) and Asc (Section 2.2.2). The medium was then filter-sterilised through a 0.2μm bottle top filter and stored at 4°C. The medium was replenished with 2mM L-glutamine at fortnightly intervals.

2.2.4 α-MEM For Murine Mineralisation (m-αMEM)

α-MEM was supplemented with 20% (v/v) FCS, Adds (Section 2.2.1), Asc (Section 2.2.2), 10^{-8}M Dexamethasone (catalogue number: RAH688A; Royal Adelaide Hospital Pharmacy, South Australia, Australia) and 4mM potassium phosphate (catalogue number: 10203; BDH AnalaR, Victoria, Australia). The medium was then filter-sterilised through a 0.2μm bottle top filter and stored at 4°C. The medium was replenished with 2mM L-glutamine at fortnightly intervals.

2.2.5 α-MEM For Murine Bone Marrow Monocyte (mBM) Culture (o-αMEM)

α-MEM was supplemented with 10% (v/v) FCS and Adds (Section 2.2.1). The medium was filter-sterilised through a 0.2μm bottle top filter and stored at 4°C. The medium was replenished with 2mM L-glutamine at fortnightly intervals.

2.2.6 Blocking Buffer (for Flow Analysis)

1M stock was prepared by dissolving calcium chloride (11.098g) in RO water (100mL) and stored at room temperature until use. On the day of use, 5mM HEPES (250μL, 1M stock solution) and 2.5mM calcium chloride (125μL, 1M stock solution) were added to 50mL sterile serum-free Hanks' buffered saline solution (HBSS) and mixed by inversion. The blocking buffer was kept on ice while in use.

2.2.7 Calcium Standards

Calcium chloride was prepared as per Section 2.2.6. A standard curve for the Arsenazo III Method assay (Section 2.6.2) was prepared by diluting the stock solution from 2.5–0.25mM in RO water. Diluted standards were stored at 4°C until use.

2.2.8 Dexamethasone, 10^{-5}M Stock Solution

Dexamethasone (65µL of 4mg/mL solution) was added to 50mL serum free α-MEM and mixed thoroughly by inversion. The stock solution was stored at 4°C until use.

2.2.9 DMEM for RAW264.7 Cell Culture (c-DMEM)

DMEM was supplemented with 10% (v/v) FCS and Adds (Section 2.2.1). The medium was then filter-sterilised through a 0.2µm bottle top filter and stored at 4°C. The medium was replenished with 2mM L-glutamine at fortnightly intervals.

2.2.10 DNA Standards

A stock solution of 1mg/mL salmon sperm DNA (10mg) was dissolved in 10mL RO water at 4°C overnight. 100µl aliquots were stored at -20°C. To prepare standards for the Pico Green DNA assay, 4M sodium chloride (4mL) and 0.1M sodium phosphate (4mL) were mixed and salmon sperm DNA was diluted in the sodium chloride/sodium phosphate solution for final concentrations of 1.56–100µg/mL DNA. Diluted standards were stored at 4°C until use.

2.2.11 HHF Wash Buffer

Sterile Hank's Balanced Salt Solution (HBSS) was supplemented with 5% (v/v) sterile FCS, filter-sterilised through a 0.2µm bottle top filter and stored at 4°C.

2.2.12 Iscove's Modified Dulbecco's Medium (IMDM) for Murine Myeloma Cell Culture (c-IMDM)

IMDM was supplemented with 20% (v/v) FCS and Adds (Section 2.2.1). The medium was then filter-sterilised through a 0.2µm bottle top filter and stored at 4°C. The medium was replenished with 2mM L-glutamine at fortnightly intervals.

2.2.13 NVP-BEZ235 (BEZ235) For Tissue Culture

BEZ235 (6.4176mg) was dissolved in 1mL DMSO, for a 10mM stock solution. 100µL aliquots were stored at -20°C. Serial dilutions (1-100mM) of the 10mM stock solution were prepared in DMSO and stored in the dark at room temperature for 2 weeks. For *in vitro* experiments, BEZ235 was used at 1-100nM in 0.1% DMSO by diluting the 1000x serial

dilutions in c-αMEM (Section 2.2.3), m-αMEM (Section 2.2.4), o-αMEM (Section 2.2.5), c-DMEM (Section 2.2.9), c-IMDM (Section 2.2.12) or c-RPMI (Section 2.2.17).

2.2.14 NVP-BKM120 (BKM120) For Tissue Culture

BKM120 (46.488mg) was dissolved in 1mL DMSO, for a 100mM stock solution. 100µL aliquots were stored at -20°C. Serial dilutions (125-2000mM) of the 100mM stock solution were prepared in DMSO and stored in the dark at room temperature for 2 weeks. For *in vitro* experiments, BKM120 was used at 125-2000nM in 0.1% DMSO by diluting the 1000x serial dilutions in c-αMEM (Section 2.2.3), m-αMEM (Section 2.2.4), o-αMEM (Section 2.2.5), c-DMEM (Section 2.2.9), c-IMDM (Section 2.2.12) or c-RPMI (Section 2.2.17).

2.2.15 Proteinase K, 10mg/mL Stock Solution

Proteinase K (100mg) was dissolved in 10mL RO water and 25µL and 50 µL aliquots were stored at -20°C until use. Aliquots were thawed fresh on the day of use.

2.2.16 Potassium phosphate, 400mM Stock Solution

Potassium phosphate (13.6g) was dissolved in 250mL HBSS, filter-sterilised using a 0.2µm syringe filter and 10mL aliquots were stored at -20°C until use.

2.2.17 Roswell Park Memorial Institute Medium (RPMI-1640) for Human Myeloma Cell Culture (c-RPMI)

RPMI-1640 was supplemented with 10% (v/v) FCS and Adds (Section 2.2.1). The medium was subsequently filter-sterilised through a 0.2µm bottle top filter and stored at 4°C. The medium was replenished with 2mM L-glutamine at fortnightly intervals.

2.2.18 rhM-CSF, 25µg/mL Stock Solution

Milli-Q water (1mL) was added to 100µg rhM-CSF and incubated at room temperature for 30 minutes to dissolve. The solution was quickly centrifuged, mixed with 3mL HBSS and filtered through a 0.2µm syringe filter. 20µL aliquots were stored at -80°C until use. Thawed aliquots were stored at 4°C for up to 1 week.

2.2.19 rhPDGF-BB, 10µg/mL Stock Solution

Milli-Q water (1mL) was added to 10µg rhPDGF-BB and incubated at room temperature for 30 minutes to dissolve. The solution was mixed, quickly centrifuged and filtered through a 0.2µm syringe filter. 10µL aliquots were stored at -80°C until use. Thawed aliquots were stored at 4°C for up to 1 week.

2.2.20 rhRANKL, 500µg/mL Stock Solution

Milli-Q water (200µL) was added to 100µg rhRANKL and incubated at room temperature for 30 minutes to dissolve. The solution was quickly centrifuged and filtered through a 0.2µm syringe filter. 5µL aliquots were stored at -80°C until use. Thawed aliquots were stored at 4°C for up to 1 week.

2.2.21 Serum-free α-MEM (sf-αMEM)

α-MEM was supplemented with Adds (Section 2.2.1). The medium was filter-sterilised through a 0.2µm bottle top filter and stored at 4°C. The medium was replenished with 2mM L-glutamine at fortnightly intervals.

2.2.22 Serum-free DMEM (sf-DMEM)

DMEM was supplemented with Adds (Section 2.2.1). The medium was filter-sterilised through a 0.2µm bottle top filter and stored at 4°C. The medium was replenished with 2mM L-glutamine at fortnightly intervals

2.2.23 Trypsin, 0.05%

0.5% Trypsin-EDTA (1mL) was thawed at 37°C, mixed with 9mL HBSS and stored at 4°C for up to 1 week.

2.3 Stains, Buffers and Solutions for Histology and Immunohistochemistry

2.3.1 3,3'-Diamino Benzidine Tetrahydrochloride Hydrate (DAB) Working Solution

On the day of use, RO water (24mL), 13.6mL hydrochloric acid (0.2N) and 13.4mL Tris (0.2M) were combined, mixed on a magnetic stirrer and adjusted to pH7.65-7.70 before the addition of 75mg/mL DAB (Catalogue Number: D5637; Sigma-Aldrich) and 50µL 30% Hydrogen Peroxide.

2.3.2 Acetate-Tartrate Buffer

On the day of use, 200mM sodium acetate (2.72g) and 100mM sodium tartrate (2.3g) were dissolved in 80mL RO water and adjusted to pH5.2 with 1.2% acetic acid. RO water was added for a final volume of 100mL.

2.3.3 Acid Alcohol

RO water (297mL), 70% (v/v) ethanol (700mL) and 0.3% (v/v) hydrochloric acid (3mL) were mixed. The solution was stored at room temperature and used to differentiate Haematoxylin staining.

2.3.4 Citrate/Acetone/Formaldehyde Fixative

4.6mM citric acid solution (5mL), 66.3% (v/v) acetone (13mL) and 3.3% (v/v) formaldehyde (1.6mL) were mixed thoroughly. The fixative was made fresh on the day of use.

2.3.5 Decalcification Solution

Approximately 50g NaOH pellets were dissolved in 3L RO water before the addition of 200mL PBS (20x solution). 0.5M EDTA (744.2g) was then dissolved at room temperature and adjusted to pH8.0 with additional NaOH pellets, as required. 0.5% (w/v) paraformaldehyde (20g) was then added to the EDTA solution and dissolved with heating in a fume cupboard. The final volume was made up to 4L with RO water. Decalcification solution was stored at 4°C for up to 1 month.

2.3.6 Eosin

RO water (22mL), 83% (v/v) ethanol (420.5mL), 11% (w/v) eosin Y (57mL; 1% solution), 1.1% (w/v) phloxine (5.7mL; 1% solution) and acetic acid (2.3mL) were combined and mixed well. The prepared stain was stored at 4°C until use.

2.3.7 Fast Garnet TRAP Stain

Just prior to use, 0.09mg/mL fast garnet GBC (150µL) base solution was combined with 150µL sodium nitrite solution in a 1.5mL microfuge tube. The solutions were mixed by inversion and left to stand for 2 minutes. The freshly diazotised fast garnet GBC salt thus formed was mixed thoroughly with 15mL RO water, 126µg/mL naphthol AS-BI

phosphoric acid solution (150µL), 6.77mM sodium- L-tartrate solution (300µL) and 101µg/mL sodium acetate solution (600µL).

2.3.8 Gelatin/Chromic Potassium Sulphate Solution

1% Gelatine (10g, catalogue number: G9391; Sigma-Aldrich) was dissolved in 1L RO water and heated, with stirring, until dissolved. The solution was allowed to cool and 0.05% chromium (III) potassium sulphate dodecahydrate (500mg, catalogue number: 243361; Sigma-Aldrich) was added. The solution was mixed thoroughly and stored at room temperature until use.

2.3.9 Mayer's Haematoloxylin

5% (w/v) aluminium ammonium sulphate (100g, catalogue number: 100073A; Merck Millipore) was dissolved in 1400mL RO water by heating. The solution was cooled and 0.5% (w/v) haematoxylin (10g), 1% (v/v) ethanol (20mL), 0.1% (w/v) sodium iodate (2g), 2% (v/v) acetic acid (40mL) and 30% (v/v) glycerol (600mL) were added. The solution was stored at room temperature until use.

2.3.10 Methyl green, 0.5mg/mL

Methyl green (25mg, catalogue number: M8884; Sigma-Aldrich) was dissolved in 50mL RO water and was stored at room temperature until use.

2.3.11 Naphthol AS-BI Phosphate, 0.39mg/mL

Naphthol AS-BI phosphate (20mg) was dissolved in 1mL N,N-dimethylformamide and diluted in 50mL acetate-tartrate buffer. The solution was heated to 37°C prior to use.

2.3.12 Pararosaniline, 40mg/mL Stock Solution

Pararosaniline (1g) was heated in 20mL RO water in a fume cupboard until almost completely dissolved. Hydrochloric acid (5mL) was added and the solution was filtered with a 0.45µm syringe filter and then stored at 4°C in the dark for up to 1 month.

2.3.13 Pararosaniline TRAP Stain

Sodium nitrite (80mg) was mixed with 2mL RO water until dissolved. Immediately before use, pararosaniline was hexaazotised by mixing 2mL pararosaline stock solution with 2mL

sodium nitrite solution and incubating at room temperature for 5 minutes. Hexaazotised pararosaniline solution (2.5mL) was added to 50mL acetate-tartrate buffer, heated to 37°C, for a final concentration of 1mg/mL pararosaniline.

2.3.14 Silver Nitrate, 1% (w/v)

Silver nitrate (5g) was dissolved in 500mL RO water and the solution was stored at 4°C in the dark. The solution was used neat or was diluted 1:4 in RO water prior to use

2.3.15 Silver Nitrate, 5% (w/v)

Silver nitrate (25g) was dissolved in 500mL RO water and the solution was stored at 4°C in the dark. The solution was used neat or was diluted 1:4 in RO water prior to use.

2.3.16 Saline Sodium Citrate Buffer (SSC Buffer)

RO water (100mL), 1.753g Sodium Chloride (300mM) and 0.88g Sodium Citrate (30mM) were combined and mixed on a magnetic stirrer. The buffer was made fresh a day before use, stored at 4°C and allowed to reach room temperature before use on the day of use.

2.3.17 Spreading Solution

30% (v/v) 2-ethylene glycol monoethyl ether (300mL) was mixed with 49% (v/v) ethanol (490mL) and 210mL RO water. Spreading solution was stored at room temperature until use.

2.3.18 Sodium Bicarbonate, 1% (w/v)

Sodium bicarbonate (500mg) was dissolved in 500mL RO water on the day of use. Solution was used as a blueing agent for haematoxylin staining.

2.3.19 Sodium Carbonate, 5% (w/v)

Sodium carbonate (12.5g) was dissolved in 250mL RO water and the solution was stored at room temperature until use.

2.3.20 Sodium Phosphate/Citrate Buffer

8.22mM Citric acid (1.58g) and 4.575mM sodium phosphate (0.75g) were dissolved in 800mL RO water and adjusted to pH3.7. The volume was made up to 1L and the solution stored at room temperature until use.

2.3.21 Tris Buffer

RO water (1L) and 1.21g TRIS (10mM) were combined, mixed on a magnetic stirrer and adjusted to pH8. The buffer is made fresh a day before use, stored at 4°C and allowed to reach room temperature before use on the day of use.

2.3.22 Terminal Deoxynucleotidyl Transferase Buffer (TdT Buffer)

RO water (100mL), 363mg TRIS (30mM), 3g Sodium Cacodylate (140mM) and 23.8mg Cobalt Chloride (1mM) were combined, mixed on a magnetic stirrer and adjusted to pH7.2. The buffer was made fresh a day before use, stored at 4°C and allowed to reach room temperature before use on the day of use.

2.3.23 Toluidine Blue Stain, 2% (w/v)

Toluidine blue (2g) was dissolved in 80mL sodium phosphate/citrate buffer and adjusted to pH3.7. The volume was then made up to 100mL with sodium phosphate/citrate buffer and filtered through a 0.45µm syringe filter. The solution was stored at room temperature until use.

2.3.24 TUNEL Reaction Solution

TdT buffer (986.5µL), TdT (4.5µL, Catalogue Number: M1875; Promega, Wisconsin, USA) and Biotinylated 16-dUTP (Catalogue Number: 11093070910; Roche, Basel, Switzerland) were combined and mixed by inversion. Solution was made fresh on the day of use.

2.4 Cell Culture Techniques

2.4.1 Cell Lines and Standard Culture Conditions

All tissue culture techniques were performed in a Class II laminar flow hood (Top Safe 1.2, Bio Air, Siziano, Italy). Cell lines were maintained in a humidified environment at 37°C

with 5% carbon dioxide. All media were warmed in a 37°C water bath before use. All tissue culture plates were obtained from BD Biosciences (North Ryde, NSW).

2.4.1.1 Human Myeloma Cell Cultures

Myeloma cell lines RPMI-8226 and U266 were purchased from the American Type Culture Collection. The WL2 cell line was kindly provided by Professor Doug Joshua (Royal Prince Alfred Hospital, Sydney, Australia). The myeloma cell lines JIM-1, LP-1, OPM-2, and NCI-H929 were kindly provided by Professor Andrew Spencer (The Alfred Hospital, Melbourne, Australia). All myeloma cell lines were cultured in RPMI-1640-10, and cultured at a cell density of $2x10^5$ cells/mL (unless otherwise specified), to ensure that the majority of cells were in a logarithmic phase of growth. Cells were subcultured into fresh media every two to three days and maintained at a cell density of $2x10^5$ cells/mL.

2.4.1.2 Murine 5TGM1 Myeloma Cell Culture

The murine myeloma cell line 5TGM1 was kindly provided by Dr Claire Edwards (Nuffield Department of Orthopaedics, Rheumatology and Musculoskeletal Sciences, University of Oxford, Oxford, England). These cells were cultured in c-IMDM at a cell density of $1x10^5$ cells/mL. Cells were subcultured into fresh media every two to three days.

2.4.1.3 Murine 5TGM1-SFG-NES-TGL Myeloma Cell Culture (5TGM1-SFG)

The 5TGM1 cell line (Section 2.4.1.2) was transduced with the SFG-$_{NES}$-TGL luciferase construct[1] by Dr Peter Diamond (Discipline of Physiology, School of Medical Sciences, Faculty of Health Science, University of Adelaide, South Australia, Australia). The SFG-NES-TGL construct enables the assessment of tumour growth *in vivo* by bioluminescence scanning. These transduced cells were cultured in c-IMDM at a cell density of $1x10^5$ cells/mL. Cells were subcultured into fresh media every two to three days and maintained at a cell density of $1x10^5$ cells/mL.

2.4.1.4 RAW264.7 cell culture

The murine monocyte/macrophage-like cell line RAW264.7 was kindly provided by Associate Professor Gerald Atkins (Orthopaedics and Trauma, Institute of Medical and Veterinary Science, Adelaide, South Australia). These cells were maintained at less than 80% confluence in c-DMEM and were subcultured 1:15 once per week by cell scraping

2.4.2 Trypsinisation of Adherent Cell Lines

Cells were washed with pre-warmed HBSS and detached from the flasks by treating the cells with 2mL 0.05% trypsin-EDTA for 3–5 minutes at 37ºC. Cells were dislodged by firmly tapping the flask and trypsin activity was inhibited by the addition of 5mL HHF. The cells were centrifuged at 800g for 5 minutes at 4°C in an Eppendorf 5810 centrifuge (Eppendorf South Pacific, North Ryde, NSW). The supernatant was aspirated; the cell pellet resuspended in an appropriate volume of culture medium and tapped gently to obtain a single cell suspension. Cells were then transferred into a new culture flask containing medium at a cell density of $1x10^5$ cells/mL and cultured at 37ºC.

2.4.3 Cell Counts and Viability Staining

Enumeration of viable cells was performed following trypan blue staining. 20µL of cell suspension was added to 80µL 0.4% (w/v) trypan blue. The cells were then loaded onto a haemocytometer (Weber Scientific International, Teddington, England) in duplicate. At least 100 cells were counted using a haemocytometer under a light microscope (Olympus BX40, Tokyo, Japan). The cell concentration and viability was calculated using the equation:

(number of cells counted / number of squares) x dilution factor x 10^4

2.4.4 Cryopreservation and Storage of Cells

Cells were cryopreserved in FCS containing 10% (v/v) DMSO which acts as a cryoprotectant. Immediately prior to freezing, 0.5mL sterile freeze mix (20% (v/v) DMSO in FCS) was added to 0.5mL FCS containing 5–10 x 10^6 cells. The cell mixture was immediately transferred to cryoampoules (Greiner Labortechnik, Germany) and placed in a "Mr Frosty" freezing container (Nalgene, USA) at -80°C for at least 3 hours. Cryoampoules were then transferred into the vapour phase liquid nitrogen for extended storage at -196°C.

2.4.5 Thawing of Cryopreserved Cells

Ampoules of cells were rapidly thawed by placing the cryoampoules from liquid nitrogen storage directly into a 37°C waterbath. As soon as the ice crystals had melted, the cells were tapped gently to form a cell suspension and transferred to 9mL pre-warmed culture

medium. Cells were centrifuged at 400g in an Eppendorf 5810R centrifuge for 5 minutes, the supernatant aspirated, and the cell pellet resuspended in 15mL culture medium. The cells were then seeded in a 75cm^2 flask and placed in the 37ºC incubator. After thawing, cells were passaged at least once before use in experiments.

2.4.6 Establishment of mBM Cultures (Isolation of Osteoclast Precursor)

mBM cultures were established as previously described by[2]. Briefly, 6 – 8-week-old female C57BL6/KaLwRijHsd mice (Harlan Netherlands, Horst, The Netherlands) were humanely killed by carbon dioxide overdose. Under sterile conditions, the femurs and tibiae were dissected free of tissue and a scalpel blade was used to remove the ends of the bones. Using a 23-gauge needle, bone marrow was flushed from femurs and tibiae using ice-cold o-αMEM (Section 2.2.5). Bone marrow cells were washed once in HBSS, resuspended in o-αMEM and tapped gently to obtain a single-cell suspension. The bone marrow cells were then seeded at 9x10^5 cells/cm^2 in 175cm^2 flasks. Cells were incubated overnight at 37°C to allow stromal cells to adhere. The next day, non-adherent mBM were aspirated, pelleted at 400g in an Eppendorf 5810R centrifuge at 4°C for 5 minutes and then used as monocyte/macrophage osteoclast precursor cells in osteoclast formation and function assays.

2.4.7 Establishment of mBMSC Cultures

mBMSC cultures were established as previously described[3]. Briefly, 6 – 8-week-old C57BL6/KaLwRijHsd mice (Harlan Netherlands, Horst, The Netherlands) were humanely killed by carbon dioxide overdose. The bone marrow was flushed from femora and tibiae, as described in section 2.4.6, and the bones were cut into 1 – 2mm pieces with a sterile scalpel. The bone chips were then resuspended in 12.5mL c-αMEM, seeded into a 75cm^2 flask and incubated at 37°C with for 2 weeks to allow mBMSC to proliferate. mBMSC were passaged twice before use in mineralisation, proliferation and Western blot experiments. For routine culture, mBMSC were seeded at 8x10^3 cells/cm^2 and media were replaced twice weekly. Cells were sub-cultured by trypsinisation.

2.5 Osteoclastogenesis Assays

2.5.1 mBM Osteoclast Formation and Activity Assays

For TRAP staining or calcium phosphate resorption assays, mBM cells were cultured as previously described[2] in 96-well plates or on 16-well calcium phosphate-coated slides (Corning Osteo Assay Surface Multiwell Plates, catalogue number: CLS3989; Sigma-Aldrich). Briefly, mBM cells were cultured at $3.1x10^5$ cells/cm^2 in 200µL o-αMEM supplemented with 75ng/mL rhM-CSF. Following overnight incubation to allow the cells to adhere, the media were aspirated and replaced with 200µL o-αMEM containing 75ng/mL rhM-CSF, 75ng/mL rhRANKL and BEZ235 or BKM120 (at indicated concentrations, in a final concentration of 0.05% DMSO vehicle) or vehicle alone (day 0). Treatment media were replaced on days 3 and 6. The formation of TRAP-positive bone-resorbing osteoclasts was assessed after 6 days. The resorption of calcium phosphate was assessed after 9 days.

2.5.2 RAW264.7 Osteoclastogenesis Assays

RAW264.7 cells were cultured at $5x10^2$ cells/cm^2 in 96-well plates or on calcium phosphate-coated slides (Corning Osteo Assay Surface Multiwell Plates) in 200µL c-DMEM supplemented with 100ng/mL rhRANKL. Following overnight incubation, the media were replaced with c-DMEM containing 100ng/mL rhRANKL and BEZ235 or BKM120 (at indicated concentrations, in a final concentration of 0.05% DMSO vehicle) or vehicle alone (day 0). Treatment media were replaced on day 2 and 3. The formation of TRAP-positive bone-resorbing osteoclasts was assessed after 4 days. The resorption of calcium phosphate was assessed after 6 days.

2.5.3 TRAP Stain

Cells were stained for TRAP activity with the Leukocyte Acid Phosphatase (TRAP) kit (catalogue number 387-1KT; Sigma-Aldrich) as per the manufacturer's recommendations. Briefly, cells were fixed with 100µL/well freshly prepared citric acid/acetone/formaldehyde solution (Section 2.3.4) for 3–5 minutes. Cells were then carefully washed 3 times with 250µL/well RO water and incubated with freshly-prepared fast garnet TRAP stain (Section 2.3.7) for 15 – 20 minutes at 37°C in the dark. Wells were washed 4 times with 250µL/well RO water and the plates were left to dry by evaporation. The number of osteoclasts

(defined as TRAP-positive cells containing 3 or more nuclei) per well were enumerated in quadruplicate wells. Cells were visualised and photographed with an Olympus CKX41 inverted microscope and an Olympus DP11 digital camera (Olympus Japan) at 200x magnification.

2.5.4 von Kossa Silver Stain

Calcium phosphate-coated slides were stained for mineral using von Kossa silver stain. The slides were washed once with 250µL/well RO water and were bleached with 12.5% (w/v) sodium hypochlorite for 5 minutes. The wells were then washed 3 times with 250µL RO water to remove cell debris. The calcium phosphate layer was stained with 100µL/well 5% silver nitrate solution for 30 minutes under ultra violet light. The developer was prepared fresh by diluting formaldehyde 1:4 in sodium carbonate for a final concentration of 4% (w/v) sodium carbonate and 9.25% (w/v) formaldehyde. The slides were washed 3 times with 250µL/well RO water and were then incubated with 100µL/well developer for 30 to 60 seconds. Following a further 3 washes with 250µL/well RO water, the stain was fixed with 100µL/well 5% sodium thiosulphate for 2 minutes followed by a final wash in RO water.

Slides were left to dry by evaporation and photographed with Olympus CKX41 inverted microscope with an Olympus DP11 digital camera at 40 x final magnification. Resorption area (cleared, unstained foci in the mineral layer) was quantitated with Adobe Photoshop CS3 following the protocol recommended by BD Biosciences.

2.6 Osteoblastogenesis Assay

2.6.1 Murine Mineralisation Assay

For murine mineralisation assays, mBMSC cells were cultured in 48-well plates in 200µL c-αMEM. Cells were cultured overnight, to adhere, and the following day the media were replaced with 200µL m-αMEM media supplemented with BEZ235 or BKM120 (at indicated concentrations, containing 0.1% DMSO vehicle) or vehicle alone. Treatment media were changed twice weekly for 2 weeks and cultured in a hypoxic in vitro cabinet (Coy Laboratory Products, Michigan, USA), under hypoxic condition at 37°C with 5% oxygen, 10% carbon dioxide and 85% nitrogen.

2.6.2 Mineral Quantitation

After 2 weeks of culture, the wells were washed 3 times in 250μL calcium- and magnesium-free PBS and the mineralised matrix was dissolved in 100μL 0.6M hydrochloric acid for 1 hour at room temperature. The supernatant was then transferred to a 96-well microtitre plate and calcium levels were quantitated by the Calcium Arsenazo III assay (catalogue number TR29226; Thermo Scientific, Illinois, USA) according to the manufacturer's instructions. Briefly, supernatants were diluted 1:4 in RO water and 4μL volumes were transferred to single wells of a fresh microtitre plate. A calcium chloride standard curve was also established in triplicate (Section 2.2.7). Arsenazo III reagent (200uL) was added to each well and the absorbance was read immediately at 595nm on a microplate reader (Ultra Microplate Reader, EL808, BIO-TEK Instruments INC, Vermont, USA) after a 10 second shake step.

Following dissolution of the mineral with hydrochloric acid, the wells were washed 3 times with 250μL PBS and the cells were digested with 100μL proteinase K (100μg/mL) for 2 hours at 37°C. After the 1st hour, the cells were resuspended thoroughly to ensure complete disruption of the cells and incubated for a further 1 hour. 50μL volumes were then transferred to a black 96-well microtitre plate (catalogue number 3915; Corning, New York, USA). DNA content per well was then determined using the Pico Green DNA assay (section 2.6.3).

2.6.3 Pico Green DNA Assay

DNA content was measured using Pico Green (catalogue number P11496; Invitrogen, New York, USA) as a surrogate marker of cell number. Pico Green solution (1:300 dilution in TE Buffer, 150uL) was added to samples and DNA standards (Section 2.2.12) in a black polystyrene 96-well plate (catalogue number 3915; Corning, New York, USA) and the plate was mixed by gentle agitation. Fluorescence was then measured using the POLARstar Optima microplate reader (BMGLabtech, Ortenberg, Germany) with an excitation wavelength of 480 nm and an emission wavelength of 520 nm.

2.7 WST-1 Assay

To determine the effects of BEZ235 and BKM120 on cell survival/proliferation, mBMSC ($5x10^3$ cells per well in c-αMEM), human MM cell lines ($1x10^4$ cells per well in c-RPMI),

5TGM1-SFG cells ($1x10^4$ cells per well in c-IMDM) and RAW264.7 cells ($7.5x10^2$ cells per well in c-DMEM) were plated in 96-well plates and allowed to settle overnight. Cells were then treated with inhibitors or vehicle in 150μL media. The relative number of viable cells in each well was determined at days 0, 1, 3, and 5 (human MM cell lines, 5TGM1-SFG cells and RAW264.7 cells) or days 0, 2, 4, and 6 (mBMSC) using the colorimetric assay reagent WST-1 (4-[3-(4-Iodophenyl)-2-(4-nitrophenyl)-2H-5-tetrazolio)-1,3-benzene disulphonate) following the manufacturer's instructions (Roche, Basel, Switzerland). Briefly, 20μL of WST-1 in 30μL of media was added to each well and to wells containing media alone (to enable background determination). The cells were incubated at 37°C in humidified carbon dioxide for 30 minutes (for RAW264.7 cells) or 2 hours (for mBMSC, human MM cell lines and 5TGM1-SFG cells) to allow colour to develop. The optical density of the media was then read at 450nm using a microtitre plate reader (BioTek Instruments, Winooski, USA).

2.8 Cell Apoptosis Analysis by Immunofluorescence Staining: FOXO3a

To determine the effects of BEZ235 and BKM120 on cellular apoptosis, $1x10^6$ cells (human MM cell lines: RPMI-8226, U266, OPM2, WL2 and NCI-H929 or the murine MM cell line, 5TGM1-SFG), were treated with 10μL of ½ IC_{50}, IC_{50} and 2x IC_{50} (as determined by the WST-1 assay) in 10mL of media for 2 hours at 37°C. Cells were then washed with HBSS and resuspended in FCS (1mL). 100μL of cells were cytospun onto ethanol cleaned slides at 1000rpm in a Shandon cytospin (Shandon Cytospin 2; Block Scientific Inc., New York, USA) for 5 minutes and left overnight to dry. The next day, a "wall" was drawn around the cells using a DAKO pen (catalogue number: S2002; DAKO, Golstrup, Denmark), fixed with 200μL 4% paraformaldehyde for 15 minutes at room temperature and permeabilized with 200μL 0.5% (v/v) Triton X-100 in PBS for 4 minutes on ice. Cells were then blocked for 30 minutes at room temperature with 200μL blocking buffer (5% BSA in PBS). Following blocking, cells were incubated with 1:500 dilution of anti-FOXO3a antibody (Catalogue Number: 07-1719, Millipore, Massachusetts, USA) for 1 hour, washed 3 times with ice-cold PBS and then treated with 1:500 dilution of secondary antibody, donkey anti-rabbit-Cy3 (Catalogue Number: AP182C, Millipore, Massachusetts, USA), for 1 hour at room temperature in the dark. Cells were then washed 3 times with ice-cold PBS and counterstained with 300nM DAPI (catalogue number: D9542; Sigma-Aldrich) for 15 minutes at room temperature in the dark. Finally, cells were washed twice with ice-cold PBS, coverslipped with Prolong Gold Antifade Reagent (catalogue number:

P36934, Invitrogen, New York, USA) and stored in the dark at 4°C. The slides were visualised using the Zeiss LSM700 Confocal Microscope (Carl Zeiss AG, Oberkuchen, Germany).

2.9 Cell Apoptosis Analysis by Flow Cytometry: Annexin-V (AnnV) and 7-AAD

To determine the effects of BEZ235 and BKM120 on cellular apoptosis, $1x10^6$ cells (human MM cell lines: RPMI-8226, U266, OPM2, WL2 and NCI-H929 or the murine MM cell line, 5TGM1), were treated with 10µL of ½x IC_{50}, 1x IC_{50} and 2x IC_{50} (as determined by the WST-1 assay) in 10mL of media for 18 hours at 37°C. The next day, cells were pelleted by centrifugation for 5 minutes at 4°C. Cells were washed twice with ice-cold blocking buffer, transferred into 5ml polypropylene tubes and resuspended in 500µL of ice-cold blocking buffer. $1x10^5$ cells (in a 50µL volume) were then incubated with 100µL diluted AnnV Alexa488 (20µL AnnV) in 1000µL blocking buffer, catalogue number: A13201; Invitrogen, New York, USA) and 20µL 7-AAD (catalogue number: A07704; Beckman-Coulter, California, USA) for 15 minutes in the dark at room temperature. Cells were washed twice in ice-cold blocking buffer and resuspended in 250µL ice-cold blocking buffer. Cells were kept on ice in the dark and analysed immediately using a Coulter Cytomics FC500 Series flow cytometer (Beckman Coulter, USA). Typically, for each sample, 5000-10000 events were analysed by flow cytometry, and stored as list mode data for further analysis using Denovo FCS Express 4 software (Denovo Software, California, USA).

2.10 Cell Cycle Arrest Analysis by Flow Cytometry: Propidium Iodide (PI)

To determine the effects of BEZ235 and BKM120 on cell cycle arrest, $1x10^6$ cells (human MM cell lines: RPMI-8226, U266, OPM2, WL2 and NCI-H929 or the murine MM cell line, 5TGM1), were treated with 10µL of ½ IC_{50}, IC_{50} and 2x IC_{50} (as determined by the WST-1 assay) in 10mL of media for 18, 36 and 72 hours at 37°C. At each time point, cells were pelleted by centrifugation for 5 minutes at 4°C. Cells were washed once with ice-cold PBS, transferred into 5ml polypropylene tubes and resuspended in 1mL of ice-cold PBS. $1x10^5$ cells (in a 100µL volume) were then resuspended in 1.2mL ice-cold PBS. 2.8mL 100% -20°C ethanol was added to each tube drop wise on gentle vortex to achieve a final concentration of 70% ethanol and cells were fixed at -20°C overnight. The following day, cells were centrifuged at 1200rpm for 5 minutes. Supernatant was discarded and the pellets

were resuspended with 2mL ice-cold PBS and dispersed by high-speed vortexing. Cells were pelleted and rehydrated with 1ml 0.25% Triton X-100 in PBS with gentle vortexing. Cells were again pelleted and stained overnight at 4°C in the dark with 500µL of PI staining solution consisting of 25µg/mL PI (1mg/ml PI diluted from 25mg/mL PI, catalogue number: P4170, Sigma-Aldrich) and 40µg/ml RNAse A (100µg/mL, catalogue number: 19101, Qiagen, Venlo, Netherlands) in PBS. The following days, cells were analysed using a Coulter Cytomics FC500 Series flow cytometer (Beckman Coulter, USA). Typically, for each sample, 50000-100000 events were analysed by flow cytometry, and stored as list mode data for further analysis using Denovo FCS Express 4 software (Denovo Software, California, USA).

2.11 In Vivo Mouse Studies

2.11.1 Animals

C57BL6/KaLwRijHsd mice (Harlan Netherlands, Horst, The Netherlands) were obtained from Professor Andrew Spencer (The Alfred Hospital, Melbourne) and bred at the Veterinary Services Division, IMVS. Mice were provided standard commercial mouse chow and tap water *ad libitum*. All procedures were approved by the Animal Ethics Committees of the University of South Australia and of the IMVS/SA Pathology.

2.11.2 Experimental Design

Prior to study commencement and at weekly intervals thereafter, blood was collected from female C57BL6/KaLwRijHsd mice by tail tipping (approximately 100µL/sample). These samples were then spun at 800 x g for 10 minutes and sera collected and stored at -20°C until analysis. Animals were then intravenously injected with 5x10^{5} 5TGM1-SFG cells (resuspended in 100µL PBS) via the tail vein. After 2 weeks, animals were randomly assigned to 2 groups: group 1 received vehicle alone (0.5% methyl cellulose) by daily gavage (n=10); group 2 received 50mg/kg BEZ235 in 0.5% methyl cellulose vehicle or 40mg/kg BKM120 in 0.5% methyl cellulose vehicle by daily gavage (n=10). Gavage (10µL volume) was performed using 15 gauge, 78mm polypropylene gavage needles (catalogue number FTP-15-78; Solomon Scientific, San Antonio, USA), and drug treatments were carried out for 2 weeks. At weekly intervals, following the start of drug treatment, tumour growth was assessed by bioluminescence imaging (section 2.10.3).

After 2 weeks of drug treatment, animals were anaesthetised with isoflurane and blood was collected by cardiac puncture prior to sacrifice by cervical dislocation. Both femurs and tibiae were fixed in 10% NBF at 4°C for 48 hours. The left tibiae underwent scanning by μ-CT (Section 2.11). Following scanning, the left tibiae were embedded in methyl methacrylate for histological analyses as described in section 2.13.1 while the tibiae were decalcified and embedded in paraffin for histological analyses as described in section 2.13.2.

2.11.3 *In vivo* Bioluminescence Scanning

As described in section 2.4.1.3, the murine 5TGM1 myeloma cells were transduced with the SFG-NES-TGL luciferase construct, to enable the ongoing assessment of tumour growth by bioluminescence scanning. For *in vivo* bioluminescence imaging, mice were administered 150mg/kg D-luciferin K+ substrate (Xenogen, USA) in sterile calcium- and magnesium-free PBS by intraperitoneal injection. Levels of bioluminescence emitted from injected tumour cells were detected with the Xenogen IVIS^{TM} system (Xenogen, USA).

Twenty minutes after administration of D-luciferin, mice were anaesthetised by 3% (v/v) isofluorane inhalation and placed onto a warmed stage inside the light-ight chamber, with continuous exposure to anaesthetic via a nose-cone. Bioluminescence images were recorded for 5 minutes. Using the Living Image 2.50.1® software (Xenogen, USA), levels of bioluminescence were quantified at tumour sites. Mice were imaged weekly for the duration of the experiment.

2.11.4 BEZ235 and BKM120 Preparation for Oral Gavage

50mg/kg BEZ235 in 0.5% methyl cellulose (10μL), 40mg/kg BKM120 (10μL) in 0.5% methyl cellulose or the vehicle (10μL, 0.5% methyl cellulose) were administered to the mice after they were divided randomly into 2 groups on Week 2. Once mice were divided into each group, weight of each mouse was taken and the average weight of mice in each group was determined. Each treatment was solubilised in 0.5% methyl cellulose by sonication to ensure even dispersion and administered by oral gavage immediately. Mice were monitored to ensure no adverse reaction to the drugs or to the procedure.

2.12 Micro-CT (μ-CT)

The 3-dimensional microarchitechture of mouse proximal tibiae were evaluated using μ-CT (Skyscan 1174 X-ray Microtomograph, Skyscan). Bone samples were scanned at 74 kV/100*m*A, with an isometric resolution of 8.7μm/pixel using a 2.5mm aluminium filter and 2 frame averaging. Reconstruction of the original scan data was performed using NRecon (SkyScan).

Analysis of microarchitectural parameters was performed using CTAn (SkyScan). A trabecular polygonal region of interest was manually defined to exclude the cortex. A total of 150 slices (0.645mm) were analysed for each tibia, commencing 50 slices (0.215mm) distal to the growth plate.

Digital segmentation of the bone from air/tissues was performed by adaptive (median-C) thresholding. Despeckling and smoothing protocols were run to minimise background noise.

For trabecular bone regions, bone volume fraction (BV/TV), bone surface fraction (BS/BV), trabecular thickness (Tb.Th.), trabecular number (Tb.N), trabecular spacing (Tb.Sp), structure model index (SMI) and trabecular pattern factor (Tb.Pf) were calculated using CTAn. Tb.Th measurements were calibrated by scanning and analysing 4 aluminum foils with thicknesses of 20, 50, 125 and 250μm (SkyScan)[4]. Bone mineral density was calculated using CTAn, using phantoms of known density (0.25g/cm^3 and 0.75g/cm^2) and a region corresponding to water as a reference.

The volumes of interest were reconstructed in 3 dimensions using adaptive 3-dimensional modelling and visualised using ANT software (SkyScan). To assess the degree of osteolysis between treated and untreated animals, the reconstructed 3 dimension images were sliced in half using the ANT software (SkyScan) and the number of cortical holes present were counted.

2.13 Histology

2.13.1 Methacrylate Embedding

Murine femurs and tibiae were embedded in methylmethacrylate as described previously[5]. The fixed samples were dehydrated in sequential changes of graded acetone (70% acetone for 1 hour; 90% acetone, 1 hour; 100% acetone, 1 hour; 100% acetone, 1 hour) at 4°C and

subsequently infiltrated in 91% methylmethacrylate/9% PEG 400 under a vacuum for 1 week at room temperature in polypropylene specimen containers. After infiltration, the samples were embedded in 10mL methylmethacrylate/PEG 400 (10:1) with Perkadox 16 (0.4% w/v) at 37°C for 48 hours. Blocks were attached to aluminium block holders with Araldite epoxy resin (Selleys, Padstow, NSW) prior to sectioning.

Using a D-profile blade, 5µm thick sections were taken from each block using a Leica SM2500 motorised sledge microtome (Leica Microsystems). Gelatine-coated slides were prepared by dipping clean, dust-free slides (SuperFrost, Menzel-Gläser) in gelatine/chromic potassium sulphate solution and allowing the slides to dry overnight prior to use. Sections were attached to gelatine-coated slides using spreading solution heated to 60 – 70°C and the sections were covered with a polyethylene sheet which was pre-soaked in spreading solution for 10 seconds. The slides were interleaved with blotting paper, clamped together using a bulldog clip and were incubated at 42°C for 18 – 48 hours to dry. Sections were deplasticised by submersion in 100% acetone for 15 minutes prior to staining.

2.13.2 Paraffin Embedding

Fixed tibiae were decalcified in 0.5M EDTA/0.5% parafomaldehyde decalcification solution, changed twice weekly, for 2 weeks. Complete decalcification of the samples was confirmed by X-ray. The cortex was cut from the medial facet of the tibia and the samples were processed through sequential changes of ethanol, xylene and paraffin and then embedded in paraffin. Longitudinal sections (5µm) were cut and were mounted on Snowcoat X-tra slides (Surgipath, Richmond, USA).

2.13.3 TRAP Stain

Sections were stained for TRAP using naphthol AS-BI as a substrate and pararosaniline as a coupler. Briefly, slides were incubated at 37°C for 30 minutes in acetate-tartate buffer (200mM sodium acetate, 100mM sodium tartrate, pH 5.2) containing 0.4mg/mL naphthol AS-BI phosphate. The slides were then transferred to pararosaniline TRAP stain solution and were incubated at 37°C for a further 30 minutes. Slides were rinsed in water and were counterstained in methyl green (0.5mg/mL) for 5–60 seconds. Slides were rinsed in water and were then dehydrated through ethanol and cleared in xylene before cover slipping using DePeX mounting medium.

2.13.4 Toluidine Blue Stain

For toluidine blue staining, de-plasticised slides were incubated for 5 minutes in 2% toluidine blue stain. The slides were then washed in 2 changes of sodium phosphate-citrate buffer, dehydrated through ethanol, cleared in xylene and coverslipped using DePeX mounting medium.

2.13.5 von Kossa Stain

For von Kossa silver stain, de-plasticised slides were stained with 1% silver nitrate for 60 minutes under ultraviolet light at room temperature. The brown stain was developed in 4% sodium carbonate and 10% formaldehyde for 60 seconds. The slides were washed with RO water and then fixed in 2.5% sodium thiosulphate for 2 minutes. The slides were then rinsed in RO water and the sections were counterstained with haematoxylin and eosin before being dehydrated through ethanol, cleared in xylene and coverslipped using DePeX.

2.14 Serum Paraprotein Analysis

Serum samples collected during the mouse studies were analysed for serum paraprotein levels using the Hydragel 30 β1-β2 kit (catalogue number: 4141, Sebia, Georgie, USA), following the manufacturer's protocols. Once the gels were prepared, they were run on the Hydrasys Focusing Electrophoresis System (Sebia, Georgia, USA) and scanned on an Epson Expression 1680 Professional scanner (Epson, Nagano, Japan) Using the software provided, the percentage of serum paraprotein present was measured against the total protein.

2.15 Serum Bone Marker Analyses – Total Procollagen Type 1 N-terminal Propeptide (P1NP) and Tartrate-resistant Acid Phosphatase (TRAP) 5b

Mouse P1NP serum levels were assessed using a commercial ELISA (catalogue number: AC33F1, Immuno Diagnostic Systems, Boldon, United Kingdom) according to the manufacturer's instruction. The intra- and inter-assay coefficients of variance of 8% and 12%, respectively.

Mouse TRAP5b serum levels in rat sera were assessed using a commercial ELISA (catalogue number: SBTR103; Immuno Diagnostic Systems, Boldon) according to the

manufacturer's instruction. The intra- and inter-assay coefficients of variance of 4% and 3% respectively.

2.16 Immunohistochemistry Staining

2.16.1 Terminal deoxynucleotidyl transferase dUTP nick end labelling (TUNEL) Staining

Five micron sections of paraffin-embedded tibiae were stained to detect nuclei undergoing apoptosis using TUNEL staining. De-waxed slides were incubated for 15 minutes with 20µg/ml Proteinase K (Catalogue Number: 21627; Millipore, Massachusetts, USA) at room temperature. Subsequently, slides were washed twice in RO water for 2 minutes per wash and incubated for 5 minutes with 1% Hydrogen Peroxidase (30% H_2O_2 stock) in Tris Buffer. The slides were then pre-incubated with TdT buffer for 10 minutes and incubated with the reaction solution at 37°C for 1 hour. The reaction was stopped by immersing the slides for 15 minutes into the SSC buffer twice, rinsed with PBS and blocked with 2% BSA in PBS for 10 minutes. Following blocking, slides were incubated with 1:1000 dilution streptavidin horseradish-peroxidase conjugate (catalogue number: 21127; Thermo Scientific, USA) at 37°C for 30 minutes and then with DAB in 1% H_2O_2 for 6 minutes. Slides were washed in RO water, counterstained with haematoxylin and differentiated in acid alcohol and 0.1% sodium bicarbonate solutions. Slides were dehydrated through ethanol, cleared in xylene and coverslipped using DePex mounting medium.

2.17 Western Blotting Reagents

2.17.1 Blocking Solution

On the day of use, 1g membrane blocking agent was dissolved in 40mL TBS-Tween with 1% BSA at room temperature with agitation.

2.17.2 Lysis Buffer

One protease inhibitor tablet was dissolved in 7.27mL RO water with agitation. 200µL Tris (1M; pH 7.4), 40µL EDTA (0.5M), 750µL sodium chloride (2M), 100µL Triton X-100 (catalogue number: 9002-93-1, MP Biomedicals, NSW), 100µL sodium vanadate (200mM), 40µL sodium fluoride (500mM), 100µL SDS (10% w/v), 400µL sodium pyrophosphate (250mM) and 1mL glycerol (100% v/v) were then added and mixed

thoroughly. The resulting solution of 1% Triton-X, 20mM Tris, 150mM sodium chloride, 2mM EDTA, 2mM sodium fluoride, 0.1% (w/v) SDS, 10mM sodium phosphate, 2mM sodium vanadate and 10% (v/v) glycerol, supplemented with complete protease inhibitors, was stored in 1mL aliquots at -20°C for up to 3 months.

2.17.3 10% Polyacrylamide Gel (Separating Gel)

7.9mL RO water, 6.7mL bis-acrylamide, 5mL Tris (1.5 M; pH 8.8), 200µL SDS (10% w/v) and 200µL APS (10% w/v) were combined and were mixed by inversion. Immediately before use, 8µL TEMED was added and the solution was mixed carefully to avoid creating bubbles.

2.17.4 15% Polyacrylamide Gel (Separating Gel)

4.6mL RO water, 10mL bis-acrylamide, 5mL Tris (1.5 M; pH 8.8), 200µL SDS (10% w/v) and 200µL APS (10% w/v) were combined and were mixed by inversion. Immediately before use, 8µL TEMED was added and the solution was mixed carefully to avoid creating bubbles.

2.17.5 Reducing Loading Buffer, 4x

20mL Glycerol, 20 L Tris (1.0M, pH 6.8), 6.4g SDS, 320mg bromophenol blue, 6.4mL β-mercaptoethanol and 20mL RO water were mixed, the solution was filtered using a 0.45µm syringe filter and 2.5mL aliquots were stored at -20°C. Thawed aliquots were stored at 4°C until use. Cell lysates were diluted 1:4 in loading buffer for a final concentration of 50mM Tris, 1.6% SDS, 0.08% (w/v) bromophenol blue and 1.6% β-mercaptoethanol.

2.17.6 Stacking Gel

3.4mL RO water, 830µL bis-acrylamide, 630µL Tris (1M; pH 6.8), 50µL SDS (10% w/v) and 50µL APS (10% w/v) were combined and were mixed by inversion. Immediately before use, 5µL TEMED was added and the solution was mixed carefully to avoid creating bubbles.

2.17.7 Running Buffer, 10x

30.3g Tris, 144g glycine and 10g SDS were dissolved in RO water, the pH was adjusted to 8.3 and the volume was made up to 1L. The solution was stored at room temperature and

was diluted 1:9 in RO water prior to use for a final concentration of 0.3% (w/v) Tris-HCl, 1.44% (w/v) glycine and 0.1% (w/v) SDS.

2.17.8 Tris-Buffered Saline (TBS), 10x

24.2g Tris and 80g sodium chloride were dissolved in RO water, the pH was adjusted to 7.6 and the volume was made up to 1L. The solution was stored at room temperature and was diluted 1:9 in RO water before use.

2.17.9 0.1% Tween/TBS (TBS-Tween)

Tween-20 (1mL) was added to 100 mL TBS (10x) and 899 mL RO water and was carefully mixed to avoid bubbles. Solution was stored at room temperature until use.

2.17.10 TBS-Tween with 10% BSA

BSA (0.5g) was dissolved in 50mL TBS-Tween, with agitation. The solution was filtered using a 0.45μM syringe filter and was stored at 4°C. The solution was diluted 1:9 in TBS-Tween prior to use.

2.17.11 Transfer Buffer

12.104g Tris and 57.66g glycine were dissolved in 3L RO water, 0.6L methanol was added and the volume was made up to 4L. The solution was stored at 4°C and was used up to 2 times before discarding.

2.18 Western Blotting

2.18.1 Preparation of Cell Lysates

For Western blotting experiments, human MM cell lines and 5TGM1 cells were cultured at $1x10^6$ cells in a $25cm^2$ flask in 10mL c-RPMI or c-IMDM with BEZ235 or BKM120 (containing 0.1% DMSO vehicle) or vehicle alone for 4 hours. For apoptosis analyses, human MM cell lines and 5TGM1 cells were cultured at $1x10^6$ cells in a $25cm^2$ flask in 10mL c-RPMI or c-IMDM with BEZ235 or BKM120 (containing 0.1% DMSO vehicle) or vehicle alone for 18 hours. mBMSC were cultured at $3.13x10^5$ cells/cm^2 in 60mm dishes with 5ml of c-αMEM and allowed to settle overnight. Cells were washed with 5ml HBSS and serum starved for 4 hours in 5ml sf-α-MEM. Following that, cells were treated with BEZ235 or BKM120 (containing 0.1% DMSO vehicle) or vehicle alone in 2.7ml sf-αMEM

for 1 hour. Prior to being harvested, cells were stimulated with 300µL 100ng/mL rhPDGF-BB for 5 minutes at 37°C.

RAW264.7 cells were seeded in a 6-well plate in 2 mL in c-DMEM at $9.38x10^3$ cells/cm^2 and allowed to settle overnight. The wells were washed with 3 mL HBSS and the cells were starved with sf-DMEM overnight. Prior to being harvested, the cells were then treated with BEZ235 or BKM120 (containing 0.1% DMSO vehicle) or vehicle alone in 2mL sf-DMEM for 2 hours.

Following treatment, cells were washed twice in 5ml ice-cold PBS and lysed with 150µL ice-cold lysis buffer. The lysates were transferred to 1.5mL microfuge tubes (Eppendorf, North Ryde, NSW) and the cells were lysed by sonication at 3 watts for 10 seconds using a probe sonicator (model number XL2007; MiSonix, Farmindale, USA). The lysates were cleared by centrifugation at 13000 x g for 10 minutes at 4°C and the supernatants were transferred to 1.5mL microfuge tubes. The protein concentration of the supernatant was determined using a RCDC protein assay kit (catalogue number: 500-0120; BioRad Laboratories, California, USA), following the protocol of the manufacturer (see section 2.16.2). The lysates were then stored at -20°C until being used for SDS-polyacrylamide gel electrophoresis (SDS-PAGE).

2.18.2 RCDC Protein Estimation

The protein concentration of all cell extracts was determined using the RCDC Protein Assay Kit (BioRad, USA) according to manufacturer's instructions. Serial dilutions of BSA (2mg/mL stock) were used to create a standard curve.

2.18.3 Preparation of Samples for SDS-PAGE

Cell lysates were thawed on ice and equivalent amounts of protein, as determined by RCDC protein assay kit were transferred to 1.5mL microfuge tubes. Appropriate volumes of 4x reducing loading buffer were added and the samples were incubated for 4 minutes at 100°C on a heat block. The samples were cooled on ice, quickly centrifuged and loaded onto SDS-PAGE gels with a pre-stained protein marker (Bench-mark; catalogue number 10748-010; Invitrogen, New York, USA).

2.18.4 SDS-PAGE Gel Preparation

Spacer plates (1.5mm; catalogue number: 1653312; Bio-Rad) and short plates (catalogue number: 1653308; Bio-Rad) were assembled in a gel-casting frame. Immediately following addition of TEMED, separating gel was poured until it was 2cm below the top of the short plate. The gel was then covered with RO water to remove bubbles and was left for 15 minutes to set.

When the gel was set, the RO water was blotted off, the stacking gel was poured, a 10 or 15-well comb (catalogue number: 1653365/1653366; Bio-Rad) was inserted and the gel was left to set for 15 minutes.

2.18.5 Loading and Running of SDS-PAGE Gels

The gels were assembled with the Mini-Protean® 3 (Bio-Rad) electrode assembly and clamping frame, the assembly was placed in a tank and the combs were removed. The inner chamber was filled with running buffer, ensuring the wells were well-rinsed with buffer. The tank was then half-filled with running buffer and the prepared samples and protein markers were loaded in appropriate wells. The lysates were run through the stacking gel at 20 mA and were then resolved through the separating gel at 40mA.

2.18.6 Transfer of Protein to Polyvinylidene Difluoride (PVDF) Membranes

PVDF membrane (Hybond-P membrane, Amersham Biosciences, GE Healthcare, Little Chalfont, UK) was cut to size (8 x 9 cm) and pre-equilibrated in methanol for 5 minutes. The membrane, blotting paper and fibre pads were then soaked in transfer buffer until use. Following electrophoresis, the gel assembly was dismantled and the electrophoretic transfer cell (Mini Trans-Blot, Bio-Rad) was assembled, following the instructions of the manufacturer. Briefly, 2 sheets of blotting paper were placed on a fibre pad on the black side of the gel cassette holder and the gel was carefully placed on top. The pre-equilibrated membrane was laid over the gel, followed by 2 sheets of blotting paper, any air bubbles were expelled by rolling over the filter paper with a pipette and a final fibre pad was placed on top. The assembly was then placed in a tank with a cooling unit (cooled to -20°C), the tank was filled with transfer buffer and the protein transfer was carried out overnight at 30mA or for 2 hours at 200mA.

2.18.7 Protein Detection

Following Western blotting, the PVDF membrane was rinsed in TBS-Tween before being incubated for 2 hours in blocking buffer with agitation. The membrane was rinsed briefly in TBS-Tween and was then probed with primary antibody (detailed in table 2.2) diluted in 1% BSA in TBS-Tween either overnight at 4°C or for 2 hours at room temperature with agitation. The membranes were then washed 3 times for 5 minutes in TBS-Tween and the immunoreactive proteins were subsequently detected by incubation with alkaline-phosphatase-conjugated antibodies against rabbit immunoglobulin (Ig) (catalogue number AP182A; Chemicon, Melbourne, VIC) or mouse Ig (catalogue number AP322A; Chemicon), diluted 1:2000 in 1% BSA/TBS-Tween, for 1 hour at room temperature with agitation. The membranes were then washed 3 times for 5 minutes at room temperature with agitation, followed by a final rinse in TBS. The protein was then detected by incubation with 1mL enhanced chemifluorescence (ECF™) substrate (catalogue number RPN5785; Amersham) prior to imaging using a Typhoon 9410 fluorimager (Amersham) at 488 nm excitation.

Quantitation was performed using ImageQuant software (version 7.0, GE Healthcare). Where required, membranes were stripped of antibodies using a commercial stripping buffer (Western blot recycling kit; catalogue number 90100; Alpha Diagnostics, San Antonio, USA), following the instructions of the manufacturer. The blots were then rinsed in TBS and incubated for 1 hour in blocking buffer before reprobing with primary antibody.

Table 2.2 List of Antibodies for Western Blotting				
Reagent	Supplier	Catalogue number	Dilution	Isotype
α-Tubulin	Abcam, Massachusetts, USA	ab6160	1/5000	Rat IgG
Phosphorylated p70S6k Thr389	Cell Signalling, Denver, USA	9206	1/1000	Mouse IgG
Total p70S6k	Cell Signalling	9202	1/1000	Rabbit IgG
Phosphorylated Akt Ser473	Cell Signalling	4051	1/1000	Mouse IgG
Phosphorylated Akt Thr308	Cell Signalling	9275	1/1000	Rabbit IgG
Total Akt	Cell Signalling	9272	1/1000	Rabbit IgG
Caspase-3	Cell Signalling	9262	1/1000	Rabbit IgG
Caspase-9	Cell Signalling	9502	1/1000	Rabbit IgG
Cyclin D1	Cell Signalling	2926	1/1000	Mouse IgG
Deptor	LifeSpan BioSciences, Seattle, USA		1/1000	Rabbit IgG

2.19 Statistical Analyses

Data points are reported as the mean ± standard error of the mean (SEM). Analysis of the variance to determine significant differences between treatments was performed using a two-tailed paired Student's T-test, one-way ANOVA with Dunnett's post-hoc test or Pearson Product Moment test on the SigmaStat® 3.0 software package (Systat, USA). Statistical significance was determined for a two-tailed test and Ho (null hypothesis, $\mu = \mu o$) was rejected at significance $p \leq 0.05$. Each experiment was repeated at least three times for these analyses.

The calculation of 50% inhibitory concentration (IC50) values was performed using the Hill equation: $y = 100/(1 + 10_{50}^{(logIC-x)*Hillslope})$, where y is the level of inhibition and x is the logarithmic drug concentration.

Reference:

1. Ponomarev, V., Doubrovin, M., Serganova, I., Vider, J., Shavrin, A., Beresten, T., Ivanova, A., Ageyeva, L., Tourkova, V., Balatoni, J., Bornmann, W., Blasberg, R. & Gelovani Tjuvajev, J. (2004). A novel triple-modality reporter gene for whole-body fluorescent, bioluminescent, and nuclear noninvasive imaging. *European journal of nuclear medicine and molecular imaging* **31**, 740-51.
2. Wani, M. R., Fuller, K., Kim, N. S., Choi, Y. & Chambers, T. (1999). Prostaglandin E2 cooperates with TRANCE in osteoclast induction from hemopoietic precursors: synergistic activation of differentiation, cell spreading, and fusion. *Endocrinology* **140**, 1927-35.
3. Pitsillides, A. A., Rawlinson, S. C., Suswillo, R. F., Bourrin, S., Zaman, G. & Lanyon, L. E. (1995). Mechanical strain-induced NO production by bone cells: a possible role in adaptive bone (re)modeling? *FASEB J* **9**, 1614-22.
4. Perilli, E., Baruffaldi, F., Bisi, M. C., Cristofolini, L. & Cappello, A. (2006). A physical phantom for the calibration of three-dimensional X-ray microtomography examination. *J Microsc* **222**, 124-34.
5. McNeil, P. J., Durbridge, T. C., Parkinson, I. H. & Moore, R. J. (1997). Simple method for the simultaneous demonstration of formation and resorption in undecalcified bone embedded in methyl methacrylate. *J Histotechnol* **20**, 307-311.

Chapter 3

The Effect of BEZ235 and BKM120 on MM cells *in vitro*

3.1 *Introduction*

Tissues in the body go through cellular renewal on a daily basis through cell growth, proliferation, survival and apoptosis. This homeostatic turnover of cells is controlled by a number of important signalling pathways. Among these pathways are the PI3k and mTOR pathways. In tumour cells, mutations in the PI3k and mTOR pathways result in uncontrolled proliferation and the development of chemotherapy and radiotherapy resistance[1; 2; 3; 4].

In MM tumour cells, multiple genetic mutations have been found to affect the PI3k and mTOR pathways. Chromosomal translocations 11q13, 4p16.3, 16q32 and 6p25 have been linked to mutations of Cyclin D1, fibroblast growth factor receptor 3 (FGFR3) and MMSET, c-MAF and MUM1/IRF4 respectively with 10-15% of MM patients identified as possessing t(4;14)(p16q;q32) [5; 6; 7; 8; 9; 10; 11]. PTEN, a tumour suppressor gene which negatively regulates anti-apoptotic action of Akt phosphorylation, has been shown to be deleted or mutated in both solid tumours and MM resulting in uncontrolled cell proliferation and inhibition of apoptosis [12; 13; 14; 15]. Mutations of the RAS oncogene, small GTPases which are able to trigger the activity of the PI3k pathway[16], have been reported in 30-50% of MM patients[17; 18; 19] and while they have been identified at each clinical stage of disease progression, they are particularly prevalent in relapsed patients[17; 18; 19]. p53 tumour suppressor gene, which suppresses PI3k activation directly or through PTEN, has also been identified as being mutated in MM cells[17].

In addition to PI3k mutations, DEPTOR, an mTOR interacting protein that negatively regulates mTORC1 and mTORC2, has recently been shown to aberrantly overexpressed in MM[20]. Studies have also shown that over-expressing DEPTOR can suppress p70S6k phosphorylation[20; 21; 22]. However, via a feedback loop, DEPTOR over-expression can activate Akt while mTORC1 is inhibited[20; 21; 22].

A number of the common genetic translocations found in patients are present in a number of human MM cell lines that are regularly used for examining the pathogenesis of MM. Translocation of t(4;14) which coincides with mutation of FGFR3 and MMSET has been identified in OPM2, NCI-H929, KMS-11, LP-1 and JIM-1 MM cell lines[3; 17]. The t(11;14) translocation found in the U266 cell line induces Cyclin D1 resulting in increased cell proliferation[10; 23] while the t(14;16) translocation found in the RPMI-8226 and KMS-11 MM cell lines lead to over-expression of c-MAF[23]. Deletion

of PTEN has been identified in OPM2 cells[14] while DEPTOR over-expression, due to over-expression of c-MAF, was recently identified in RPMI-8226 cells[20].

With these mutations, one would hypothesise that the cells would be susceptible to cell apoptosis due to the instability of the cell's DNA. A study by Stengel discovered that primary MM patient cells with t(4;14) translocation were more susceptible to cell apoptosis compared to primary MM cells with t(11;14) and t(15;14) translocation following exposure to the dual PI3k/mTOR inhibitors, PI103 and BEZ235, or a combination of PIK90, a PI3k inhibitor, with Rapamycin[23]. Recently, McMillin and colleagues demonstrated that BEZ235 inhibits cell survival in human MM cell lines (KMS-11, NCI-H929 OPM2 and U266) at concentrations of 100nM BEZ235 and higher[24] while Zheng showed BKM120, a PI3k inhibitor was able to induce U266 cell apoptosis from 1μM BKM120[25].

With this information in hand, we hypothesised that BEZ235 and BKM120 would inhibit human and murine MM cell proliferation and induce cell apoptosis. The studies outlined in this chapter were performed to investigate the effects of BEZ235 and BKM120 on MM cell proliferation and survival.

3.2 *Results*

3.2.1 The effect of BEZ235 and BKM120 on human and murine MM cell lines *in vitro*

3.2.1.1 The effect of BEZ235 and BKM120 on the PI3K and mTOR signalling pathways

To investigate the effect of BEZ235 and BKM120 on PI3K and mTOR signalling in MM cells, a panel of human (U266, OPM2, NCI-H929, RPMI-8226 and WL2) and murine (5TGM1) MM cell lines were treated with BEZ235 (1-100nM), BKM120 (125-2000nM) or vehicle alone (0.1% DMSO) for 4 hours prior to the preparation of cell lysates. The cell lysates were then examined by Western immunoblot to determine the effects of BEZ235 and BKM120 on phosphorylation of Akt and $p70^{S6K}$, downstream effectors of the PI3k and mTOR pathways. As shown in Figures 3.1A, 3.2A, 3.3A, 3.4A, 3.5A and 3.6A, BEZ235 and BKM120 inhibit phosphorylation of $p70^{S6k}$ in a dose-dependent manner from concentrations of 1nM BEZ235 and 500nM BKM120. Notably, the phosphorylation of Akt_{Ser473} and Akt_{Thr308} was unaffected at all

concentrations examined except in the NCI-H929 cell line, where Akt_{Ser473} was inhibited by both BEZ235 and BKM120 at concentrations of 5nM and 750nM, respectively.

Quantitation of the intensity of the phosphorylated Akt_{Ser473} and $p70^{S6K}$ bands, normalised to the intensity of the total Akt and total $p70^{S6K}$ bands respectively, enabled the determination of the IC_{50} for inhibition of BEZ235 and BKM120 on phosphorylation of Akt and $p70^{S6K}$ in these cell lines (Figures 3.1B, 3.2B, 3.3B, 3.4B, 3.5B and 3.6B).

3.2.1.2 The effect of BEZ235 and BKM120 on Deptor expression in human and murine MM cells

As discussed in Section 3.1, Deptor, a novel binding partner of mTOR, negatively regulates mTORC1 and mTORC2 and was recently discovered to be overexpressed in MM. To investigate whether Deptor was expressed in our MM cell lines and to determine whether BEZ235 and BKM120 were able to inhibit Deptor expression, human (U266, OPM2, NCI-H929, RPMI-8226 and WL2) and murine (5TGM1) MM cell lines were treated with BEZ235 (1-100nM), BKM120 (125-2000nM) or vehicle alone (0.1% DMSO) for 4 hours prior to the preparation of cell lysates. The cell lysates were then examined by Western immunoblot to determine the effects of BEZ235 and BKM120 on Deptor. Figures 3.1A, 3.2A, 3.3A, 3.4A, 3.5A and 3.6A show that Deptor is expressed in these cell lines. BEZ235 and BKM120 treatment inhibited Deptor expression at concentrations between 50nM BEZ235 and 1750nM BEZ235.

3.2.1.3 The effect of BEZ235 and BKM120 on cell proliferation in human and murine MM cells

To examine whether the inhibition of the PI3K and mTOR pathways with BEZ235 and BKM120 affected MM cell growth, human (U266, OPM2, NCI-H929, RPMI-8226 and WL2) and murine (5TGM1) MM cell lines were seeded in 96 well plates and treated with BEZ235 (1-100nM), BKM120 (125-2000nM) or vehicle alone (0.1% DMSO) for 1, 3, and 5 days. At each of these time points, the number of viable cells was determined using the WST-1 assay. As shown in left panels of Figures 3.7 and 3.8, human and murine cell lines cultured in the presence of the vehicle alone displayed a

Figure 3.1. BEZ235 and BKM120 mediate a dose-dependent inhibition of $p70^{S6k}$ phosphorylation but have no effect on Akt phosphorylation and Deptor expression in U266 cells. U266 cells were treated with BEZ235 (1-100nM), BKM120 (125-2000nM) or the vehicle alone (0.1% DMSO) for 4 hours and lysates prepared for immunoblotting. An RCDC protein assay was performed to ensure equal amounts of protein were loaded in each lane, and proteins (50ug/lane) were resolved on 10% SDS-PAGE gels. **(A)** Levels of phosphorylated Akt_{Ser473}, Akt_{Thr308}, and $p70^{S6K}$ and total Akt, $p70^{S6K}$ and Deptor protein expression were detected using Western immunoblotting. **(B)** The IC_{50} for BEZ235- and BKM120-mediated inhibition of $p70^{S6K}$ phosphorylation was determined using Graphpad Prism software.

A

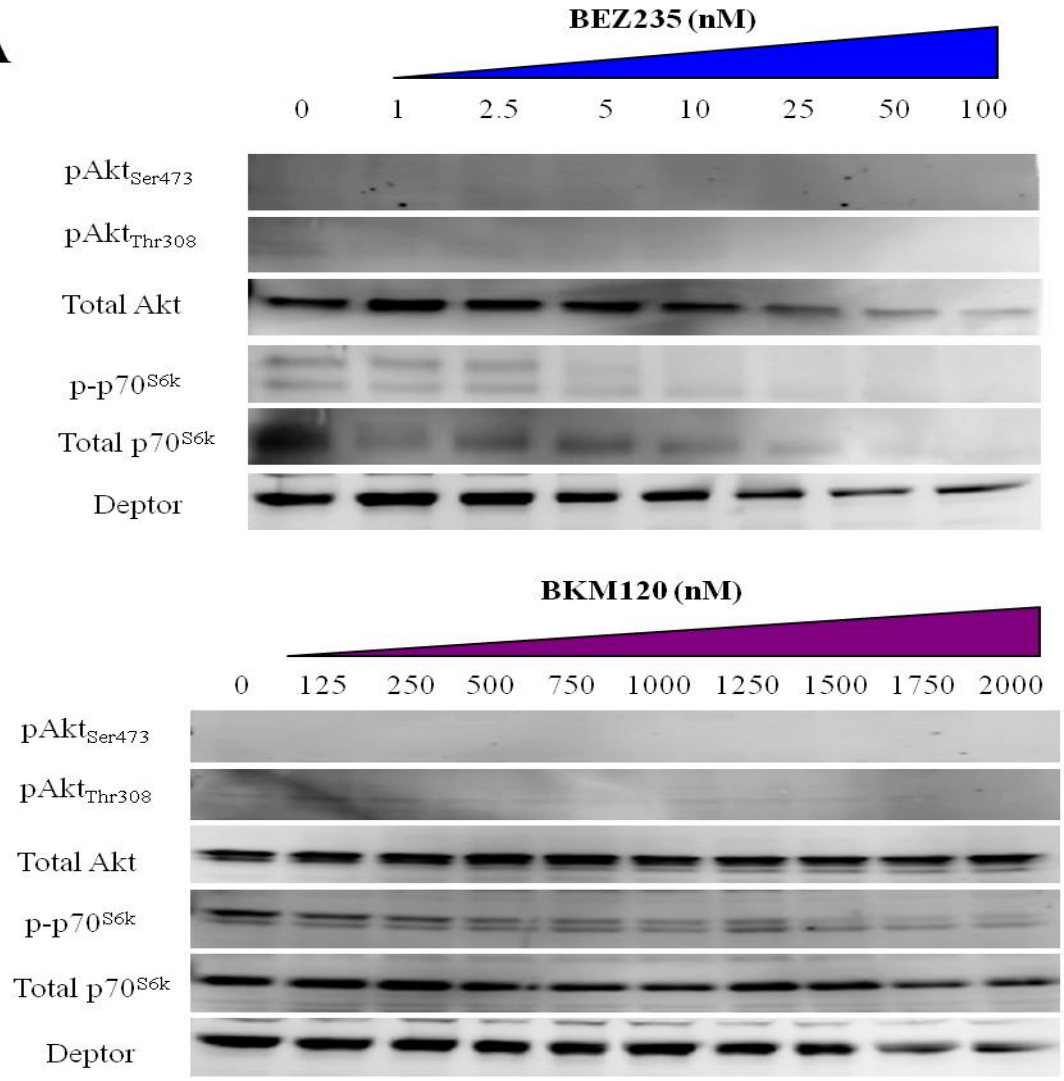

B

	pAkt^{Ser473} IC$_{50}$	pAkt^{Thr308} IC$_{50}$	P-p70^{S6k} IC$_{50}$
BEZ235	N/A	N/A	2nM 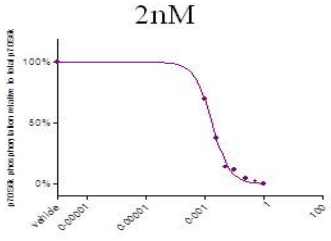
BKM120	N/A	N/A	411nM 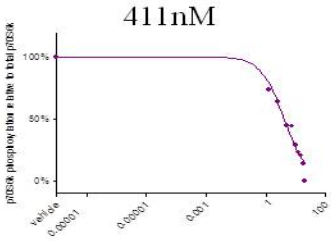

Figure 3.2. BEZ235 and BKM120 mediate a dose-dependent inhibition of $p70^{S6k}$ phosphorylation but have no effect on Akt phosphorylation and Deptor expression in OPM2 cells. OPM2 cells were treated with BEZ235 (1-100nM), BKM120 (125-2000nM) or the vehicle alone (0.1% DMSO) for 4 hours and lysates prepared for immunoblotting. An RCDC protein assay was performed to ensure equal amounts of protein were loaded in each lane, and proteins (50ug/lane) were resolved on 10% SDS-PAGE gels. **(A)** Levels of phosphorylated Akt_{Ser473}, Akt_{Thr308}, and $p70^{S6K}$ and total Akt, $p70^{S6K}$ and Deptor protein expression were detected using Western immunoblotting. **(B)** The IC_{50} for BEZ235- and BKM120-mediated inhibition of $p70^{S6K}$ phosphorylation was determined using Graphpad Prism software.

A

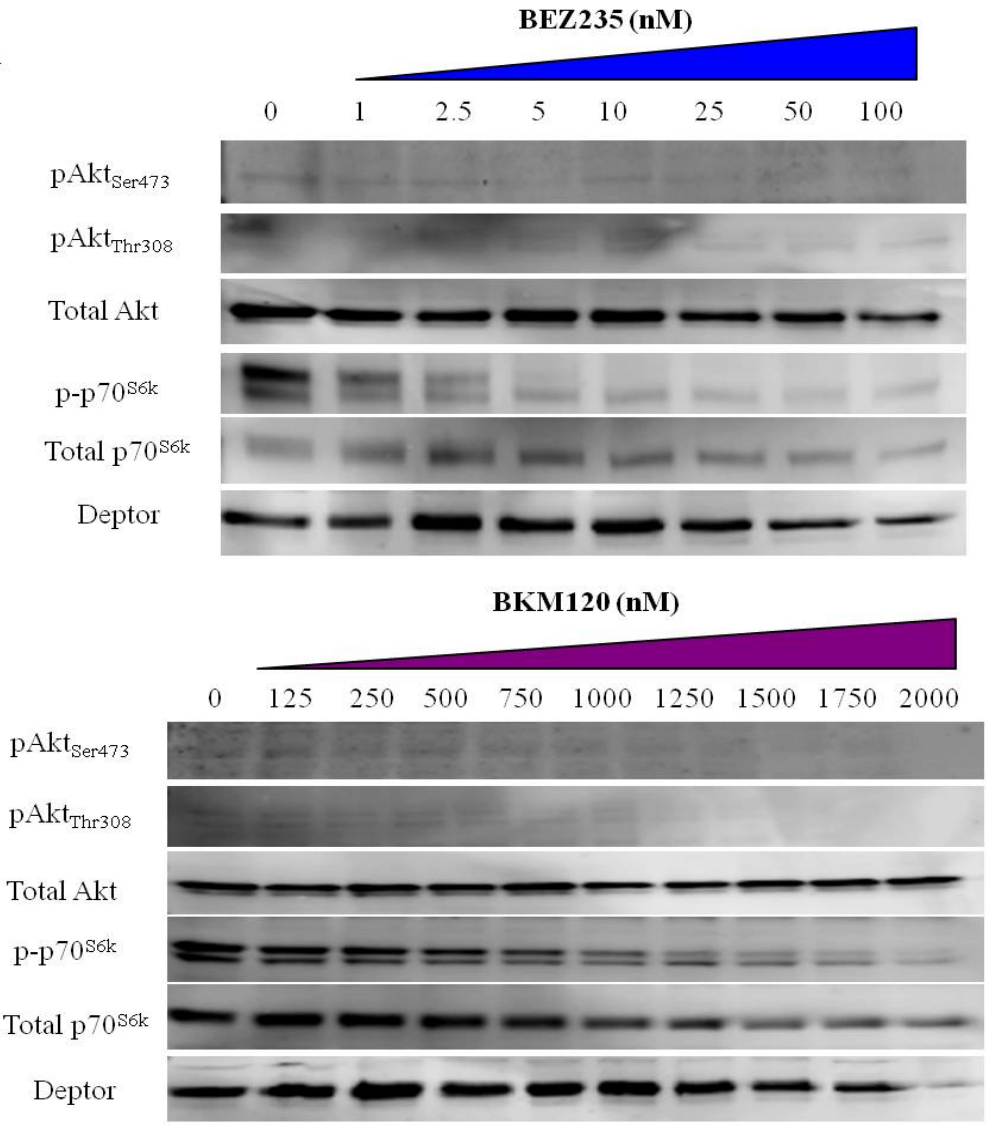

B

	pAkt^{Ser473} IC$_{50}$	pAkt^{Thr308} IC$_{50}$	P-p70^{S6k} IC$_{50}$
BEZ235	N/A	N/A	1nM 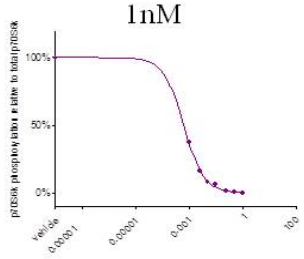
BKM120	N/A	N/A	175nM 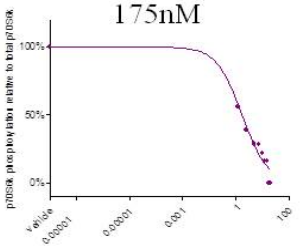

Figure 3.3. BEZ235 and BKM120 mediate a dose-dependent inhibition of $p70^{S6k}$ phosphorylation but have no effect on Akt phosphorylation and Deptor expression in NCI-H929 cells. NCI-H929 cells were treated with BEZ235 (1-100nM), BKM120 (125-2000nM) or the vehicle alone (0.1% DMSO) for 4 hours and lysates prepared for immunoblotting. An RCDC protein assay was performed to ensure equal amounts of protein were loaded in each lane, and proteins (50ug/lane) were resolved on 10% SDS-PAGE gels. **(A)** Levels of phosphorylated Akt_{Ser473}, Akt_{Thr308}, and $p70^{S6K}$ and total Akt, $p70^{S6K}$ and Deptor protein expression were detected using Western immunoblotting. **(B)** The IC_{50} for BEZ235- and BKM120-mediated inhibition of $p70^{S6K}$ phosphorylation was determined using Graphpad Prism software.

A

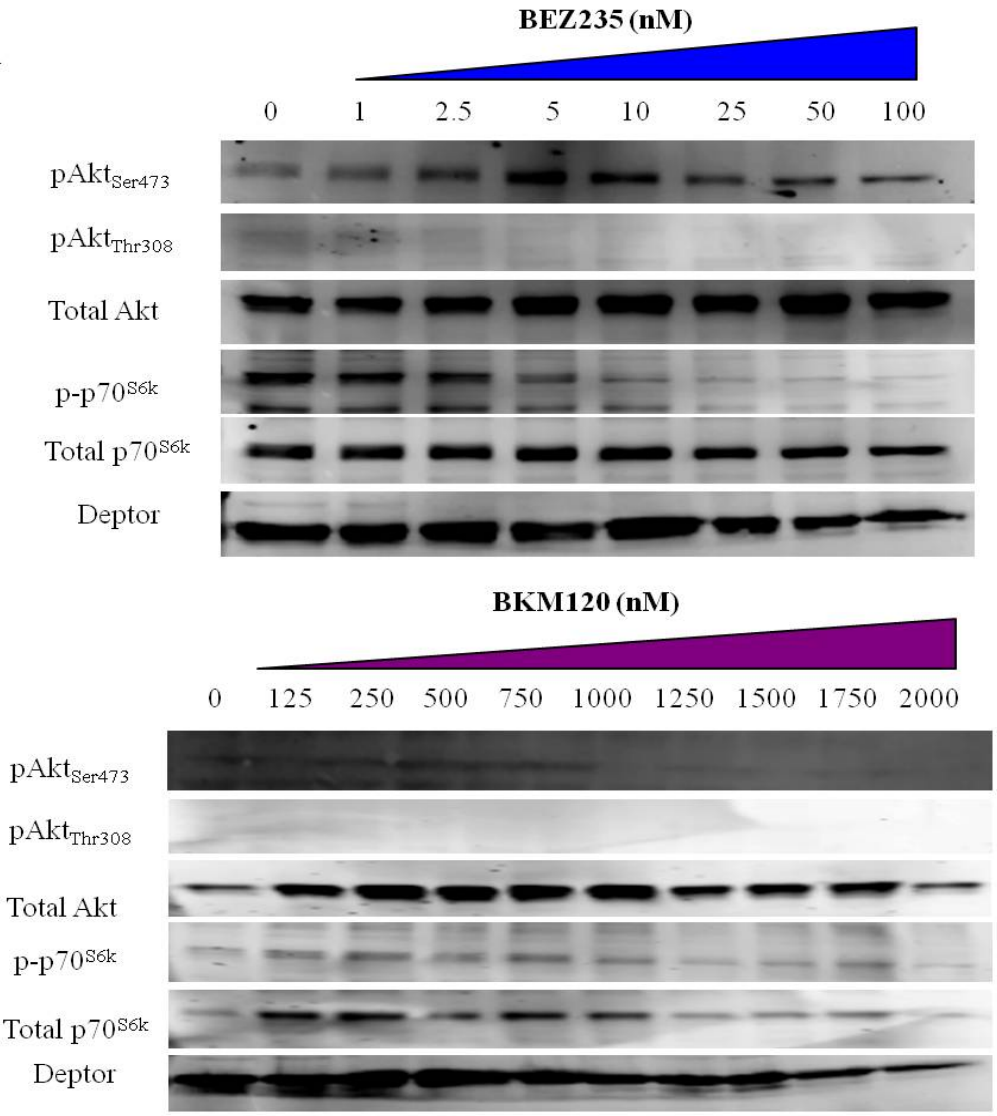

B

	pAkt^{Ser473} IC$_{50}$	pAkt^{Thr308} IC$_{50}$	P-p70^{S6k} IC$_{50}$
BEZ235	6nM 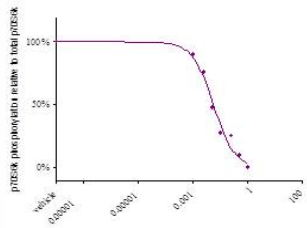	N/A	15nM 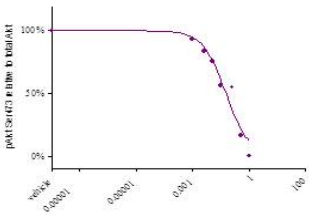
BKM120	905nM 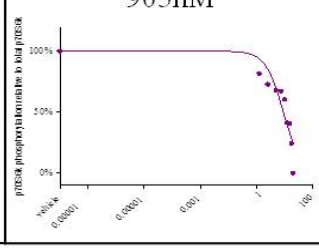	N/A	904nM 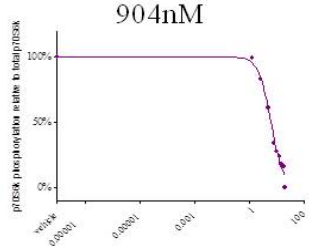

Figure 3.4. BEZ235 and BKM120 mediate a dose-dependent inhibition of $p70^{S6k}$ phosphorylation but have no effect on Akt phosphorylation and Deptor expression in RPMI-8226 cells. RPMI-8226 cells were treated with BEZ235 (1-100nM), BKM120 (125-2000nM) or the vehicle alone (0.1% DMSO) for 4 hours and lysates prepared for immunoblotting. An RCDC protein assay was performed to ensure equal amounts of protein were loaded in each lane, and proteins (50ug/lane) were resolved on 10% SDS-PAGE gels. **(A)** Levels of phosphorylated Akt_{Ser473}, Akt_{Thr308}, and $p70^{S6K}$ and total Akt, $p70^{S6K}$ and Deptor protein expression were detected using Western immunoblotting. **(B)** The IC_{50} for BEZ235- and BKM120-mediated inhibition of $p70^{S6K}$ phosphorylation was determined using Graphpad Prism software.

A

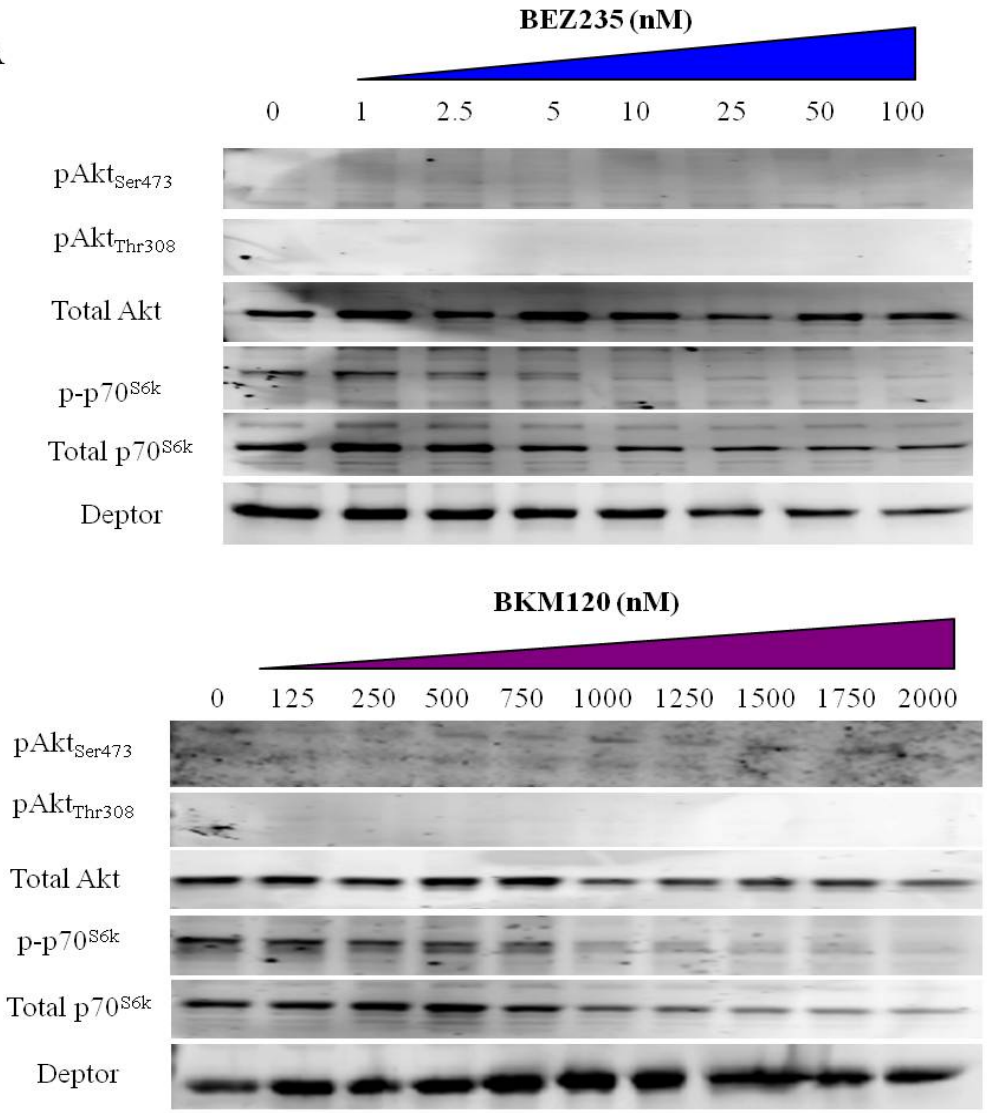

B

	pAkt^{Ser473} IC$_{50}$	pAkt^{Thr308} IC$_{50}$	P-p70^{S6k} IC$_{50}$
BEZ235	N/A	N/A	6.5nM 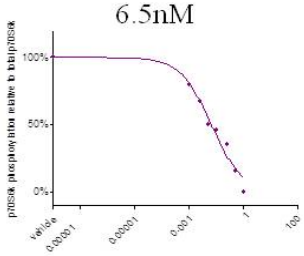
BKM120	N/A	N/A	614nM 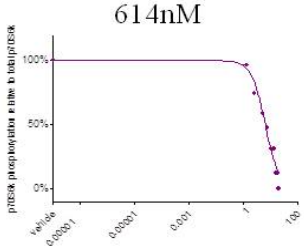

Figure 3.5. BEZ235 and BKM120 mediate dose-dependent inhibition of $p70^{S6k}$ phosphorylation but have no effect on Akt phosphorylation and Deptor expression in WL2 cells. WL2 cells were treated with BEZ235 (1-100nM), BKM120 (125-2000nM) or the vehicle alone (0.1% DMSO) for 4 hours and lysates prepared for immunoblotting. An RCDC protein assay was performed to ensure equal amounts of protein were loaded in each lane, and proteins (50ug/lane) were resolved on 10% SDS-PAGE gels. **(A)** Levels of phosphorylated Akt_{Ser473}, Akt_{Thr308}, and $p70^{S6K}$ and total Akt, $p70^{S6K}$ and Deptor protein expression were detected using Western immunoblotting. **(B)** The IC_{50} for BEZ235- and BKM120-mediated inhibition of $p70^{S6K}$ phosphorylation was determined using Graphpad Prism software.

A

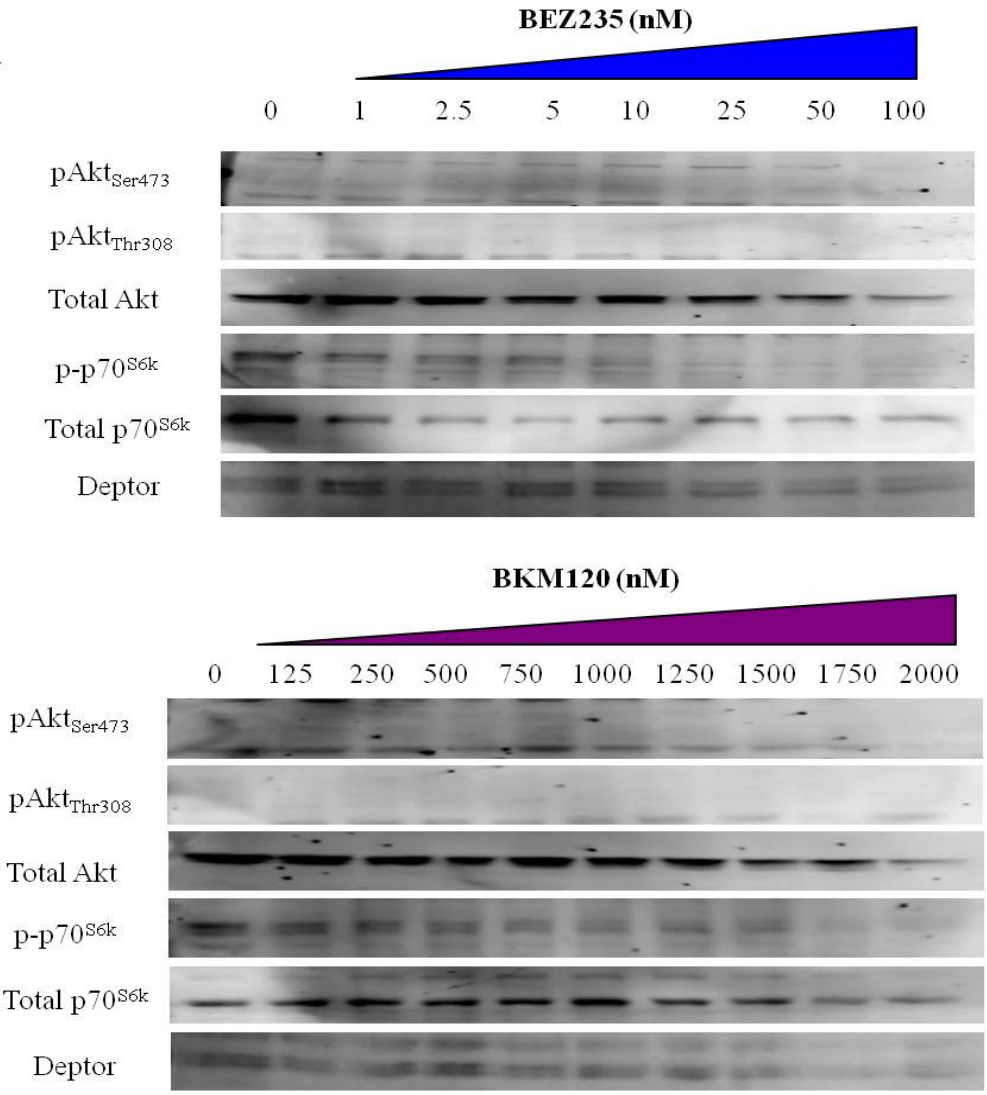

B

	pAkt^{Ser473} IC$_{50}$	pAkt^{Thr308} IC$_{50}$	P-p70^{S6k} IC$_{50}$
BEZ235	N/A	N/A	2nM 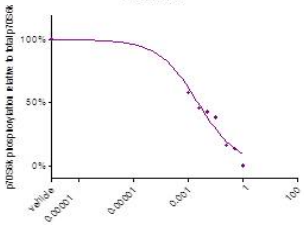
BKM120	N/A	N/A	87nM 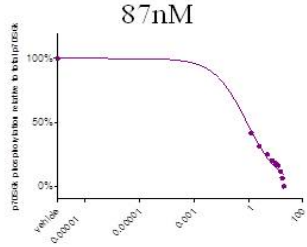

Figure 3.6. BEZ235 and BKM120 mediate dose-dependent inhibition of $p70^{S6k}$ phosphorylation but have no effect on Akt phosphorylation and Deptor expression in murine 5TGM1 cells. Murine 5TGM1 cells were treated with BEZ235 (1-100nM), BKM120 (125-2000nM) or the vehicle alone (0.1% DMSO) for 4 hours and lysates prepared for immunoblotting. An RCDC protein assay was performed to ensure equal amounts of protein were loaded in each lane, and proteins (50ug/lane) were resolved on 10% SDS-PAGE gels. **(A)** Levels of phosphorylated Akt_{Ser473}, Akt_{Thr308}, and $p70^{S6K}$ and total Akt, $p70^{S6K}$ and Deptor protein expression were detected using Western immunoblotting. **(B)** The IC_{50} for BEZ235- and BKM120-mediated inhibition of $p70^{S6K}$ phosphorylation was determined using Graphpad Prism software.

A

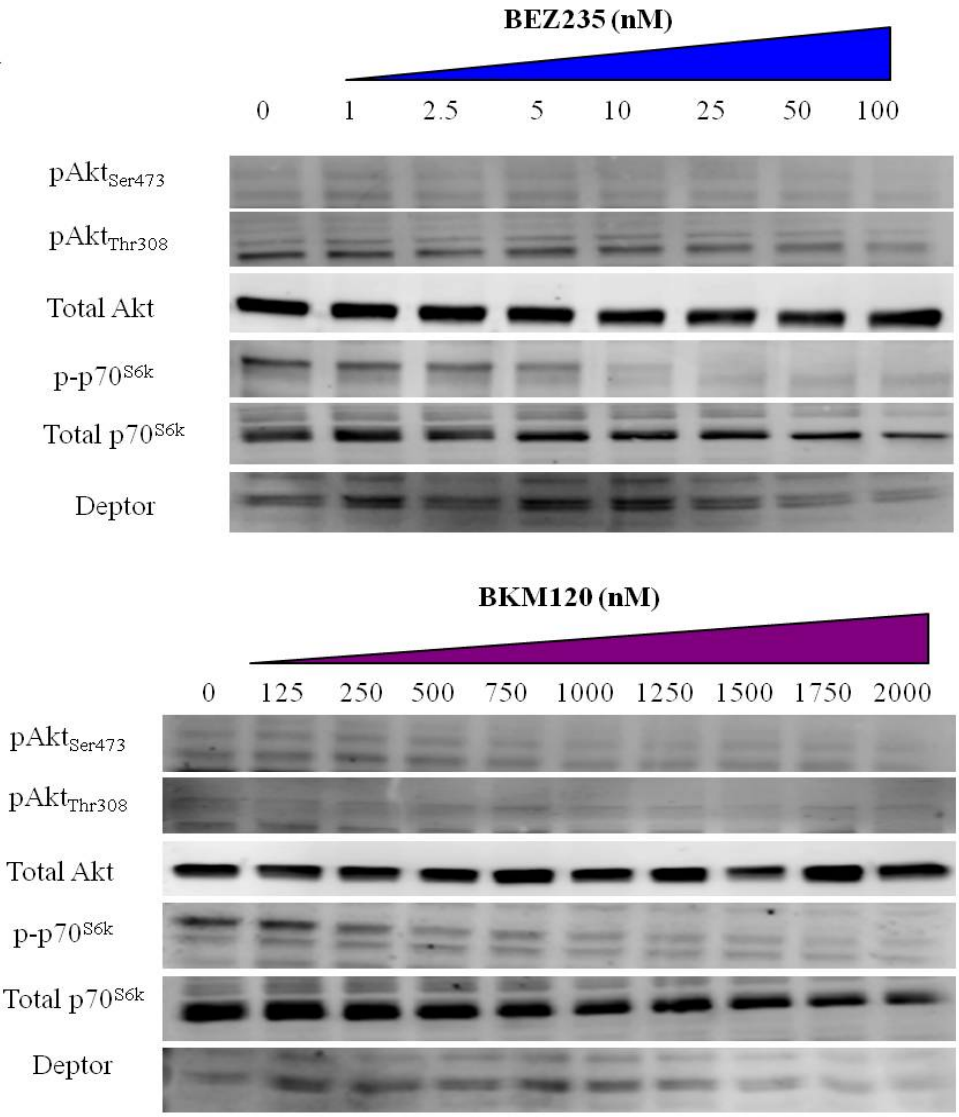

B

	pAkt^{Ser473}IC$_{50}$	pAkt^{Thr308}IC$_{50}$	P-p70^{S6k} IC$_{50}$
BEZ235	N/A	N/A	3nM 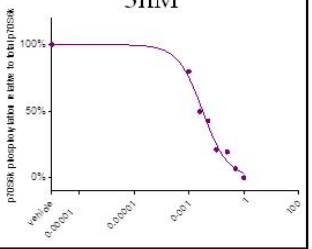
BKM120	N/A	N/A	461nM 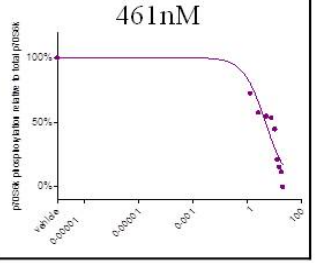

progressive increase in cell number over the 5 days of culture, with a plateau reached at day 5 as the cells reached confluence. In the presence of BEZ235, a dose-dependent decrease in cell number was observed, with a significant decrease in cell proliferation observed at concentrations of 1nM and higher (Figures 3.7 right panel, 3.8 right panel, $p < 0.05$; one-way ANOVA).

As shown in the left panels of Figures 3.9 and 3.10, MM cells cultured in the presence of BKM120 demonstrated a dose-dependent decrease in cell proliferation when compared with vehicle alone, with a significant decrease in cell proliferation observed at concentrations of 125nM and higher (Figures 3.9 right panel, 3.10 right panel, $p < 0.01$; one-way ANOVA). The IC_{50} for BEZ235 and BKM120-mediated inhibition of cell growth in each MM cell line is summarised in Table 3.1.

3.2.1.4 The effect of PIK75 on cell proliferation in human and murine MM cells

As shown in Section 3.2.1.1 the phosphorylation of Akt was not observed in all MM cell lines examined, with the exception of the human MM cell line, NCI-H929. As such, we next investigated whether the p110 subunit of the PI3k receptor was active. To do this, human (U266, OPM2, NCI-H929, RPMI-8226 and WL2) and murine (5TGM1) MM cells were seeded in 96 well plates and treated with PIK-75, a p110α inhibitor[26] (1-100nM) or vehicle alone (0.1% DMSO) for 1, 3, and 5 days. At each of these time points, the number of viable cells was evaluated using the WST-1 assay. As shown in Figures 3.11 and 3.12, MM cells cultured in the presence of PIK-75 resulted in a dose-dependent decrease in cell proliferation was observed when compared to vehicle alone, with a significant decrease in cell proliferation observed at concentrations of 1nM and higher (Figures 3.11 right panel, 3.12 right panel, $p < 0.01$; one-way ANOVA). The ability of PIK-75 to inhibit MM cell proliferation suggests that the p110 subunit of the PI3k receptor is active in these cell lines.

3.2.2 The effect of BEZ235 and BKM120 on apoptosis in human and murine MM cell lines *in vitro*

3.2.2.1 The effect of BEZ235 and BKM120 on Cyclin D1 expression, Caspase-3 and Caspase-9 phosphorylation in MM cell lines in vitro

To determine whether BEZ235 and BKM120 induces apoptosis of the MM cell lines, human (U266, OPM2, NCI-H929, RPMI-8226 and WL2) and murine (5TGM1) cells

Figure 3.7. BEZ235 inhibits the proliferation of U266, OPM2 and NCI-H929 human myeloma cell lines *in vitro*. Human myeloma cells **(A)** U266, **(B)** OPM2 and **(C)** NCI-H929 were seeded at a density of 10,000 cells/well in 96-well tissue culture plates and cultured in the presence of 0-100nM BEZ235 for 5 days. At day 0, 1, 3, and 5 time points, the number of proliferating cells was assessed using WST-1 reagent. **(Left panels)** WST-1 data were plotted for each cell line over the 5-day time course. Data are expressed as the mean ± standard deviation of replicate samples of a representative experiment of three. **(Right panels)** The significance of the inhibition of the human myeloma cells growth was determined from day 5 results. *$p<0.05$, **$p<0.01$ and ***$p<0.001$, compared to vehicle, one-way ANOVA.

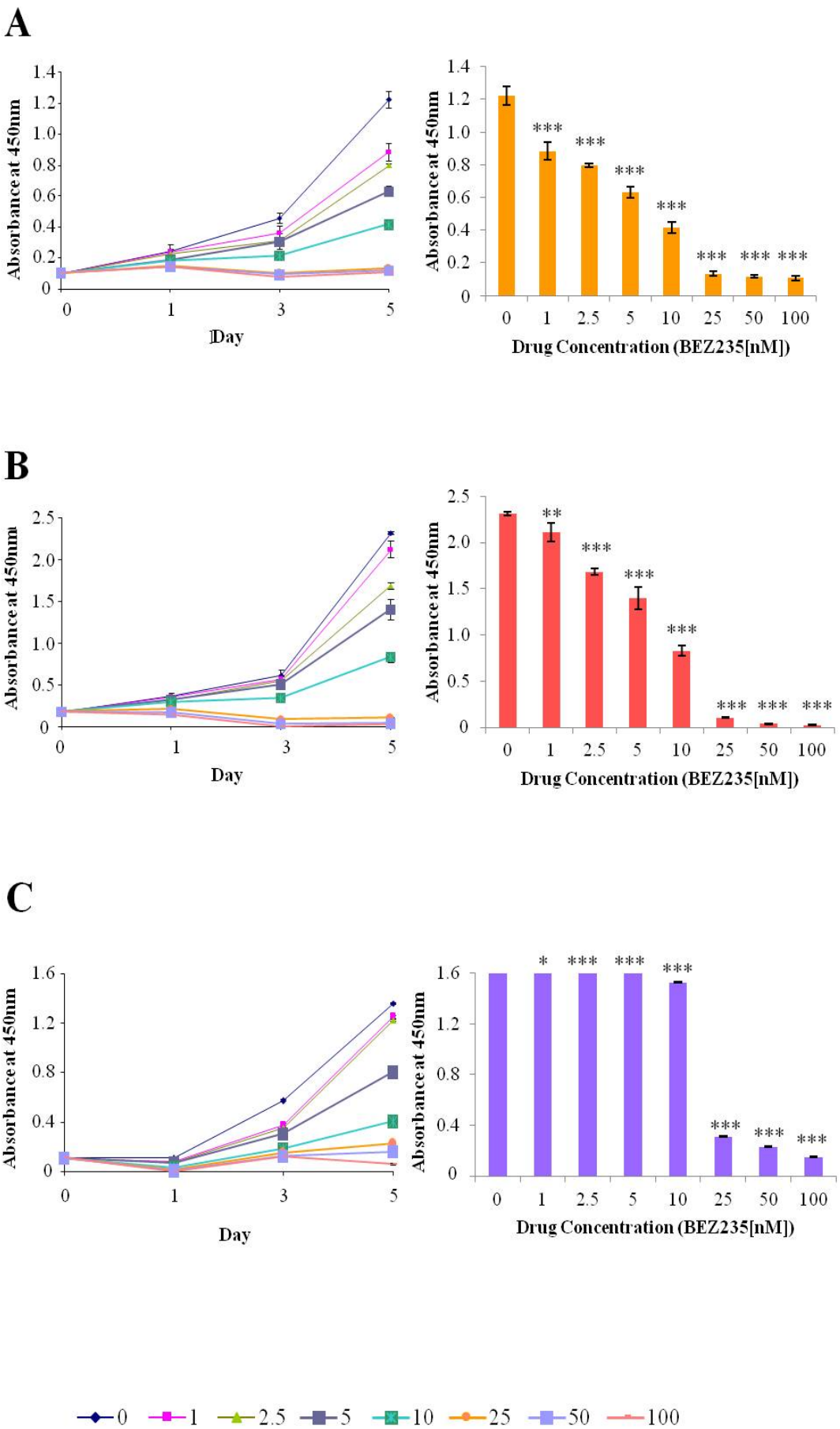
A
Absorbance at 450nm
Day
Drug Concentration (BEZ235[nM])
B
Absorbance at 450nm
Day
Drug Concentration (BEZ235[nM])
C
Absorbance at 450nm
Day
Drug Concentration (BEZ235[nM])
0
1
2.5
5
10
25
50
100

Figure 3.8. BEZ235 inhibits the proliferation of RPMI-8226 and WL2 human myeloma cell lines and murine 5TGM1 myeloma cell lines *in vitro*. Human myeloma cells **(A)** RPMI-8226 and **(B)** WL2 and **(C)** murine 5TGM1 myeloma cells were seeded at a density of 10,000 cells/well in 96-well tissue culture plates and cultured in the presence of 0-100nM BEZ235 for 5 days. At day 0, 1, 3, and 5 time points, the number of proliferating cells was assessed using WST-1 reagent. **(Left panels)** WST-1 data were plotted for each cell line over the 5 day time course. Data are expressed as the mean ± standard deviation of replicate samples of a representative experiment of three. **(Right panels)** The significance of the inhibition of the human myeloma cells growth was determined from day 5 results. ***$p<0.001$, compared to vehicle, one-way ANOVA.

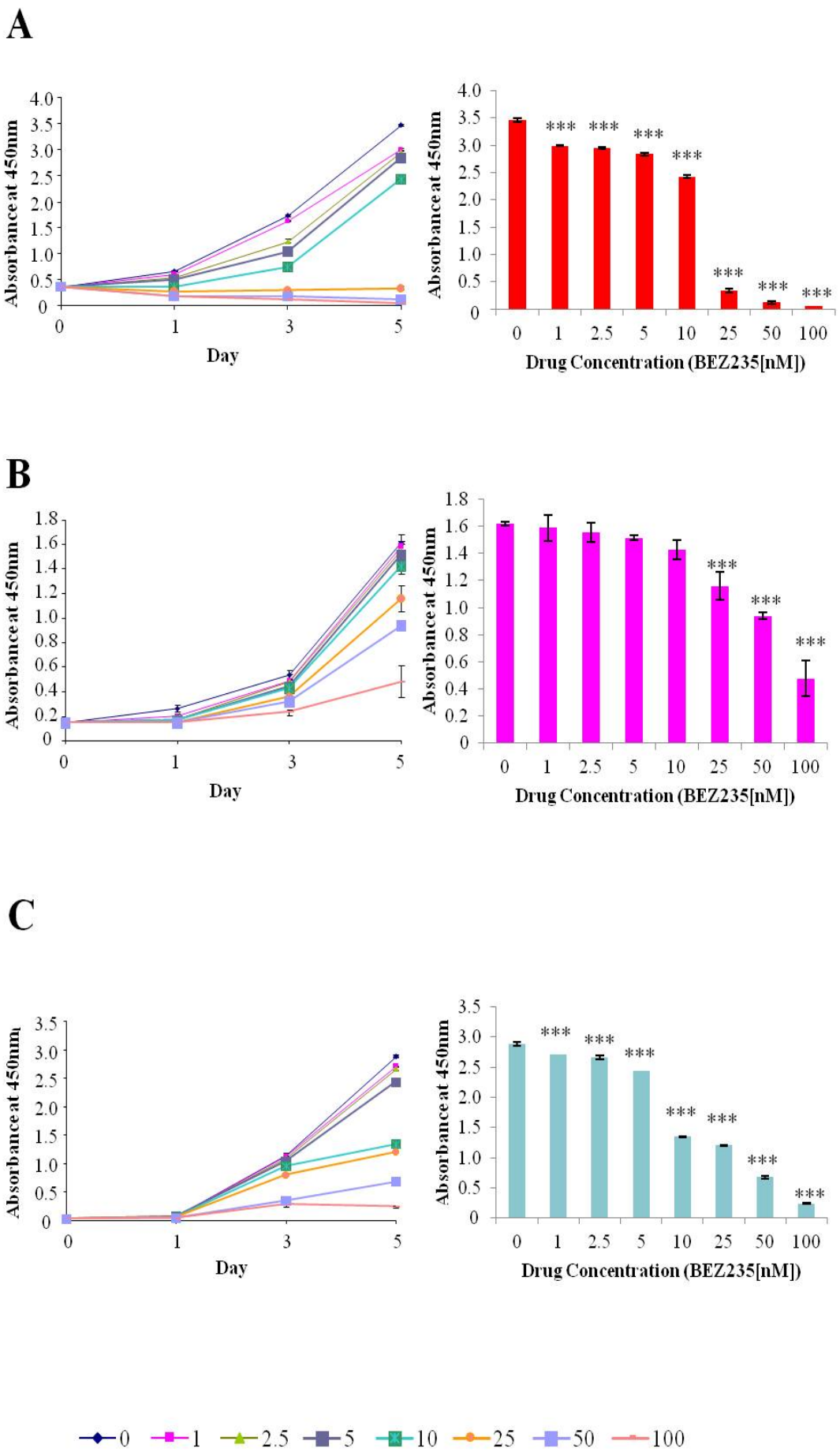
A
Absorbance at 450nm
Day
Drug Concentration (BEZ235[nM])
B
Absorbance at 450nm
Day
Drug Concentration (BEZ235[nM])
C
Absorbance at 450nm
Day
Drug Concentration (BEZ235[nM])
0
1
2.5
5
10
25
50
100

Figure 3.9. BKM120 inhibits the proliferation of U266, OPM2 and NCI-H929 human myeloma cell lines *in vitro*. Human myeloma cells **(A)** U266, **(B)** OPM2 and **(C)** NCI-H929 were seeded at a density of 10,000 cells/well in 96-well tissue culture plates and cultured in the presence of 0-2000nM BKM120 for 5 days. At day 0, 1, 3, and 5 time points, the number of proliferating cells was assessed using WST-1 reagent. **(Left panels)** WST-1 data were plotted for each cell line over the 5 day time course. Data are expressed as the mean ± standard deviation of replicate samples of a representative experiment of three. **(Right panels)** The significance of the inhibition of the human myeloma cell line growth was determined from day 5 results. **$p<0.01$ and ***$p<0.001$, compared to vehicle, one-way ANOVA.

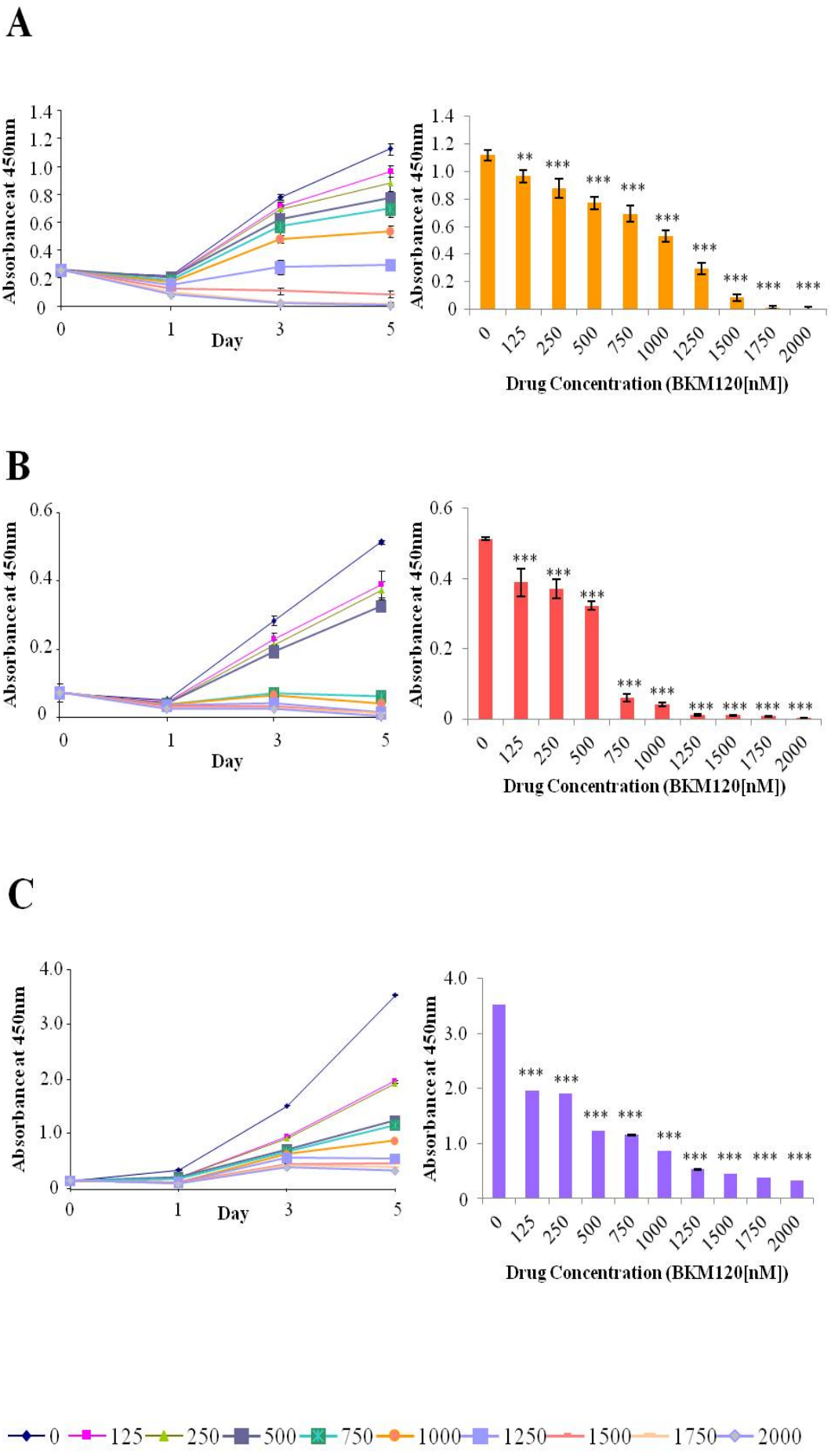
A
Absorbance at 450nm
Day
Drug Concentration (BKM120[nM])
B
Absorbance at 450nm
Day
Drug Concentration (BKM120[nM])
C
Absorbance at 450nm
Day
Drug Concentration (BKM120[nM])
0
125
250
500
750
1000
1250
1500
1750
2000

Figure 3.10. BKM120 inhibits the proliferation RPMI-8226 and WL2 human myeloma cell lines and murine 5TGM1 myeloma cell lines *in vitro*. Human myeloma cells **(A)** RPMI-8226 and **(B)** WL2 and **(C)** murine 5TGM1 myeloma cells were seeded at a density of 10,000 cells/well in 96-well tissue culture plates and cultured in the presence of 0-2000nM BKM120 for 5 days. At day 0, 1, 3, and 5 time points, the number of proliferating cells was assessed using WST-1 reagent. **(Left panels)** WST-1 data were plotted for each cell line over the 5-day time course. Data are expressed as the mean ± standard deviation of replicate samples of a representative experiment of three. **(Right panels)** The significance of the inhibition of the human myeloma cells growth was determined from day 5 results. ***$p<0.001$, compared to vehicle, one-way ANOVA.

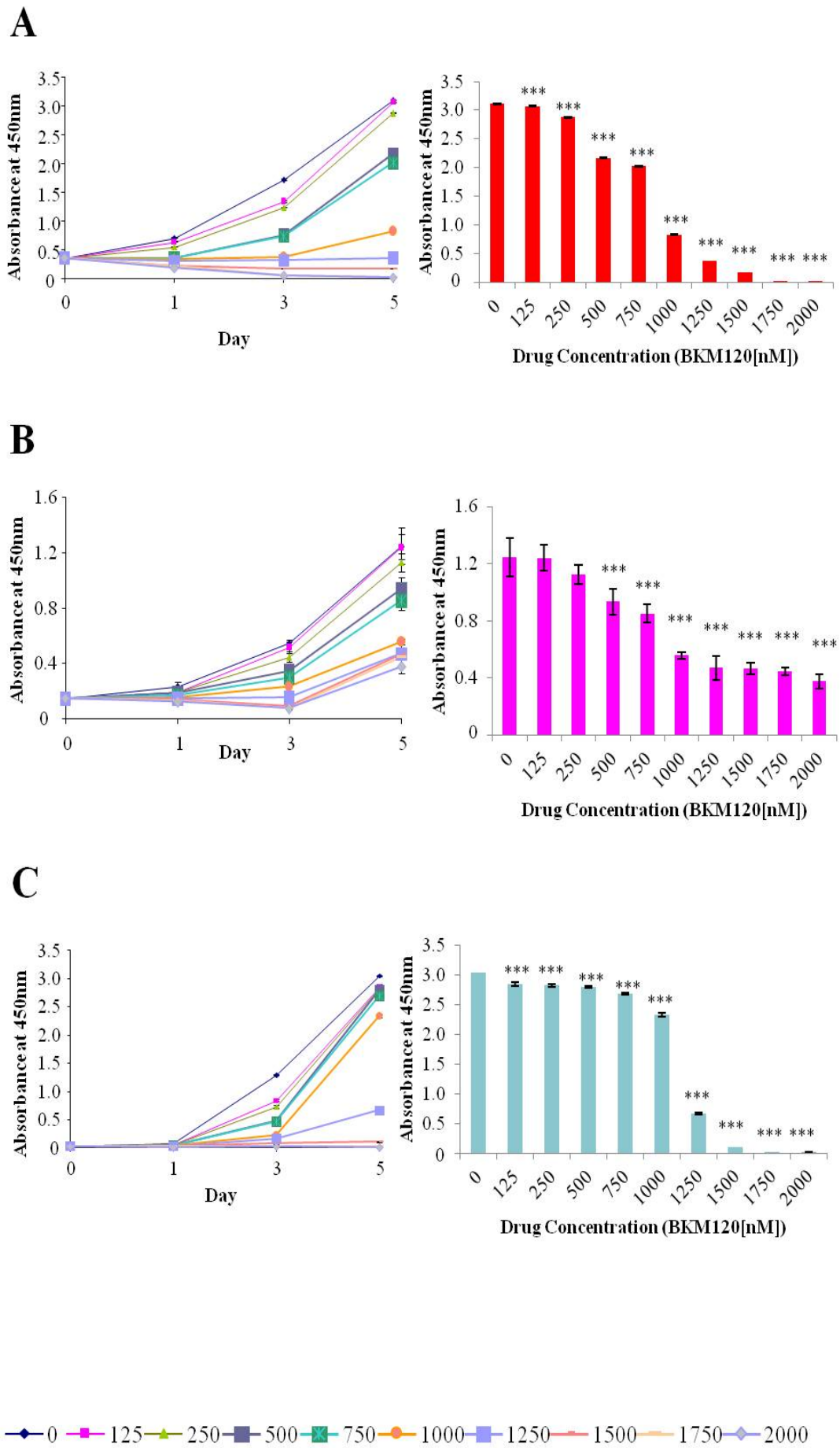
A
Absorbance at 450nm
Day
Drug Concentration (BKM120[nM])
B
Absorbance at 450nm
Day
Drug Concentration (BKM120[nM])
C
Absorbance at 450nm
Day
Drug Concentration (BKM120[nM])
0
125
250
500
750
1000
1250
1500
1750
2000

Table 3.1 BEZ235 and BKM120 WST-1 cell proliferation assay IC_{50}

Cell Line	BEZ235 IC_{50}	BKM120 IC_{50}
U266	4nM	785nM
OPM2	6nM	432nM
NCI-H929	7nM	395nM
RPMI-8226	12nM	765nM
WL2	56nM	1048nM
Murine 5TGM1-SFG	15nM	1111nM

Figure 3.11. PIK-75 inhibits the proliferation of U266, OPM2 and NCI-H929 human myeloma cell lines *in vitro*. Human myeloma cells **(A)** U266, **(B)** OPM2 and **(C)** NCI-H929 were seeded at a density of 10,000 cells/well in 96-well tissue culture plates and cultured in the presence of 0-100nM PIK-75 for 5 days. At day 0, 1, 3, and 5 time points, the number of proliferating cells was assessed using WST-1 reagent. **(Left panels)** PIK-75 WST-1 data were plotted for each cell line over the 5-day time course. Data are expressed as the mean ± standard deviation of replicate samples of a representative experiment of three. **(Right panels)** The significance of the inhibition of the human myeloma cells growth was determined from day 5 results. ***$p<0.001$, compared to vehicle, one-way ANOVA.

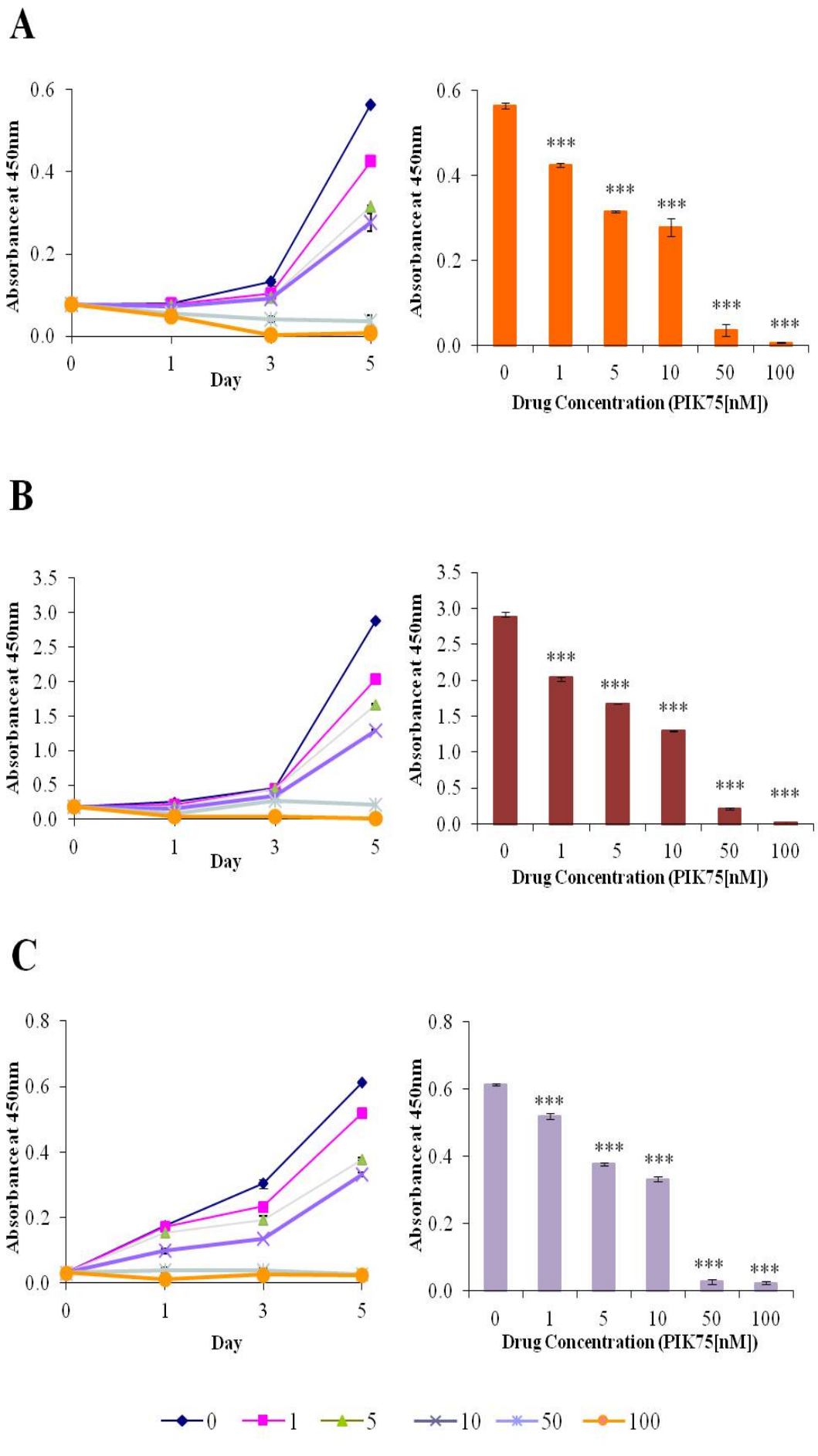
A
Absorbance at 450nm
0.6
0.4
0.2
0.0
0
1
3
5
Day
***
Drug Concentration (PIK75[nM])
0
1
5
10
50
100
B
3.5
3.0
2.5
2.0
1.5
1.0
0.5
C
0.8
0.6
0.4
0.2
0
1
5
10
50
100

Figure 3.12. PIK-75 inhibits the proliferation of RPMI-8226 and WL2 human myeloma cell lines and murine 5TGM1 myeloma cell lines *in vitro*. Human myeloma cells **(A)** RPMI-8226 and **(B)** WL2 and **(C)** murine 5TGM1 myeloma cells were seeded at a density of 10,000 cells/well in 96-well tissue culture plates and cultured in the presence of 0-100nM PIK-75 for 5 days. At day 0, 1, 3, and 5 time points, the number of proliferating cells was assessed using WST-1 reagent. **(Left panels)** PIK-75-WST-1 data were plotted for each cell line over the 5-day time course. Data are expressed as the mean ± standard deviation of replicate samples of a representative experiment of three. **(Right panels)** The significance of the inhibition of the human myeloma cells growth was determined from day 5 results. **p<0.01 and ***p<0.001, compared to vehicle, one-way ANOVA.

Mapsoft TOCBuilder Tryout

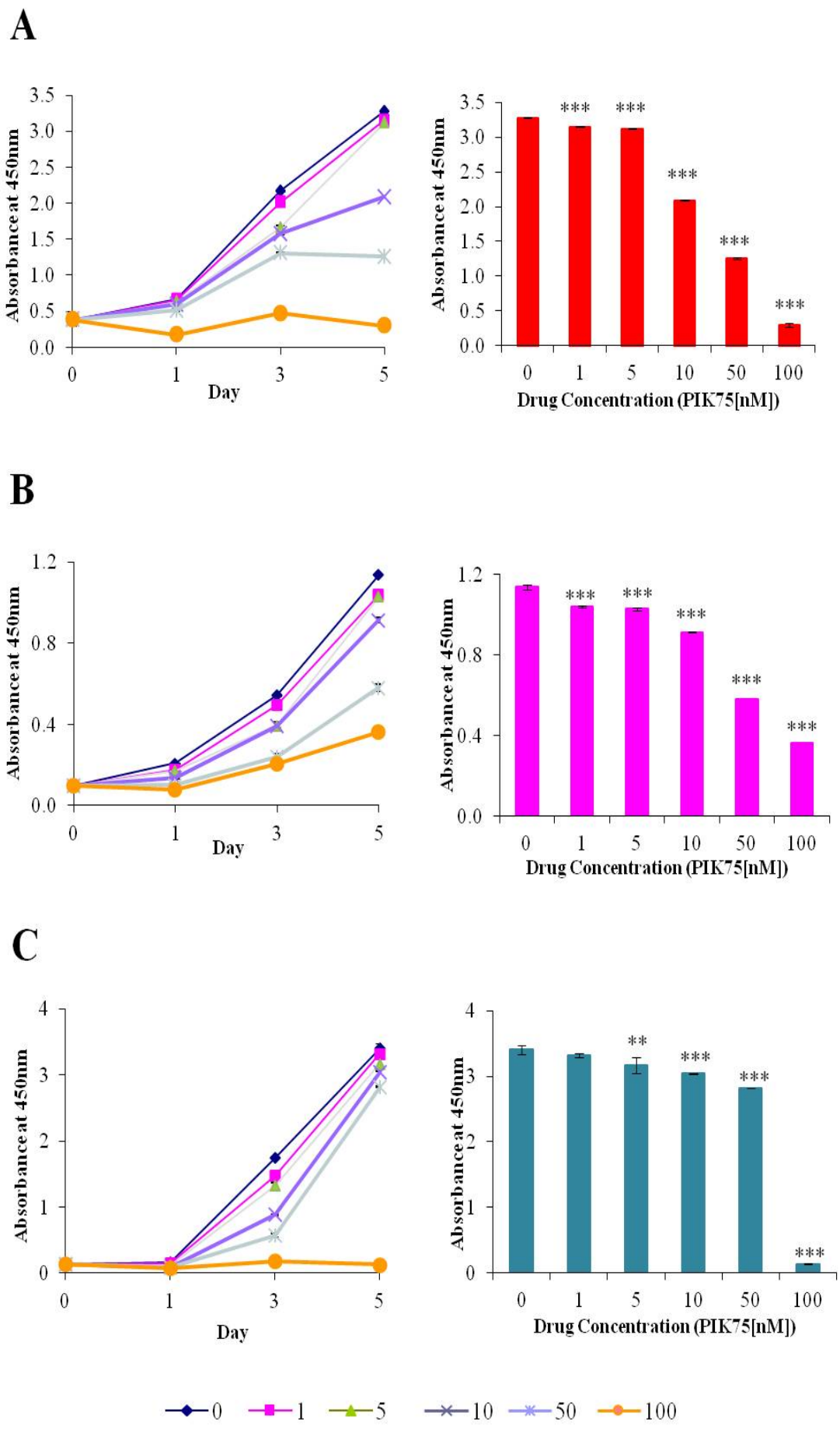
A
Absorbance at 450nm
Day
Drug Concentration (PIK75[nM])
***
B
Absorbance at 450nm
Day
Drug Concentration (PIK75[nM])
***
C
Absorbance at 450nm
Day
Drug Concentration (PIK75[nM])
**
***
0
1
5
10
50
100

were treated with BEZ235 (1-100nM), BKM120 (125-2000nM) or vehicle alone (0.1% DMSO) for 18 hours prior to the preparation of cell lysates. The cell lysates were then examined by Western immunoblot to determine the effects of BEZ235 and BKM120 on phosphorylation of Caspase-3 and Caspase-9 (markers of apoptosis) and Cyclin D1 (marker of cell cycle cycle). As shown in Figures 3.13A, 3.15A and 3.16A, BEZ235 and BKM120 inhibit the expression of Cyclin D1 in a dose dependent manner from 10nM BEZ235 and 500nM BKM120. While BEZ235 did not inhibit the expression of Cyclin D1 in WL2 and 5TGM1 cell lines, BKM120 inhibited the expression of Cyclin D1 in a dose dependent manner from 750nM BKM120 in WL2 and 5TGM1 cell lines (Figures 3.17A and 3.18A). In contrast, the phosphorylation of Caspase-3 and Caspase-9 was not observed in any of the cell lines examined, and the expression of Cyclin D1 was not affected in OPM2 cell line (Figure 3.14A) in response to either BEZ235 or BKM120 treatment.

Quantitation of the intensity of the expression of Cyclin D1 bands enabled the determination of the IC_{50} for inhibition of BEZ235 and BKM120 on the expression of Cyclin D1 (Figures 3.13B, 3.15B, 3.16B, 3.17B and 3.18B). The results suggest that both BEZ235 and BKM120 inhibit cell cycle progression.

3.2.2.2 The effect of BEZ235 and BKM120 on MM cell apoptosis in vitro

To further examine the effects of BEZ235 and BKM120 on human and murine MM cell apoptosis, human (U266, OPM2, NCI-H929, RPMI-8226 and WL2) and murine 5TGM1 MM cell lines were incubated with ½ IC_{50}, IC_{50} and 2x IC_{50} BEZ235 (see IC_{50} data in Table 3.1), ½ IC_{50}, IC_{50} and 2x IC_{50} BKM120 (see IC_{50} data in Table 3.1), or vehicle alone (0.1% DMSO) for 18 hours. The cells were then stained with AnnV (marker of early apoptosis) and 7AAD (marker of necrotic cells) and analysed immediately using the Coulter Cytomics FC500 Series flow cytometer. These markers enable the analysis of 4 distinct cell populations: viable cells (AnnV-/7AAD-), cells undergoing early apoptosis (AnnV+/7AAD-), cells in late apoptosis (AnnV-/7AAD+) and dead cells (AnnV+/7AAD+).

A representation of the dot plots illustrating the percentage and distribution of the 4 cell populations for each BEZ235 treatments is shown in Figure 3.19A. Graphical representations of the 4 cell populations of each BEZ235-treated human (U266, OPM2, NCI-H929 and WL2) and murine 5TGM1 MM cell lines showed that less than 5% of

Figure 3.13. BEZ235 and BKM120 mediate a dose-dependent inhibition of Cyclin D1 but have no effect on Caspase 3 and Caspase 9 phosphorylation in U266 cells. U266 cells were treated with BEZ235 (1-100nM), BKM120 (125-2000nM) or the vehicle alone (0.1% DMSO) for 18 hours and lysates prepared for immunoblotting. An RCDC protein assay was performed to ensure equal amounts of protein were loaded in each lane, and proteins (50ug/lane) were resolved on 10% SDS-PAGE gels. **(A)** Levels of active Caspase 3, active Caspase 9, Cyclin D1 and α-tubulin protein were detected using Western immunoblotting. **(B)** The IC_{50} for BEZ235- and BKM120-mediated inhibition of Cyclin D1 was determined using Graphpad Prism software.

A

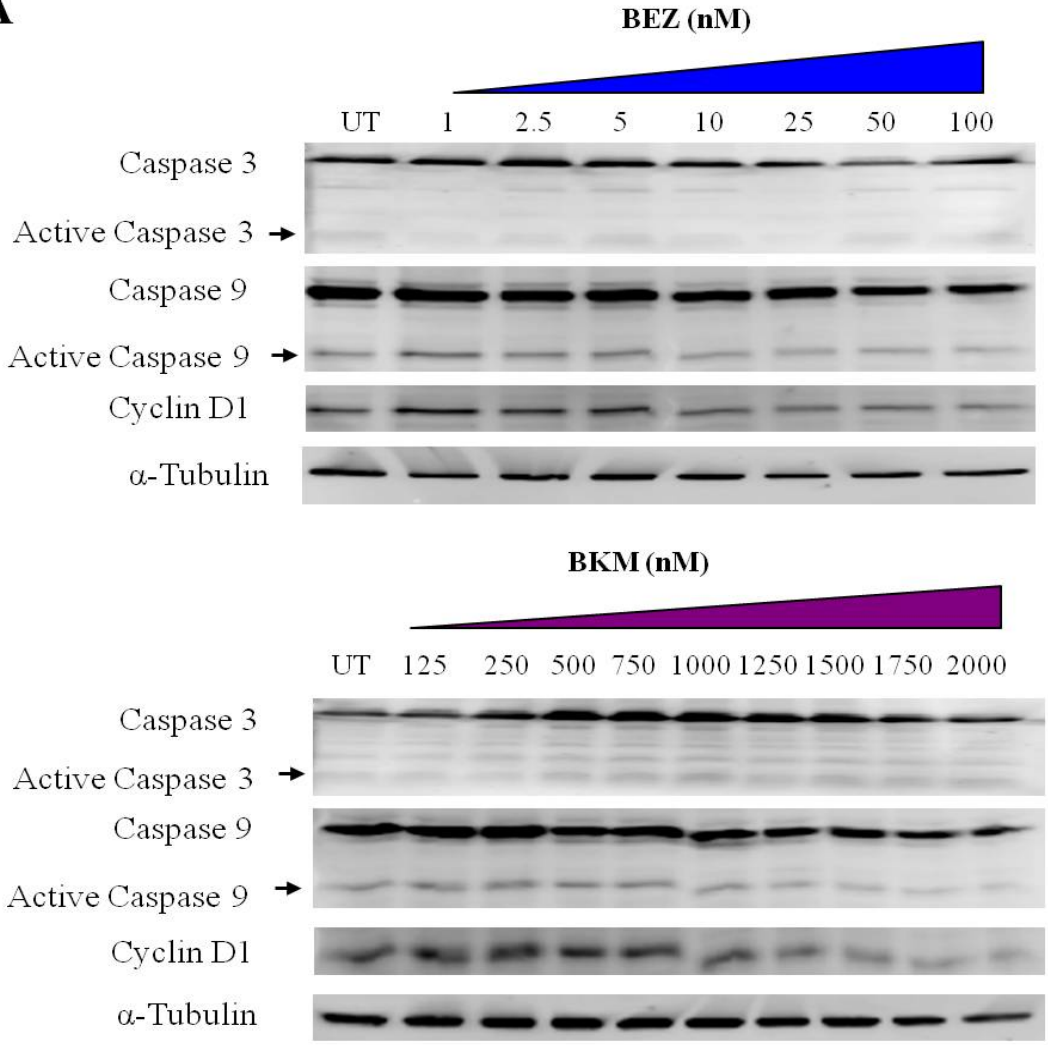

B

	Active Caspase 3 IC_{50}	Active Capase 9 IC_{50}	Cyclin D1 IC_{50}
BEZ235	N/A	N/A	9.7nM 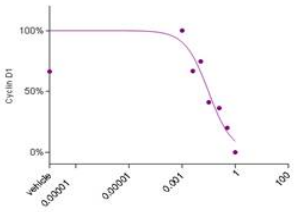
BKM120	N/A	N/A	1164nM 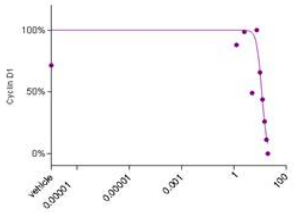

Figure 3.14. BEZ235 and BKM120 have no effect on Caspase 3, Caspase 9 and Cyclin D1 phosphorylation in OPM2 cells. OPM2 cells were treated with BEZ235 (1-100nM), BKM120 (125-2000nM) or the vehicle alone (0.1% DMSO) for 18 hours and lysates prepared for immunoblotting. An RCDC protein assay was performed to ensure equal amounts of protein were loaded in each lane, and proteins (50ug/lane) were resolved on 10% SDS-PAGE gels. **(A)** Levels of active Caspase 3, active Caspase 9, Cyclin D1 and α-tubulin protein were detected using Western immunoblotting. **(B)** The IC_{50} for BEZ235- and BKM120-mediated inhibition of Cyclin D1 was determined using Graphpad Prism software.

A

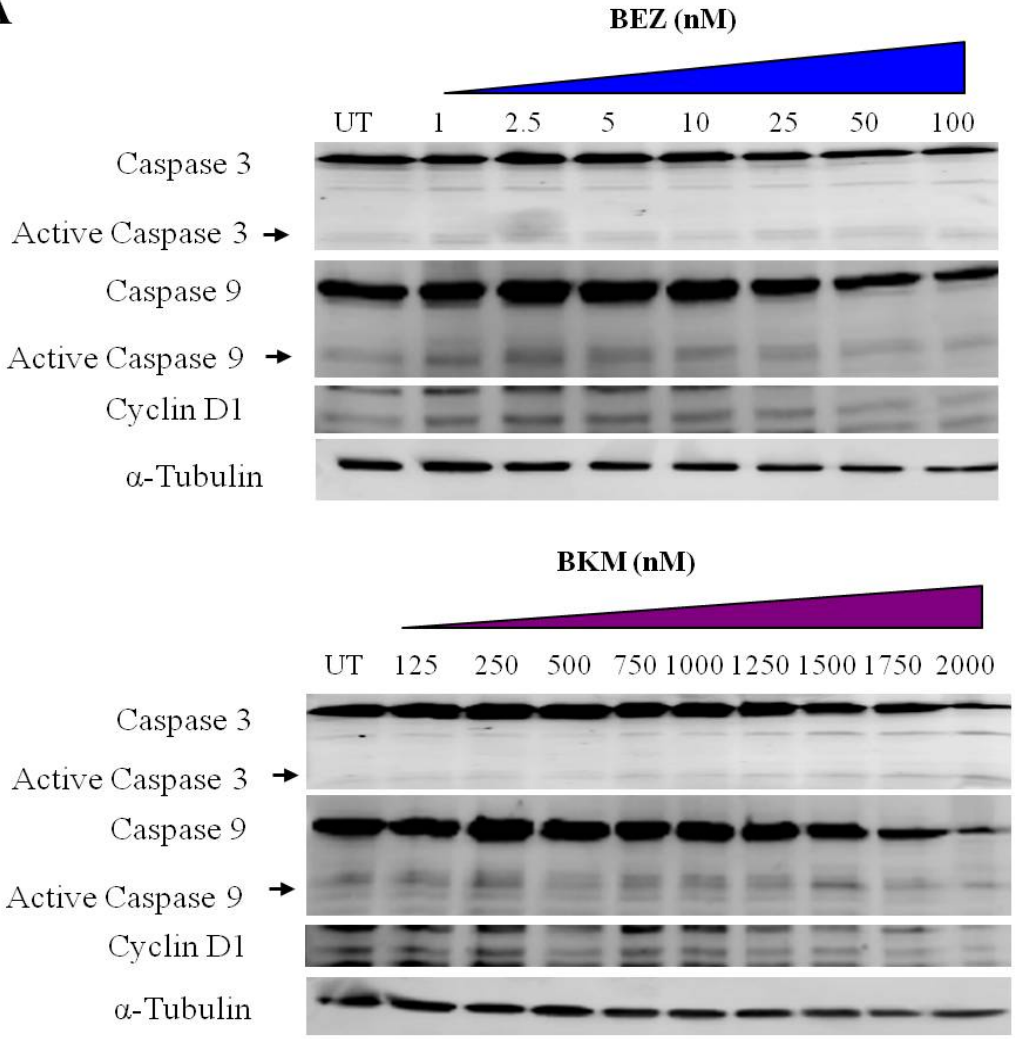

B

	Active Caspase 3 IC_{50}	Active Capase 9 IC_{50}	Cyclin D1 IC_{50}
BEZ235	N/A	N/A	N/A
BKM120	N/A	N/A	N/A

Figure 3.15. BEZ235 and BKM120 mediate a dose-dependent inhibition of Cyclin D1 but have no effect on Caspase 3 and Caspase 9 phosphorylation in NCI-H929 cells. NCI-H929 cells were treated with BEZ235 (1-100nM), BKM120 (125-2000nM) or the vehicle alone (0.1% DMSO) for 18 hours and lysates prepared for immunoblotting. An RCDC protein assay was performed to ensure equal amounts of protein were loaded in each lane, and proteins (50ug/lane) were resolved on 10% SDS-PAGE gels. **(A)** Levels of active Caspase 3, active Caspase 9, Cyclin D1 and α-tubulin protein were detected using Western immunoblotting. **(B)** The IC_{50} for BEZ235- and BKM120-mediated inhibition of Cyclin D1 was determined using Graphpad Prism software.

A

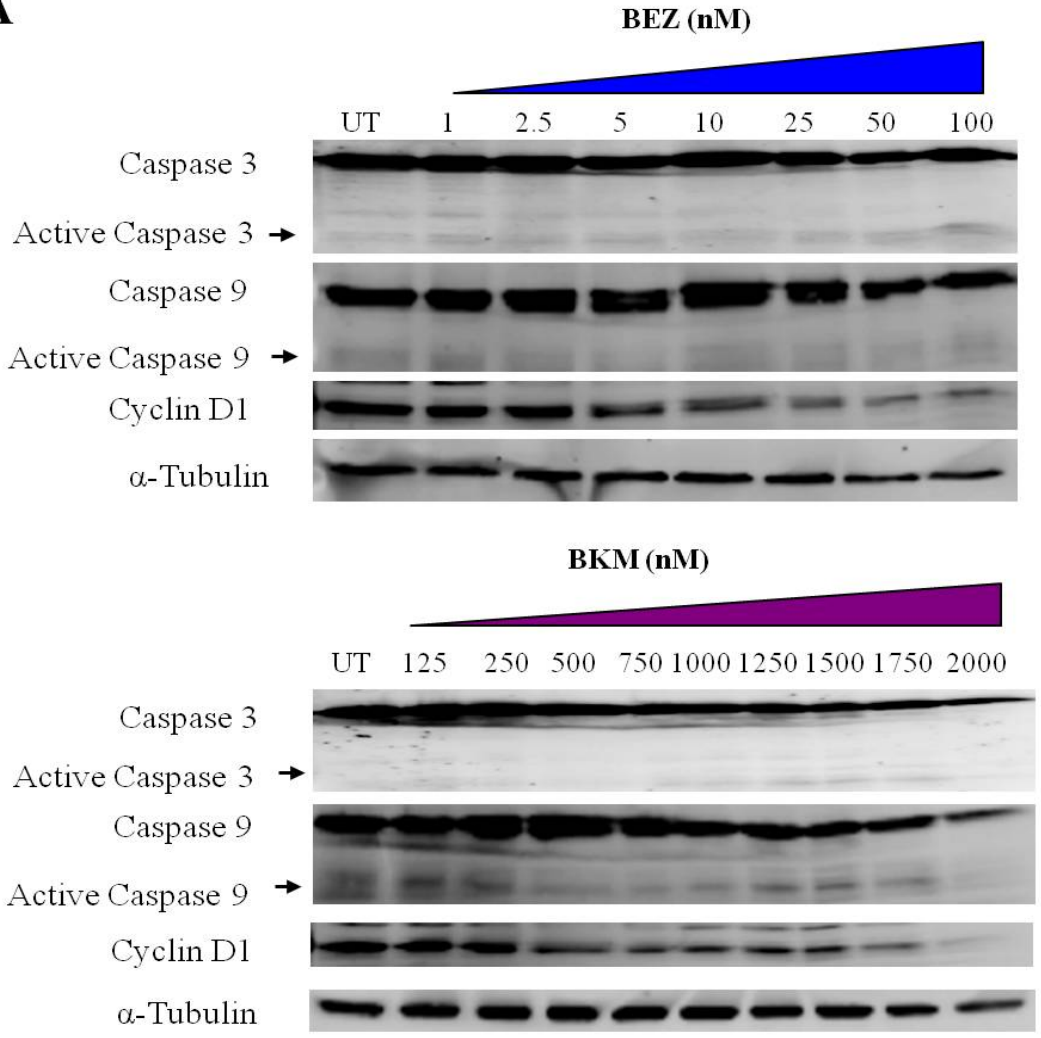

B

	Active Caspase 3 IC_{50}	Active Capase 9 IC_{50}	Cyclin D1 IC_{50}
BEZ235	N/A	N/A	3.5nM 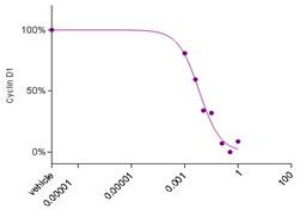
BKM120	N/A	N/A	456nM 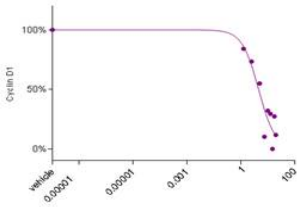

Figure 3.16. BEZ235 and BKM120 mediate a dose-dependent inhibition of Cyclin D1 but have no effect on Caspase 3 and Caspase 9 phosphorylation in RPMI-8226 cells. RPMI-8226 cells were treated with BEZ235 (1-100nM), BKM120 (125-2000nM) or the vehicle alone (0.1% DMSO) for 18 hours and lysates prepared for immunoblotting. An RCDC protein assay was performed to ensure equal amounts of protein were loaded in each lane, and proteins (50ug/lane) were resolved on 10% SDS-PAGE gels. **(A)** Levels of active Caspase 3, active Caspase 9, Cyclin D1 and α-tubulin protein were detected using Western immunoblotting. **(B)** The IC_{50} for BEZ235- and BKM120-mediated inhibition of Cyclin D1 was determined using Graphpad Prism software.

A

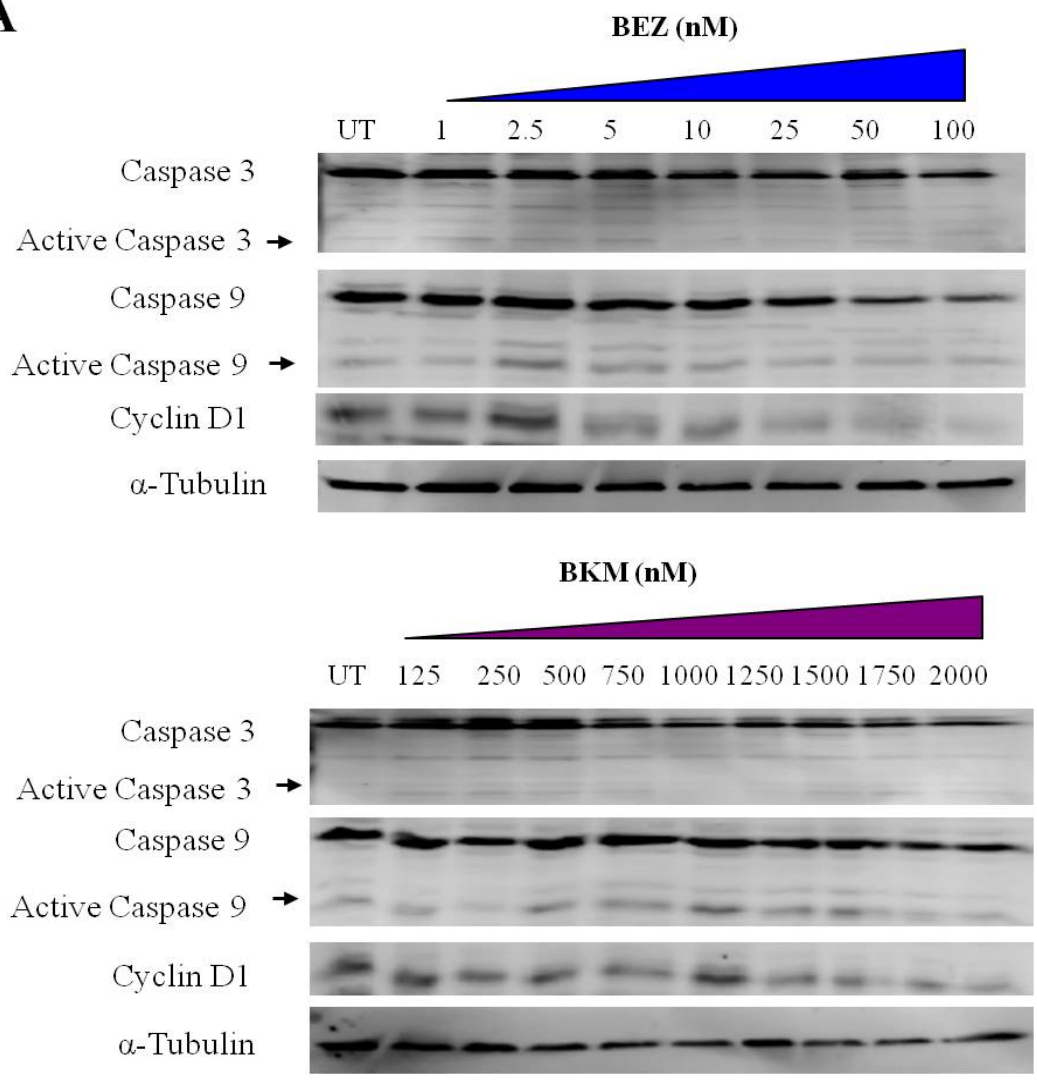

B

	Active Caspase 3 IC_{50}	Active Capase 9 IC_{50}	Cyclin D1 IC_{50}
BEZ235	N/A	N/A	706nM 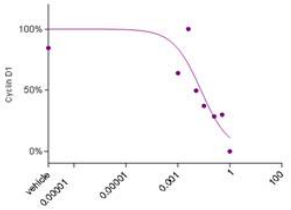
BKM120	N/A	N/A	1209nM 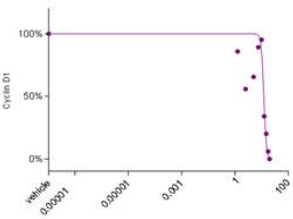

Figure 3.17. BEZ235 has no effect on Caspase 3, Caspase 9 and Cyclin D1 phosphorylation but BKM120 inhibits Cyclin D1 in WL2 cells. WL2 cells were treated with BEZ235 (1-100nM), BKM120 (125-2000nM) or the vehicle alone (0.1% DMSO) for 18 hours and lysates prepared for immunoblotting. An RCDC protein assay was performed to ensure equal amounts of protein were loaded in each lane, and proteins (50ug/lane) were resolved on 10% SDS-PAGE gels. **(A)** Levels of active Caspase 3, active Caspase 9, Cyclin D1 and α-tubulin protein were detected using Western immunoblotting. **(B)** The IC_{50} for BEZ235- and BKM120-mediated inhibition of Cyclin D1 was determined using Graphpad Prism software.

A

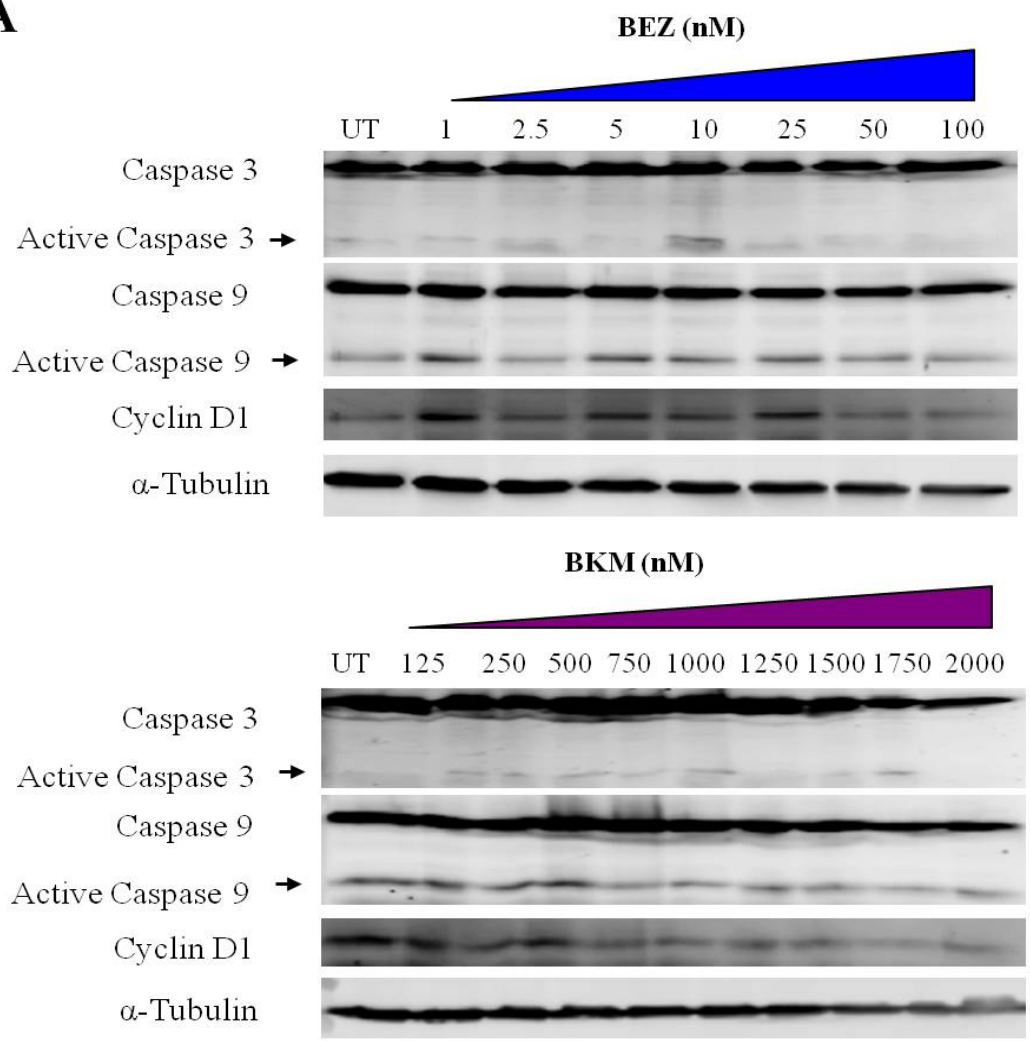

B

	Active Caspase 3 IC_{50}	Active Capase 9 IC_{50}	Cyclin D1 IC_{50}
BEZ235	N/A	N/A	N/A
BKM120	N/A	N/A	714nM 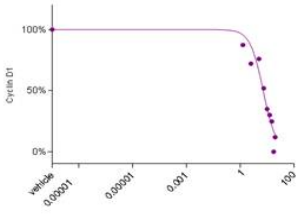

Figure 3.18. BEZ235 has no effect on Caspase 3, Caspase 9 and Cyclin D1 phosphorylation but BKM120 inhibits Cyclin D1 in murine 5TGM1 cells. Murine 5TGM1 cells were treated with BEZ235 (1-100nM), BKM120 (125-2000nM) or the vehicle alone (0.1% DMSO) for 18 hours and lysates prepared for immunoblotting. An RCDC protein assay was performed to ensure equal amounts of protein were loaded in each lane, and proteins (50ug/lane) were resolved on 10% SDS-PAGE gels. **(A)** Levels of active Caspase 3, active Caspase 9, Cyclin D1 and α-tubulin protein were detected using Western immunoblotting. **(B)** The IC_{50} for BEZ235- and BKM120-mediated inhibition of Cyclin D1 was determined using Graphpad Prism software.

A

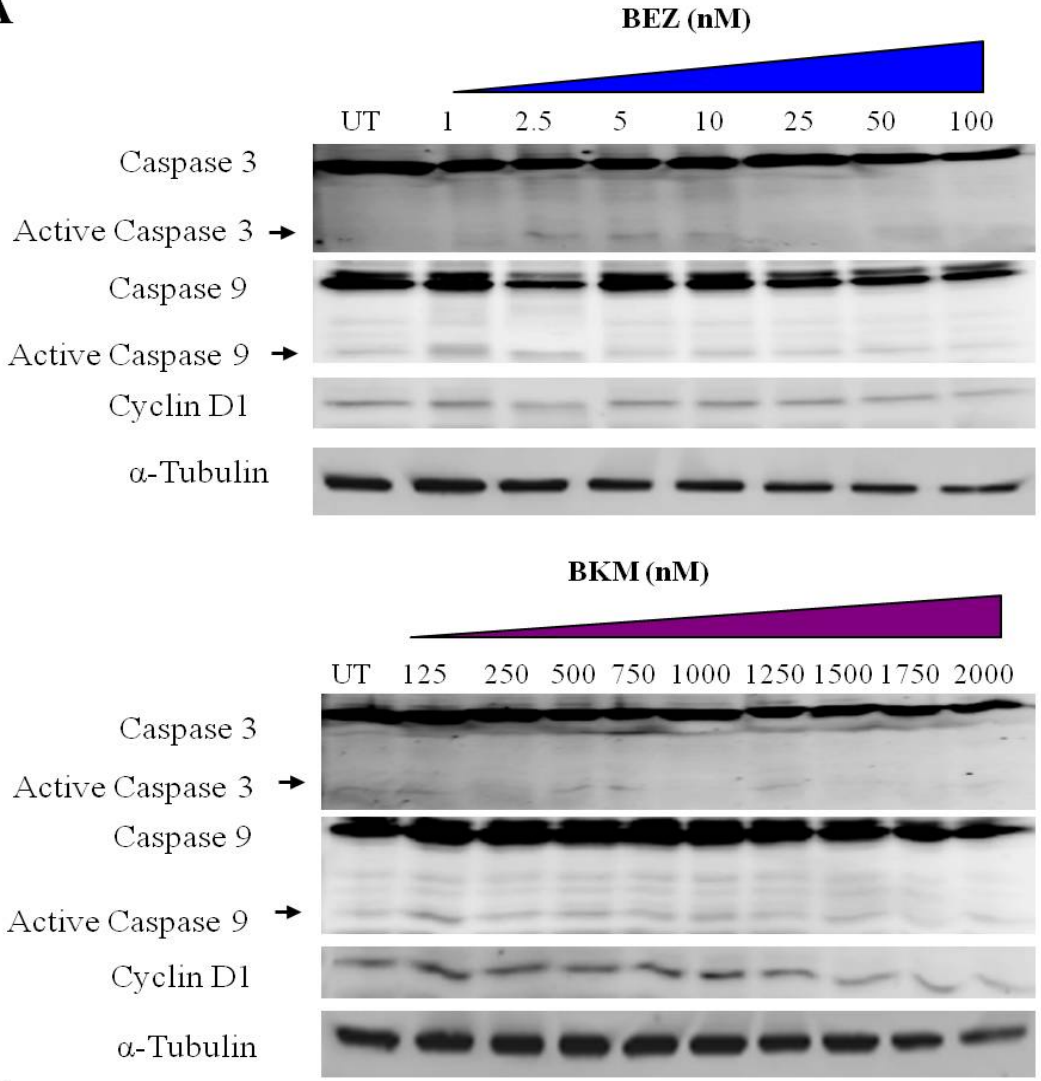

B

	Active Caspase 3 IC_{50}	Active Capase 9 IC_{50}	Cyclin D1 IC_{50}
BEZ235	N/A	N/A	N/A
BKM120	N/A	N/A	1054nM 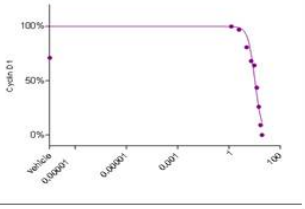

t

the cell population underwent apoptosis when compared to the viable cell populations (Figures 3.19B and C, 3.20 A, C and D). In contrast, when the human MM cell line (RPMI-8226) was treated with BEZ235, between 2-10% of the cell population underwent late apoptosis (indicated by AnnV-/7AAD+ cell population) and a dose-dependent increase in apoptotic cells (indicated by AnnV+/7AAD+ cell population) compared to the viable cell population was observed (Figure 3.26B).

Similar to BEZ235, a representation of the dot plots illustrating the percentage and distribution of the 4 cell populations for each BKM120 treatments is shown in Figure 3.21A. Graphical representations of the 4 cell populations of each BKM120-treated human (U266, RPMI-8226 and WL2) and murine 5TGM1 MM cell lines showed a dose-dependent increase in apoptotic cells when compared to the viable cell population (Figure 3.21B, 3.22B, C and D). In contrast, less than 5% of the cell population underwent apoptosis when compared to the viable cell populations when human MM cell lines (OPM2 and NCI-H929) were treated with BKM120 when compared to the viable cell population (Figure 3.21C and 3.22A).

3.2.2.3 The effect of BEZ235 and BKM120 in inducing oxidative stress in MM cell

Oxidative stress, as defined by Betteridge, is "the disturbance in the balance between the production of reactive oxygen species (free radicals) and antioxidant defences"[27]. In drug-treated cells, the level of oxidative stress has been shown to increase, which in turn, can lead to apoptosis[28]. We next investigated whether there was an increase in oxidative stress levels in the cell nuclei of BEZ235- and BKM120-treated human and murine MM cell lines. Human (U266, OPM2, NCI-H929, RPMI-8226 and WL2) and murine (5TGM1) MM cell lines were incubated with ½ IC_{50}, IC_{50} and 2x IC_{50} BEZ235 (see IC_{50} data in Table 3.1), ½ IC_{50}, IC_{50} and 2x IC_{50} BKM120 (see IC_{50} data in Table 3.1), or vehicle alone (0.1% DMSO) for 2 hours (a time that has been shown to be sufficient to induce oxidative stress in MM cells[24]) and stained with FOXO3a (marker of oxidative stress) and DAPI (DNA stain). An increase in the uptake of FOXO3a antibody into the nucleus was observed in human (U266 and NCI-H929) MM cells treated with IC_{50} BEZ235 when compared to the vehicle-treated cells (Figures 3.23A and 3.25A). In contrast, the increase of FOXO3a antibody uptake

Figure 3.19. BEZ235 does not induce apoptosis in U266 and OPM2 human MM cell lines. Human myeloma cells (U266 and OPM2) were treated with BEZ235 (½IC_{50}, 1x IC_{50} and 2x IC_{50}) and 0.1% DMSO for 18 hours. Cells were then stained with Annexin V and 7-AAD for 15 minutes and analysed by flow cytometry. **(A)** A representation of the flow cytometry images of WL2 cells. The percentage of viable, AnnV+, 7AAD+ and AnnV/7AAD+ **(B)** U266 and **(C)** OPM2 myeloma cells determined by flow cytometry was graphed.

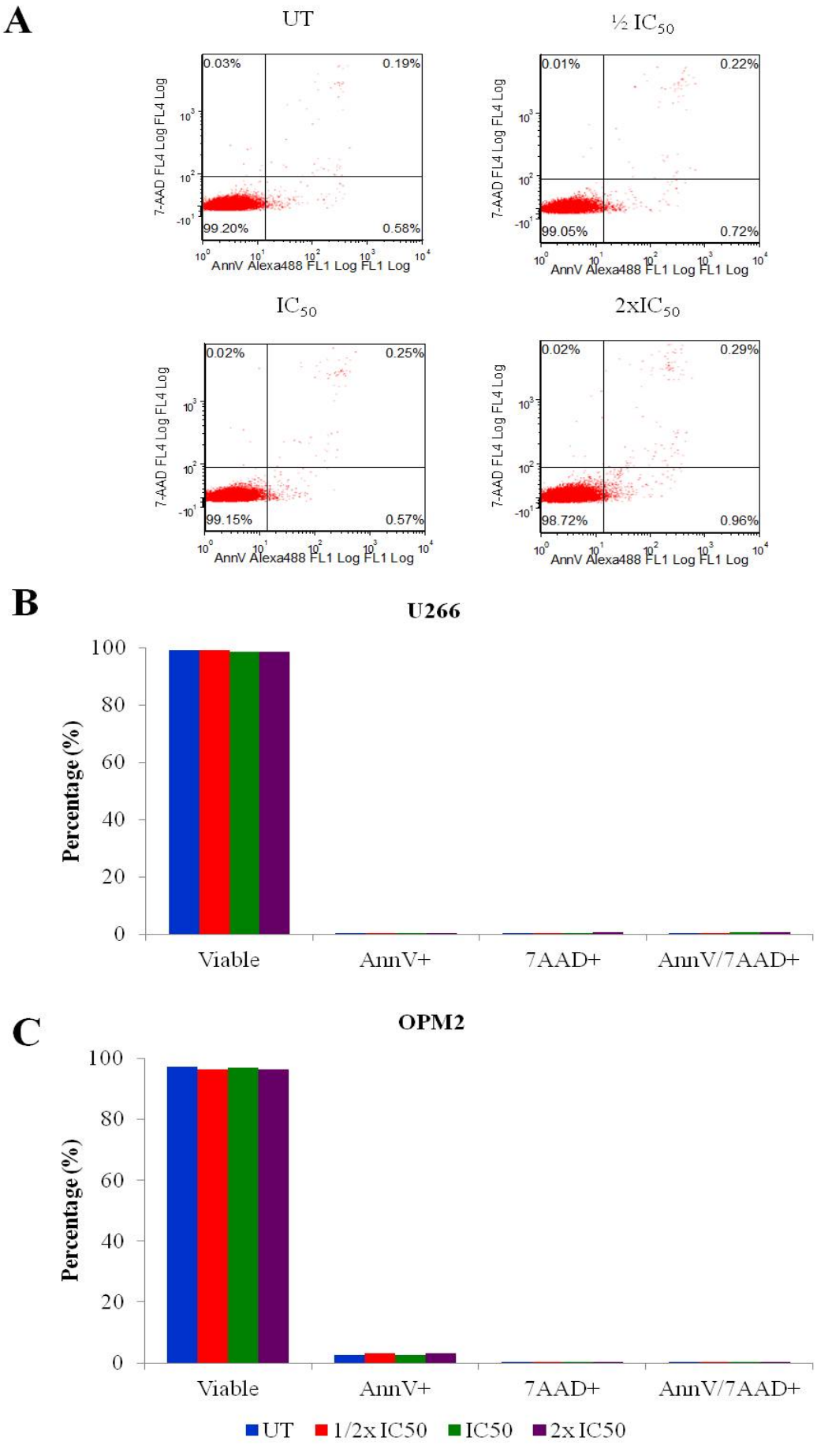
A
UT
0.03%
0.19%
99.20%
0.58%
½ IC50
0.01%
0.22%
99.05%
0.72%
IC50
0.02%
0.25%
99.15%
0.57%
2xIC50
0.02%
0.29%
98.72%
0.96%
7-AAD FL4 Log FL4 Log
AnnV Alexa488 FL1 Log FL1 Log
B
U266
Percentage (%)
Viable
AnnV+
7AAD+
AnnV/7AAD+
C
OPM2
Percentage (%)
Viable
AnnV+
7AAD+
AnnV/7AAD+
UT
1/2x IC50
IC50
2x IC50

Figure 3.20. BEZ235 do not induce apoptosis in NCI-H929, RPMI-8226 and WL2 human and murine 5TGM1 myeloma cell lines. Human (NCI-H929, RPMI-8226 and WL2) and murine 5TGM1 myeloma cells were treated with BEZ235 (½IC_{50}, 1x IC_{50} and 2x IC_{50}) and 0.1% DMSO for 18 hours. Cells were then stained with Annexin V and 7-AAD for 15 minutes and analysed by flow cytometry. The percentage of viable, AnnV+, 7AAD+ and AnnV/7AAD+ **(A)** NCI-H929, **(B)** RPMI-8226, **(C)** WL2 and **(D)** 5TGM1 myeloma cells determined by flow cytometry was graphed.

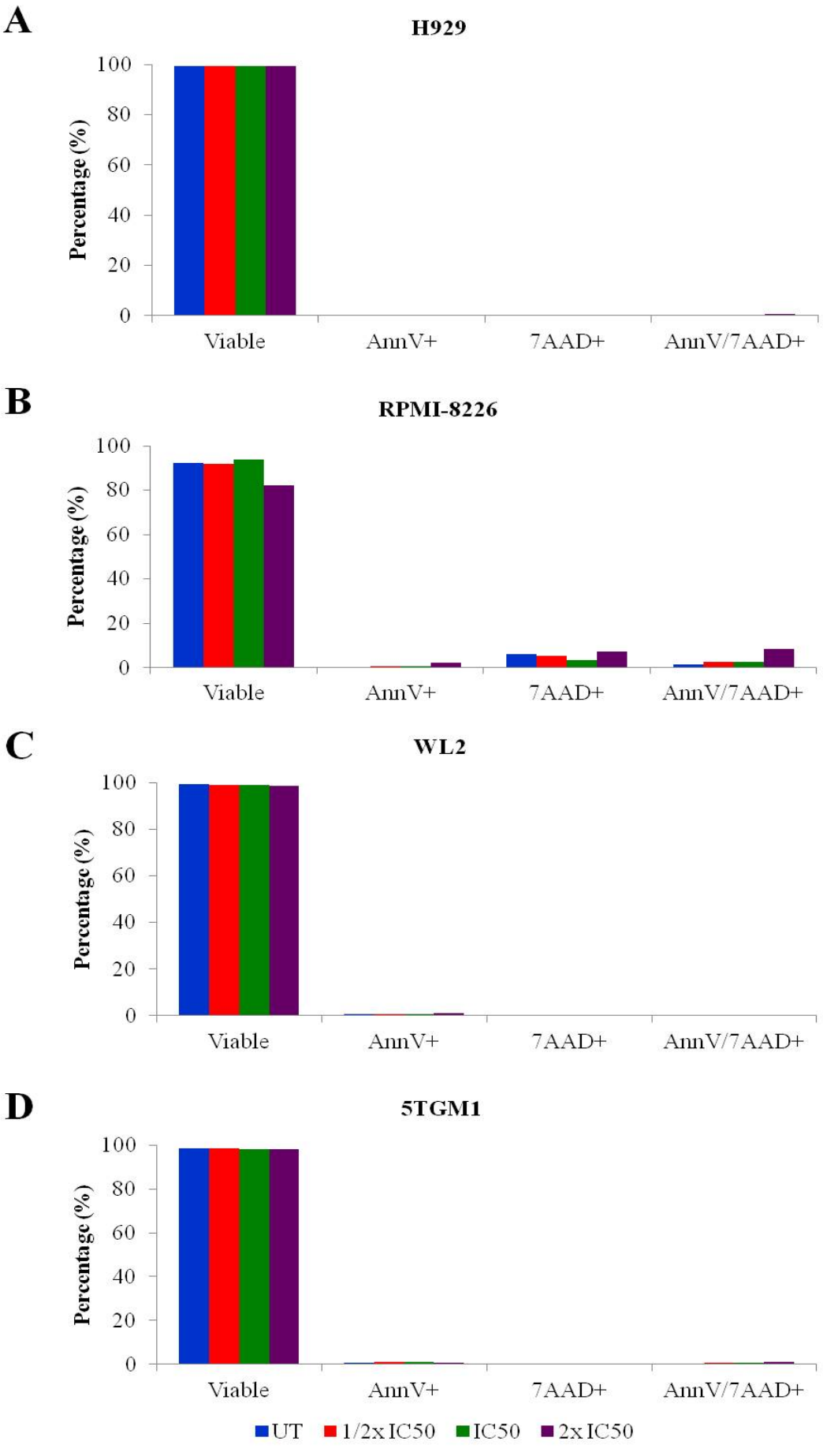
A
H929
Percentage (%)
100
80
60
40
20
0
Viable
AnnV+
7AAD+
AnnV/7AAD+
B
RPMI-8226
Percentage (%)
100
80
60
40
20
0
Viable
AnnV+
7AAD+
AnnV/7AAD+
C
WL2
Percentage (%)
100
80
60
40
20
0
Viable
AnnV+
7AAD+
AnnV/7AAD+
D
5TGM1
Percentage (%)
100
80
60
40
20
0
Viable
AnnV+
7AAD+
AnnV/7AAD+
UT
1/2x IC50
IC50
2x IC50

Figure 3.21. BKM120 do not induce apoptosis in U266 and OPM2 human MM cell lines. Human myeloma cells (U266 and OPM2) were treated with BKM120 (½IC_{50}, 1x IC_{50} and 2x IC_{50}) and 0.1% DMSO for 18 hours. Cells were then stained with Annexin V and 7-AAD for 15 minutes and analysed by flow cytometry. **(A)** A representation of the flow cytometry images of WL2 cells. The percentage of viable, AnnV+, 7AAD+ and AnnV/7AAD+ **(B)** U266 and **(C)** OPM2 myeloma cells determined by flow cytometry was graphed.

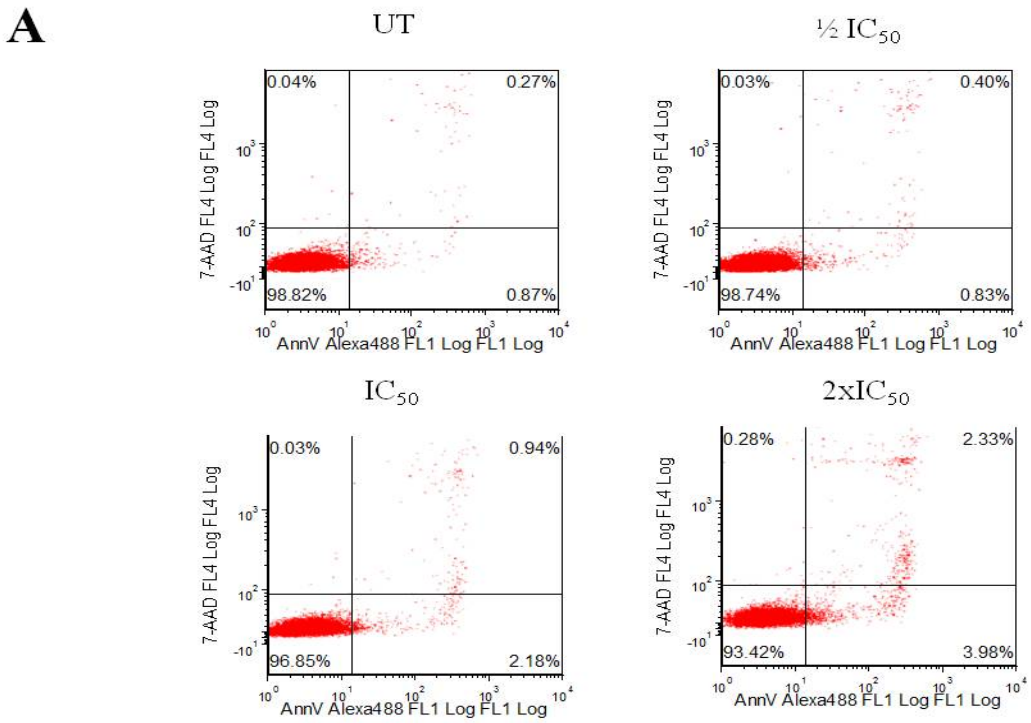
A
UT
½ IC50
IC50
2xIC50
0.04%
0.27%
98.82%
0.87%
0.03%
0.40%
98.74%
0.83%
0.03%
0.94%
96.85%
2.18%
0.28%
2.33%
93.42%
3.98%
7-AAD FL4 Log FL4 Log
AnnV Alexa488 FL1 Log FL1 Log

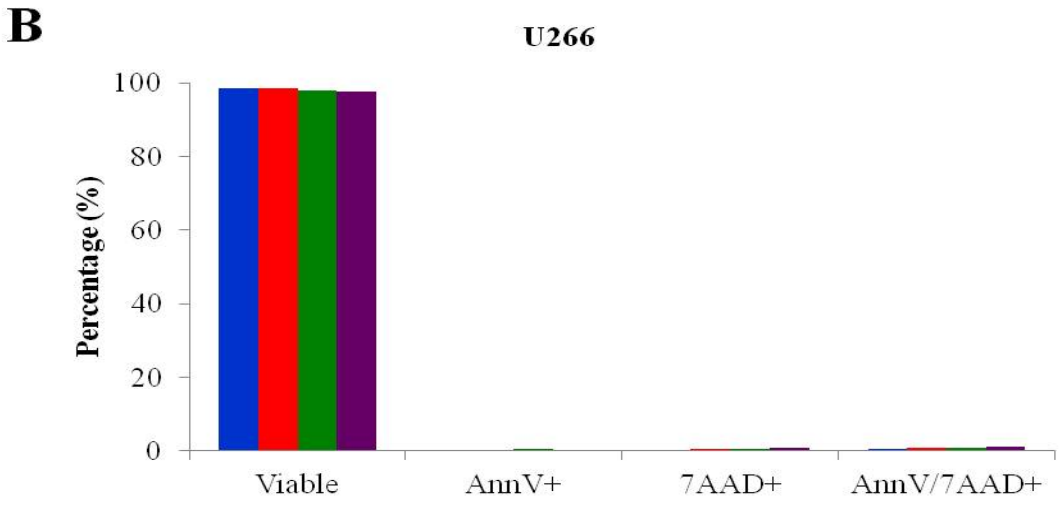
B
U266
Percentage (%)
100
80
60
40
20
0
Viable
AnnV+
7AAD+
AnnV/7AAD+

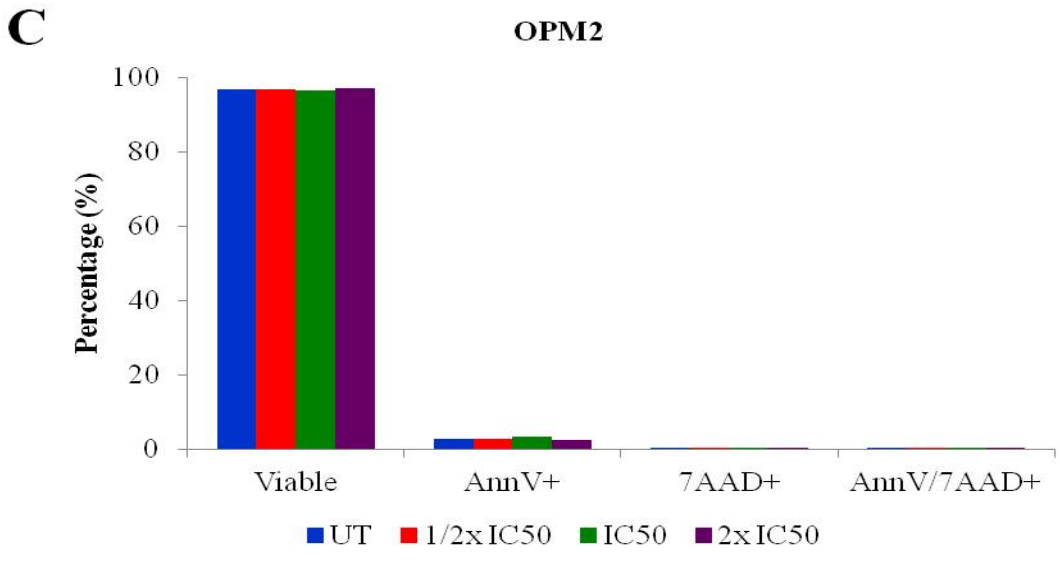
C
OPM2
Percentage (%)
100
80
60
40
20
0
Viable
AnnV+
7AAD+
AnnV/7AAD+
UT
1/2x IC50
IC50
2x IC50

Figure 3.22. BKM120 do not induce apoptosis in NCI-H929, RPMI-8226 and WL2 human and murine 5TGM1 myeloma cell lines. Human (NCI-H929, RPMI-8226 and WL2) and murine 5TGM1 myeloma cells were treated with BKM120 (½IC_{50}, 1x IC_{50} and 2x IC_{50}) and 0.1% DMSO for 18 hours. Cells were then stained with Annexin V and 7-AAD for 15 minutes and analysed by flow cytometry. The percentage of viable, AnnV+, 7AAD+ and AnnV/7AAD+ **(A)** NCI-H929, **(B)** RPMI-8226, **(C)** WL2 and **(D)** 5TGM1 myeloma cells determined by flow cytometry was graphed.

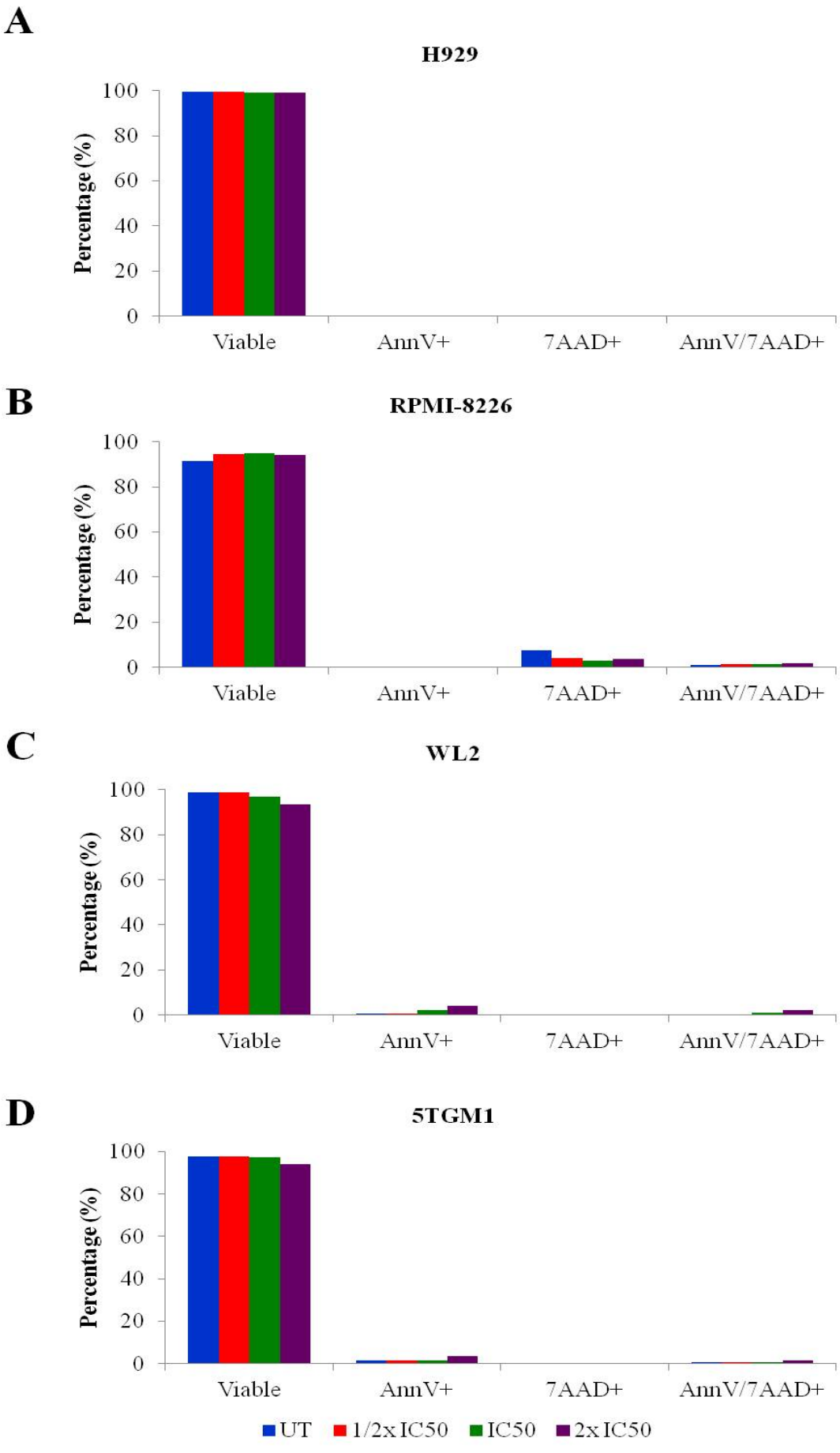
A
H929
Percentage (%)
100
80
60
40
20
0
Viable
AnnV+
7AAD+
AnnV/7AAD+
B
RPMI-8226
Percentage (%)
100
80
60
40
20
0
Viable
AnnV+
7AAD+
AnnV/7AAD+
C
WL2
Percentage (%)
100
80
60
40
20
0
Viable
AnnV+
7AAD+
AnnV/7AAD+
D
5TGM1
Percentage (%)
100
80
60
40
20
0
Viable
AnnV+
7AAD+
AnnV/7AAD+
UT
1/2x IC50
IC50
2x IC50

was only observed in human (OPM2, RPMI-8226 and WL2) and murine (5TGM1) MM cells that were treated with 2x IC_{50} BEZ235 (Figures 3.24A, 3.26A, 3.27A and 3.28A).

In the BKM120 treated cells, an increase in FOXO3a antibody uptake was observed in human (U266 and NCI-H929) MM cells treated with IC_{50} BKM120 when compared to vehicle treated cells (Figures 3.23B and 3.25B). In contrast, the increase of FOXO3a antibody uptake was only observed in human (OPM2, RPMI-8226 and WL2) and murine (5TGM1) MM cells that were treated with 2x IC_{50} BKM120 (Figures 3.24B, 3.26B, 3.27B and 3.28B).

3.2.2.4 The effect of BEZ235 and BKM120 on cell cycle in MM cell lines in vitro

To investigate the effect on BEZ235 and BKM120 on cell cycle arrest, human (U266, OPM2, NCI-H929, RPMI-8226 and WL2) and murine 5TGM1 MM cell lines were incubated with ½ IC_{50}, IC_{50} and 2x IC_{50} BEZ235 (see IC_{50} data in Table 3.1), ½ IC_{50}, IC_{50} and 2x IC_{50} BKM120 (see IC_{50} data in Table 3.1), or vehicle alone (0.1% DMSO) for 18, 36 and 72 hours. The cells were then washed and stained with PI (which stains the DNA of dead cells) and analysed on the Coulter Cytomics FC500 Series flow cytometer.

The graphical representations in Figures 3.29, 3.30, 3.31, 3.32, 3.33 and 3.34 show the percentage of cells in sub G1 (apoptotic phase), G1 (interphase), S (synthesis phase) and G2/M (mitotic phase) phases in response to either BEZ235 (top panels) or BKM120 (bottom panels) treatment. A trend towards the onset of apoptosis was observed in all BEZ235-treated MM cell lines in a dose- and time-dependent manner as indicated by the increase in the proportion of hypo-diploid cells in the sub G1 phase compared to the vehicle treated cells (Figures 3.32A, 3.33A, 3.34A and 3.36A).

Consistent with disruption in cell cycle regulation, as observed by the inhibition of Cyclin D1 in BKM120-treated human and murine MM cell lines (Section 3.2.2.1), an increase in sub G1 population was observed. When the MM cell lines were treated with 2x IC_{50} BKM120 for 72hours, a 2-fold increase in the sub G1 population (a marker of necrotic cells) was observed in the U266 and RPMI-8226 MM cell lines (Figure 3.29B and 3.32B), a 1-fold increase in the NCI-H929 MM cell line (Figure 3.31B), a 17-fold increase in WL2 MM cell line (Figure 3.33B) and a 8-fold increase in the murine 5TGM1 MM cell line (Figure 3.34B) when compared to the vehicle treated cells. While

Figure 3.23. BEZ235 and BKM120 induce translocation of FOXO3a to the nucleus in U266 cells. U266 cells were treated with **(A)** BEZ235 (½IC_{50}, 1xIC_{50} and 2xIC_{50}), **(B)** BKM120 (½IC_{50}, 1x IC_{50} and 2x IC_{50}) or vehicle alone (UT, 0.1% DMSO) for 2 hours and stained for FOXO3a and DAPI and visualized by immunofluorescence. Scale: 30μm.

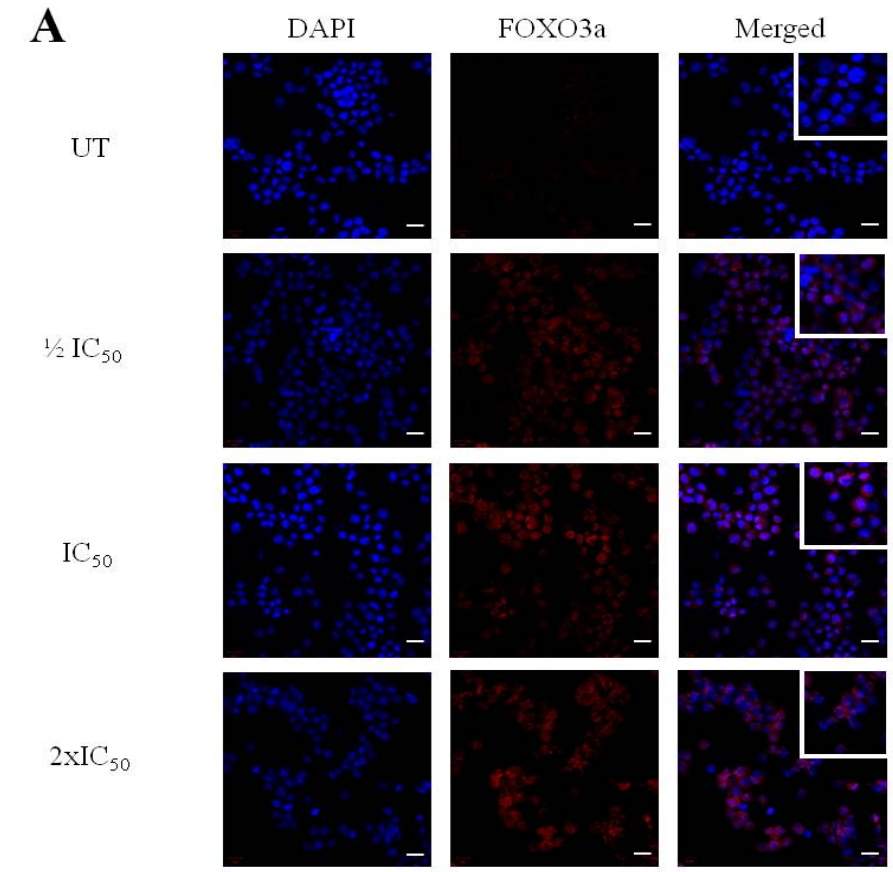
A
DAPI
FOXO3a
Merged
UT
½ IC50
IC50
2xIC50

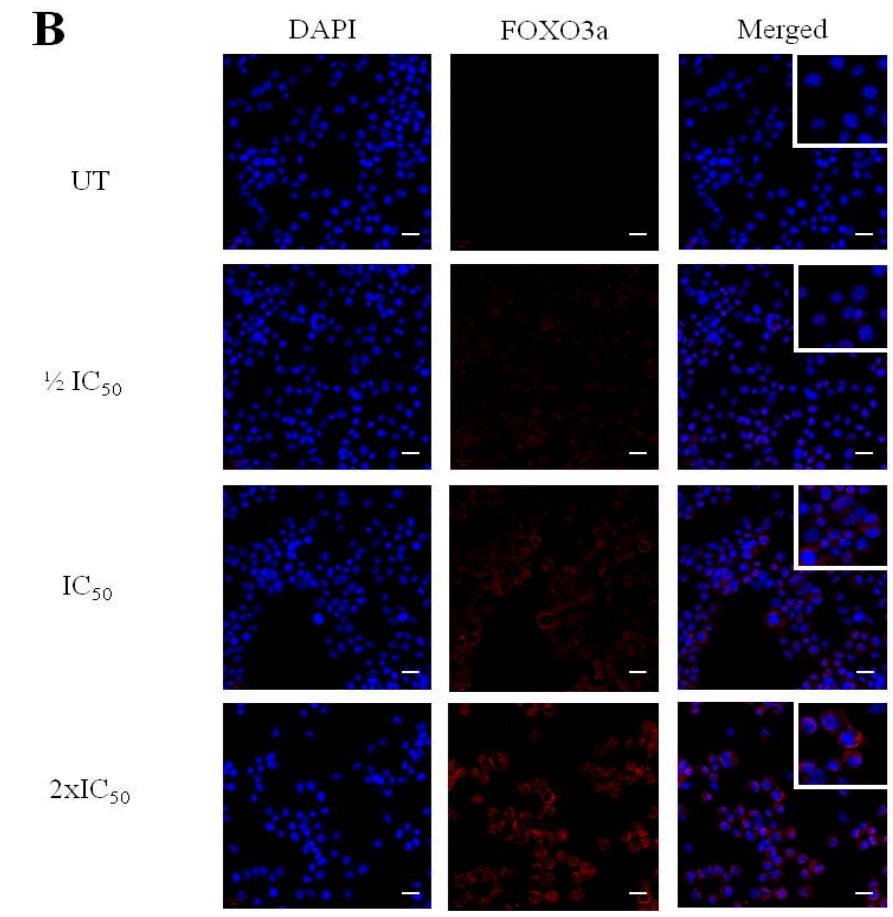
B
DAPI
FOXO3a
Merged
UT
½ IC50
IC50
2xIC50

Figure 3.24. BEZ235 and BKM120 induce translocation of FOXO3a to the nucleus in OPM2 cells. OPM2 cells were treated with **(A)** BEZ235 (½IC_{50}, 1xIC_{50} and 2xIC_{50}), **(B)** BKM120 (½IC_{50}, 1x IC_{50} and 2x IC_{50}) or vehicle alone (UT, 0.1% DMSO) for 2 hours and stained for FOXO3a and DAPI and visualized by immunofluorescence. Scale: 30µm.

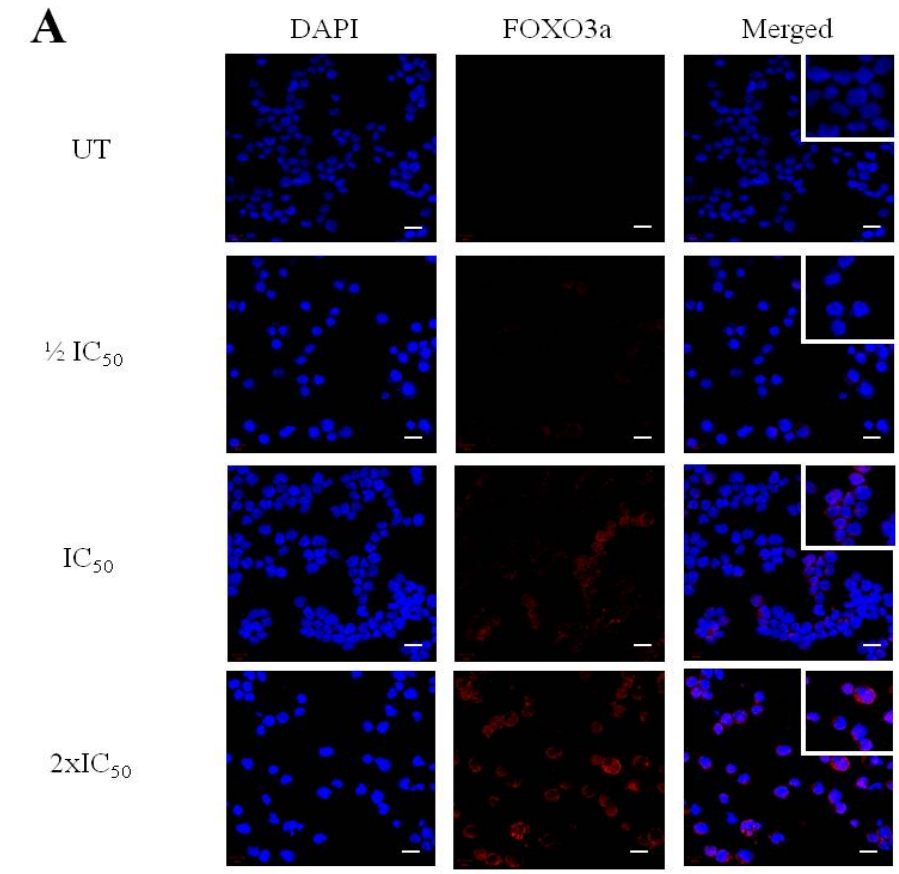
A
DAPI
FOXO3a
Merged
UT
½ IC50
IC50
2xIC50

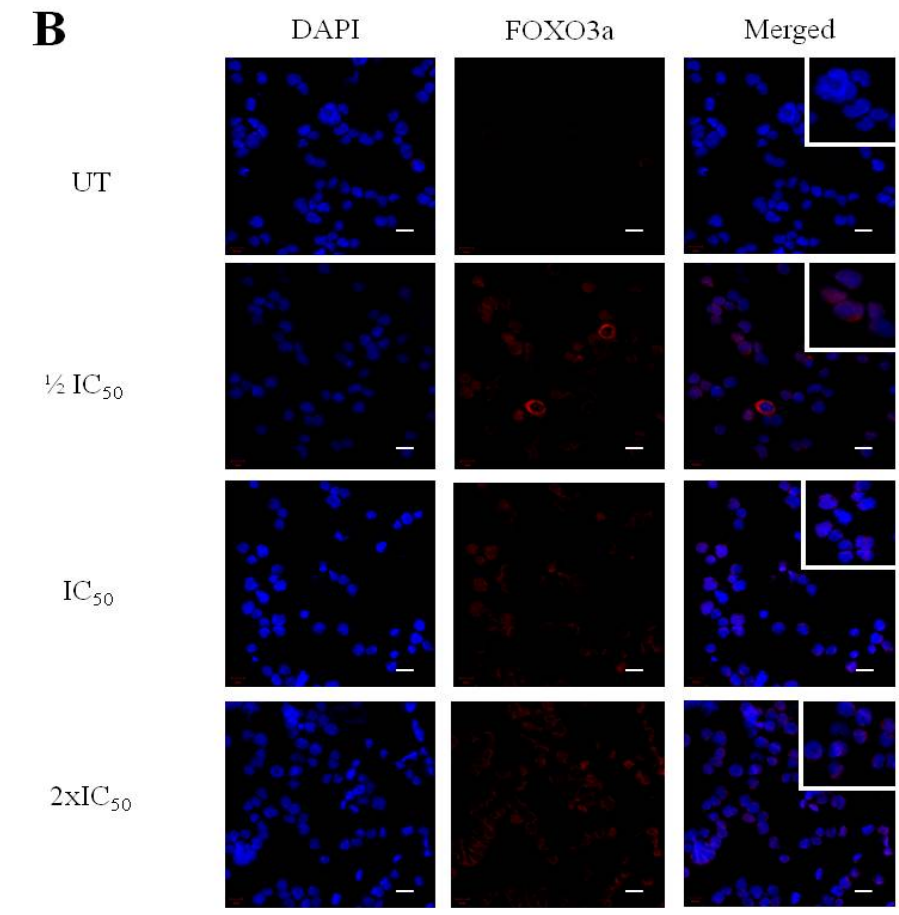
B
DAPI
FOXO3a
Merged
UT
½ IC50
IC50
2xIC50

Figure 3.25. BEZ235 and BKM120 induce translocation of FOXO3a to the nucleus in NCI-H929 cells. NCI-H929 cells were treated with **(A)** BEZ235 (½IC_{50}, 1xIC_{50} and 2xIC_{50}), **(B)** BKM120 (½IC_{50}, 1x IC_{50} and 2x IC_{50}) or vehicle alone (UT, 0.1% DMSO) for 2 hours and stained for FOXO3a and DAPI and visualized by immunofluorescence. Scale: 30µm.

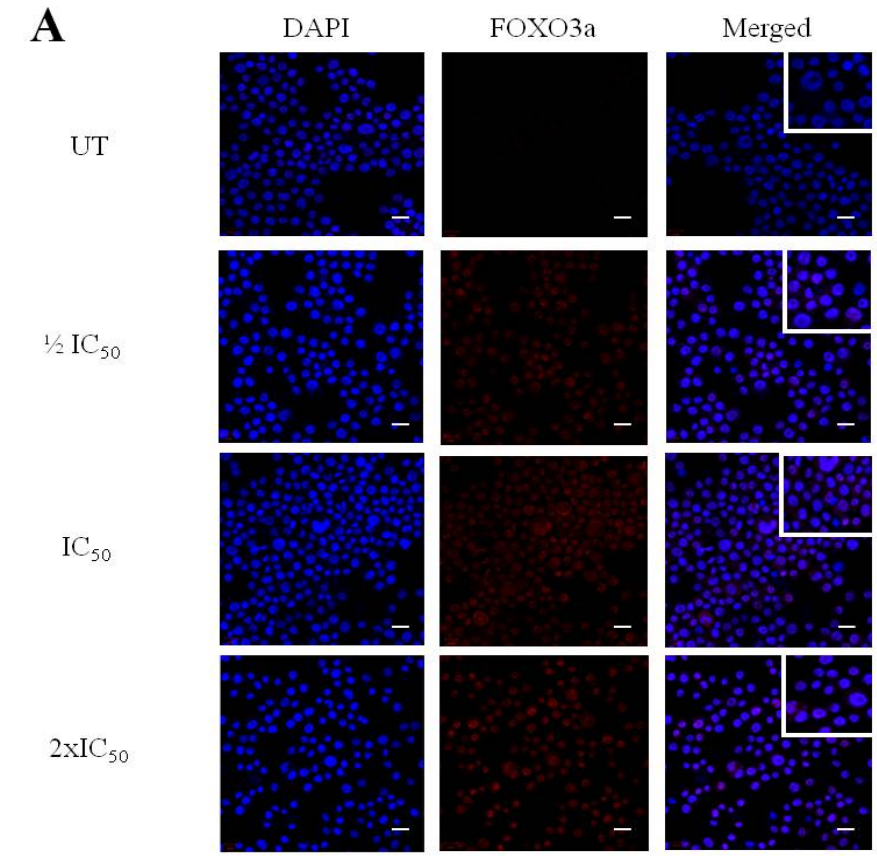
A
DAPI
FOXO3a
Merged
UT
½ IC50
IC50
2xIC50

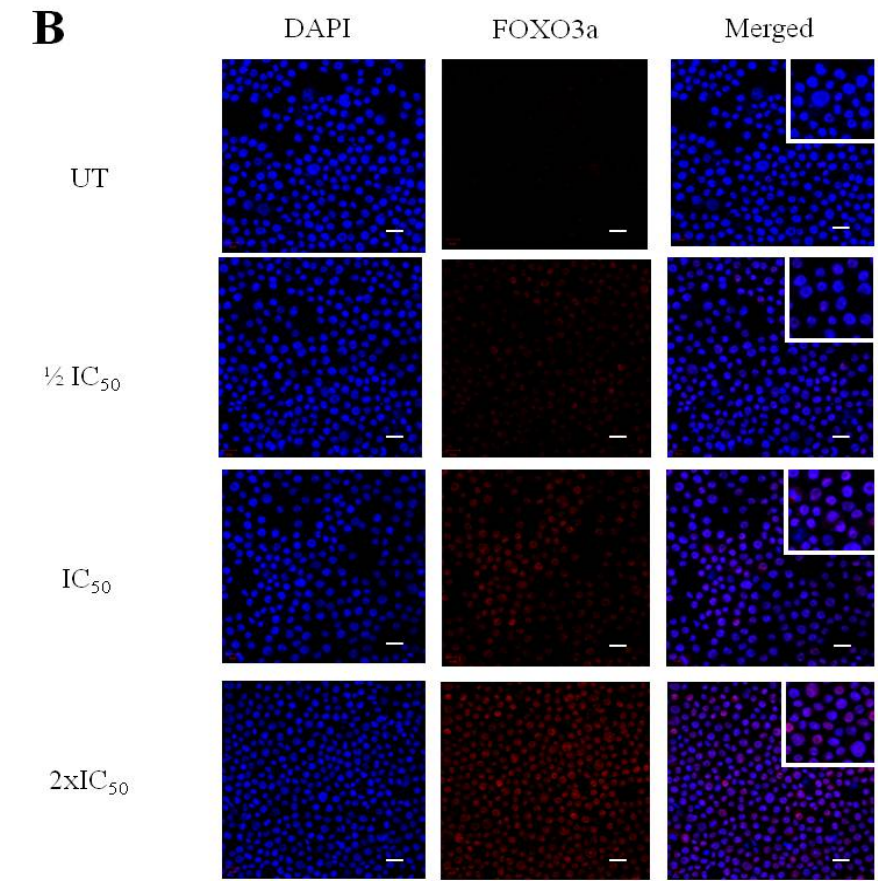
B
DAPI
FOXO3a
Merged
UT
½ IC50
IC50
2xIC50

Figure 3.26. BEZ235 and BKM120 induce translocation of FOXO3a to the nucleus in RPMI-8226 cells. RPMI-8226 cells were treated with **(A)** BEZ235 (½IC_{50}, 1xIC_{50} and 2xIC_{50}), **(B)** BKM120 (½IC_{50}, 1x IC_{50} and 2x IC_{50}) or vehicle alone (UT, 0.1% DMSO) for 2 hours and stained for FOXO3a and DAPI and visualized by immunofluorescence. Scale: 30µm.

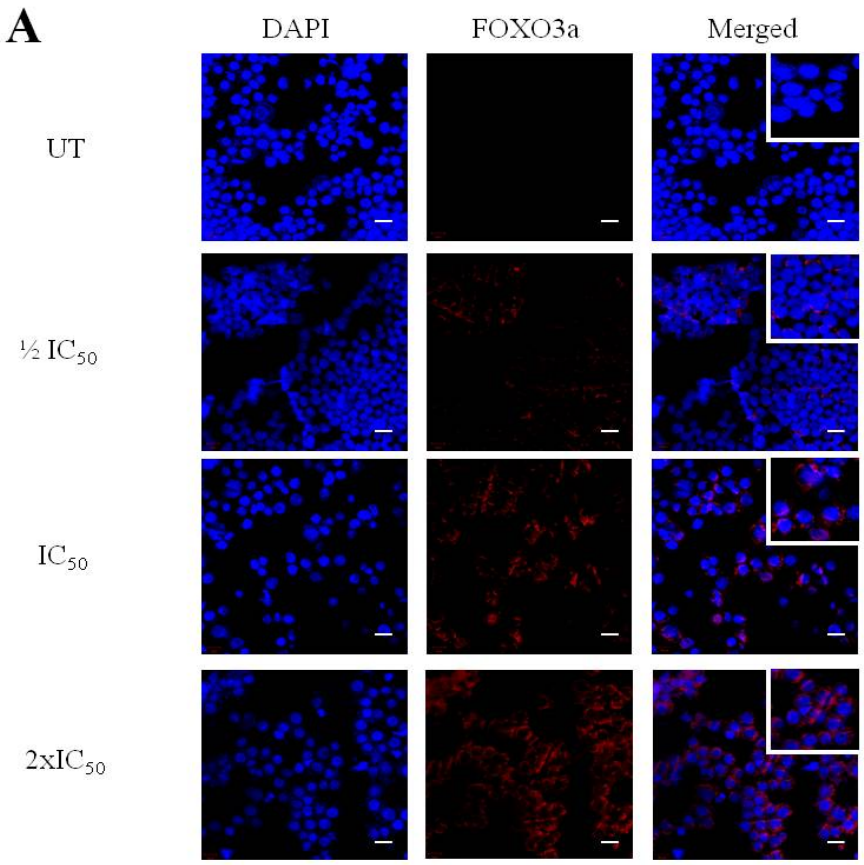
A
DAPI
FOXO3a
Merged
UT
½ IC50
IC50
2xIC50

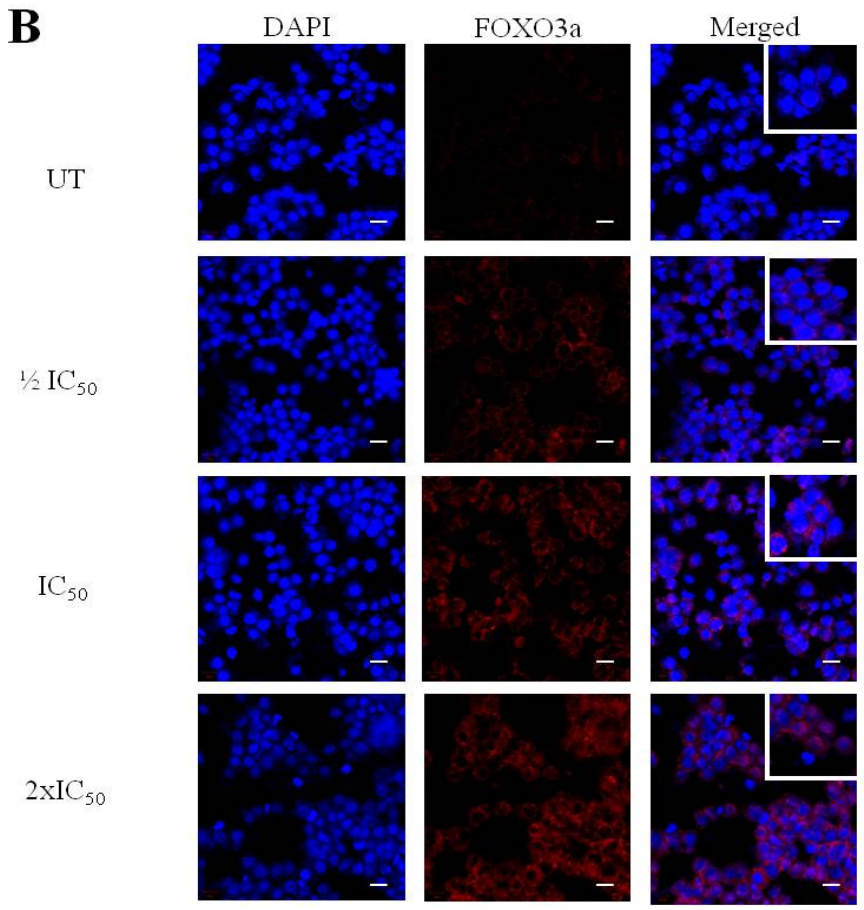
B
DAPI
FOXO3a
Merged
UT
½ IC50
IC50
2xIC50

Figure 3.27. BEZ235 and BKM120 induce translocation of FOXO3a to the nucleus in WL2 cells. WL2 cells were treated with **(A)** BEZ235 (½IC_{50}, 1xIC_{50} and 2xIC_{50}), **(B)** BKM120 (½IC_{50}, 1x IC_{50} and 2x IC_{50}) or vehicle alone (UT, 0.1% DMSO) for 2 hours and stained for FOXO3a and DAPI and visualized by immunofluorescence. Scale: 30µm.

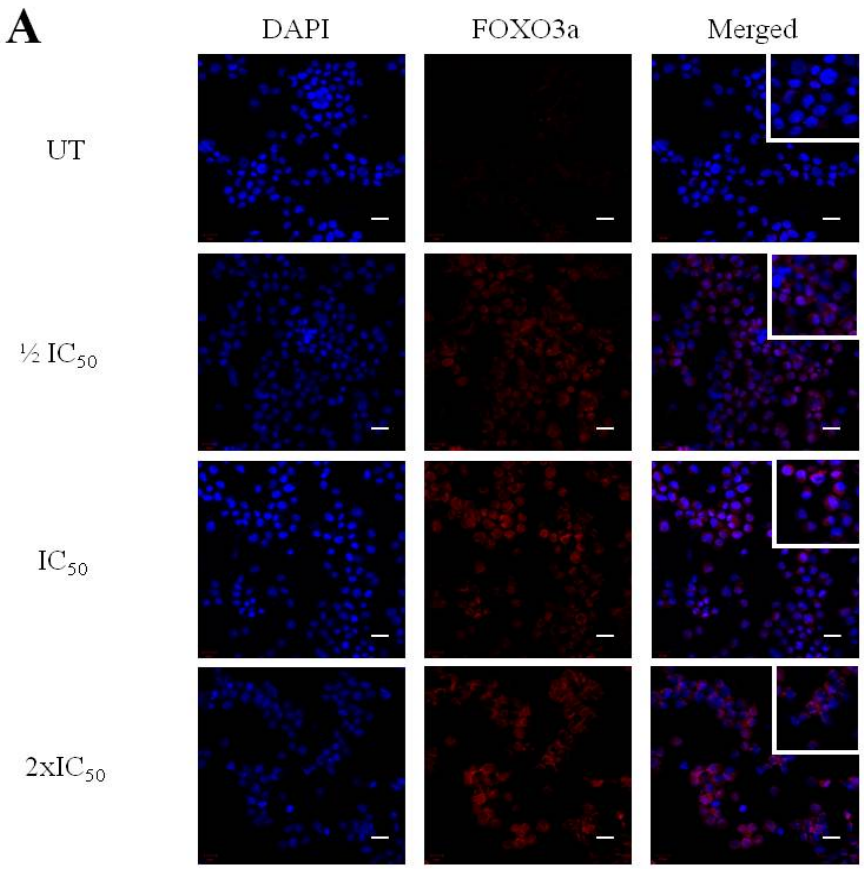
A
DAPI
FOXO3a
Merged
UT
½ IC50
IC50
2xIC50

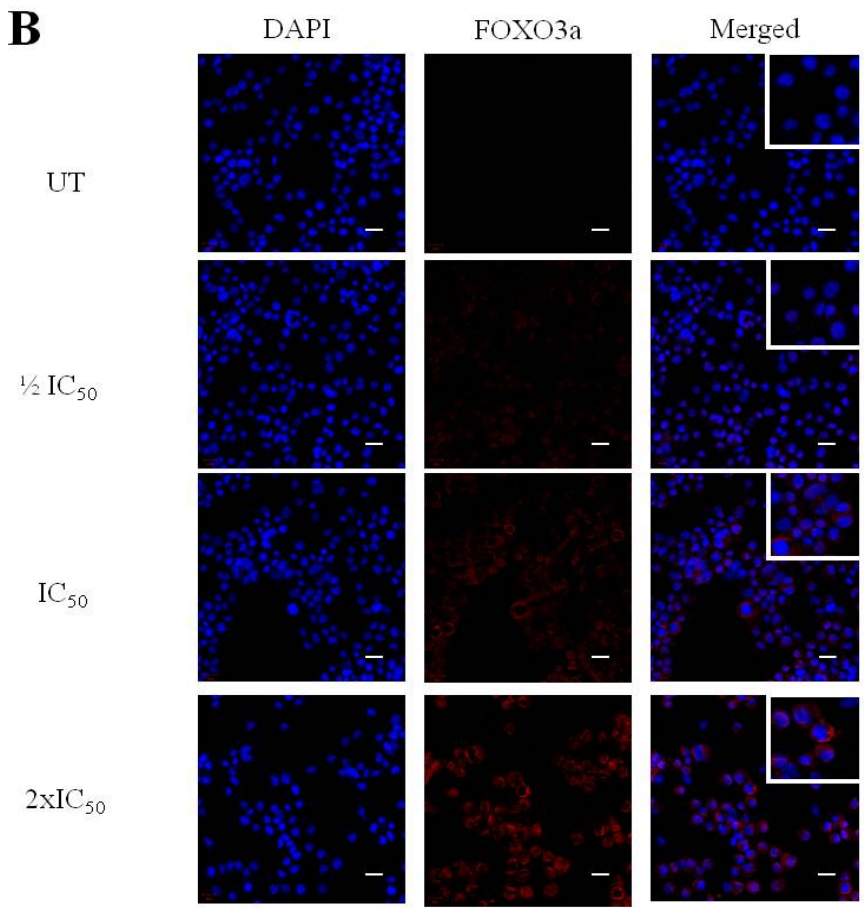
B
DAPI
FOXO3a
Merged
UT
½ IC50
IC50
2xIC50

Figure 3.28. BEZ235 and BKM120 induce translocation of FOXO3a to the nucleus in murine 5TGM1 cells. Murine 5TGM1cells were treated with **(A)** BEZ235 (½IC_{50}, 1xIC_{50} and 2xIC_{50}), **(B)** BKM120 (½IC_{50}, 1x IC_{50} and 2x IC_{50}) or vehicle alone (UT, 0.1% DMSO) for 2 hours and stained for FOXO3a and DAPI and visualized by immunofluorescence. Scale: 30μm.

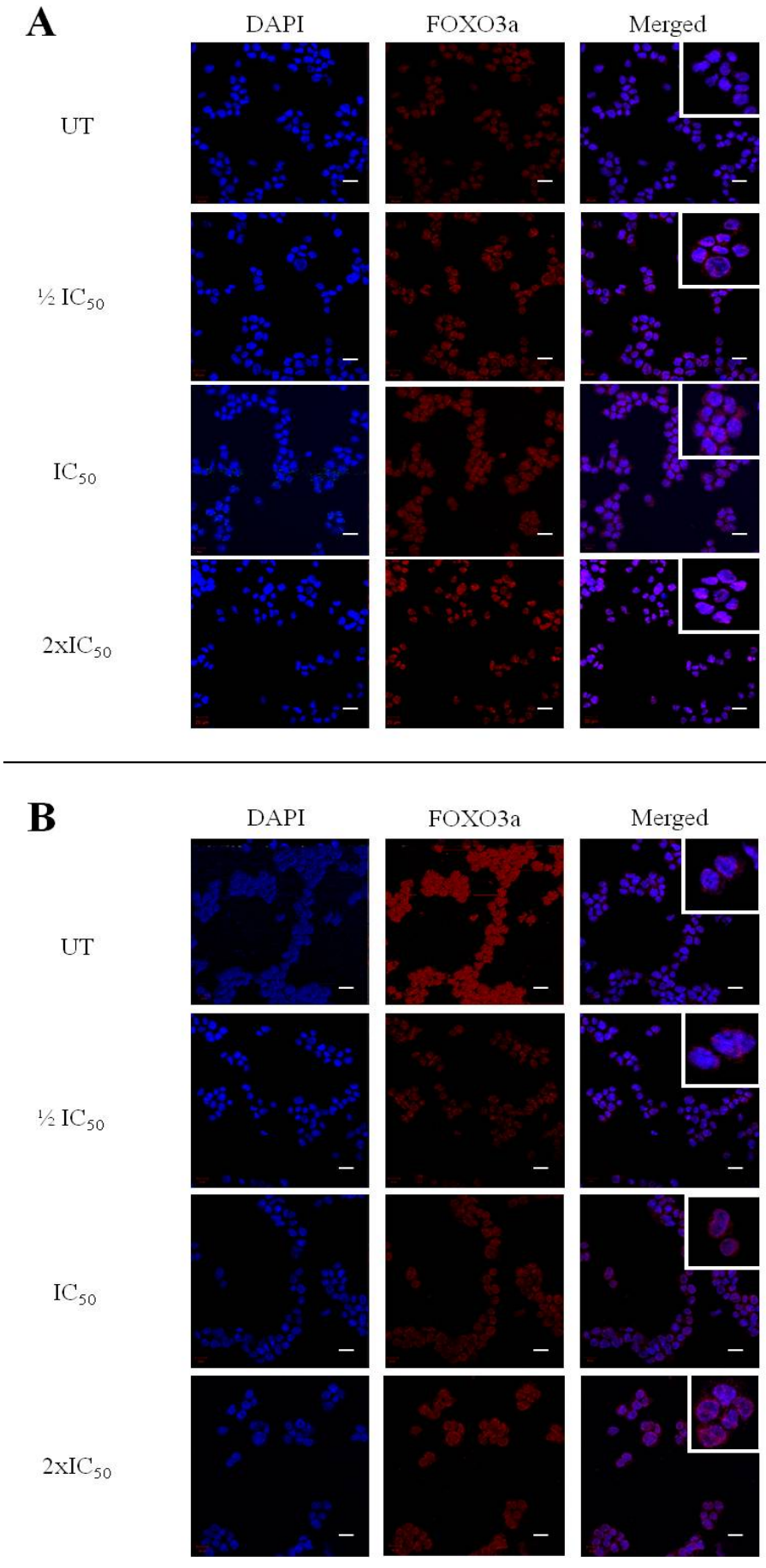
A
DAPI
FOXO3a
Merged
UT
½ IC50
IC50
2xIC50
B
DAPI
FOXO3a
Merged
UT
½ IC50
IC50
2xIC50

the OPM2 MM cell line did not show a dose dependent increase in sub G1 population when compared to the vehicle treated cells; a time dependent increase in apoptotic cells was observed (Figure 3.31B). Furthermore, a 2-, 5- and 6-fold increase in G1 phase population was observed in U266, WL2 and murine 5TGM1 MM cell lines, respectively (Figures 3.29B, 3.33B and 3.34B). These findings were in line with the results from the Caspase-3 and -9 studies (Section 3.2.2.1) where phosphorylation of active Caspase-3 and -9 were not observed.

3.3 *Discussion*

Mutations in the PI3k and mTOR pathways in MM cells cause uncontrolled cell proliferation and protection against apoptosis. In this study, the effects of the dual pan Class-I PI3k and mTOR inhibitor, BEZ235 and the single pan Class-I PI3k inhibitor, BKM120, on MM cell growth and survival was examined. Similar to other PI3k and mTOR inhibitors such as PIK90 (PI3k inhibitor), Rapamycin (mTOR inhibitor) and PI103 (PI3k/mTOR inhibitor)[23], BEZ235 and BKM120 were found to inhibit the proliferation of human and murine MM cell lines *in vitro*. While the phosphorylation of Akt in MM cell lines has been reported in several studies[24; 25], with the exception of NCI-H929, phosphorylation of Akt was not observed in any of the other MM cell lines examined. A recent study by Breitkopf identified the presence of the BCR-ABL oncogene, commonly found in Chronic Myeloid Leukemia cells, in the p85 regulatory subunit of PI3k in the NCI-H929 human MM cell line[29]. The presence of this gene has been shown to activate Akt phosphorylation[29]. While Deptor has been shown to inhibit Akt phosphorylation through mTORC2 inhibition[20; 21; 22], it is possible that the presence of the BCR-ABL gene in the NCI-H929 human MM cell line inhibited the effect of Deptor, thus enabling the phosphorylation of Akt.

Given that the PI3k subunit is made up of 2 subunits, the p110 and p85 subunits, we investigated the possibility of the PI3k subunit being inactive (thus contributing to the absence of Akt phosphorylation in the MM cell lines investigated) by inhibiting the PI3k pathway with PIK-75, a p110α inhibitor. As shown in Figures 3.11 and 3.12, PIK-75 was able to inhibit cell proliferation, suggesting that the PI3k subunit is indeed active. However, this finding does not explain the absence of Akt phosphorylation in our cells. Although we have not looked at PDK-1 and PTEN activity in our cell lines,

Figure 3.29. BEZ235 and BKM120 induce cell cycle arrest in U266 cells. U266 cells were incubated with **(A)** BEZ235 (½IC_{50}, 1x IC_{50} and 2x IC_{50}), **(B)** BKM120 (½IC_{50}, 1x IC_{50} and 2x IC_{50}) or vehicle alone (0.1% DMSO) for 18, 36 and 72 hours. At each time point, cells were ethanol fixed, stained with propridium iodide (PI) and analysed by flow cytometry. The data is presented as the percentage of cells in each phase of cell cycling (sub G1, G1, S and G2/M) for each concentration of drug at the 18, 36 and 72 hour time points.

A

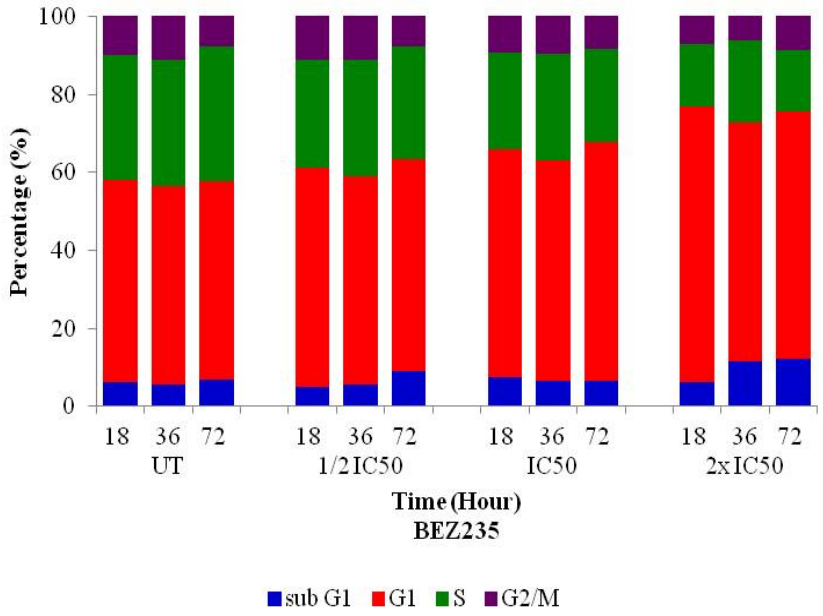
100
80
60
40
20
0
Percentage (%)
18 36 72 18 36 72 18 36 72 18 36 72
UT 1/2IC50 IC50 2xIC50
Time (Hour)
BEZ235
sub G1 G1 S G2/M

B

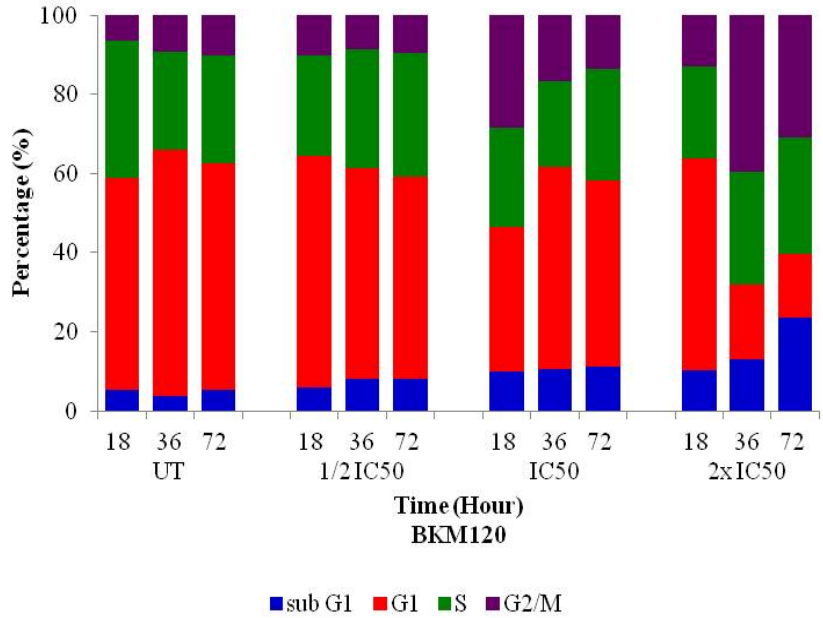
100
80
60
40
20
0
Percentage (%)
18 36 72 18 36 72 18 36 72 18 36 72
UT 1/2IC50 IC50 2xIC50
Time (Hour)
BKM120
sub G1 G1 S G2/M

Figure 3.30. BEZ235 and BKM120 induce cell cycle arrest in OPM2 cells. OPM2 cells were incubated with **(A)** BEZ235 (½IC_{50}, 1x IC_{50} and 2x IC_{50}), **(B)** BKM120 (½IC_{50}, 1x IC_{50} and 2x IC_{50}) or vehicle alone (0.1% DMSO) for 18, 36 and 72 hours. At each time point, cells were ethanol fixed, stained with propridium iodide (PI) and analysed by flow cytometry. The data is presented as the percentage of cells in each phase of cell cycling (sub G1, G1, S and G2/M) for each concentration of drug at the 18, 36 and 72 hour time points.

A

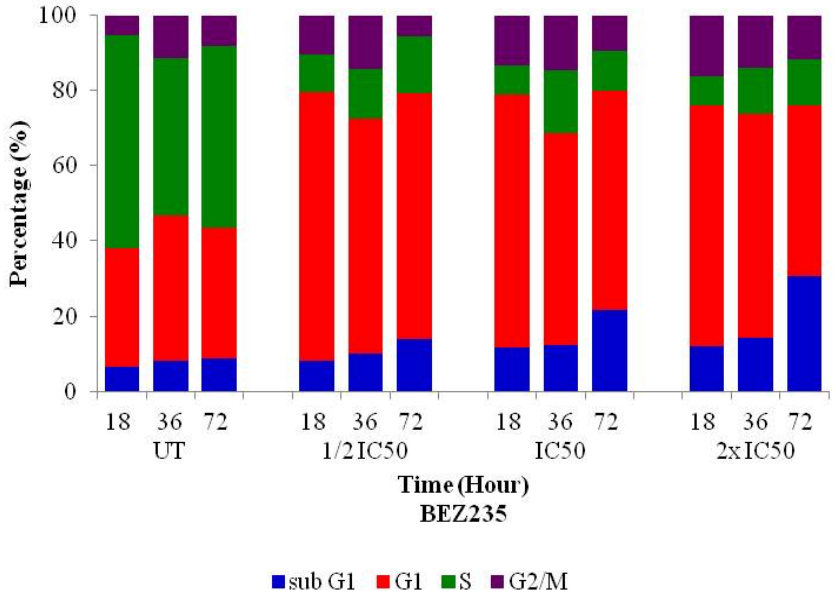
100
80
60
40
20
0
Percentage (%)
18 36 72 18 36 72 18 36 72 18 36 72
UT
1/2IC50
IC50
2xIC50
Time (Hour)
BEZ235
sub G1
G1
S
G2/M

B

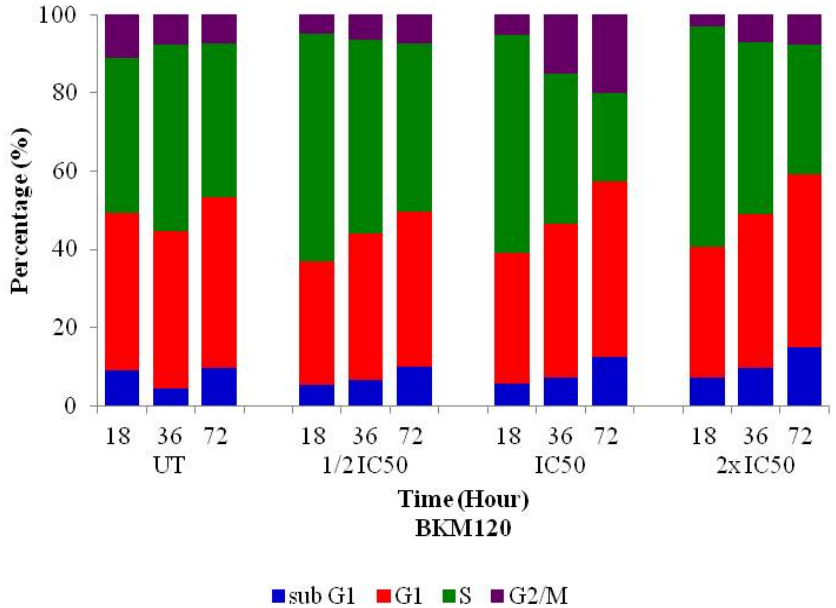
100
80
60
40
20
0
Percentage (%)
18 36 72 18 36 72 18 36 72 18 36 72
UT
1/2IC50
IC50
2xIC50
Time (Hour)
BKM120
sub G1
G1
S
G2/M

Figure 3.31. BEZ235 and BKM120 induce cell cycle arrest in NCI-H929 cells. NCI-H929 cells were incubated with **(A)** BEZ235 (½IC_{50}, 1x IC_{50} and 2x IC_{50}), **(B)** BKM120 (½IC_{50}, 1x IC_{50} and 2x IC_{50}) or vehicle alone (0.1% DMSO) for 18, 36 and 72 hours. At each time point, cells were ethanol fixed, stained with propridium iodide (PI) and analysed by flow cytometry. The data is presented as the percentage of cells in each phase of cell cycling (sub G1, G1, S and G2/M) for each concentration of drug at the 18, 36 and 72 hour time points.

A

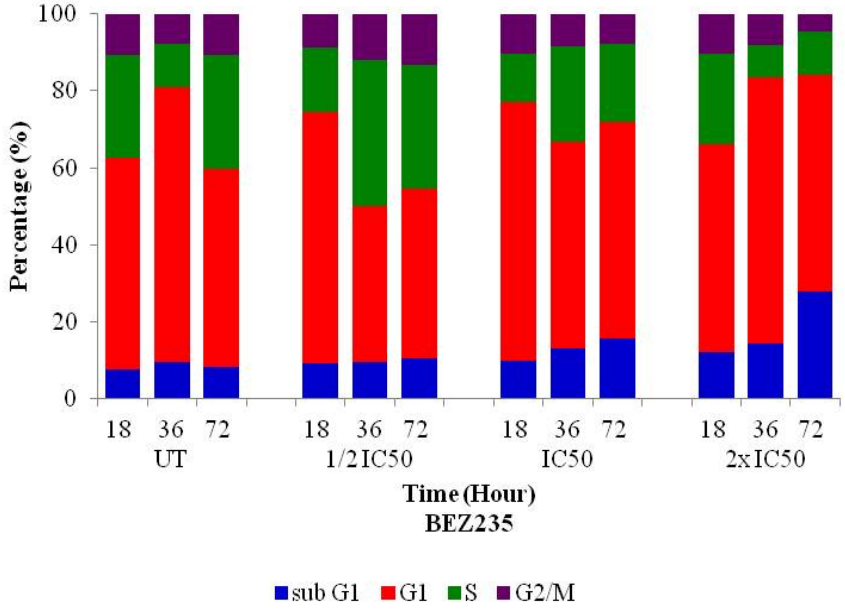
100
80
60
40
20
0
Percentage (%)
18 36 72 18 36 72 18 36 72 18 36 72
UT
1/2IC50
IC50
2xIC50
Time (Hour)
BEZ235
sub G1
G1
S
G2/M

B

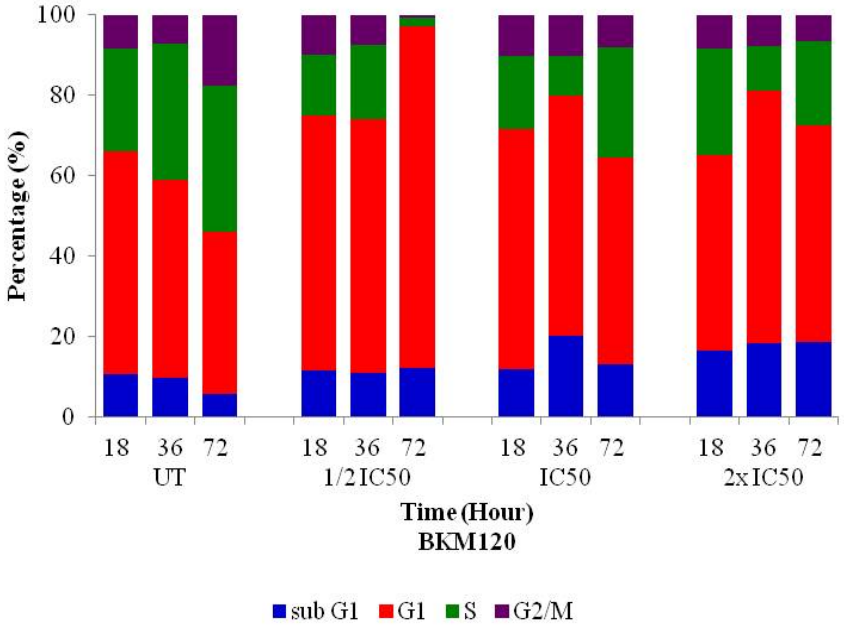
100
80
60
40
20
0
Percentage (%)
18 36 72 18 36 72 18 36 72 18 36 72
UT
1/2IC50
IC50
2xIC50
Time (Hour)
BKM120
sub G1
G1
S
G2/M

Figure 3.32. BEZ235 and BKM120 induce cell cycle arrest in RPMI-8226 cells. RPMI-8226 cells were incubated with **(A)** BEZ235 (½IC_{50}, 1x IC_{50} and 2x IC_{50}), **(B)** BKM120 (½IC_{50}, 1x IC_{50} and 2x IC_{50}) or vehicle alone (0.1% DMSO) for 18, 36 and 72 hours. At each time point, cells were ethanol fixed, stained with propridium iodide (PI) and analysed by flow cytometry. The data is presented as the percentage of cells in each phase of cell cycling (sub G1, G1, S and G2/M) for each concentration of drug at the 18, 36 and 72 hour time points.

A

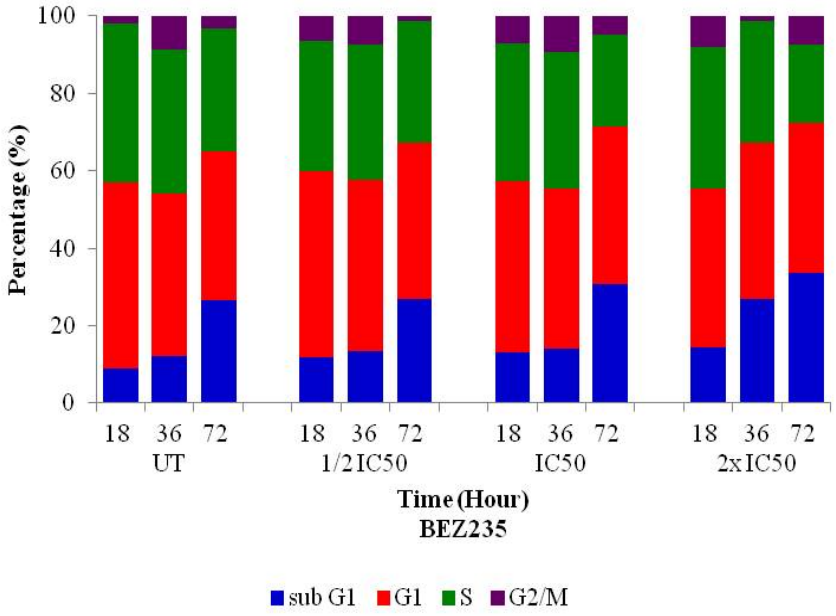
100
80
60
40
20
0
Percentage (%)
18 36 72 18 36 72 18 36 72 18 36 72
UT
1/2IC50
IC50
2xIC50
Time (Hour)
BEZ235
sub G1
G1
S
G2/M

B

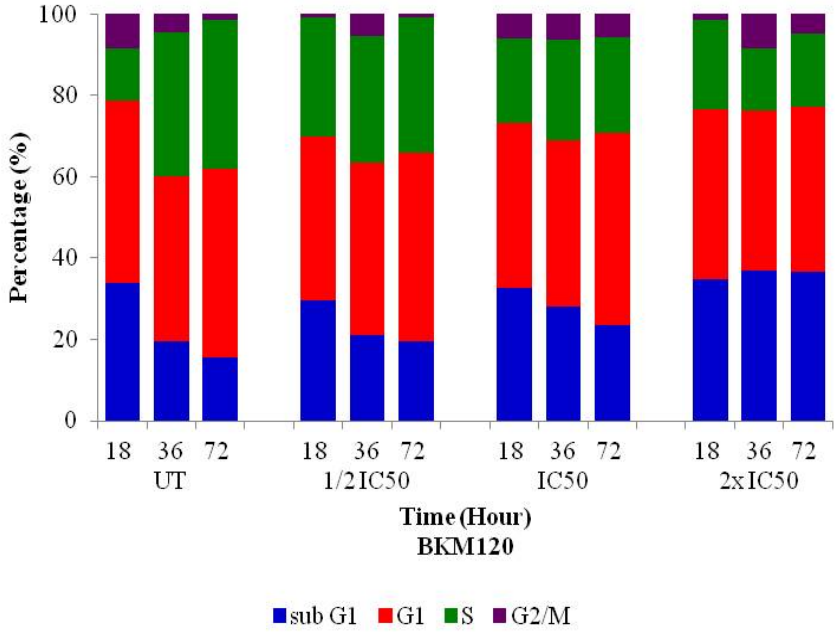
100
80
60
40
20
0
Percentage (%)
18 36 72 18 36 72 18 36 72 18 36 72
UT
1/2IC50
IC50
2xIC50
Time (Hour)
BKM120
sub G1
G1
S
G2/M

Figure 3.33. BEZ235 and BKM120 induce cell cycle arrest in WL2 cells. WL2 cells were incubated with **(A)** BEZ235 (½IC_{50}, 1x IC_{50} and 2x IC_{50}), **(B)** BKM120 (½IC_{50}, 1x IC_{50} and 2x IC_{50}) or vehicle alone (0.1% DMSO) for 18, 36 and 72 hours. At each time point, cells were ethanol fixed, stained with propridium iodide (PI) and analysed by flow cytometry. The data is presented as the percentage of cells in each phase of cell cycling (sub G1, G1, S and G2/M) for each concentration of drug at the 18, 36 and 72 hour time points.

A

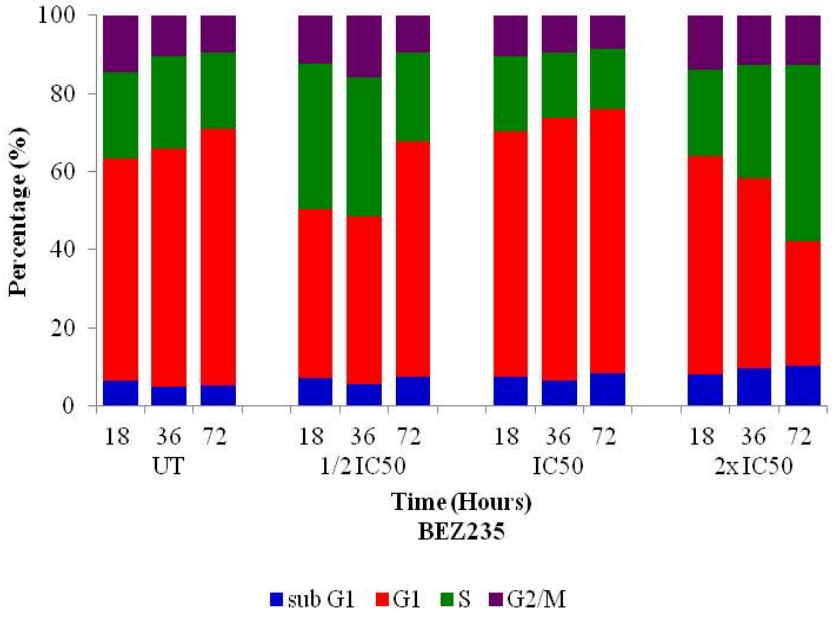
100
80
60
40
20
0
Percentage (%)
18 36 72 18 36 72 18 36 72 18 36 72
UT
1/2IC50
IC50
2xIC50
Time (Hours)
BEZ235
sub G1
G1
S
G2/M

B

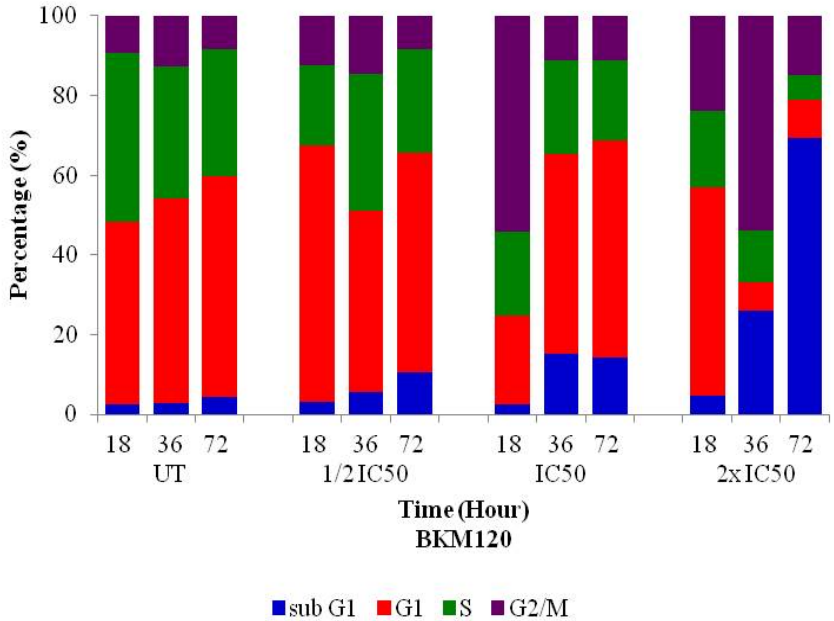
100
80
60
40
20
0
Percentage (%)
18 36 72 18 36 72 18 36 72 18 36 72
UT
1/2IC50
IC50
2xIC50
Time (Hour)
BKM120
sub G1
G1
S
G2/M

Figure 3.34. BEZ235 and BKM120 induce cell cycle arrest in murine 5TGM1 cells. Murine 5TGM1 cells were incubated with **(A)** BEZ235 (½IC_{50}, 1x IC_{50} and 2x IC_{50}), **(B)** BKM120 (½IC_{50}, 1x IC_{50} and 2x IC_{50}) or vehicle alone (0.1% DMSO) for 18, 36 and 72 hours. At each time point, cells were ethanol fixed, stained with propridium iodide (PI) and analysed by flow cytometry. The data is presented as the percentage of cells in each phase of cell cycling (sub G1, G1, S and G2/M) for each concentration of drug at the 18, 36 and 72 hour time points.

A

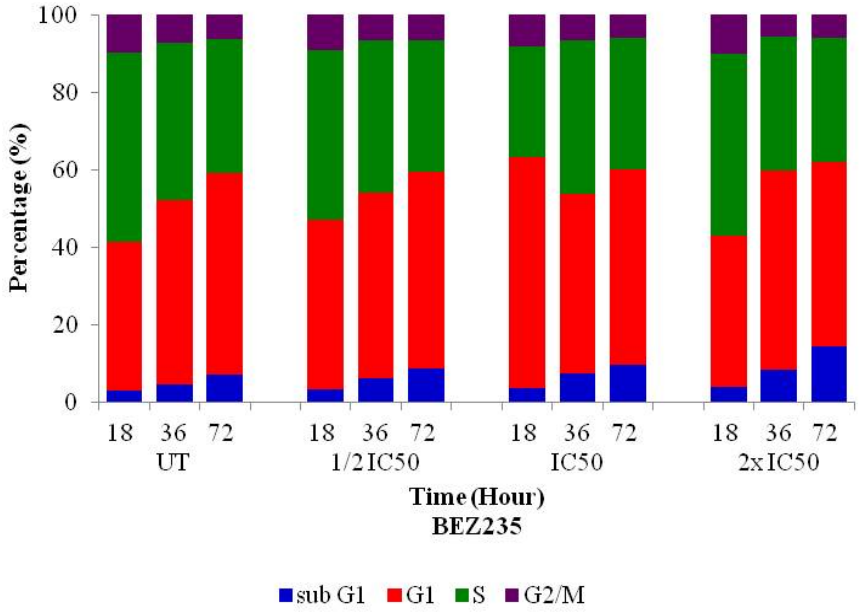
100
80
60
40
20
0
Percentage (%)
18 36 72 18 36 72 18 36 72 18 36 72
UT
1/2IC50
IC50
2xIC50
Time (Hour)
BEZ235
sub G1
G1
S
G2/M

B

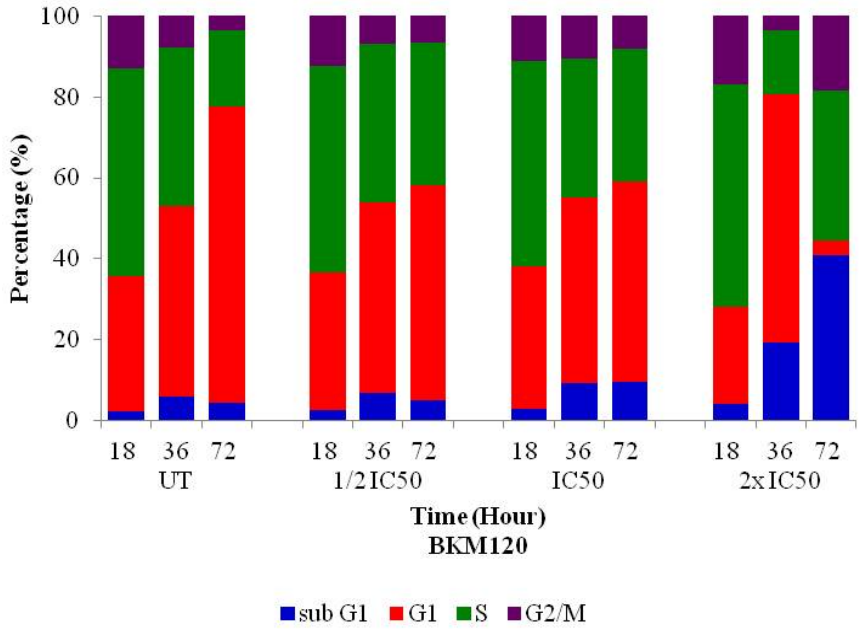
100
80
60
40
20
0
Percentage (%)
18 36 72 18 36 72 18 36 72 18 36 72
UT
1/2IC50
IC50
2xIC50
Time (Hour)
BKM120
sub G1
G1
S
G2/M

no published studies have reported that PDK-1, downstream of PI3k, is deleted or inactive or that PTEN is over-expressed in the cell lines examined in this study. A number of studies have demonstrated that deletion of PTEN leads to constitutive phosphorylation of Akt in MM cells[14; 30; 31; 32; 33].

Previously published findings by McMillin *et al* have demonstrated phosphorylation of Akt_{Ser473} in the human MM.1S cell line[24]. Furthermore, Zheng *et al* showed phosphorylation of Akt_{Thr308} and Akt_{Ser473} human myeloma cell lines MM.1S, ARP-1 and MM.1R[25]. There is no evidence in the literature to explain the absence of Akt phosphorylation in the human WL2 MM cell line and the murine 5TGM1 MM cell line in our study. Several studies have shown that Akt_{Thr308} and Akt_{Ser473} are phosphorylated when MM cells are serum-starved and pulsed with IGF-1 or IL-6 [34; 35; 36; 37]. In an attempt to induce Akt phosphorylation in our cells, we stimulated MM cells with each of these factors but were unable to detect Akt phosphorylation (data not shown).

As shown in by the AnnV/7AAD apoptosis assay (Figures 3.19, 3.20 3.21 and 3.22), treatment of 2x IC50 BEZ235 and BKM120 for 18 hours induced cytostasis in the MM cell lines. While the cells did not undergo apoptosis, they could have undergone quiescence, indicated by the inhibition of $p70^{S6k}$ phosphorylation. This phenomenon has been shown in a number of studies where $p70^{S6k}$ phosphorylation was inhibited in quiescent cells[38; 39].

Another interesting finding from these *in vitro* studies was that BKM120, a PI3k inhibitor, was able to inhibit the phosphorylation of $p70^{S6k}$ in MM cells at concentrations well within the therapeutic range of 10μM BKM120[40]. Despite not being a direct mTOR inhibitor, BKM120 has been shown to be able to either partially or fully inhibit $p70^{S6k}$ phosphorylation at doses between 1μM-10μM in MM, colon, gastric and brain cancer cell lines[25; 40; 41]. Given that the PI3-Akt-mTOR pathway is highly interconnected, our studies and those of Maira *et al.* suggest that BKM120 is able to inhibit all the downstream effectors of Akt[40].

Previously published studies have demonstrated that LY294002, Wortmannin and Rapamycin, in conjunction with Dexamethasone, induce apoptosis in human OPM2, U266 and MM.1S MM cell lines[42; 43; 44; 45; 46]. Furthermore, McMillin *et al* demonstrated that 100nM BEZ235 was able to induce MM cell apoptosis, as evidenced by an increase in AnnV/7AAD double positive cells after 48 hours[24]. Although Zheng

et al did not show that BKM120 induced apoptosis; they demonstrated an increase in G1 cell cycle arrest when the MM cells were treated with 1μM BKM120 for 24 hours[25]. In line with these findings, our data showed that treatment with 2x IC_{50} of BEZ235 (IC_{50} in Table 3.1) and BKM120 (IC_{50} in Table 3.1) for 72 hours induced an increase in sub G1 population in the cell cycle arrest analyses. While BEZ235 and BKM120 treatment for 2 hours increased oxidative stress levels in the MM cell lines, cell apoptosis was not observed when MM cell lines were treated with BEZ235 and BKM120 for 18 hours as only a small population of AnnV/7AAD double positive cells was observed.

In summary, the data presented here shows that BEZ235 and BKM120 are able to inhibit human and murine MM cell proliferation, and while not significant, there was some evidence to suggest that these inhibitors could induce low levels of apoptosis when cells were treated with BEZ235 and BKM120 for 72 hours *in vitro*. In this next results chapter, these findings will be translated into a murine model of MM, to further understand the anti-MM properties of BEZ235 and BKM120 in a more complex biological setting.

Reference:

1. West, K. A., Castillo, S. S. & Dennis, P. A. (2002). Activation of the PI3K/Akt pathway and chemotherapeutic resistance. *Drug resistance updates : reviews and commentaries in antimicrobial and anticancer chemotherapy* **5**, 234-48.
2. Clark, A. S., West, K., Streicher, S. & Dennis, P. A. (2002). Constitutive and inducible Akt activity promotes resistance to chemotherapy, trastuzumab, or tamoxifen in breast cancer cells. *Molecular cancer therapeutics* **1**, 707-17.
3. Grunwald, V., DeGraffenried, L., Russel, D., Friedrichs, W. E., Ray, R. B. & Hidalgo, M. (2002). Inhibitors of mTOR reverse doxorubicin resistance conferred by PTEN status in prostate cancer cells. *Cancer research* **62**, 6141-5.
4. Steelman, L. S., Navolanic, P. M., Sokolosky, M. L., Taylor, J. R., Lehmann, B. D., Chappell, W. H., Abrams, S. L., Wong, E. W., Stadelman, K. M., Terrian, D. M., Leslie, N. R., Martelli, A. M., Stivala, F., Libra, M., Franklin, R. A. & McCubrey, J. A. (2008). Suppression of PTEN function increases breast cancer chemotherapeutic drug resistance while conferring sensitivity to mTOR inhibitors. *Oncogene* **27**, 4086-95.
5. Malgeri, U., Baldini, L., Perfetti, V., Fabris, S., Vignarelli, M. C., Colombo, G., Lotti, V., Compasso, S., Bogni, S., Lombardi, L., Maiolo, A. T. & Neri, A. (2000). Detection of t(4;14)(p16.3;q32) chromosomal translocation in multiple myeloma by reverse transcription-polymerase chain reaction analysis of IGH-MMSET fusion transcripts. *Cancer research* **60**, 4058-61.
6. Chesi, M., Nardini, E., Brents, L. A., Schrock, E., Ried, T., Kuehl, W. M. & Bergsagel, P. L. (1997). Frequent translocation t(4;14)(p16.3;q32.3) in multiple myeloma is associated with increased expression and activating mutations of fibroblast growth factor receptor 3. *Nature genetics* **16**, 260-4.
7. Chesi, M., Nardini, E., Lim, R. S., Smith, K. D., Kuehl, W. M. & Bergsagel, P. L. (1998). The t(4;14) translocation in myeloma dysregulates both FGFR3 and a novel gene, MMSET, resulting in IgH/MMSET hybrid transcripts. *Blood* **92**, 3025-34.
8. Ronchetti, D., Greco, A., Compasso, S., Colombo, G., Dell'Era, P., Otsuki, T., Lombardi, L. & Neri, A. (2001). Deregulated FGFR3 mutants in multiple myeloma cell lines with t(4;14): comparative analysis of Y373C, K650E and the novel G384D mutations. *Oncogene* **20**, 3553-62.
9. Lauring, J., Abukhdeir, A. M., Konishi, H., Garay, J. P., Gustin, J. P., Wang, Q., Arceci, R. J., Matsui, W. & Park, B. H. (2008). The multiple myeloma associated

MMSET gene contributes to cellular adhesion, clonogenic growth, and tumorigenicity. *Blood* **111**, 856-64.

10. Soverini, S., Cavo, M., Cellini, C., Terragna, C., Zamagni, E., Ruggeri, D., Testoni, N., Tosi, P., De Vivo, A., Amabile, M., Grafone, T., Ottaviani, E., Giannini, B., Cangini, D., Bonifazi, F., Neri, A., Fabris, S., Tura, S., Baccarani, M. & Martinelli, G. (2003). Cyclin D1 overexpression is a favorable prognostic variable for newly diagnosed multiple myeloma patients treated with high-dose chemotherapy and single or double autologous transplantation. *Blood* **102**, 1588-94.
11. Santra, M., Zhan, F., Tian, E., Barlogie, B. & Shaughnessy, J., Jr. (2003). A subset of multiple myeloma harboring the t(4;14)(p16;q32) translocation lacks FGFR3 expression but maintains an IGH/MMSET fusion transcript. *Blood* **101**, 2374-6.
12. Chang, H., Qi, X. Y., Claudio, J., Zhuang, L., Patterson, B. & Stewart, A. K. (2006). Analysis of PTEN deletions and mutations in multiple myeloma. *Leukemia research* **30**, 262-5.
13. Shi, Y., Gera, J., Hu, L., Hsu, J. H., Bookstein, R., Li, W. & Lichtenstein, A. (2002). Enhanced sensitivity of multiple myeloma cells containing PTEN mutations to CCI-779. *Cancer research* **62**, 5027-34.
14. Hyun, T., Yam, A., Pece, S., Xie, X., Zhang, J., Miki, T., Gutkind, J. S. & Li, W. (2000). Loss of PTEN expression leading to high Akt activation in human multiple myelomas. *Blood* **96**, 3560-8.
15. Zhang, J., Choi, Y., Mavromatis, B., Lichtenstein, A. & Li, W. (2003). Preferential killing of PTEN-null myelomas by PI3K inhibitors through Akt pathway. *Oncogene* **22**, 6289-95.
16. Castellano, E. & Downward, J. (2011). RAS Interaction with PI3K: More Than Just Another Effector Pathway. *Genes & cancer* **2**, 261-74.
17. Neri, A., Baldini, L., Trecca, D., Cro, L., Polli, E. & Maiolo, A. T. (1993). p53 gene mutations in multiple myeloma are associated with advanced forms of malignancy. *Blood* **81**, 128-35.
18. Bezieau, S., Devilder, M. C., Avet-Loiseau, H., Mellerin, M. P., Puthier, D., Pennarun, E., Rapp, M. J., Harousseau, J. L., Moisan, J. P. & Bataille, R. (2001). High incidence of N and K-Ras activating mutations in multiple myeloma and primary plasma cell leukemia at diagnosis. *Human mutation* **18**, 212-24.

19. Neri, A., Murphy, J. P., Cro, L., Ferrero, D., Tarella, C., Baldini, L. & Dalla-Favera, R. (1989). Ras oncogene mutation in multiple myeloma. *The Journal of experimental medicine* **170**, 1715-25.
20. Peterson, T. R., Laplante, M., Thoreen, C. C., Sancak, Y., Kang, S. A., Kuehl, W. M., Gray, N. S. & Sabatini, D. M. (2009). DEPTOR is an mTOR inhibitor frequently overexpressed in multiple myeloma cells and required for their survival. *Cell* **137**, 873-86.
21. Proud, C. G. (2009). Dynamic balancing: DEPTOR tips the scales. *Journal of molecular cell biology* **1**, 61-3.
22. Zhao, Y., Xiong, X. & Sun, Y. DEPTOR, an mTOR inhibitor, is a physiological substrate of SCF(betaTrCP) E3 ubiquitin ligase and regulates survival and autophagy. *Molecular cell* **44**, 304-16.
23. Stengel, C., Cheung, C. W., Quinn, J., Yong, K. & Khwaja, A. (2012). Optimal induction of myeloma cell death requires dual blockade of phosphoinositide 3-kinase and mTOR signalling and is determined by translocation subtype. *Leukemia : official journal of the Leukemia Society of America, Leukemia Research Fund, U.K.*
24. McMillin, D. W., Ooi, M., Delmore, J., Negri, J., Hayden, P., Mitsiades, N., Jakubikova, J., Maira, S. M., Garcia-Echeverria, C., Schlossman, R., Munshi, N. C., Richardson, P. G., Anderson, K. C. & Mitsiades, C. S. (2009). Antimyeloma activity of the orally bioavailable dual phosphatidylinositol 3-kinase/mammalian target of rapamycin inhibitor NVP-BEZ235. *Cancer research* **69**, 5835-42.
25. Zheng, Y., Yang, J., Qian, J., Zhang, L., Lu, Y., Li, H., Lin, H., Lan, Y., Liu, Z., He, J., Hong, S., Thomas, S., Shah, J., Baladandayuthapani, V., Kwak, L. W. & Yi, Q. (2012). Novel phosphatidylinositol 3-kinase inhibitor NVP-BKM120 induces apoptosis in myeloma cells and shows synergistic anti-myeloma activity with dexamethasone. *Journal of molecular medicine* **90**, 695-706.
26. Fitter, S., Vandyke, K., Gronthos, S. & Zannettino, A. C. (2012). Suppression of PDGF-induced PI3 kinase activity by imatinib promotes adipogenesis and adiponectin secretion. *Journal of molecular endocrinology* **48**, 229-40.
27. Betteridge, D. J. (2000). What is oxidative stress? *Metabolism: clinical and experimental* **49**, 3-8.
28. Deavall, D. G., Martin, E. A., Horner, J. M. & Roberts, R. (2012). Drug-induced oxidative stress and toxicity. *Journal of toxicology* **2012**, 645460.

29. Breitkopf, S. B., Yuan, M., Pihan, G. A. & Asara, J. M. (2012). Detection of a rare BCR-ABL tyrosine kinase fusion protein in H929 multiple myeloma cells using immunoprecipitation (IP)-tandem mass spectrometry (MS/MS). *Proceedings of the National Academy of Sciences of the United States of America* **109**, 16190-5.
30. Jiang, B. H. & Liu, L. Z. (2008). PI3K/PTEN signaling in tumorigenesis and angiogenesis. *Biochimica et biophysica acta* **1784**, 150-8.
31. Hennessy, B. T., Smith, D. L., Ram, P. T., Lu, Y. & Mills, G. B. (2005). Exploiting the PI3K/AKT pathway for cancer drug discovery. *Nature reviews. Drug discovery* **4**, 988-1004.
32. Hay, N. (2005). The Akt-mTOR tango and its relevance to cancer. *Cancer Cell* **8**, 179-83.
33. Dancey, J. E. (2004). Molecular targeting: PI3 kinase pathway. *Annals of oncology : official journal of the European Society for Medical Oncology / ESMO* **15 Suppl 4**, iv233-9.
34. Pene, F., Claessens, Y. E., Muller, O., Viguie, F., Mayeux, P., Dreyfus, F., Lacombe, C. & Bouscary, D. (2002). Role of the phosphatidylinositol 3-kinase/Akt and mTOR/P70S6-kinase pathways in the proliferation and apoptosis in multiple myeloma. *Oncogene* **21**, 6587-97.
35. Hideshima, T., Nakamura, N., Chauhan, D. & Anderson, K. C. (2001). Biologic sequelae of interleukin-6 induced PI3-K/Akt signaling in multiple myeloma. *Oncogene* **20**, 5991-6000.
36. Ge, N. L. & Rudikoff, S. (2000). Insulin-like growth factor I is a dual effector of multiple myeloma cell growth. *Blood* **96**, 2856-61.
37. Abroun, S., Ishikawa, H., Tsuyama, N., Liu, S., Li, F. J., Otsuyama, K., Zheng, X., Obata, M. & Kawano, M. M. (2004). Receptor synergy of interleukin-6 (IL-6) and insulin-like growth factor-I in myeloma cells that highly express IL-6 receptor alpha [corrected]. *Blood* **103**, 2291-8.
38. Takuwa, N., Fukui, Y. & Takuwa, Y. (1999). Cyclin D1 expression mediated by phosphatidylinositol 3-kinase through mTOR-p70(S6K)-independent signaling in growth factor-stimulated NIH 3T3 fibroblasts. *Molecular and cellular biology* **19**, 1346-58.
39. Frost, V., Morley, S. J., Mercep, L., Meyer, T., Fabbro, D. & Ferrari, S. (1995). The phosphodiesterase inhibitor SQ 20006 selectively blocks mitogen activation of p70S6k and transition to S phase of the cell division cycle without affecting the

steady state phosphorylation of eIF-4E. *The Journal of biological chemistry* **270**, 26698-706.

40. Maira, S. M., Pecchi, S., Huang, A., Burger, M., Knapp, M., Sterker, D., Schnell, C., Guthy, D., Nagel, T., Wiesmann, M., Brachmann, S., Fritsch, C., Dorsch, M., Chene, P., Shoemaker, K., De Pover, A., Menezes, D., Martiny-Baron, G., Fabbro, D., Wilson, C. J., Schlegel, R., Hofmann, F., Garcia-Echeverria, C., Sellers, W. R. & Voliva, C. F. (2012). Identification and characterization of NVP-BKM120, an orally available pan-class I PI3-kinase inhibitor. *Molecular cancer therapeutics* **11**, 317-28.
41. Mueller, A., Bachmann, E., Linnig, M., Khillimberger, K., Schimanski, C. C., Galle, P. R. & Moehler, M. (2012). Selective PI3K inhibition by BKM120 and BEZ235 alone or in combination with chemotherapy in wild-type and mutated human gastrointestinal cancer cell lines. *Cancer chemotherapy and pharmacology* **69**, 1601-15.
42. Grugan, K. D., Ma, C., Singhal, S., Krett, N. L. & Rosen, S. T. (2008). Dual regulation of glucocorticoid-induced leucine zipper (GILZ) by the glucocorticoid receptor and the PI3-kinase/AKT pathways in multiple myeloma. *The Journal of steroid biochemistry and molecular biology* **110**, 244-54.
43. Yan, H., Frost, P., Shi, Y., Hoang, B., Sharma, S., Fisher, M., Gera, J. & Lichtenstein, A. (2006). Mechanism by which mammalian target of rapamycin inhibitors sensitize multiple myeloma cells to dexamethasone-induced apoptosis. *Cancer research* **66**, 2305-13.
44. Stromberg, T., Dimberg, A., Hammarberg, A., Carlson, K., Osterborg, A., Nilsson, K. & Jernberg-Wiklund, H. (2004). Rapamycin sensitizes multiple myeloma cells to apoptosis induced by dexamethasone. *Blood* **103**, 3138-47.
45. Ogawa, M., Nishiura, T., Oritani, K., Yoshida, H., Yoshimura, M., Okajima, Y., Ishikawa, J., Hashimoto, K., Matsumura, I., Tomiyama, Y. & Matsuzawa, Y. (2000). Cytokines prevent dexamethasone-induced apoptosis via the activation of mitogen-activated protein kinase and phosphatidylinositol 3-kinase pathways in a new multiple myeloma cell line. *Cancer research* **60**, 4262-9.
46. Tu, Y., Gardner, A. & Lichtenstein, A. (2000). The phosphatidylinositol 3-kinase/AKT kinase pathway in multiple myeloma plasma cells: roles in cytokine-dependent survival and proliferative responses. *Cancer research* **60**, 6763-70.

Chapter 4

The Effect of BEZ235 and BKM120 on MM and MM-induced Bone Loss

4.1 *Introduction*

Studies using PI3k inhibitors, LY294002 and Wortmannin, and the mTOR inhibitor Rapamycin have demonstrated convincing pro-apoptotic effects in a number of *in vivo* tumour models. In colon cancer, non-small cell lung cancer and ovarian cancer models, LY294002 induces tumour cell apoptosis and reduces tumour size[1; 2; 3; 4]. Moreover, Wortmannin inhibits the growth and motility of tumour cells and induces apoptosis in pancreatic and human non-small cell lung cancer xenograft models[5; 6; 7]. Similarly, Rapamycin has been shown to be an effective anti-tumour agent in pancreatic, breast and oral cancer animal models[8; 9; 10; 11]. While LY294002, Wortmannin and Rapamycin alone are effective in causing tumour cell apoptosis, the combination of these drugs with conventional chemotherapy agents such as butyrate, paclitaxel, gemcitabine and doxorubicin enhances their efficacy in inducing tumour apoptosis[1; 4; 6; 8; 9].

Toxicity studies have shown that while the administration of 100mg/kg LY294002 once daily is effective in reducing tumour growth in nude mice with bladder cancer xenografts, this concentration caused severe respiratory difficulty and lethargy in the animals[12]. Similarly, Wortmannin-associated toxicity was observed at 1.5mg/kg in colon and ovarian carcinomas and leukemia in vivo tumour models[13]. While Rapamycin was well tolerated in animal models, continuous administration of 100mg/kg Rapamycin significantly impaired glucose-induced insulin secretion[14]. Studies using PI-103, a dual PI3k and mTOR inhibitor, demonstrated that treatment with drug alone was incapable of reducing tumour growth in subcutaneous human melanoma xenograft models. While these studies showed that PI-103 is effective when combined with Rapamycin[15], this combination approach leads to immunosuppression[16] in these models. These side effects and the ineffectiveness of these drugs in preclinical studies highlighted that these drugs are not suitable candidates for future clinical trials as anti-tumour agents.

Recently, a number of studies have investigated the role of the dual PI3k/mTOR inhibitor, BEZ235, and the PI3k inhibitor, BKM120, in inhibiting tumour cell growth. The effectiveness of BEZ235 as an anti-tumour agent has been shown in breast, non small-cell lung, glioblastoma, prostate and colorectal cancers[17; 18; 19; 20]. BEZ235 has been shown to inhibit tumour cell proliferation in vivo, with a reduction in tumour size observed in tumour cell xenografts[17; 18; 19; 20]. In a breast cancer study, administration of

45mg/kg BEZ235 once daily was shown to induce cell apoptosis *in vivo*, and *ex vivo* analysis of these tumour cells demonstrated a decrease in Akt_{Ser473} phosphorylation and an increase in Caspase-2, -6 and -7 phosphorylation[17]. Furthermore, decreased phosphorylation of Akt_{Ser473} and $p70^{S6k}$ was observed in breast cancer xenografts and skin tissue, 1-hour post-BEZ235 administration[18]. Of relevance to this thesis, a study by McMillin and colleagues demonstrated that BEZ235-treatment decreased the size of subcutaneously implanted human MM cells in a NOD-SCID mouse model[21]. McMillin also observed that the survival rate of BEZ235-treated animals was significantly higher than the vehicle-treated animals with no significant weight loss or signs of toxicity[21]. These findings suggest that BEZ235 is not only was well tolerated by the animals but also possesses anti-tumour properties.

BKM120 has also been shown to be a promising anti-tumour agent in subcutaneous xenograft models of gastrointestinal, ovarian and lung cancer, glioma, and myeloma[22; 23; 24; 25; 26]. BKM120 was found to completely inhibit Akt_{Ser473} phosphorylation when administered at 30, 60 or 100mg/kg/day in an ovarian cancer xenograft model[23]. Administration of 30mg/kg and 60mg/kg BKM120, once daily, was also found to be effective in inducing ovarian and glioma tumour cell apoptosis and reducing tumour growth. Importantly, both concentrations were well tolerated with minimal side effects[23; 27]. Recently, a study by Zheng *et al* investigated the efficacy of BKM120 on human MM xenografts in NOD-SCID mice and showed that administration of 40mg/kg BKM120 once daily significantly reduced tumour growth, serum light chains and prolonged the survival of the animals[26]. To date, both BEZ235 and BKM120 have been shown to be well tolerated and display minimal side effects in preclinical studies[20; 21; 23; 27]. As a result, both drugs are currently being investigated in Phase I/II human clinical trials in patients with advanced solid tumours[28; 29].

In addition to their anti-tumour properties, studies have also demonstrated that PI3k and mTOR inhibitors possess anti-osteoclastic properties. Wortmannin prevents bone degradation in ovariectomized rats by inhibiting the signalling between Akt Ser^{473} and c-Src, a tyrosine kinase which is essential for osteoclast function[30; 31]. Furthermore, studies by Ulici *et al* and Xie *et al* have found that LY294002 serves to protect bone loss by reducing the number of TRAP-positive osteoclasts and prevents bone loss in OPG and Akt1 knockout mice[32; 33]. Interestingly, administration of Rapamycin to young rats retards the growth and activity of growth plate. Analysis of the growth plate

revealed a disorganised proliferative zone characterised by a loss of the normal columnar pattern and an ill-defined transition between the proliferation and hyperthrophic zones.[34] Rapamycin administration also affects the healing of femoral fractures in young mice, by reducing callus formation and vascularisation within the fracture[35]. These results suggest that the PI3k and mTOR pathways play important roles in bone formation.

Over the years, numerous animal models have been developed to study various aspects of MM biology. These models include xenograft models in which human MM cells are injected subcutaneously or intratibially into immunocompromised animals, and systemic animal models in which murine MM cells were injected intrabially into immunocompetent animals. In 1979, it was observed that 0.5% of aging C57BL6-KaLwRijHsd (KaLwRij) mice develop a MM-like disease[36; 37; 38; 39]. From this observation, the 5T MM mouse models (5T2MM, 5T33MM and 5TGM1) have been derived and involve the intravenous propagation of KaLwRij-derived MM PCs in immunocompetent KaLwRij mice[36; 40; 41; 42]. The 5T MM models closely mimic human MM disease and develop osteolytic bone lesions, hind-limb paralysis (caused by spinal cord compression) and occasional hypercalcaemia[43]. Of the three 5T MM models, the 5TGM1 model was selected as the most suitable for the studies outlined in this chapter as 5TGM1 cells can be propagated and manipulated *in vitro* while the 5T2MM and 5T33MM cell lines require *in vivo* propagation and cannot be manipulated[41; 44]. The 5TGM1 model has been widely used and has been proven to be a suitable animal model to test novel therapies for the treatment of MM and MM-associated bone destruction[43; 45; 46].

Having shown in the previous chapter that BEZ235 and BKM120 inhibit 5TGM1 cell proliferation and induce 5TGM1 apoptosis *in vitro*, we next wanted to examine the effect of these drugs on 5TGM1 growth and MM disease progression *in vivo*. This chapter outlines *in vivo* experiments designed to investigate the effects of BEZ235 and BKM120 on MM disease progression and bone loss *in vivo*.

4.2 *Results*

4.2.1 The effect of BEZ235 tumour progression and osteolytic bone disease *in vivo*

4.2.1.1 BEZ235 slows tumour progression down in vivo

To investigate the effect of BEZ235 in a murine model of MM, 5TGM1-SFG cells were injected into the tail vein of 6-8 week old female C57BL/KaLwRij mice. 5TGM1-SFG cells were engineered to express firefly luciferase so as to enable bioluminescent monitoring of tumour growth *in vivo*[47]. Two weeks post-tumour cell injection, after the cells had homed from the peripheral circulation and established within the bone marrow, the mice were divided into two treatment groups (n=10 per group): Group 1 were administered 0.5% methyl cellulose (vehicle control) via daily oral gavage for two weeks; and Group 2 were administered 40mg/kg BEZ235 via daily oral gavage for two weeks. The dose of BEZ235 was selected based on previously published studies[48; 49]. This dose was reported as well tolerated and exert anti-tumour effects in treated animals[48; 49]. Tumour growth was assessed at weekly intervals from the time of tumour cell inoculation and for the duration of the study via bioluminescence imaging (BLI). Figure 4.1A shows consecutive BLI images of a representative animal from each treatment group throughout the study, to illustrate disease progression over time. Quantitation of the bioluminescence signal intensity from each animal revealed a decrease in signal intensity in response to BEZ235 treatment at week 3 and a significant decrease in signal intensity at week 4 (Figure 4.1B, $p < 0.05$, Student's t-test).

4.2.1.2 BEZ235 decreases serum paraprotein levels and has no effect on animal weight

Serum paraprotein relates to monoclonal immunoglobulin that is produced by clonal malignant plasma cells that can be detected in the serum[50] and is a marker of MM disease burden. To determine whether BEZ235 affects serum paraprotein levels in our model, blood was collected from all animals at weekly intervals and serum paraprotein

Figure 4.1. BEZ235 slows tumour progression in vivo. C57BL/KaLwRijHsd mice (n=10 per group) were intravenously inoculated with 5 x 105 5TGM1-SFG cells. Two weeks post-tumour cell injection, animals were treated with 50mg/kg BEZ235 or vehicle alone (0.5% methyl cellulose) via daily oral gavage for two weeks. Tumour progression was monitored weekly by live bioluminescence imaging (BLI) following intraperitoneal administration with D-luciferin. (A) Consecutive weekly BLI images of a representative mouse from the vehicle group (top panel) and BEZ235-treated group (bottom panel) are shown at weeks 1-4 following tumour inoculation. (B) The average bioluminescence signal intensity was graphed to illustrate the changes in the signal intensity at each time point for each animal group. Data are expressed as mean ± SEM luminescence signal.*$p<0.05$, Student's t-test.

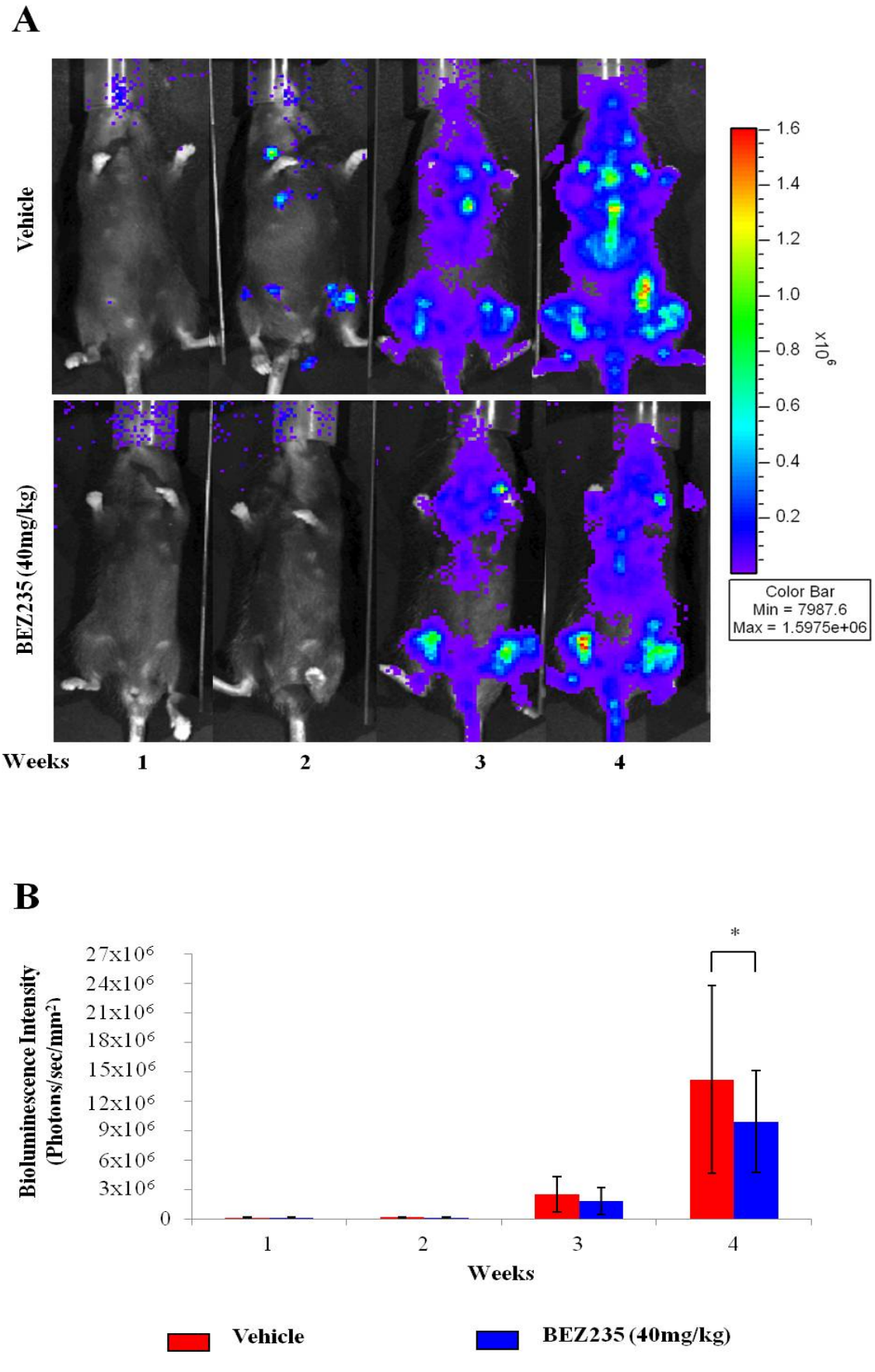
A
Vehicle
BEZ235 (40mg/kg)
1.6
1.4
1.2
1.0
0.8
0.6
0.4
0.2
x10⁶
Color Bar
Min = 7987.6
Max = 1.5975e+06
Weeks 1 2 3 4
B
Bioluminescence Intensity (Photons/sec/mm²)
27x10⁶
24x10⁶
21x10⁶
18x10⁶
15x10⁶
12x10⁶
9x10⁶
6x10⁶
3x10⁶
0
*
1
2
3
4
Weeks
Vehicle
BEZ235 (40mg/kg)

levels measured using the Sebia Hydragel 30 β1-β2 kit according to the manufacturer's instructions. As shown in Figure 4.2A, a progressive increase in serum paraprotein was observed in vehicle-treated animals, with a clear protein band evident at 3 and 4 weeks post-tumour inoculation. In contrast, there was a delay in the onset of paraprotein detection in BEZ235-treated animals, with a serum paraprotein band only observed at the 4-week time point. When the intensity of the serum paraprotein band was measured and normalised to total protein, a significant decrease in serum paraprotein was observed in response to BEZ235-treatment at week 3 (Figure 4.2A, bottom panel, $p < 0.05$, Student's t-test) and week 4 (Figure 4.2A, bottom panel, $p < 0.01$, Student's t-test), compared to vehicle-treated animals.

Throughout the duration of the study, the weight of each animal was measured twice weekly to monitor the effects of tumour burden and/or drug or vehicle administration on overall animal health. As shown as Figure 4.2B, the weight of the animals was not affected by BEZ235 treatment and evidence of toxicity was observed.

4.2.1.3 BEZ235 reduces the number of osteolytic lesions

To examine the effect of BEZ235 on osteolytic bone disease *in vivo*, formalin-fixed tibiae from vehicle- and BEZ235-treated animals were scanned on a high-resolution μCT scanner. 3D images of the tibiae were generated, and the images sliced in half on a plane parallel through the length of the tibiae and the number of osteolytic lesions that perforated the tibiae was enumerated. Figure 4.3A shows an example of the osteolytic lesions that perforate the tibiae of representative animals from the vehicle-treated group (top panel) and BEZ235-treated group (bottom panel). As shown in Figure 4.3B, a significant decrease in the number of osteolytic lesions in the tibial cortical bone was observed in BEZ235-treated animals, compared to the vehicle alone ($p < 0.01$, Student's t-test).

4.2.1.4 BEZ235 increases bone volume density and trabecular number

To examine the effect of BEZ235 treatment on trabecular bone morphometry, a 0.645mm region of the trabecular bone, commencing 0.215mm from the growth plate, was analysed for all animals using cTAN software (SkyScan). A significant increase in

Figure 4.2. BEZ235 decreases serum paraprotein levels and has no effect on animal weight. C57BL/KaLwRijHsd mice (n=10 per group) were intravenously inoculated with 5 x 105 5TGM1-SFG cells. Two weeks post-tumour cell injection, animals were treated with 50mg/kg BEZ235 or vehicle alone via daily oral gavage for two weeks. Blood was collected from vehicle- and BEZ235-treated animals at weekly intervals and serum paraprotein levels measured. (A) Serum paraprotein gels from a representative animal from the vehicle (top left) and BEZ235-treated (top right) groups are shown. The arrow indicates the protein band corresponding to serum paraprotein. Sebia image analysis software was used to quantitate the intensity of the paraprotein band relative to total serum protein bands. The data were then plotted as the mean ± SEM for each treatment group. *$p<0.05$ and **$p<0.01$, Student's t-test. (B) The weight of each animal was measured twice weekly for the duration of the study and the average weight of each group plotted. Data are expressed as the mean ± SEM.

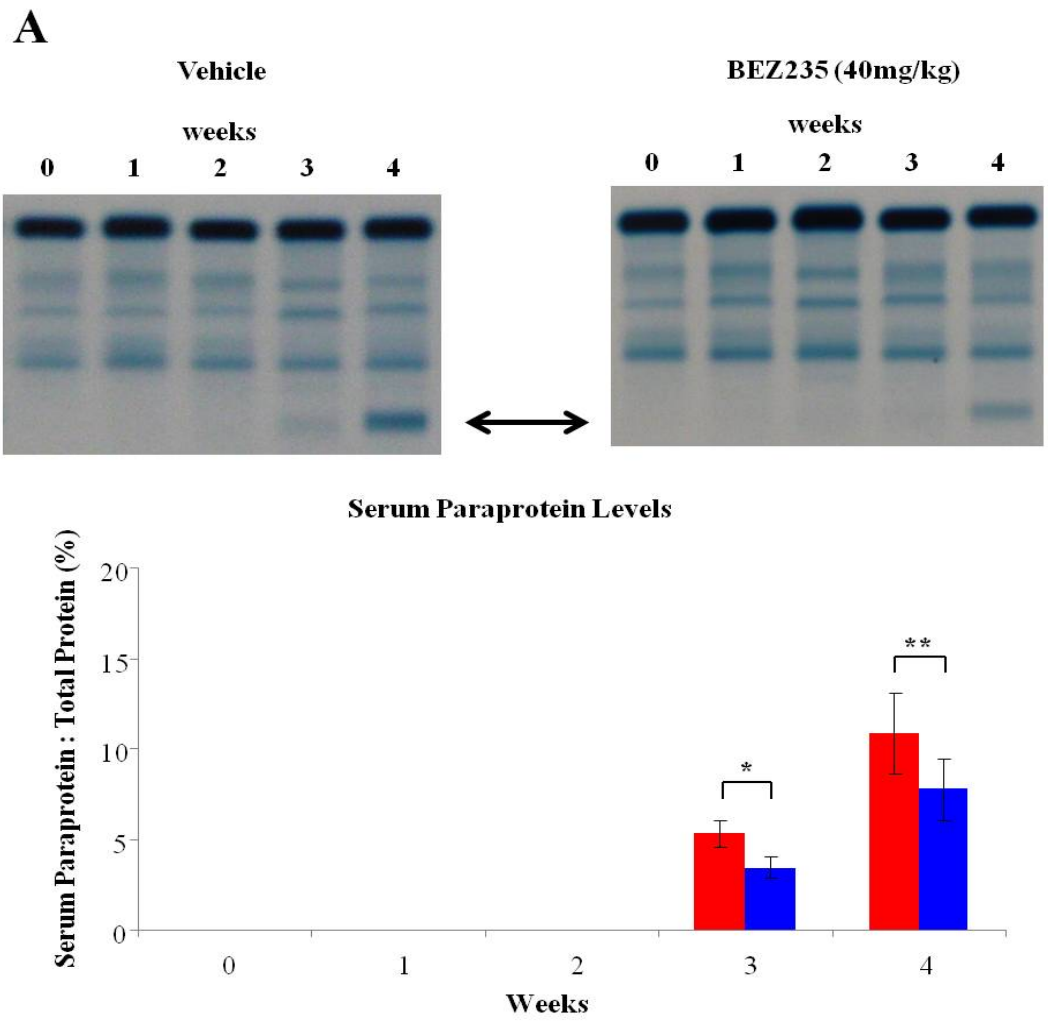
A
Vehicle
weeks
0 1 2 3 4
BEZ235 (40mg/kg)
weeks
0 1 2 3 4
Serum Paraprotein Levels
Serum Paraprotein : Total Protein (%)
20
15
10
5
0
*
**
0 1 2 3 4
Weeks
B
Weight of Animals
Weight (g)
20
15
10
5
0
0 4 7 11 14 18 21 25 28
Day
Vehicle
BEZ235 (40mg/kg)

Figure 4.3. BEZ235 reduces the number of osteolytic lesions that perforate the tibiae cortices. C57BL/KaLwRijHsd mice (n=10 per group) were intravenously inoculated with 5 x 105 5TGM1-SFG cells. Two weeks post-tumour cell injection, animals were treated with 50mg/kg BEZ235 or vehicle alone via daily oral gavage for two weeks. At the end of the study, tibiae were harvested, fixed in formalin and scanned on a high-resolution μCT scanner. (A) 3D images were generated using SkyScan ANT software, and bones were sliced in half on a plane parallel through the length of the tibia. 3D images from two representative animals from the vehicle (top panels) and BEZ235-treated (bottom panels) groups are shown. (B) The number of osteolytic lesions present in the tibial cortical bone of each animal was enumerated and the average number of osteolytic lesions per animal for each group was graphed. Data are expressed as the mean ± SEM (left panel). To better illustrate the range in the number of osteolytic lesions present in each animal cohort, the data was also plotted as a dot plot (right panel). **$p<0.01$, Student's t-test.

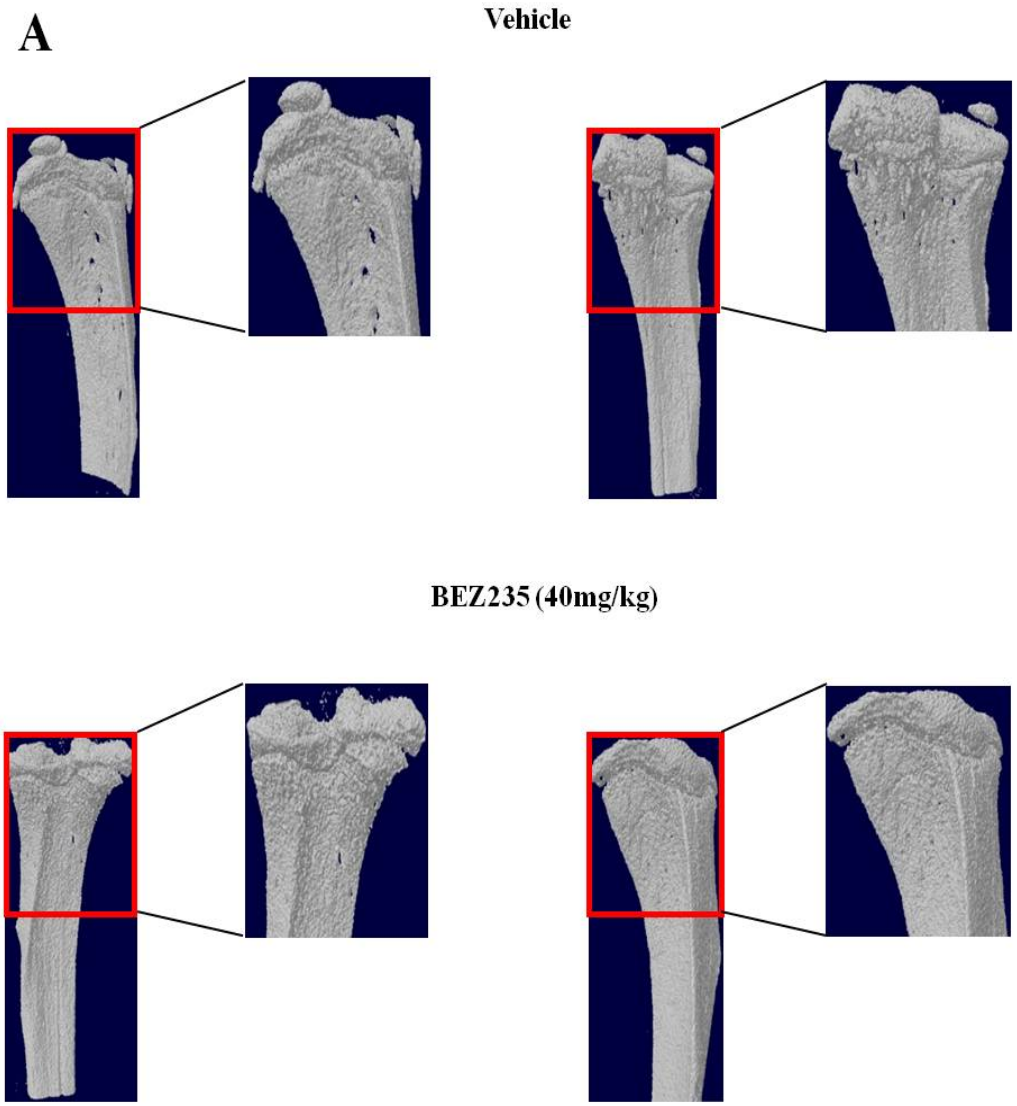
A
Vehicle
BEZ235 (40mg/kg)
B
Number of Osteolytic Lesions
60
40
20
0
**
Vehicle
BEZ235
(40mg/kg)
Number of Osteolytic Lesions
60
40
20
0
**
Vehicle
BEZ235
(40mg/kg)

bone volume density (BV/TV) (Figure 4.4A, $p < 0.01$, Student's t-test) and trabecular number (Th. N, Figure 4.4D, $p < 0.05$, Student's t-test) was observed in the BEZ235-treated group compared to the controls. In contrast, no significant difference in bone surface density (BS/TV), bone surface to volume ratio (BS/BV), trabecular thickness (Tb. Th.), trabecular pattern factor (Tb. Pf), trabecular spacing (Tb. Sp) and structure model index (SMI) was observed between the BEZ235- and vehicle-treated groups (Figure 4.4B, C, E, F, G, and H).

4.2.1.5 BEZ235 increases serum P1NP levels decreases TRAcP5 levels

To further investigate the effect of BEZ235 on bone remodelling *in vivo*, serum markers of osteoblast and osteoclast activity were examined. P1NP, or N-terminal propeptide of the type 1 procollagen, is a marker of collagen synthesis and used to measure osteoblast formation[51; 52; 53]. To examine the effect of BEZ235 on bone remodelling, levels of P1NP were measured in serum samples collected from vehicle- and BEZ235-treated animals at the end of the study using a commercial ELISA kit. As shown in Figures 4.5A and B, serum P1NP levels were significantly elevated in BEZ235-treated animals compared to vehicle alone ($p < 0.05$, Student's t-test).

Having shown a reduction in the number of osteolytic lesions in BEZ235-treated animals, serum levels of TRAcP5, a bone resorption marker, was assessed. Using a commercial ELISA, serum TRAcP5 levels were measured in samples collected from vehicle- and BEZ235-treated animals at the end of the study. As shown in Figures 4.5C and 4.5D, no significant difference in TRAcP5 serum levels was observed in BEZ235-treated animals compared to the controls ($p=0.26$, Student's t-test).

4.2.1.6 BEZ235 reduces osteoclast numbers and induces MM cell apoptosis in vivo

To evaluate the effect of BEZ235 on MM cells and osteoclasts *in vivo*, formalin-fixed tibiae from vehicle- and BEZ235-treated animals were decalcified and embedded in paraffin wax. Five-micron sections were then stained with Haematoxylin & Eosin and TRAP & methyl green to facilitate assessment of overall histology and osteoclasts, respectively. As shown in Figure 4.6, the morphology of the MM-infiltrated bone marrow of both vehicle- and BEZ235- treated tibiae was poor and the architecture of the bone marrow was disrupted. As shown in Figure 4.7, a reduction in the number of

Figure 4.4. Changes in tibial trabecular morphology in response to BEZ235 treatment. C57BL/KaLwRijHsd mice (n=10 per group) were intravenously inoculated with 5 x 105 5TGM1-SFG cells. Two weeks post-tumour cell injection, animals were treated with 50mg/kg BEZ235 or vehicle alone via daily oral gavage for two weeks. At the end of the study, formalin-fixed tibiae were scanned on a high-resolution µCT scanner and 3D morphological analysis was performed on a 0.645mm region of trabecular bone, commencing 0.215mm from the growth plate. (A) BV/TV, (B) BS/TV,(C) BS/BV, (D) Tb. N., (E) Tb. Th., (F) Tb. Pf., (G) Tb. Sp., (H) SMI. Data are expressed as the mean ± SEM. *$p<0.05$ and **$p<0.01$, Student's t-test.

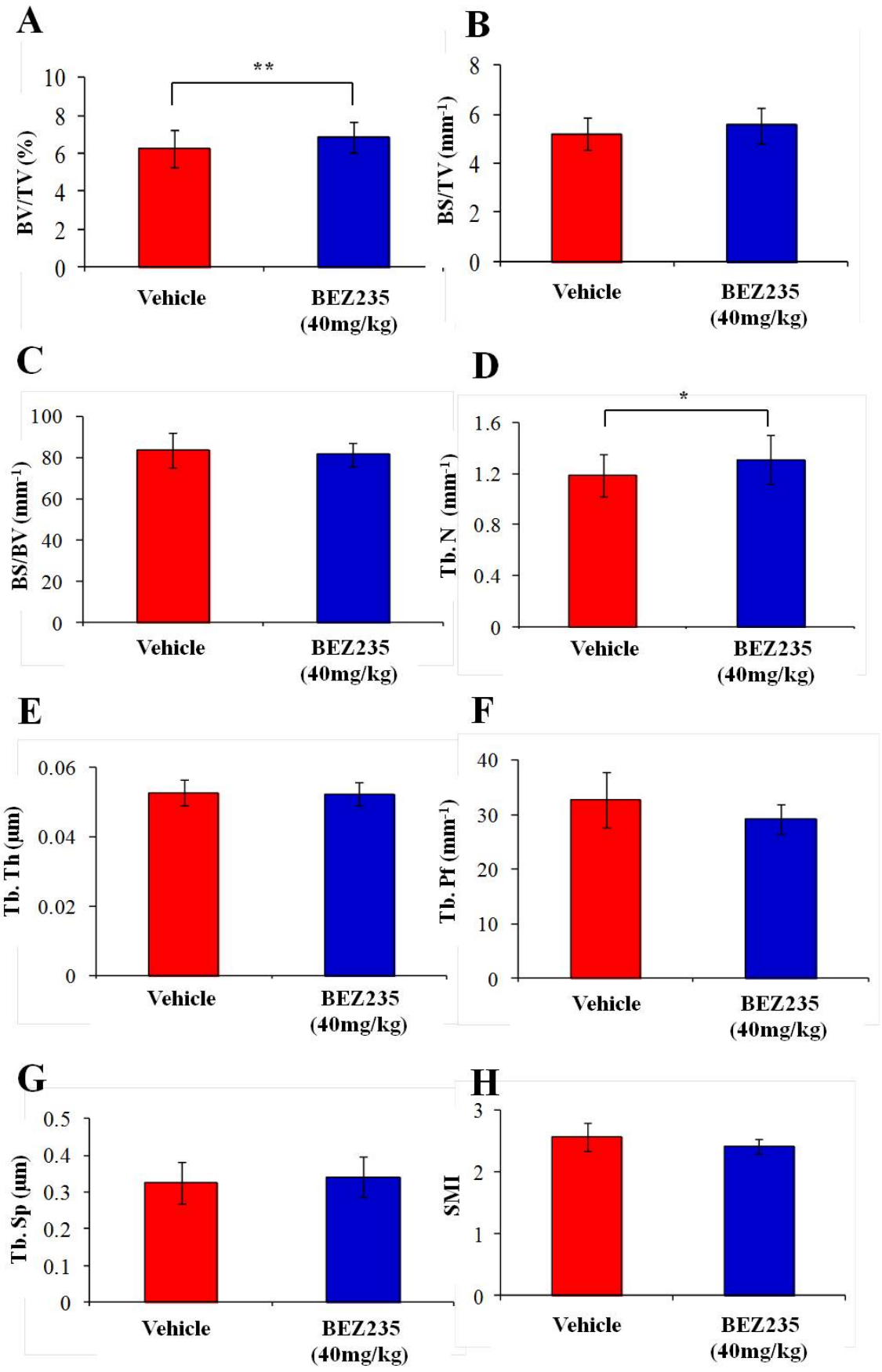
A
BV/TV (%)
10
8
6
4
2
0
**
Vehicle
BEZ235 (40mg/kg)
B
BS/TV (mm-1)
8
6
4
2
0
Vehicle
BEZ235 (40mg/kg)
C
BS/BV (mm-1)
100
80
60
40
20
0
Vehicle
BEZ235 (40mg/kg)
D
Tb.N (mm-1)
1.6
1.2
0.8
0.4
0
*
Vehicle
BEZ235 (40mg/kg)
E
Tb. Th (µm)
0.06
0.04
0.02
0
Vehicle
BEZ235 (40mg/kg)
F
Tb. Pf (mm-1)
40
30
20
10
0
Vehicle
BEZ235 (40mg/kg)
G
Tb. Sp (µm)
0.5
0.4
0.3
0.2
0.1
0
Vehicle
BEZ235 (40mg/kg)
H
SMI
3
2
1
0
Vehicle
BEZ235 (40mg/kg)

Figure 4.5. The effect of BEZ235 on serum P1NP and TRAPc5 levels. C57BL/KaLwRijHsd mice (n=10 per group) were intravenously inoculated with 5 x 105 5TGM1-SFG cells. Two weeks post-tumour cell injection, animals were treated with 50mg/kg BEZ235 or vehicle alone via daily oral gavage for two weeks. At the end of the study, blood samples were collected and serum levels of (A) P1NP and (C) TRAPc5 were measured using commercial ELISA kits. The range of (B) P1NP and (D) TRAPc5 levels in each animal cohort is plotted as dot plots. Data are expressed as the mean ± SEM. *$p<0.05$, Student's t-test.

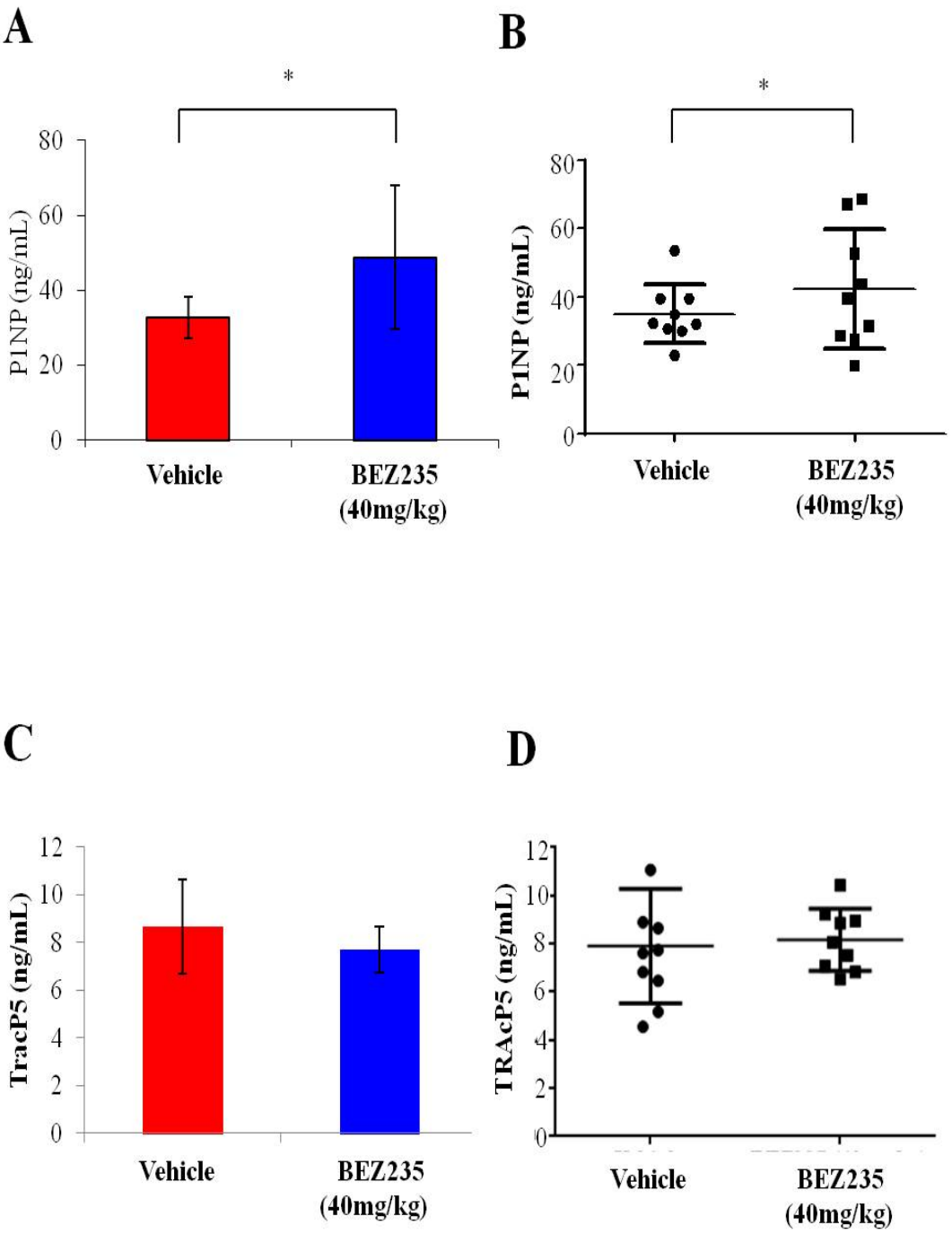
A
*
80
60
40
20
0
P1NP (ng/mL)
Vehicle
BEZ235
(40mg/kg)
B
*
80
60
40
20
0
P1NP (ng/mL)
Vehicle
BEZ235
(40mg/kg)
C
12
10
8
6
4
2
0
TracP5 (ng/mL)
Vehicle
BEZ235
(40mg/kg)
D
12
10
8
6
4
2
0
TRAcP5 (ng/mL)
Vehicle
BEZ235
(40mg/kg)

Figure 4.6. Histological examination of bone marrow in vehicle- and BEZ235-treated animals. C57BL/KaLwRijHsd mice (n=10 per group) were intravenously inoculated with 5 x 105 5TGM1-SFG cells. Two weeks post-tumour cell injection, animals were treated with 50mg/kg BEZ235 or vehicle alone via daily oral gavage for two weeks. At the end of the study, tibiae were collected, embedded in paraffin and 5µm sections were stained with haematoxylin and eosin. A representative H&E-stained section from the (A) vehicle and (B) BEZ235-treated groups are shown. Scale bar: Left panels: 0.5mm, Right panels: 1mm.

A **Vehicle**

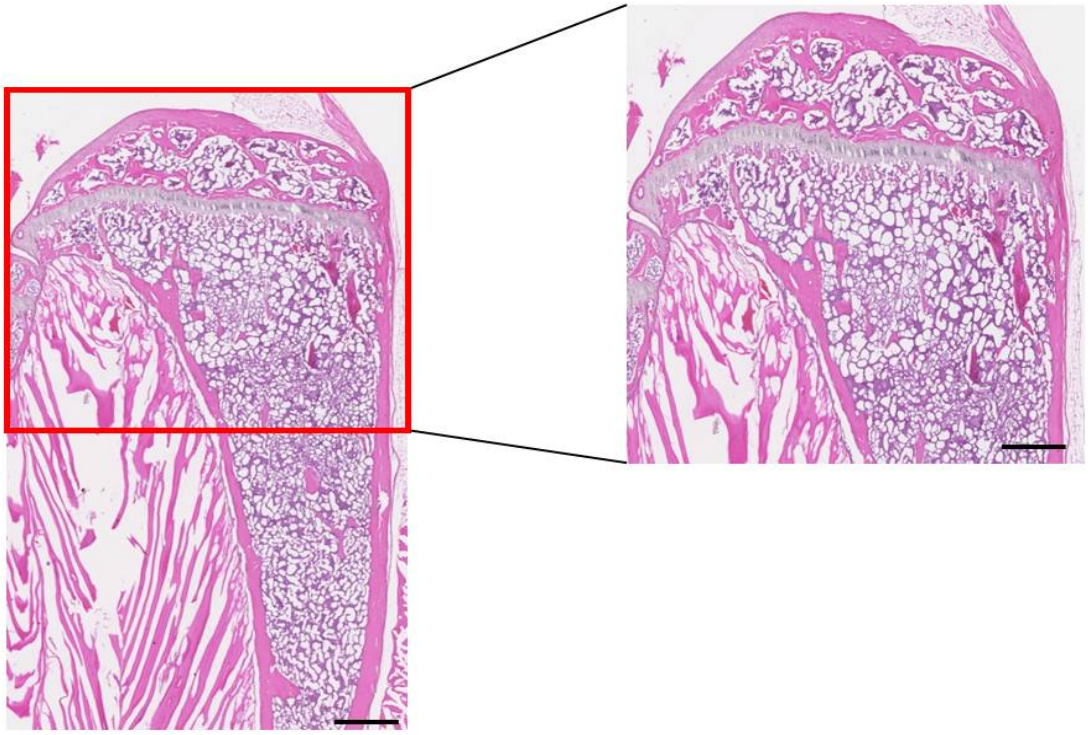

B **BEZ235 (40mg/kg)**

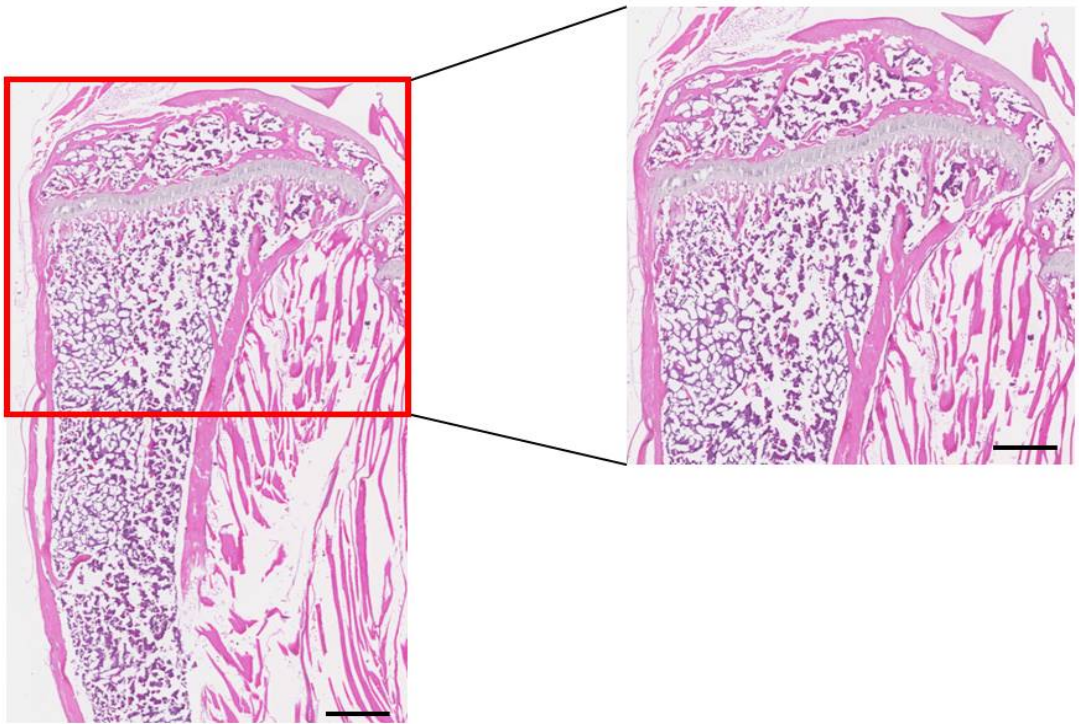

TRAP-positive osteoclasts (stained pink) was observed within the trabeculae of BEZ235-treated animals. Moreover, the number of osteoclasts per bone parameter (N.Oc/B.Pm) and percentage of bone surface occupied by osteoclasts (Oc.S/BS) was quantitated within a defined region of secondary spongiosa in these TRAP-stained sections using Image J software. As shown in Figure 4.7B, while a decrease in N.Oc/B.Pm and Oc.S/BS were observed in the BEZ235- treated animals, these differences were not statistically significant ($p=0.07$ & $p=0.06$ respectively, Student's t-test).

To determine whether BEZ235 induced MM cell apoptosis, tibial sections from vehicle- and BEZ235-treated animals were stained using the TUNEL assay, where TUNEL is a marker of apoptosis. As shown in Figure 4.8, an increase in TUNEL-positive cells (stained brown) was observed in BEZ235-treated animals (Figure 4.8B) compared to vehicle-treated animals (Figure 4.8A).

4.2.2 The effect of BKM120 on MM cells and bone *in vivo*

4.2.2.1 BKM120 *inhibits tumour progression in vivo*

Following a similar study design to that described above for BEZ235 (see section 4.2.2.1), 5TGM1-SFG cells injected into the tail vein of 6-8 week old female C57BL/KaLwRij mice and disease progression was monitored weekly using BLI. Two weeks post-tumour cell injection, after the cells had homed from the peripheral circulation to the bone marrow, the mice were divided into two treatment groups (n=10 per group): Group 1 were administered 0.5% methyl cellulose (vehicle control) via daily oral gavage for two weeks; and Group 2 were administered 50mg/kg BKM120 via daily oral gavage for two weeks. This dose of BKM120 was selected based on previously published studies reporting that no side effects were observed in the BKM120-treated animals and were able to slow tumour progression *in vivo*[54]. Figure 4.9A shows consecutive BLI images taken of a representative animal from each treatment group from week 1-4 post tumour inoculation. As shown in Figure 4.9B, quantitation of these data revealed a decrease in signal intensity between the two treatment groups at weeks 3 and a significant decrease in signal intensity at week 4 ($p < 0.05$, Student's t-test).

Figure 4.7. BEZ235 treatment has an effect on osteoclast numbers in vivo. C57BL/KaLwRijHsd mice (n=10 per group) were intravenously inoculated with 5 x 105 5TGM1-SFG cells. Two weeks post-tumour cell injection, animals were treated with 50mg/kg BEZ235 or vehicle alone via daily oral gavage for two weeks. At the end of the study, tibiae were harvested, embedded in paraffin and 5µm sections were stained for TRAP and counterstained with methyl green. (A) Representative images from a vehicle-treated (top) and BEZ235-treated (bottom) animal are shown. Arrowheads indicate TRAP-positive multinucleated osteoclasts. Scale bar: 0.2mm. (B) Using Image J analysis software, the number of osteoclasts (N.Oc/B.Pm, left panel) and percentage of bone surface occupied by osteoclasts (Oc.S/BS, right panel) were quantitated in a defined region of secondary spongiosa at the proximal tibia. Data are expressed as the mean ± SEM.

A

Vehicle

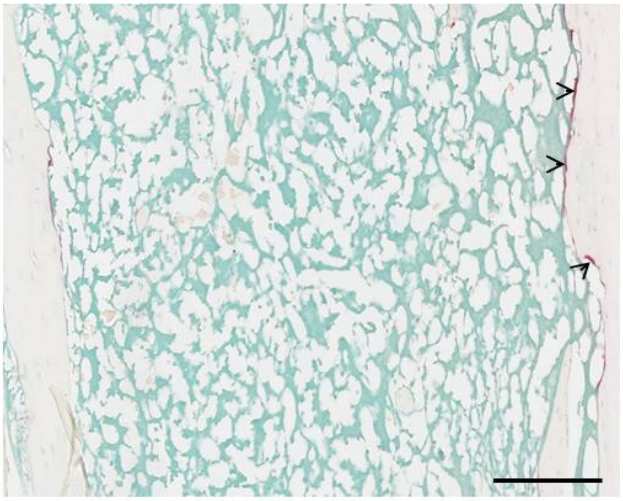

BEZ235 (40mg/kg)

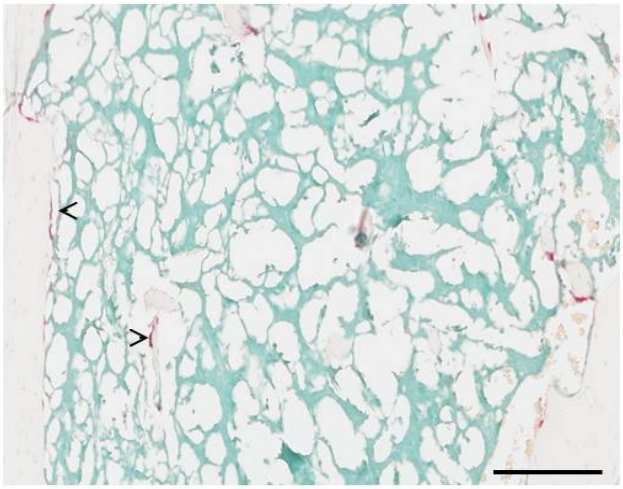

B

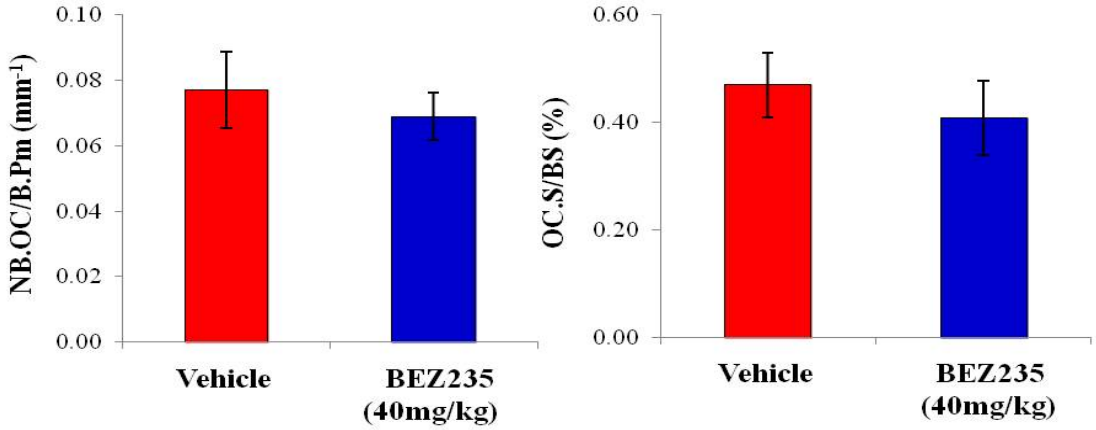

Figure 4.8. BEZ235 induces cell apoptosis in vivo. C57BL/KaLwRijHsd mice (n=10 per group) were intravenously inoculated with 5 x 105 5TGM1-SFG cells. Two weeks post-tumour cell injection, animals were treated with 50mg/kg BEZ235 or vehicle alone via daily oral gavage for two weeks. At the end of the study, tibiae were harvested, embedded in paraffin and 5µm sections were stained with TUNEL and counterstained with haematoxylin. Brown staining indicates TUNEL-positive cells. A representative image from (A) the vehicle-treated group, or (B) the BEZ235-treated group are shown. Scale bar: 0.2mm.

A

Vehicle

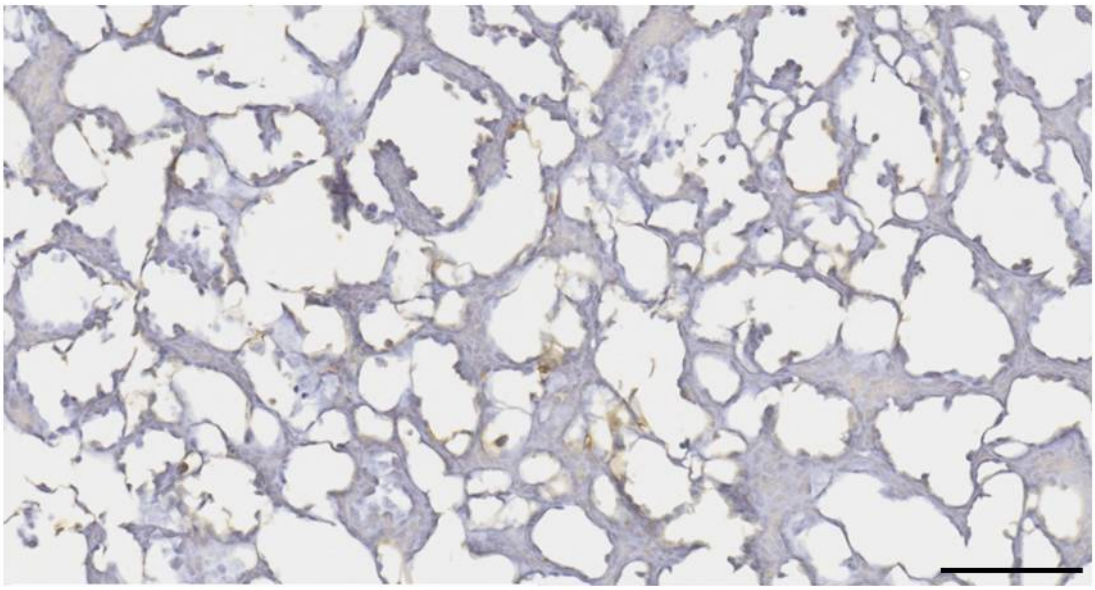

B

BEZ235 (40mg/kg)

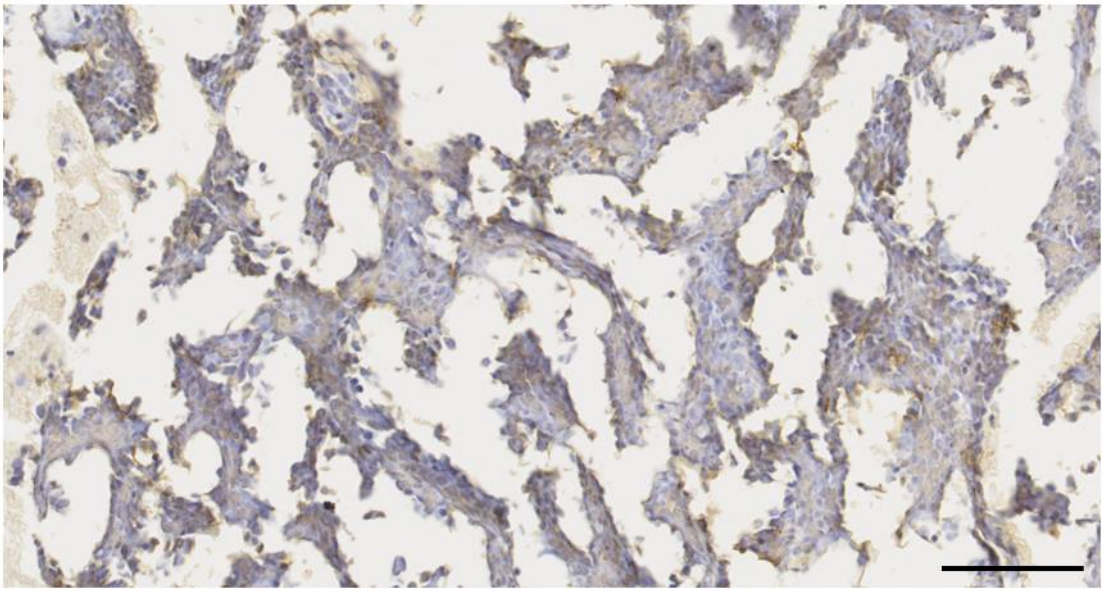

Figure 4.9. BKM120 slows tumour progression in vivo. C57BL/KaLwRijHsd mice (n=10 per group) were intravenously inoculated with 5 x 105 5TGM1-SFG cells. Two weeks post-tumour cell injection, animals were treated with 40mg/kg BKM120 or vehicle alone (0.5% methyl cellulose) via daily oral gavage for two weeks. Tumour progression was monitored weekly by live bioluminescence imaging (BLI) following intraperitoneal administration with D-luciferin. (A) Consecutive weekly BLI images of a representative mouse from the vehicle group (top panel) and BKM120-treated group (bottom panel) are shown at week 1-4 following tumour inoculation. (B) The average bioluminescence signal intensity was graphed to illustrate the changes in the signal intensity at each time point for each animal group. Data are expressed as mean ± SEM luminescence signal. *$p<0.05$, Student's t-test.

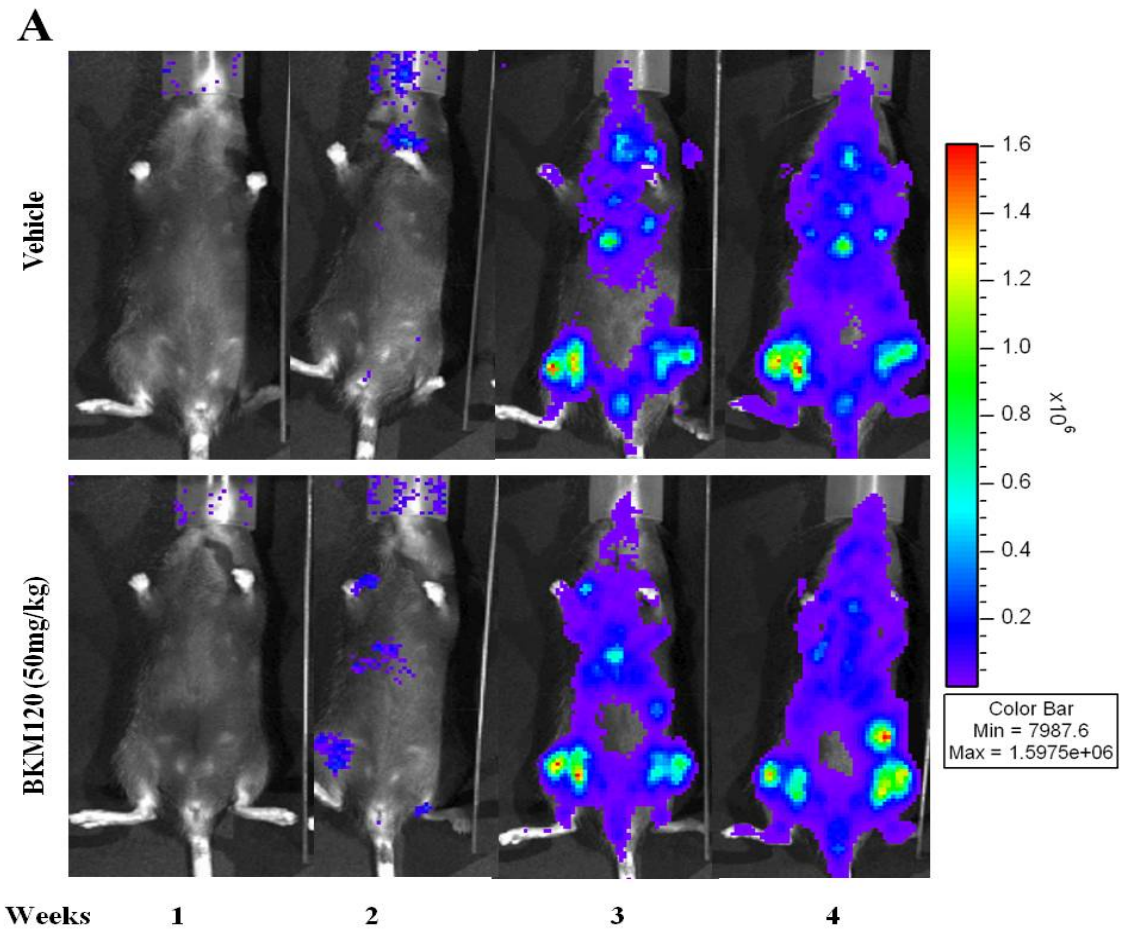
A
Vehicle
BKM120 (50mg/kg)
1.6
1.4
1.2
1.0
0.8
0.6
0.4
0.2
x10⁶
Color Bar
Min = 7987.6
Max = 1.5975e+06
Weeks 1 2 3 4

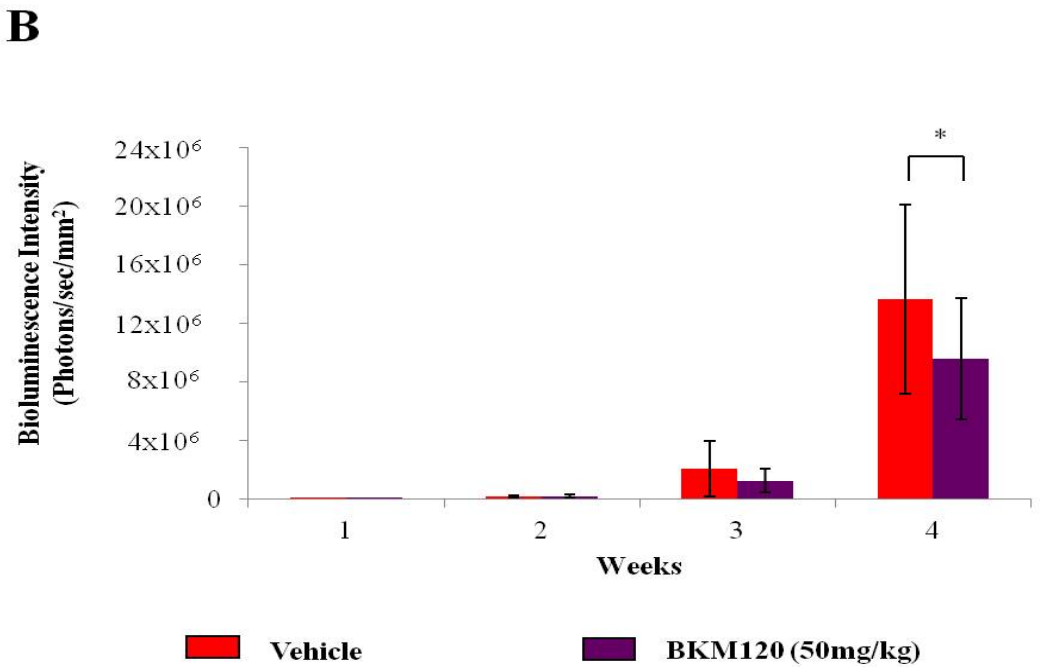
B
Bioluminescence Intensity (Photons/sec/mm²)
24x10⁶
20x10⁶
16x10⁶
12x10⁶
8x10⁶
4x10⁶
0
*
1
2
3
4
Weeks
Vehicle
BKM120 (50mg/kg)

4.2.2.2 BKM120 decreases serum paraprotein levels and has no effect animal weight

To determine whether BKM120 affects serum paraprotein levels in myelomatous mice, blood was collected from all animals at weekly intervals and serum paraprotein levels measured using the Sebia Hydragel 30 β1-β2 kit according to the manufacturer's instructions. As shown in Figure 4.10A, a progressive increase in serum paraprotein was observed in vehicle-treated animals, with a clear protein band evident at 3 and 4 weeks post-tumour inoculation. In contrast, there was a delay in the onset of paraprotein detection in BKM120-treated animals, with a clear protein band only observed at the 4-week time point. When the intensity of the serum paraprotein levels were measured and normalised to total protein, a significant decrease in serum paraprotein was observed in response to BKM120 treatment at week 3 (Figure 4.10A, bottom panel, $p < 0.05$, Student's t-test) and week 4 (Figure 4.10A, bottom panel, $p < 0.01$, Student's t-test), compared to vehicle-treated animals.

Similar to the BEZ235 animal study, the weight of each animal was measured twice weekly to monitor the effects of tumour burden and/or drug or vehicle administration on overall animal health throughout the duration of the study. As shown as Figure 4.10B, the weight of the animal increased over time and plateaued by day 28.

4.2.2.3 ***BKM120 reduces the number of osteolytic lesions perforating the tibiae cortices***

To examine the effect of BKM120 on osteolytic bone disease *in vivo*, formalin-fixed tibiae from vehicle- and BKM120-treated animals were scanned on a high-resolution μCT scanner. A 3D image of the tibia was generated, and the image sliced in half on a plane parallel through the length of the tibiae and the number of osteolytic lesions, which perforated the tibiae, was enumerated. Figure 4.11A shows the example of the osteolytic lesions that perforate the tibiae of representative animals from the vehicle-treated group (top panel) and the BKM120-treated group (bottom panel). As shown in Figure 4.11B, a significant decrease in the number of osteolytic lesions in the tibial cortical bone was observed in BKM120-treated animals, compared to the vehicle alone ($p < 0.01$, Student's t-test).

Figure 4.10. BKM120 decreases serum paraprotein levels and does not affect animal weights. C57BL/KaLwRijHsd mice (n=10 per group) were intravenously inoculated with 5 x 105 5TGM1-SFG cells. Two weeks post-tumour cell injection, animals were treated with 40mg/kg BKM120 or vehicle alone via daily oral gavage for two weeks. Blood was collected from vehicle- and BEZ235-treated animals at weekly intervals and serum paraprotein levels measured. (A) Serum paraprotein gels from a representative animal from the vehicle (top left) and BEZ235-treated (top right) groups are shown. The arrow indicates the protein band corresponding to serum paraprotein. Sebia image analysis software was used to quantitate the intensity of the paraprotein band relative to total serum protein bands. The data were then plotted as the mean ± SEM for each treatment group. *$p<0.05$ and **$p<0.01$, Student's t-test. (B) The weight of each animal was measured twice weekly for the duration of the study and the average weight of each group plotted. Data are expressed as the mean ± SEM.

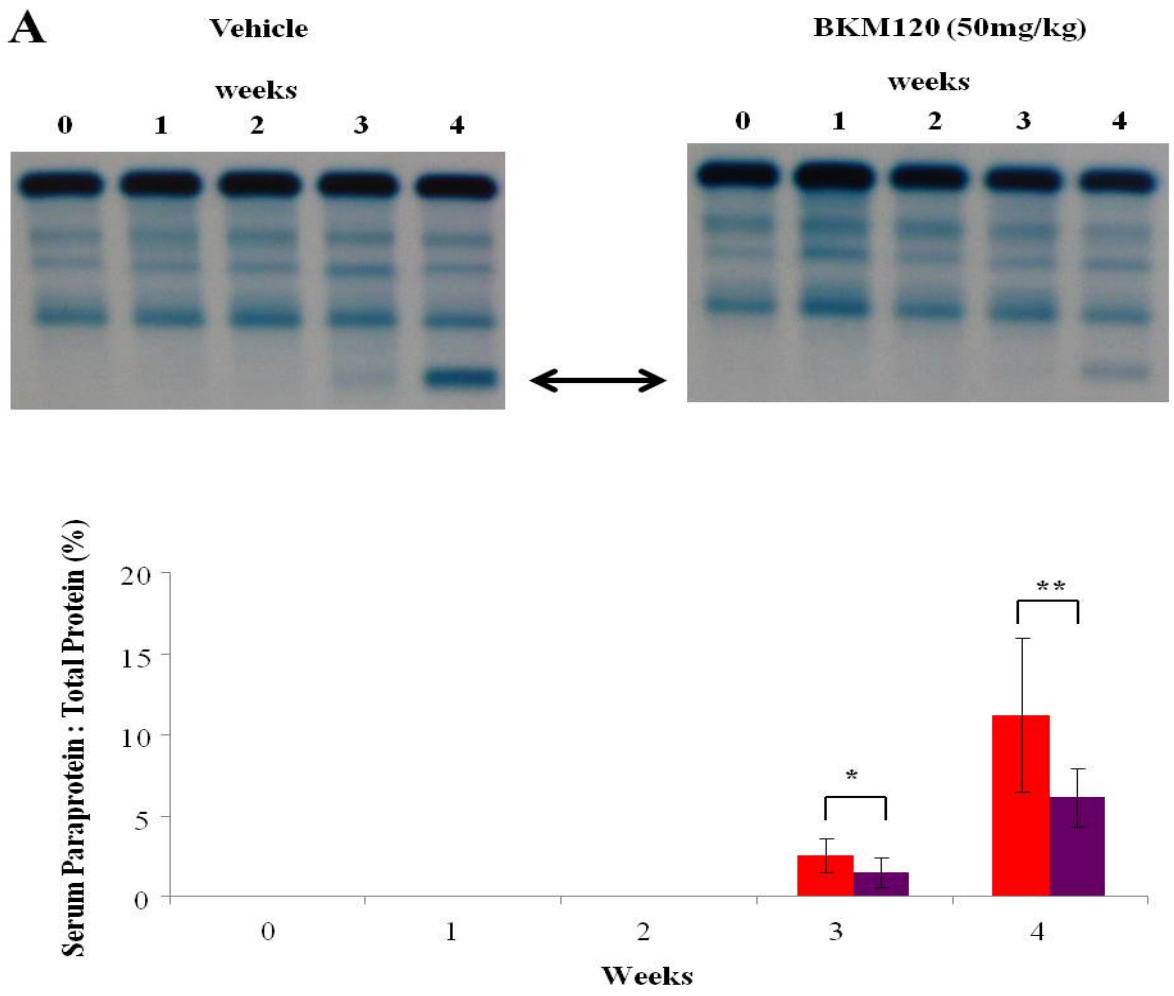
A
Vehicle
BKM120 (50mg/kg)
weeks
0 1 2 3 4
weeks
0 1 2 3 4
Serum Paraprotein : Total Protein (%)
20
15
10
5
0
*
**
0 1 2 3 4
Weeks
B
Weight (g)
20
15
10
5
0
0 4 7 11 14 18 21 25 28
Day
Vehicle
BKM120 (50mg/kg)

Figure 4.11. BKM120 reduces the number of osteolytic lesions that perforate the tibiae cortices. C57BL/KaLwRijHsd mice (n=10 per group) were intravenously inoculated with 5 x 105 5TGM1-SFG cells. Two weeks post-tumour cell injection, animals were treated with 40mg/kg BKM120 or vehicle alone via daily oral gavage for two weeks. At the end of the study, tibiae were harvested, fixed in formalin and scanned on a high-resolution μCT scanner. (A) 3D images were generated using the SkyScan ANT software, and bones were sliced in half on a plane parallel hrough the length of the tibia. 3D images from two representative animals from the vehicle (top panels) and BEZ235-treated (bottom panels) groups are shown. (B) The number of osteolytic lesions present in the tibial cortical bone of each animal was counted and the average number of osteolytic lesions per animal for each group was graphed. Data are expressed as the mean ± SEM. (left panel). To better illustrate the range in the number of osteolytic lesions present in each animal cohort, the data was also plotted as a dot plot (right panel). **$p<0.01$, Student's t-test.

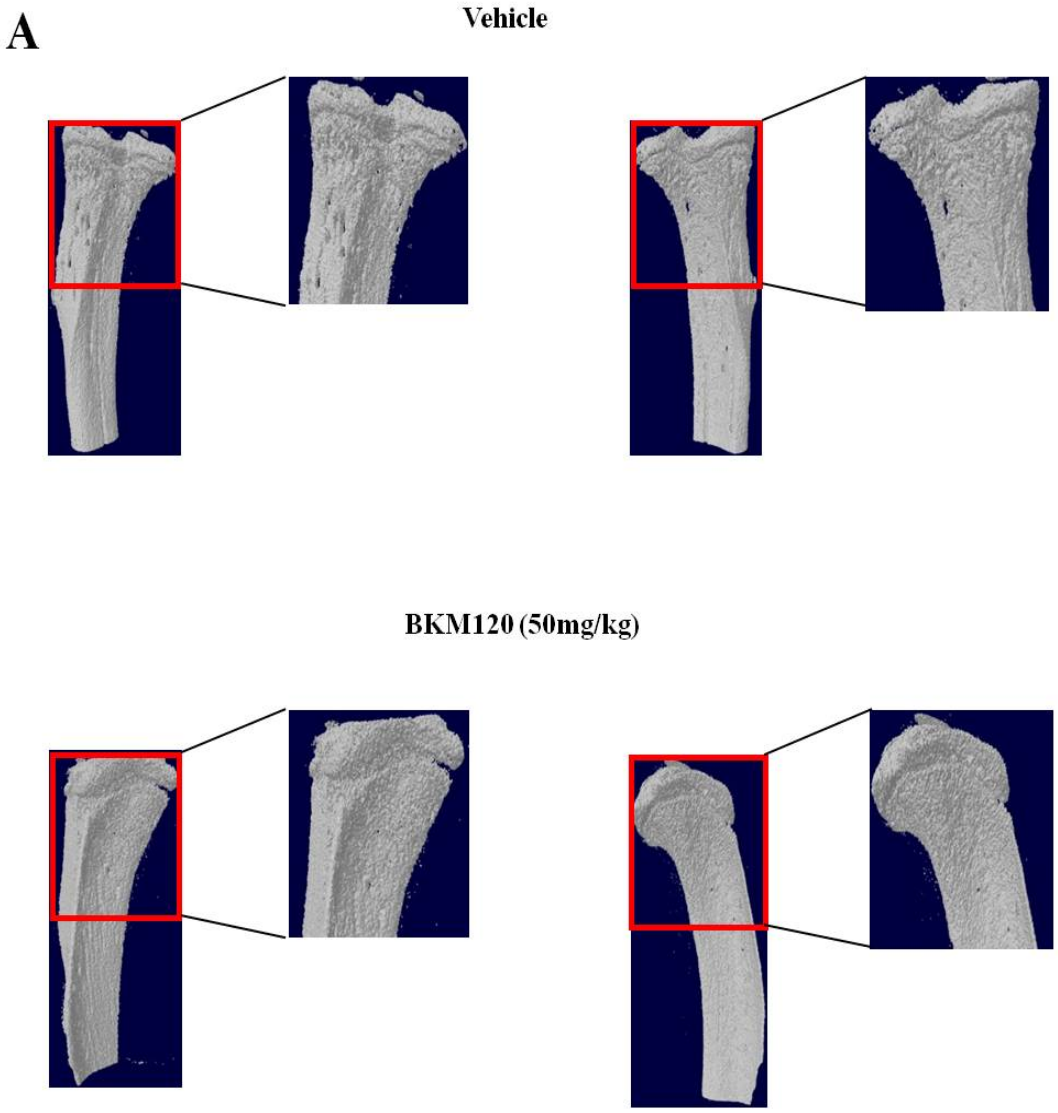
A
Vehicle
BKM120 (50mg/kg)

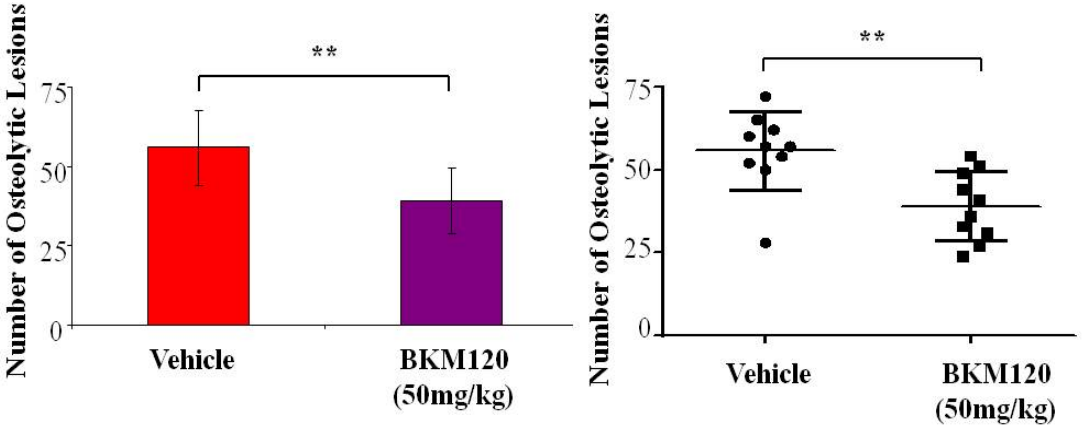
B
Number of Osteolytic Lesions
**
75
50
25
0
Vehicle
BKM120
(50mg/kg)
Number of Osteolytic Lesions
**
75
50
25
0
Vehicle
BKM120
(50mg/kg)

4.2.2.4 BKM120 increases bone density, trabecular bone surface to bone volume ratio and trabecular number

As described previously for the BEZ235 study (Section 4.2.1.4), the trabecular bone morphometry of both vehicle- and BKM120-treated animals was analysed by µCT. While a significant increase in bone density (Figure 4.12A, $p < 0.05$, Student's t-test), trabecular BS/BV (Figure 4.12C, $p < 0.001$, Student's t-test) and trabecular number (Figure 4.12D, $p < 0.05$, Student's t-test) were observed in the BKM120 treated group, a significant decrease in trabecular thickness (Figure 4.12E, $p < 0.001$, Student's t-test) and trabecular spacing (Figure 4.12G, $p < 0.001$, Student's t-test) were also observed. In contrast, no significant difference in BS/TV, Tb. Pf and SMI was observed between the vehicle- and BKM120-treated groups (Figure 4.12B, F and H).

4.2.2.5 BKM120 increases serum P1NP levels decreases serum TRAcP5 levels

To investigate the effects of BKM120 on bone serum markers *in vivo*, blood samples were collected from vehicle- and BKM120-treated mice at the end of the study and serum levels of P1NP and TRAcP5 were measured using commercial ELISA kits. As shown in Figures 4.13A and B, serum P1NP levels were significantly elevated in BKM120-treated animals compared to vehicle alone ($p < 0.001$, Student's t-test). BKM120 also significantly decreased serum TRAcP5 levels in the BKM120-treated animals (Figure 4.13C and D, $p < 0.05$, Student's t-test).

4.2.2.6 BKM120 reduces osteoclast numbers and induces MM cell apoptosis in vivo

Having shown that BEZ235 reduces the number of TRAP-positive osteoclasts and induces apoptosis, the effects of BKM120 on MM cells and osteoclast numbers *in vivo* was evaluated. Similar to BEZ235 animal study, paraffin-embedded sections were stained with Haematoxylin & Eosin to assess the overall morphology of the cells and TRAP stain to quantitate the number of TRAP positive osteoclasts present.

The Haematoxylin & Eosin staining showed poor morphology and disrupted bone marrow architecture of the MM infiltrated of both vehicle- and BKM120- treated tibiae (Figure 4.14). A reduction in the number of TRAP-positive osteoclasts (stained pink)

Figure 4.12. Trabecular morphology in animal tibiae after BKM120 treatment. C57BL/KaLwRijHsd mice (n=10 per group) were intravenously inoculated with 5 x 105 5TGM1-SFG cells. Two weeks post-tumour cell injection, animals were treated with 40mg/kg BKM120 or vehicle alone via daily oral gavage for two weeks. At the end of the study, formalin-fixed tibiae were scanned on a high resolution μCT scanner and 3D morphological analysis was performed on a 0.645mm region of trabecular bone, commencing 0.215mm from the growth plate. (A) BV/TV, (B) BS/TV, (C) BS/BV,(D) Tb. N., (E) Tb. Th., (F) Tb. Pf., (G) Tb. Sp., (H) SMI. Data are expressed as the mean ± SEM. *$p<0.05$ and ***$p<0.001$, Student's t-test.

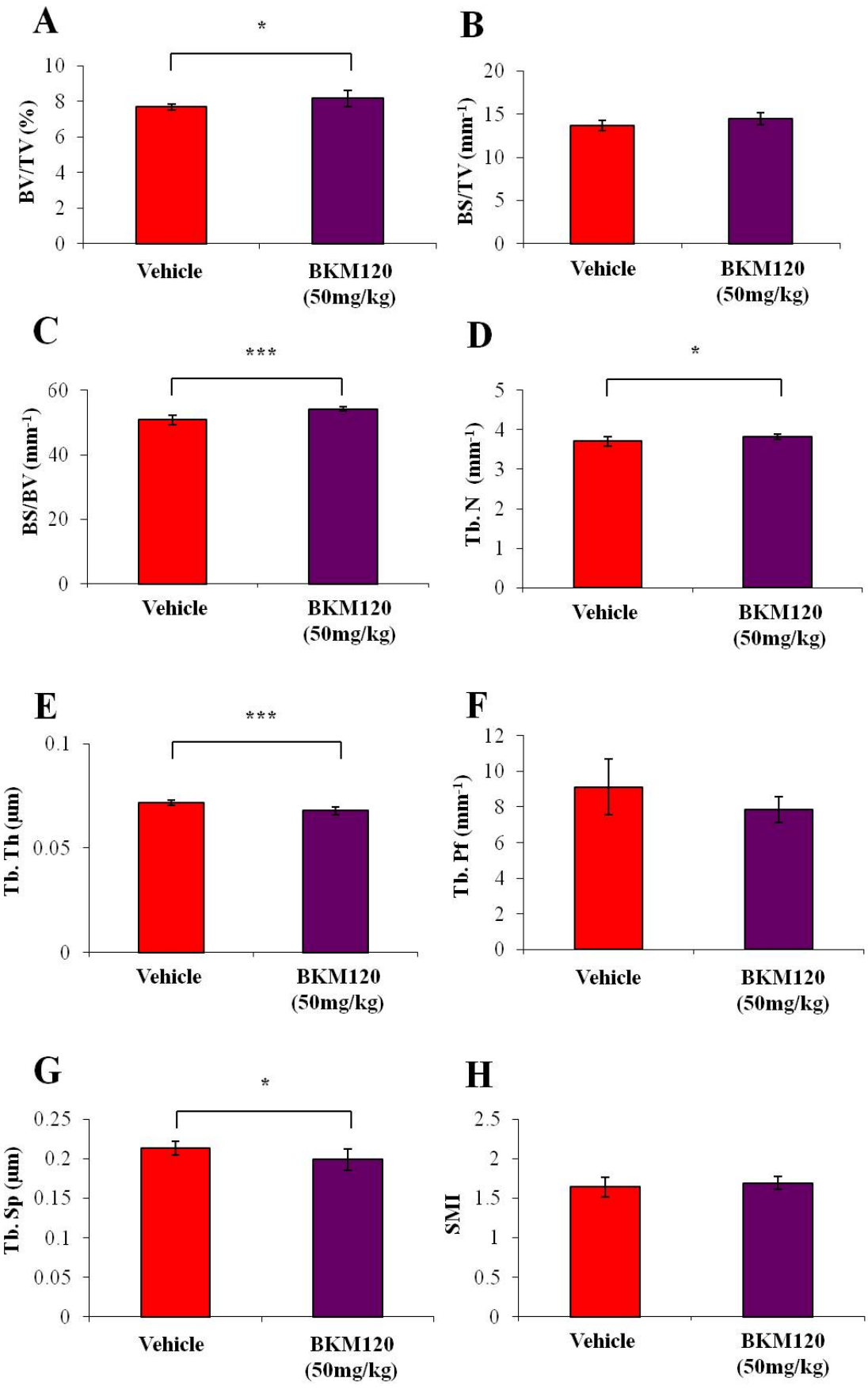
A
*
BV/TV (%)
10
8
6
4
2
0
Vehicle
BKM120 (50mg/kg)
B
BS/TV (mm-1)
20
15
10
5
0
Vehicle
BKM120 (50mg/kg)
C
***
BS/BV (mm-1)
60
40
20
0
Vehicle
BKM120 (50mg/kg)
D
*
Tb.N (mm-1)
5
4
3
2
1
0
Vehicle
BKM120 (50mg/kg)
E
***
Tb. Th (µm)
0.1
0.05
0
Vehicle
BKM120 (50mg/kg)
F
Tb. Pf (mm-1)
12
10
8
6
4
2
0
Vehicle
BKM120 (50mg/kg)
G
*
Tb. Sp (µm)
0.25
0.2
0.15
0.1
0.05
0
Vehicle
BKM120 (50mg/kg)
H
SMI
2.5
2
1.5
1
0.5
0
Vehicle
BKM120 (50mg/kg)

Figure 4.13. BKM120 increases serum P1NP levels and decreases serum TRAPc5 levels. C57BL/KaLwRijHsd mice (n=10 per group) were intravenously inoculated with 5 x 105 5TGM1-SFG cells. Two weeks post-tumour cell injection, animals were treated with 40mg/kg BKM120 or vehicle alone via daily oral gavage for two weeks. At the end of the study, blood samples were collected and serum levels of (A) P1NP and (C) TRAPc5 were measured using commercial ELISA kits according to the manufacturer's instructions. To better illustrate the range in (B) P1NP and (D) TRAPc5 levels in each animal cohort, the data were also plotted as dot plots. Data are expressed as the mean ± SEM. *$p<0.05$ and ***$p<0.001$, Student's t-test.

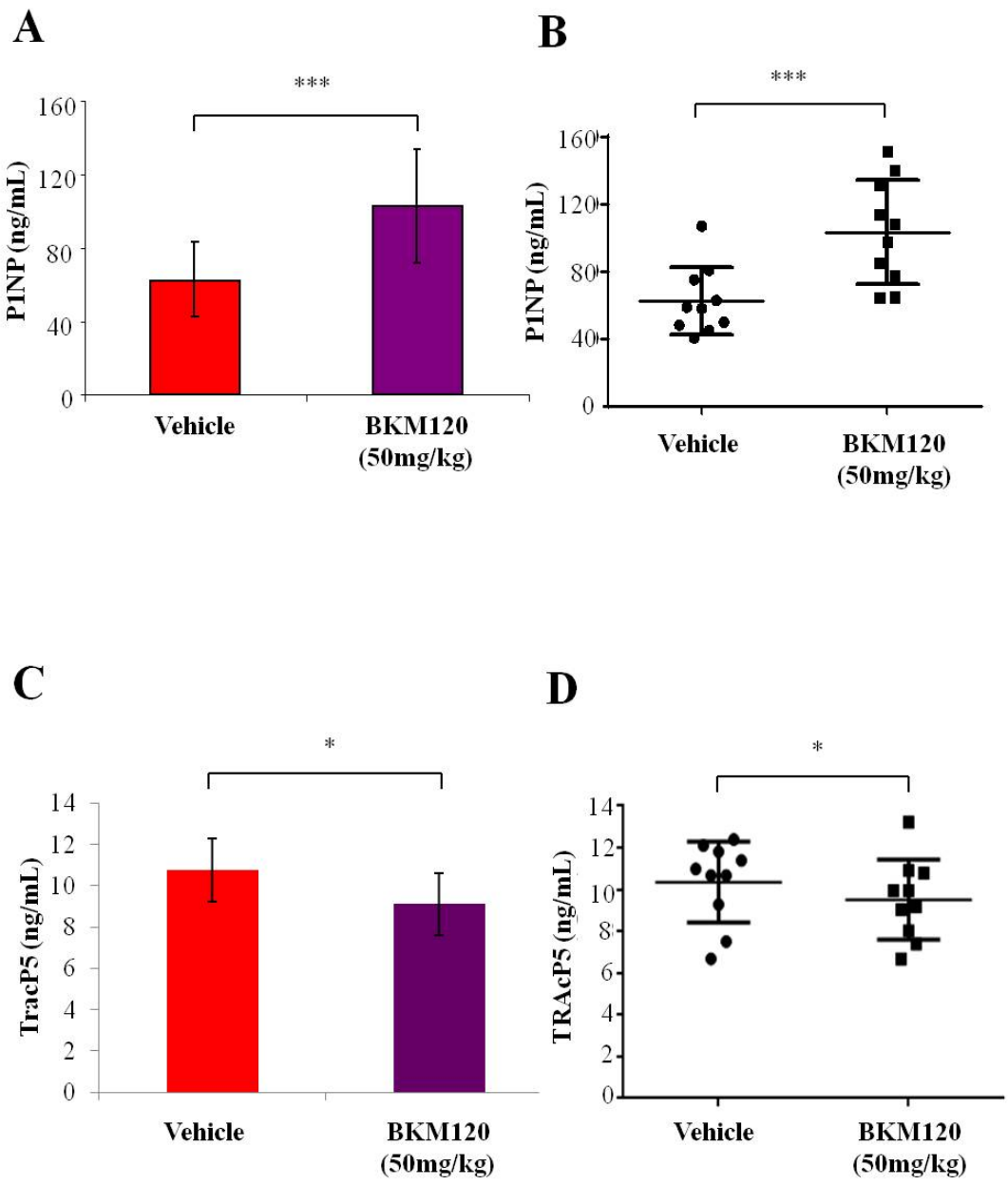
A
***
160
120
80
40
0
P1NP (ng/mL)
Vehicle
BKM120
(50mg/kg)
B
***
160
120
80
40
0
P1NP (ng/mL)
Vehicle
BKM120
(50mg/kg)
C
*
14
12
10
8
6
4
2
0
TracP5 (ng/mL)
Vehicle
BKM120
(50mg/kg)
D
*
14
12
10
8
6
4
2
0
TRAcP5 (ng/mL)
Vehicle
BKM120
(50mg/kg)

Figure 4.14. Histological examination of bone marrow in vehicle- and BKM120-treated animals. C57BL/KaLwRijHsd mice (n=10 per group) were intravenously inoculated with 5 x 10^5 5TGM1-SFG cells. Two weeks post-tumour cell injection, animals were treated with 40mg/kg BKM120 or vehicle alone via daily oral gavage for two weeks. At the end of the study, tibiae were collected, embedded in paraffin and 5µm sections were stained with haematoxylin and eosin. A representative H&E-stained section from the (A) vehicle-and (B) the BKM120-treated groups are shown. Scale bar: Left panels: 0.5mm, Right panels: 1mm.

A **Vehicle**

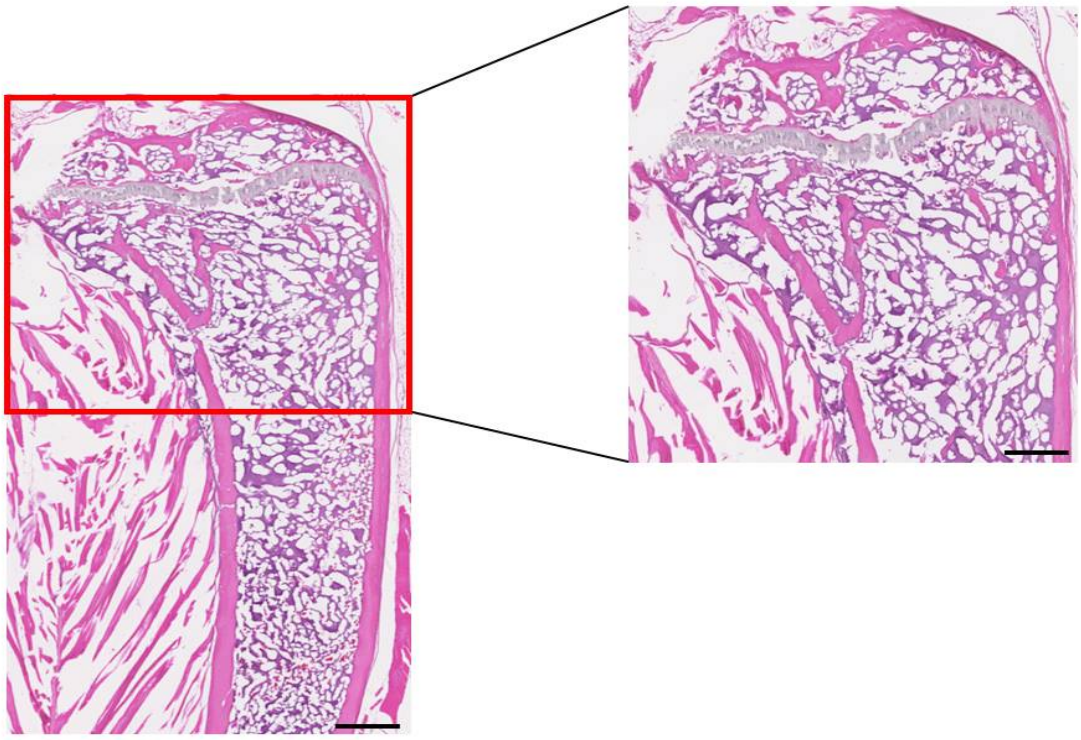

B **BKM120 (50mg/kg)**

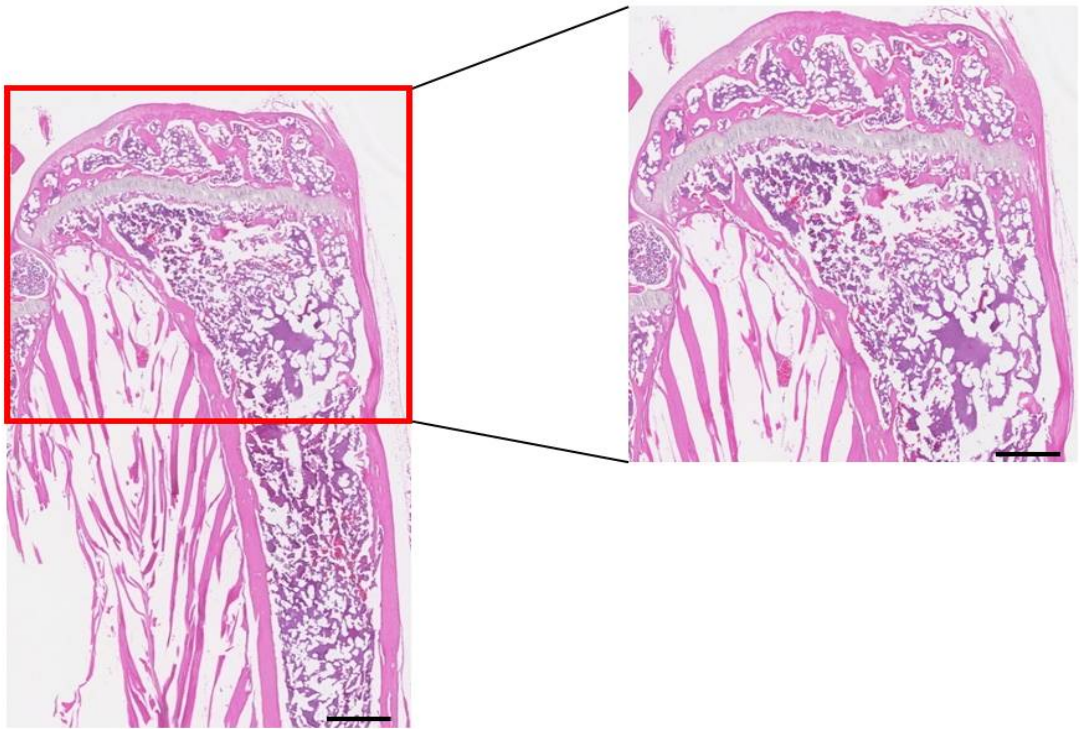

was observed within the trabeculae of BKM120-treated animals (Figure 4.15A). Similar to the BEZ235 animal study, the number of osteoclasts per bone parameter (N.Oc/B.Pm) and percentage of bone surface occupied by osteoclasts (Oc.S/BS) were measured using Image J software. As shown in Figure 4.15B, while a decrease in N.Oc/B.Pm and Oc.S/BS were observed in the BKM120-treated animals, these differences were not statistically significant ($p=0.07$ & $p=0.06$ respectively, Student's t-test). The effect of BKM120 on MM cell apoptosis was also examined by staining sections of tibiae from vehicle- and BKM120-treated mice with TUNEL. Shown in Figure 4.16, an increase in TUNEL-positive cells (stained brown) was observed in the BKM120-treated animals (Figure 4.16B) when compared to the vehicle-treated animals (Figure 4.16A).

4.3 *Discussion*

Having shown in Chapter 3 that BEZ235 and BKM120 inhibit MM PC proliferation *in vitro*, we hypothesised that BEZ235 and BKM120 would inhibit MM PC growth *in vivo*. Recent studies have examined the anti-MM effect of these drugs *in vivo* using a subcutaneous xenograft model, and found that both BEZ235 and BKM120 reduce MM tumour growth *in vivo*[21,26]. However, an inherent drawback of these studies is their use of subcutaneous xenograft models. The subcutaneous environment does not reflect the critical processes associated with MM PC homing, dissemination, and establishment of osteolytic bone disease seen in patients. To address this, we examined the effects of BEZ235 and BKM120 in the systemic 5TGM1 murine model of myeloma.

As hypothesised, BEZ235 and BKM120 inhibited MM cell growth *in vivo*, as shown by a decrease in the tumour cell-associated bioluminescence signal intensity and serum paraprotein levels in drug-treated animals compared to the vehicle-treated animals. Our findings support the findings of Mitsiades and Zheng, who showed a reduction in tumour size in MM cells implanted into NOD-SCID mice in response to BEZ235 and BKM120 treatment [21; 26]. Notably, apoptosis was observed by the increase in TUNEL staining in the BEZ235- and BKM120- treated animals. Currently, we are unable to ascertain whether the TUNEL-positive cells were MM cells, as we were unable to detect the GFP-tagged MM cells when the paraffin-embedded sections were stained with anti-

Figure 4.15. BKM120 treatment has an effect on osteoclast numbers in vivo. C57BL/KaLwRijHsd mice (n=10 per group) were intravenously inoculated with 5 x 105 5TGM1-SFG cells. Two weeks post-tumour cell injection, animals were treated with 40mg/kg BKM120 or vehicle alone via daily oral gavage for two weeks. At the end of the study, tibiae were harvested, embedded in paraffin and 5µm sections were stained for TRAP and counterstained with methyl green. (A) Representative images from a vehicle-treated (top) and BKM120-treated (bottom) animal are shown. Arrowheads indicate TRAP-positive multinucleated osteoclasts. Scale bar: 0.2mm. (B) Using Image J analysis software, the number of osteoclasts (N.Oc/B.Pm, left panel) and percentage of bone surface occupied by osteoclasts (Oc.S/BS, right panel) were quantitated in a defined region of secondary spongiosa at the proximal tibia. Data are expressed as the mean ± SEM.

A

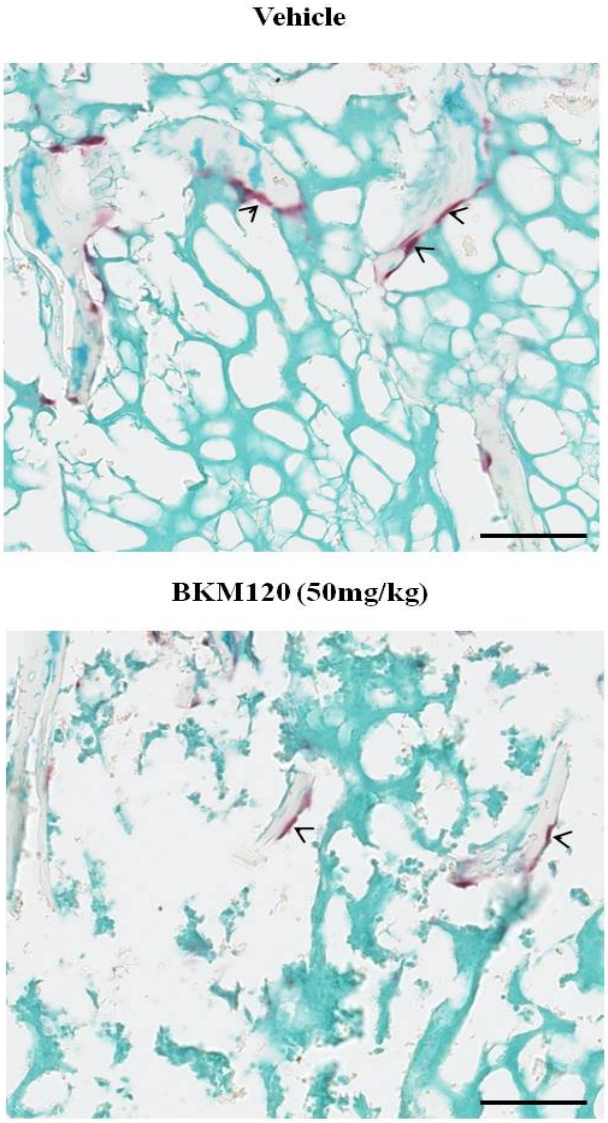
Vehicle
BKM120 (50mg/kg)

B

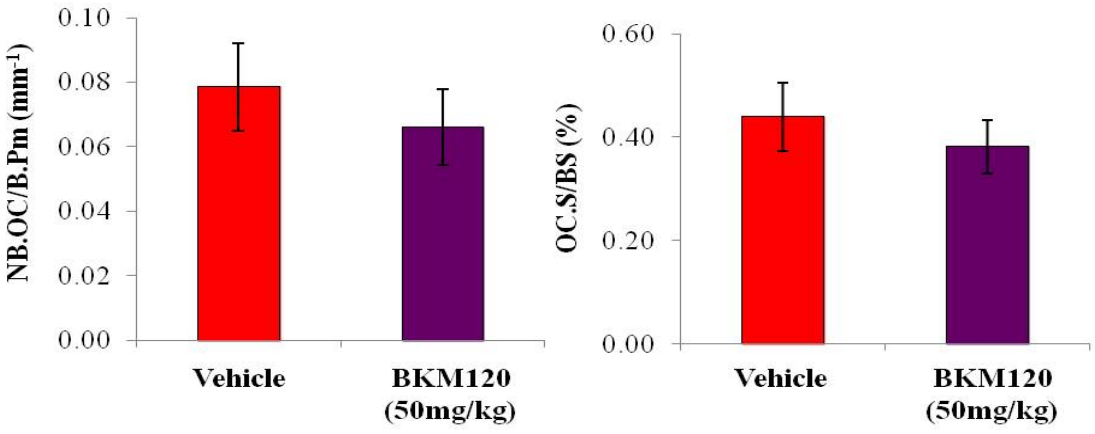
NB.OC/B.Pm (mm-1)
0.10
0.08
0.06
0.04
0.02
0.00
Vehicle
BKM120 (50mg/kg)
OC.S/BS (%)
0.60
0.40
0.20
0.00
Vehicle
BKM120 (50mg/kg)

Figure 4.16. BKM120 induces cell apoptosis in vivo. C57BL/KaLwRijHsd mice (n=10 per group) were intravenously inoculated with 5 x 105 5TGM1-SFG cells. Two weeks post-tumour cell injection, animals were treated with 40mg/kg BKM120 or vehicle alone via daily oral gavage for two weeks. At the end of the study, tibiae were harvested, embedded in paraffin and 5µm sections were stained with TUNEL and counterstained with haematoxylin. Brown staining indicates TUNEL-positive cells. Representative images from (A) the vehicle-treated group, or (B) the BKM120-treated group are shown. Scale bar: 0.2mm.

A

Vehicle

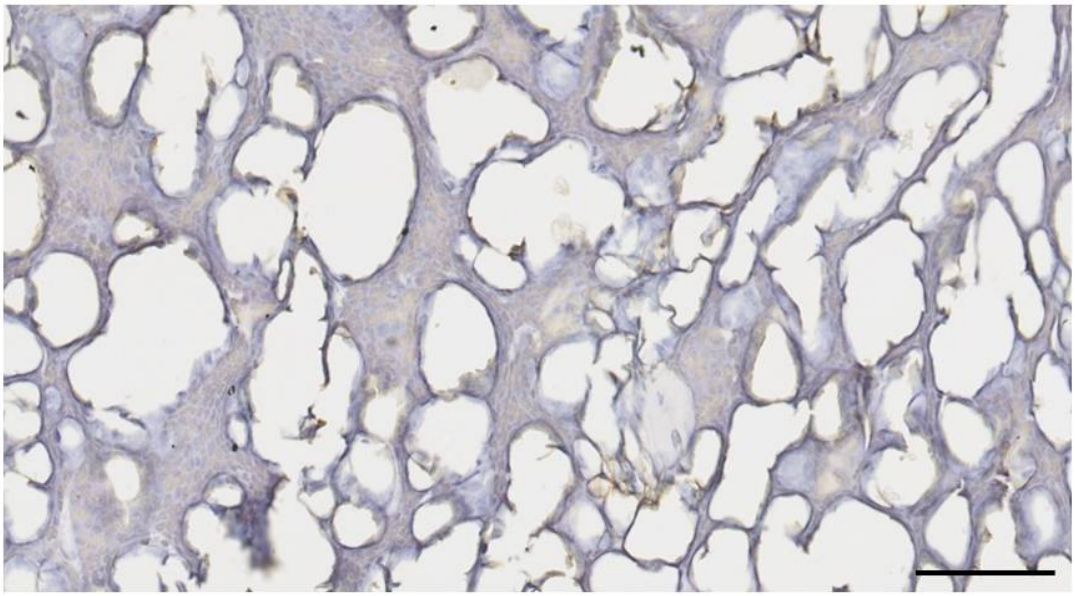

B

BKM120 (50mg/kg)

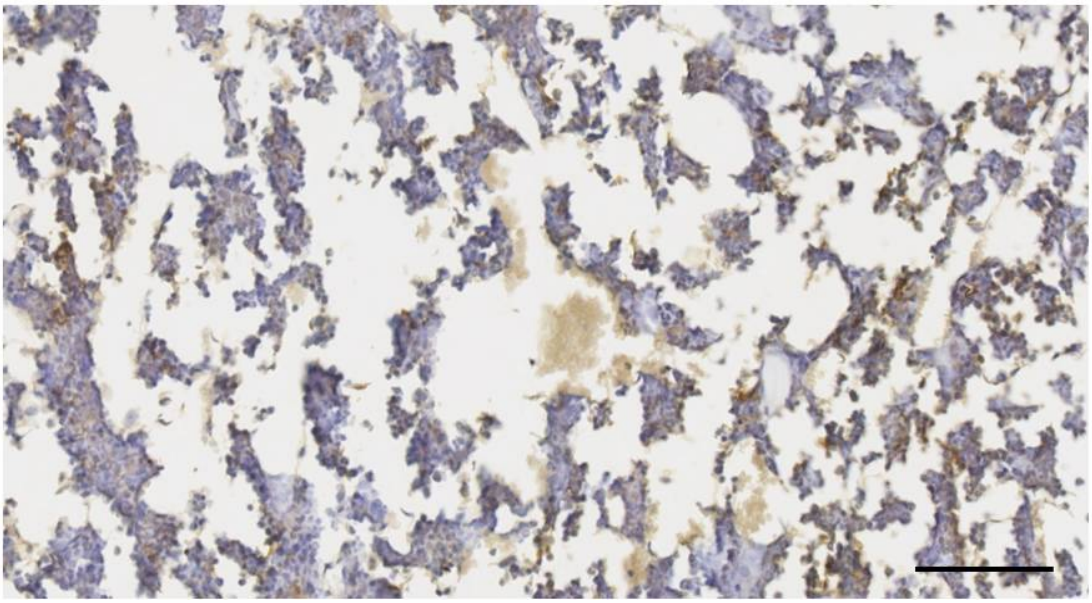

GFP (data not shown). While our *in vitro* assays showed BEZ235 and BKM120 are cytostatic, long-term administration of BEZ235 and BKM120 *in vivo,* and perhaps *in vitro,* could lead to cytotoxicity and cell apoptosis.

The PI3k and mTOR pathways are important in maintaining cellular growth in all cell types. Previous animal studies have shown that oral administration of BEZ235 and BKM120 is associated with weight loss due to drug intolerance[28; 29]. However, several studies contradict this finding with the weight of the animals being unaffected by once daily treatment of BEZ235 and BKM120[20; 21; 23; 27]. Notably, weight loss is also associated with increasing tumour burden in systemic MM tumour models such as the 5TGM1 model[55]. However in this study, the administration of 40mg/kg BEZ235 and 50mg/kg BKM120 once daily, did not affect the weight of the animals which suggests that the drugs were well tolerated by the animals.

Three dimensional images constructed from μCT scans of myelomatous long bones in our animal model showed the presence of prominent osteolytic lesions, similar to that observed in the human setting. These studies show, for the first time, that BEZ235 and BKM120 significantly reduce the number of osteolytic lesions in MM. While a reduction in serum TRAcP5 levels (which correlate with osteoclast number but not osteoclast activity)[56; 57] was observed in both BEZ235 or BKM120 treated animals, histological analyses reveal no significant change in the number of osteoclasts present or the area of bone surface occupied by osteoclasts in the trabecular bone in response to BEZ235 or BKM120. Collectively, these findings suggest that BEZ235 and BKM120 do not affect osteoclast numbers *in vivo*. Due to the poor histological morphology observed in the tibial specimens, it was difficult to identify TRAP positive, multi-nucleated osteoclasts. However, given the importance of the PI3k and mTOR pathways in osteoclast formation, we can only speculate that inhibition of these pathways *in vivo* would inhibit osteoclast formation. The effect of BEZ235 and BKM120 on osteoclast formation will be examined *in vitro* and discussed in the next chapter.

In this study, the histological analyses of tibial sections from vehicle- and drug-treated animals revealed poor tissue morphology. While the reasons for the poor morphology remain to be determined, previous studies have reported that Methyl Cellulose administration can affect cell morphology and histology[58; 59]. Specifically, Palmer *et al* and Rosa *et al* have shown that Methyl Cellulose administration can induce

splenomegaly in rats and Mongolian gerbils and disrupt cellular architecture of the spleen[58; 59].

The data presented here suggests that the administration of BEZ235 or BKM120 protects the bone from osteolytic bone disease in MM. A significant increase in bone volume (BV/TV) and trabecular number (Tb. N) was observed in BEZ235-treated animals and a significant increase in BV/TV, bone surface (BS/BV), Tb. N, trabecular thickness (Tb. Th) and trabecular spacing (Tb. Sp) was observed in BKM120-treated animals. The increase in these parameters contribute to the increase in bone volume in both studies suggesting that BEZ235 and BKM120 possess pro-osteoblastic properties which was supported by the significant increase in serum P1NP levels. Furthermore the inhibition of osteoclastic activity, indicated by the significant decrease in osteolytic lesions present on the tibial cortical bone in the BEZ235- and BKM120-treated animals, also contribute to the increase in bone volume. While a previous study from our laboratory showed that BEZ235 induces osteogenesis in human MSC *in vitro*[60], our *in vivo* results support the osteogenic properties of BEZ235. Our findings in this study also suggest that BKM120 possess both anti-osteoclastic and pro-osteoblastic properties.

To our knowledge, this is the first study showing the effects of BEZ235 and BKM120 on MM cells in a systemic *in vivo* model of MM. Our findings demonstrate that BEZ235 and BKM120 are able to decrease the proliferation of MM cells *in vivo* as shown by the decrease in BLI intensity and serum paraprotein levels. Furthermore, from the studies presented here, we speculate that BEZ235 and BKM120 could possess anti-osteoclastic and/or pro-osteoblastic properties and this will investigated in the next chapter.

Reference:

1. Denlinger, C. E., Rundall, B. K. & Jones, D. R. (2005). Inhibition of phosphatidylinositol 3-kinase/Akt and histone deacetylase activity induces apoptosis in non-small cell lung cancer in vitro and in vivo. *The Journal of thoracic and cardiovascular surgery* **130**, 1422-9.
2. Semba, S., Itoh, N., Ito, M., Harada, M. & Yamakawa, M. (2002). The in vitro and in vivo effects of 2-(4-morpholinyl)-8-phenyl-chromone (LY294002), a specific inhibitor of phosphatidylinositol 3'-kinase, in human colon cancer cells. *Clinical cancer research : an official journal of the American Association for Cancer Research* **8**, 1957-63.
3. Hu, L., Zaloudek, C., Mills, G. B., Gray, J. & Jaffe, R. B. (2000). In vivo and in vitro ovarian carcinoma growth inhibition by a phosphatidylinositol 3-kinase inhibitor (LY294002). *Clinical cancer research : an official journal of the American Association for Cancer Research* **6**, 880-6.
4. Hu, L., Hofmann, J., Lu, Y., Mills, G. B. & Jaffe, R. B. (2002). Inhibition of phosphatidylinositol 3'-kinase increases efficacy of paclitaxel in in vitro and in vivo ovarian cancer models. *Cancer research* **62**, 1087-92.
5. Teranishi, F., Takahashi, N., Gao, N., Akamo, Y., Takeyama, H., Manabe, T. & Okamoto, T. (2009). Phosphoinositide 3-kinase inhibitor (wortmannin) inhibits pancreatic cancer cell motility and migration induced by hyaluronan in vitro and peritoneal metastasis in vivo. *Cancer science* **100**, 770-7.
6. Ng, S. S., Tsao, M. S., Nicklee, T. & Hedley, D. W. (2001). Wortmannin inhibits pkb/akt phosphorylation and promotes gemcitabine antitumor activity in orthotopic human pancreatic cancer xenografts in immunodeficient mice. *Clinical cancer research : an official journal of the American Association for Cancer Research* **7**, 3269-75.
7. Boehle, A. S., Kurdow, R., Boenicke, L., Schniewind, B., Faendrich, F., Dohrmann, P. & Kalthoff, H. (2002). Wortmannin inhibits growth of human non-small-cell lung cancer in vitro and in vivo. *Langenbeck's archives of surgery / Deutsche Gesellschaft fur Chirurgie* **387**, 234-9.
8. Stephan, S., Datta, K., Wang, E., Li, J., Brekken, R. A., Parangi, S., Thorpe, P. E. & Mukhopadhyay, D. (2004). Effect of rapamycin alone and in combination with antiangiogenesis therapy in an orthotopic model of human pancreatic cancer.

Clinical cancer research : an official journal of the American Association for Cancer Research **10**, 6993-7000.

9. Mondesire, W. H., Jian, W., Zhang, H., Ensor, J., Hung, M. C., Mills, G. B. & Meric-Bernstam, F. (2004). Targeting mammalian target of rapamycin synergistically enhances chemotherapy-induced cytotoxicity in breast cancer cells. *Clinical cancer research : an official journal of the American Association for Cancer Research* **10**, 7031-42.
10. Namba, R., Young, L. J., Abbey, C. K., Kim, L., Damonte, P., Borowsky, A. D., Qi, J., Tepper, C. G., MacLeod, C. L., Cardiff, R. D. & Gregg, J. P. (2006). Rapamycin inhibits growth of premalignant and malignant mammary lesions in a mouse model of ductal carcinoma in situ. *Clinical cancer research : an official journal of the American Association for Cancer Research* **12**, 2613-21.
11. Raimondi, A. R., Molinolo, A. & Gutkind, J. S. (2009). Rapamycin prevents early onset of tumorigenesis in an oral-specific K-ras and p53 two-hit carcinogenesis model. *Cancer research* **69**, 4159-66.
12. Gupta, A. K., Cerniglia, G. J., Mick, R., Ahmed, M. S., Bakanauskas, V. J., Muschel, R. J. & McKenna, W. G. (2003). Radiation sensitization of human cancer cells in vivo by inhibiting the activity of PI3K using LY294002. *International journal of radiation oncology, biology, physics* **56**, 846-53.
13. Norman, B. H., Shih, C., Toth, J. E., Ray, J. E., Dodge, J. A., Johnson, D. W., Rutherford, P. G., Schultz, R. M., Worzalla, J. F. & Vlahos, C. J. (1996). Studies on the mechanism of phosphatidylinositol 3-kinase inhibition by wortmannin and related analogs. *Journal of medicinal chemistry* **39**, 1106-11.
14. Fabian, M. C., Lakey, J. R., Rajotte, R. V. & Kneteman, N. M. (1993). The efficacy and toxicity of rapamycin in murine islet transplantation. In vitro and in vivo studies. *Transplantation* **56**, 1137-42.
15. Werzowa, J., Koehrer, S., Strommer, S., Cejka, D., Fuereder, T., Zebedin, E. & Wacheck, V. (2011). Vertical inhibition of the mTORC1/mTORC2/PI3K pathway shows synergistic effects against melanoma in vitro and in vivo. *The Journal of investigative dermatology* **131**, 495-503.
16. Lopez-Fauqued, M., Gil, R., Grueso, J., Hernandez-Losa, J., Pujol, A., Moline, T. & Recio, J. A. (2010). The dual PI3K/mTOR inhibitor PI-103 promotes immunosuppression, in vivo tumor growth and increases survival of sorafenib-

treated melanoma cells. *International journal of cancer. Journal international du cancer* **126**, 1549-61.

17. Brachmann, S. M., Hofmann, I., Schnell, C., Fritsch, C., Wee, S., Lane, H., Wang, S., Garcia-Echeverria, C. & Maira, S. M. (2009). Specific apoptosis induction by the dual PI3K/mTor inhibitor NVP-BEZ235 in HER2 amplified and PIK3CA mutant breast cancer cells. *Proceedings of the National Academy of Sciences of the United States of America* **106**, 22299-304.
18. Serra, V., Markman, B., Scaltriti, M., Eichhorn, P. J., Valero, V., Guzman, M., Botero, M. L., Llonch, E., Atzori, F., Di Cosimo, S., Maira, M., Garcia-Echeverria, C., Parra, J. L., Arribas, J. & Baselga, J. (2008). NVP-BEZ235, a dual PI3K/mTOR inhibitor, prevents PI3K signaling and inhibits the growth of cancer cells with activating PI3K mutations. *Cancer research* **68**, 8022-30.
19. Xu, C. X., Li, Y., Yue, P., Owonikoko, T. K., Ramalingam, S. S., Khuri, F. R. & Sun, S. Y. (2011). The combination of RAD001 and NVP-BEZ235 exerts synergistic anticancer activity against non-small cell lung cancer in vitro and in vivo. *PloS one* **6**, e20899.
20. Maira, S. M., Stauffer, F., Brueggen, J., Furet, P., Schnell, C., Fritsch, C., Brachmann, S., Chene, P., De Pove, A., Schoemaker, K., Fabbro, D., Gabriel, D., Simonen, M., Murphy, L., Finan, P., Sellers, W. & Garcia-Echeverria, C. (2008). Identification and characterization of NVP-BEZ235, a new orally available dual phosphatidylinositol 3-kinase/mammalian target of rapamycin inhibitor with potent in vivo antitumor activity. *Molecular cancer therapeutics* **7**, 1851-63.
21. McMillin, D. W., Ooi, M., Delmore, J., Negri, J., Hayden, P., Mitsiades, N., Jakubikova, J., Maira, S. M., Garcia-Echeverria, C., Schlossman, R., Munshi, N. C., Richardson, P. G., Anderson, K. C. & Mitsiades, C. S. (2009). Antimyeloma activity of the orally bioavailable dual phosphatidylinositol 3-kinase/mammalian target of rapamycin inhibitor NVP-BEZ235. *Cancer research* **69**, 5835-42.
22. Mueller, A., Bachmann, E., Linnig, M., Khillimberger, K., Schimanski, C. C., Galle, P. R. & Moehler, M. (2012). Selective PI3K inhibition by BKM120 and BEZ235 alone or in combination with chemotherapy in wild-type and mutated human gastrointestinal cancer cell lines. *Cancer chemotherapy and pharmacology* **69**, 1601-15.
23. Burger, M. T., Pecchi, S., Wagman, A., Ni, Z.-J., Knapp, M., Hendrickson, T., Atallah, G., Pfister, K., Zhang, Y., Bartulis, S., Frazier, K., Ng, S., Smith, A.,

Verhagen, J., Haznedar, J., Huh, K., Iwanowicz, E., Xin, X., Menezes, D., Merritt, H., Lee, I., Wiesmann, M., Kaufman, S., Crawford, K., Chin, M., Bussiere, D., Shoemaker, K., Zaror, I., Maira, S.-M. & Voliva, C. F. (2011). Identification of NVP-BKM120 as a Potent, Selective, Orally Bioavailable Class I PI3 Kinase Inhibitor for Treating Cancer. *ACS Medicinal Chemistry Letters* **2**, 774-779.

24. Kinross, K. M., Brown, D. V., Kleinschmidt, M., Jackson, S., Christensen, J., Cullinane, C., Hicks, R. J., Johnstone, R. W. & McArthur, G. A. (2011). In vivo activity of combined PI3K/mTOR and MEK inhibition in a Kras(G12D);Pten deletion mouse model of ovarian cancer. *Molecular cancer therapeutics* **10**, 1440-9.
25. Ren, H., Chen, M., Yue, P., Tao, H., Owonikoko, T. K., Ramalingam, S. S., Khuri, F. R. & Sun, S. Y. (2012). The combination of RAD001 and NVP-BKM120 synergistically inhibits the growth of lung cancer in vitro and in vivo. *Cancer letters* **325**, 139-46.
26. Zheng, Y., Yang, J., Qian, J., Zhang, L., Lu, Y., Li, H., Lin, H., Lan, Y., Liu, Z., He, J., Hong, S., Thomas, S., Shah, J., Baladandayuthapani, V., Kwak, L. W. & Yi, Q. (2012). Novel phosphatidylinositol 3-kinase inhibitor NVP-BKM120 induces apoptosis in myeloma cells and shows synergistic anti-myeloma activity with dexamethasone. *Journal of molecular medicine* **90**, 695-706.
27. Maira, S. M., Pecchi, S., Huang, A., Burger, M., Knapp, M., Sterker, D., Schnell, C., Guthy, D., Nagel, T., Wiesmann, M., Brachmann, S., Fritsch, C., Dorsch, M., Chene, P., Shoemaker, K., De Pover, A., Menezes, D., Martiny-Baron, G., Fabbro, D., Wilson, C. J., Schlegel, R., Hofmann, F., Garcia-Echeverria, C., Sellers, W. R. & Voliva, C. F. (2012). Identification and characterization of NVP-BKM120, an orally available pan-class I PI3-kinase inhibitor. *Molecular cancer therapeutics* **11**, 317-28.
28. Cramer, J., Capples, D., KHackl, W., Lorand, D., Maira, M. S., Martus, H., Mukhopadhyay, S. & Zehender, H. (2009). BEZ235 Investigator's Brochure.
29. Ru, Q. & Cosaert, J. (2010). BKM120 Investigator's Brochure.
30. Sato, M., Bryant, H. U., Dodge, J. A., Davis, H., Matter, W. F. & Vlahos, C. J. (1996). Effects of wortmannin analogs on bone in vitro and in vivo. *The Journal of pharmacology and experimental therapeutics* **277**, 543-50.
31. Dodge, J. A., Bryant, H. U., Kim, J., Matter, W. F., Norman, B. H., Srinivasan, U., Vlahos, C. J. & Sato, M. (1995). 17β-hydroxywortmannin: A potent inhibitor of

bone resorption and phosphatidylinositol-3-kinase. *Bioorganic & medicinal chemistry letters* **5**, 1713-1718.

32. Xie, H., Xie, P. L., Wu, X. P., Chen, S. M., Zhou, H. D., Yuan, L. Q., Sheng, Z. F., Tang, S. Y., Luo, X. H. & Liao, E. Y. (2011). Omentin-1 attenuates arterial calcification and bone loss in osteoprotegerin-deficient mice by inhibition of RANKL expression. *Cardiovascular research* **92**, 296-306.
33. Ulici, V., Hoenselaar, K. D., Agoston, H., McErlain, D. D., Umoh, J., Chakrabarti, S., Holdsworth, D. W. & Beier, F. (2009). The role of Akt1 in terminal stages of endochondral bone formation: angiogenesis and ossification. *Bone* **45**, 1133-45.
34. Alvarez-Garcia, O., Carbajo-Perez, E., Garcia, E., Gil, H., Molinos, I., Rodriguez, J., Ordonez, F. A. & Santos, F. (2007). Rapamycin retards growth and causes marked alterations in the growth plate of young rats. *Pediatric nephrology* **22**, 954-61.
35. Holstein, J. H., Klein, M., Garcia, P., Histing, T., Culemann, U., Pizanis, A., Laschke, M. W., Scheuer, C., Meier, C., Schorr, H., Pohlemann, T. & Menger, M. D. (2008). Rapamycin affects early fracture healing in mice. *British journal of pharmacology* **154**, 1055-62.
36. Radl, J., De Glopper, E. D., Schuit, H. R. & Zurcher, C. (1979). Idiopathic paraproteinemia. II. Transplantation of the paraprotein-producing clone from old to young C57BL/KaLwRij mice. *Journal of immunology* **122**, 609-13.
37. Vanderkerken, K., De Raeve, H., Goes, E., Van Meirvenne, S., Radl, J., Van Riet, I., Thielemans, K. & Van Camp, B. (1997). Organ involvement and phenotypic adhesion profile of 5T2 and 5T33 myeloma cells in the C57BL/KaLwRij mouse. *British journal of cancer* **76**, 451-60.
38. Vanderkerken, K., Asosingh, K., Croucher, P. & Van Camp, B. (2003). Multiple myeloma biology: lessons from the 5TMM models. *Immunological reviews* **194**, 196-206.
39. Vanderkerken, K., De Greef, C., Asosingh, K., Arteta, B., De Veerman, M., Vande Broek, I., Van Riet, I., Kobayashi, M., Smedsrod, B. & Van Camp, B. (2000). Selective initial in vivo homing pattern of 5T2 multiple myeloma cells in the C57BL/KalwRij mouse. *British journal of cancer* **82**, 953-9.
40. Alici, E., Konstantinidis, K. V., Aints, A., Dilber, M. S. & Abedi-Valugerdi, M. (2004). Visualization of 5T33 myeloma cells in the C57BL/KaLwRij mouse:

establishment of a new syngeneic murine model of multiple myeloma. *Experimental hematology* **32**, 1064-72.

41. Asosingh, K., Radl, J., Van Riet, I., Van Camp, B. & Vanderkerken, K. (2000). The 5TMM series: a useful in vivo mouse model of human multiple myeloma. *The hematology journal : the official journal of the European Haematology Association / EHA* **1**, 351-6.
42. Radl, J., Punt, Y. A., van den Enden-Vieveen, M. H., Bentvelzen, P. A., Bakkus, M. H., van den Akker, T. W. & Benner, R. (1990). The 5T mouse multiple myeloma model: absence of c-myc oncogene rearrangement in early transplant generations. *British journal of cancer* **61**, 276-8.
43. Dallas, S. L., Garrett, I. R., Oyajobi, B. O., Dallas, M. R., Boyce, B. F., Bauss, F., Radl, J. & Mundy, G. R. (1999). Ibandronate reduces osteolytic lesions but not tumor burden in a murine model of myeloma bone disease. *Blood* **93**, 1697-706.
44. Oyajobi, B. O., Munoz, S., Kakonen, R., Williams, P. J., Gupta, A., Wideman, C. L., Story, B., Grubbs, B., Armstrong, A., Dougall, W. C., Garrett, I. R. & Mundy, G. R. (2007). Detection of myeloma in skeleton of mice by whole-body optical fluorescence imaging. *Molecular cancer therapeutics* **6**, 1701-1708.
45. Oyajobi, B. O., Franchin, G., Williams, P. J., Pulkrabek, D., Gupta, A., Munoz, S., Grubbs, B., Zhao, M., Chen, D., Sherry, B. & Mundy, G. R. (2003). Dual effects of macrophage inflammatory protein-1alpha on osteolysis and tumor burden in the murine 5TGM1 model of myeloma bone disease. *Blood* **102**, 311-9.
46. Edwards, C. M., Edwards, J. R., Lwin, S. T., Esparza, J., Oyajobi, B. O., McCluskey, B., Munoz, S., Grubbs, B. & Mundy, G. R. (2008). Increasing Wnt signaling in the bone marrow microenvironment inhibits the development of myeloma bone disease and reduces tumor burden in bone in vivo. *Blood* **111**, 2833-42.
47. Diamond, P., Labrinidis, A., Martin, S. K., Farrugia, A. N., Gronthos, S., To, L. B., Fujii, N., O'Loughlin, P. D., Evdokiou, A. & Zannettino, A. C. (2009). Targeted disruption of the CXCL12/CXCR4 axis inhibits osteolysis in a murine model of myeloma-associated bone loss. *Journal of bone and mineral research : the official journal of the American Society for Bone and Mineral Research* **24**, 1150-61.
48. Nyfeler, B., Chen, Y., Li, X., Pinzon-Ortiz, M., Wang, Z., Reddy, A., Pradhan, E., Das, R., Lehar, J., Schlegel, R., Finan, P. M., Cao, Z. A., Murphy, L. O. & Huang,

A. (2012). RAD001 enhances the potency of BEZ235 to inhibit mTOR signaling and tumor growth. *PloS one* **7**, e48548.

49. Fuereder, T., Wanek, T., Pflegerl, P., Jaeger-Lansky, A., Hoeflmayer, D., Strommer, S., Kuntner, C., Wrba, F., Werzowa, J., Hejna, M., Muller, M., Langer, O. & Wacheck, V. (2011). Gastric cancer growth control by BEZ235 in vivo does not correlate with PI3K/mTOR target inhibition but with [18F]FLT uptake. *Clinical cancer research : an official journal of the American Association for Cancer Research* **17**, 5322-32.
50. Maniatis, A. (1998). Pathophysiology of paraprotein production. *Renal failure* **20**, 821-8.
51. Ohbayashi, Y., Miyake, M., Sawai, F., Minami, Y., Iwasaki, A. & Matsui, Y. (2013). Adjunct teriparatide therapy with monitoring of bone turnover markers and bone scintigraphy for bisphosphonate-related osteonecrosis of the jaw. *Oral surgery, oral medicine, oral pathology and oral radiology* **115**, e31-7.
52. Reid, I. R., Davidson, J. S., Wattie, D., Wu, F., Lucas, J., Gamble, G. D., Rutland, M. D. & Cundy, T. (2004). Comparative responses of bone turnover markers to bisphosphonate therapy in Paget's disease of bone. *Bone* **35**, 224-30.
53. Jorgensen, N. R., Henriksen, Z., Sorensen, O. H. & Civitelli, R. (2004). Dexamethasone, BMP-2, and 1,25-dihydroxyvitamin D enhance a more differentiated osteoblast phenotype: validation of an in vitro model for human bone marrow-derived primary osteoblasts. *Steroids* **69**, 219-26.
54. Juvekar, A., Burga, L. N., Hu, H., Lunsford, E. P., Ibrahim, Y. H., Balmana, J., Rajendran, A., Papa, A., Spencer, K., Lyssiotis, C. A., Nardella, C., Pandolfi, P. P., Baselga, J., Scully, R., Asara, J. M., Cantley, L. C. & Wulf, G. M. (2012). Combining a PI3K inhibitor with a PARP inhibitor provides an effective therapy for BRCA1-related breast cancer. *Cancer discovery* **2**, 1048-63.
55. Goel, A., Dispenzieri, A., Geyer, S. M., Greiner, S., Peng, K. W. & Russell, S. J. (2006). Synergistic activity of the proteasome inhibitor PS-341 with non-myeloablative 153-Sm-EDTMP skeletally targeted radiotherapy in an orthotopic model of multiple myeloma. *Blood* **107**, 4063-70.
56. Halleen, J. M., Tiitinen, S. L., Ylipahkala, H., Fagerlund, K. M. & Vaananen, H. K. (2006). Tartrate-resistant acid phosphatase 5b (TRACP 5b) as a marker of bone resorption. *Clinical laboratory* **52**, 499-509.

57. Rissanen, J. P., Suominen, M. I., Peng, Z. & Halleen, J. M. (2008). Secreted tartrate-resistant acid phosphatase 5b is a Marker of osteoclast number in human osteoclast cultures and the rat ovariectomy model. *Calcified tissue international* **82**, 108-15.
58. Palmer, J. G., Eichwald, E. J., Cartwright, G. E. & Wintrobe, M. M. (1953). The experimental production of splenomegaly, anemia and leukopenia in Albino rats. *Blood* **8**, 72-80.
59. Rosa, R. A. & Glomski, C. A. (1981). The Mongolian gerbil (Meriones unguiculatus): its histological and haematological response to methylcellulose. *Laboratory animals* **15**, 131-6.
60. Martin, S. K., Fitter, S., Bong, L. F., Drew, J. J., Gronthos, S., Shepherd, P. R. & Zannettino, A. C. (2010). NVP-BEZ235, a dual pan class I PI3 kinase and mTOR inhibitor, promotes osteogenic differentiation in human mesenchymal stromal cells. *Journal of bone and mineral research : the official journal of the American Society for Bone and Mineral Research* **25**, 2126-37.

Chapter 5

The Role of the PI3k and mTOR pathways on Osteoblasts and Osteoclasts

5.1 *Introduction*

Bone remodelling is a coordinated process by which old bone is resorbed by osteoclasts and new bone is formed by osteoblasts. Bone remodelling is a tightly coupled process so as to ensure that the net ratio of bone formation to bone resorption is balanced.

Osteoblasts, derived from multipotent MSCs, are responsible for secreting bone matrix comprised mainly of type I collagen and a number of non-collagenous proteins[1]. BMPs, the Wnt pathway, Runx2 and Osterix play critical regulatory roles in differentiation of MSCs into osteoblasts[2; 3; 4; 5; 6; 7]. The downstream effector of the PI3k pathway, Akt, and in particular Akt1, is highly expressed in bone cells[8]. Akt1 deficiency impairs Runx2-dependent differentiation and function of osteoblasts[8].

Osteoclasts are multinucleated cells that originate from the monocyte/macrophage lineage[9; 10; 11]. Osteoclasts rely on RANK and M-CSF for their growth and function. The RANK receptor, present on the surface of mature osteoclasts interacts with RANKL, which is expressed on osteoblasts and BMSCs, to stimulate osteoclastogenesis[12; 13]. RANKL and M-CSF have been shown to promote osteoclast survival by activating Akt[8]. The PI3k pathway has been shown to induce osteoclast differentiation, activation and survival by transducing signals from RANKL and M-CSF[14; 15]. Kawamura and colleagues demonstrated that Akt1 is necessary for the function of osteoclasts, as dysfunction of Akt1 leads to reduced RANKL expression by osteoblasts, leading to a reduction in osteoclastic bone resorption *in vitro*[8]. The mTOR pathway is also involved in osteoclast formation, survival and bone resorption[16]. The mTOR pathway inhibits osteoprotegerin, an inhibitor of RANKL, thus promoting the formation and proliferation of osteoclasts[17].

Several studies using Wortmannin, LY294002 or Rapamycin have shown that these drugs possess both pro-osteoblastic and anti-osteoclastic properties. LY294002 and Rapamycin have been shown to stimulate BMP-2 expression in the mouse myoblast cell line, C2C12[18]. Vinals and colleagues also demonstrated the inhibition of Akt and $p70^{S6k}$ increases Runx2 expression, an early marker of osteoblast differentiation, and induces the expression of late-stage markers of osteoblast differentiation, alkaline phosphatase (ALP) and osteocalcin[18]. Furthermore, inhibition of the PI3K and mTOR pathways increases Runx2 expression. Ogawa demonstrated that inhibition of the

mTOR pathway with Rapamycin increased ALP activity and osteopontin and osteocalcin mRNA expression in rat osteosarcoma cells[19].

In contrast to this body of literature, there are also a number of studies that demonstrate that inhibition of the PI3k and mTOR pathways suppresses osteoblastogenesis. Using rat BMSCs, Isomoto *et al* showed that Rapamycin inhibits osteogenic differentiation *in vitro*, as evidenced by low ALP activity after 2 weeks of culture in osteogenic conditions and low calcium incorporation and osteocalcin levels after 4 weeks of osteoinductive culture[20]. Singha and colleagues also showed that inhibition of the mTOR pathway significantly reduced osteocalcin, bone sialoprotein and Osterix mRNA levels and the capacity of mBMSCs to mineralise under osteogenic conditions[21]. To further understand the role of mTOR in osteogenesis, Singha also showed that the overexpression of $p70^{S6k}$ significantly increased the levels of Runx2 protein[21].

There are several potential explanations for these contradictory findings, such as differences in the cell types and treatment conditions used. Furthermore, Rapamycin predominantly inhibits mTORC1 and to a much lesser extent, mTORC2, and ultimately activates the PI3k pathway through several feedback loops such as the S6k-PI3k-Ras pathway or the insulin-like growth factor-1 receptor signalling pathway[22; 23].

Previous studies from our laboratory using primary human MSCs showed that inhibition of the PI3k and mTOR pathways with BEZ235 induced osteogenesis[24]. Martin and colleagues demonstrated that BEZ235 significantly increased mineralisation, Runx2, BMP and ALP mRNA levels and neonatal mouse calvarial bone formation *in vitro*[24]. To our knowledge, this is the only study to demonstrate that dual inhibition of the PI3k and mTOR pathways drives osteogenesis.

Inhibition of the PI3k and mTOR pathway has also been found to inhibit osteoclastogenesis. Bradley and colleagues showed that M-CSF activates the PI3k pathway in osteoclasts[25], which inhibits the survival of RANKL-dependent osteoclasts[14; 15; 26; 27]. Inhibition of PTEN, which negatively regulates the PI3k pathway, has also been shown to inhibit RANKL- and Osteopontin-activated pathways and inhibit osteoclast differentiation, survival and migration[26]. Furthermore, Mogi and colleagues demonstrated that the inhibition of the mTOR pathway by Rapamycin increased osteoprotegerin levels leading to a reduction in osteoclastogenesis[17].

As outlined in the previous chapter, data from our *in vivo* studies demonstrated a decrease in the number of osteolytic lesions present along the cortical bone of both BEZ235- and BKM120-treated animals compared with the vehicle control groups. Furthermore, our *in vivo* studies showed an overall increase in bone volume and a significant increase in serum P1NP levels (a bone formation marker) in BEZ235- and BKM120-treated animals. These findings suggest that these drugs may possess pro-osteoblastic and/or anti-osteoclastic properties. To our knowledge, the effect of BKM120 on osteogenesis has not been examined, nor have the effects of BEZ235 and BKM120 on osteoclastogenesis. To address this and extend our *in vivo* findings, this final results chapter outlines *in vitro* experiments conducted to investigate the effects of BEZ235 and BKM120 on murine osteoblasts and osteoclasts, and their ability to produce mineral and resorb bone, respectively, *in vitro*.

5.2 *Results*

5.2.1 The effect of BEZ235 and BKM120 on osteoblastogenesis *in vitro*

5.2.1.1 BEZ235 and BKM120 inhibit the PI3k and mTOR pathways in mBMSCs

To investigate the effect of BEZ235 and BKM120 on PI3K and mTOR signalling in murine MSCs, primary mBMSC cultures, prepared from the long bones of C57BL6/KaLwRij mice, were stimulated with PDGF, a potent MSC mitogen that suppresses differentiation[28; 29; 30] and the phosphorylation status of downstream effector molecules assessed by immunoblotting. To do this, primary mBMSCs were serum-starved overnight and treated with BEZ235 (1-100nM), BKM120 (125-2000nM) or vehicle alone (0.1% DMSO) for 1 hour. Cells were then pulsed with rhPDGF-BB for 5 minutes prior to the preparation of cell lysates. The cell lysates were then examined by Western immunoblot to determine the effects of BEZ235 and BKM120 on PDGF-induced phosphorylation of Akt and $p70^{S6K}$, downstream effectors of the PI3k and mTOR pathways, respectively. As shown in Figure 5.1A, stimulation of mBMSCs with rhPDGF in the presence of vehicle alone induced the phosphorylation of Akt and $p70^{S6K}$. In the presence of BEZ235, a dose-dependent inhibition of rhPDGF-induced phosphorylation of Akt_{Ser473} and $p70^{S6k}$ was observed at concentrations of 10nM and above. In contrast, the phosphorylation of Akt_{Thr308} was unaffected at all concentrations examined. In the presence of BKM120, a dose-dependent inhibition of the rhPDGF-

Figure 5.1. BEZ235 mediates a dose-dependent inhibition of Akt and p70S6k phosphorylation in mBMSCs. (A) Serum-starved mBMSCs were treated with BEZ235 (0-100nM) for 1 hour and pulsed with PDGF-BB (10ng/mL) for 5 minutes prior to the preparation of lysates for immunoblotting. An RCDC protein assay was performed to ensure equal amounts of protein were loaded in each lane, and proteins (50ug/lane) were resolved on 10% SDS-PAGE gels. Levels of phosphorylated AktSer473, AktThr308, and p70S6K and total Akt and p70S6K protein expression were detected using Western immunoblotting. (B) The IC50 for BEZ235-mediated inhibition of AktSer473, AktThr308 and p70S6K phosphorylation was determined using Graphpad Prism software.

A

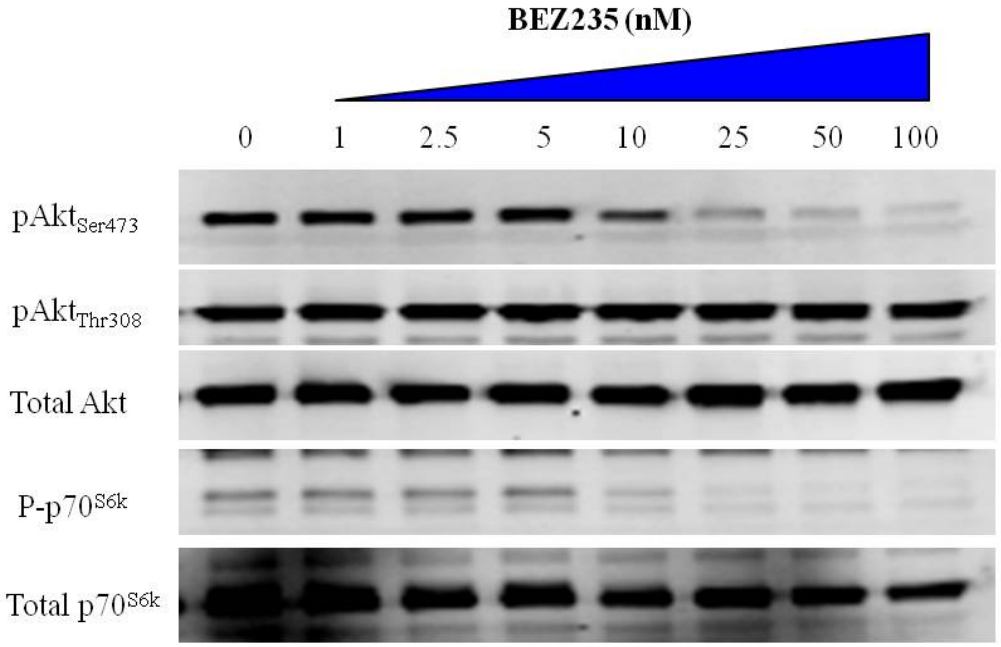

B

pAkt^{Ser473} IC$_{50}$	pAkt^{Thr308} IC$_{50}$	P-p70^{S6k} IC$_{50}$
12nM 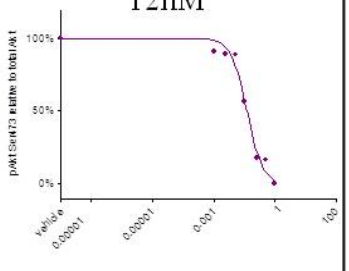	N/A	6.5nM 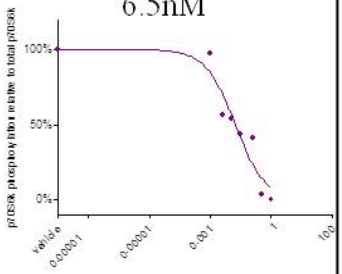

Figure 5.2. BKM120 mediates a dose-dependent inhibition of Akt and p70S6k phosphorylation in mBMSCs. (A) Serum-starved mBMSCs were treated with BKM120 (0-2000nM) for 1 hour and pulsed with PDGF-BB (10ng/mL) for 5 minutes prior to the preparation of lysates for immunoblotting. An RCDC protein assay was performed to ensure equal amounts of protein were loaded in each lane, and proteins (50ug/lane) were resolved on 10% SDS-PAGE gels. Levels of phosphorylated AktSer473, AktThr308, and p70S6K and total Akt and p70S6K protein expression were detected using Western immunoblotting. (B) The IC50 for BKM120-mediated inhibition of AktSer473, AktThr308 and p70S6K phosphorylation was determined using Graphpad Prism software.

A

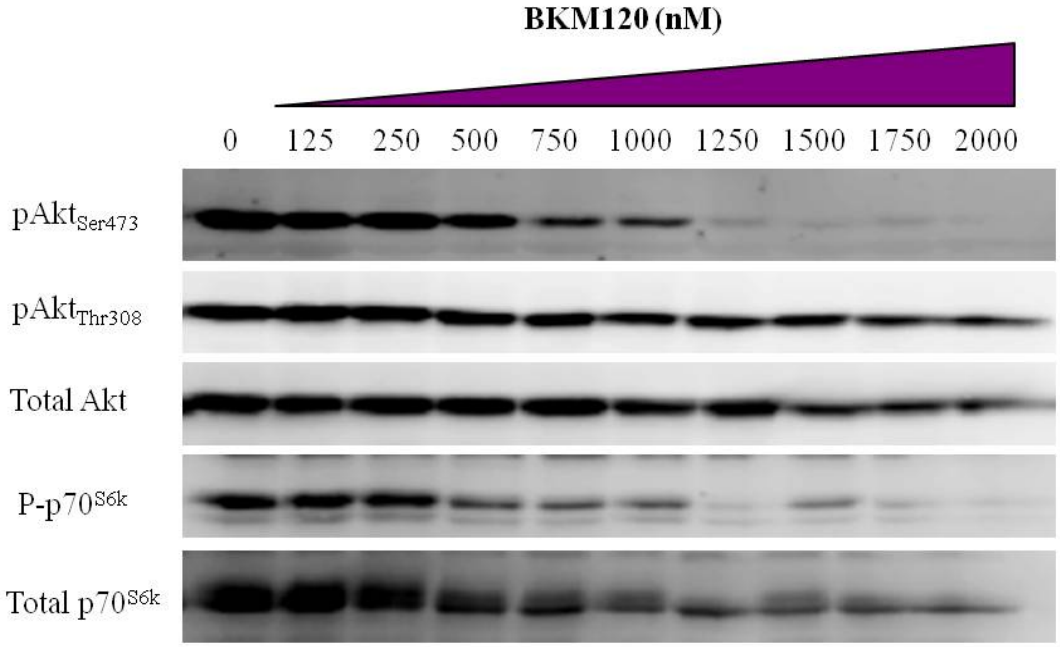

B

pAkt^{Ser473} IC$_{50}$	pAkt^{Thr308} IC$_{50}$	P-p70^{S6k} IC$_{50}$
236nM 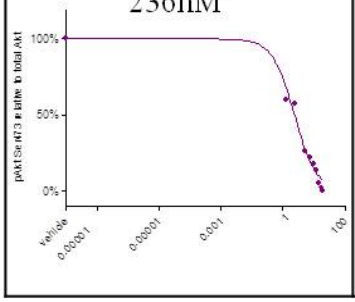	N/A	794nM 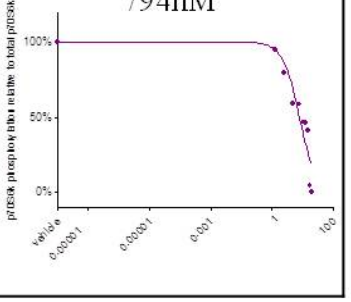

induced phosphorylation of Akt_{Ser473} and $p70^{S6k}$ was also observed at concentrations of 500nM and above (Figure 5.2A). Similar to BEZ235, phosphorylation of Akt_{Thr308} was unaffected by all concentrations of BKM120 examined.

Quantitation of the intensity of the phosphorylated Akt_{Ser473} and $p70^{S6k}$ bands, normalised to the intensity of the total Akt and total $p70^{S6K}$ bands respectively, enabled the determination of the IC_{50} for inhibition of rhPDGF-induced phosphorylation of Akt and $p70^{S6K}$ for each drug. As shown in Figure 5.1B, the IC_{50} for BEZ235-mediated inhibition of Akt and $p70^{S6K}$ phosphorylation were found to be 12nM and 6.5nM respectively, and for BKM120, the IC_{50} values were 236nM and 794nM respectively (Figure 5.2B).

5.2.1.2 BEZ235 and BKM120 inhibit mBMSC proliferation

As discussed in Chapter 1, the PI3k and mTOR pathways are important in maintaining cell proliferation, growth and survival. To examine whether the inhibition of the PI3K and mTOR pathways with BEZ235 and BKM120 inhibited mBMSC growth, the effect of BEZ235 and BKM120 on mBMSC proliferation was examined. mBMSCs were seeded into 96 well plates and allowed to adhere overnight before being treated with BEZ235 (1-100nM), BKM120 (125-2000nM) or vehicle alone (0.1% DMSO) for 2, 4, and 6 days. At each of these time points, the number of cells present in each well was determined using the WST-1 assay. As shown in left panel of Figure 5.3A, mBMSCs cultured in the presence of the vehicle alone displayed a progressive increase in cell number over the 6 days of culture, with a plateau reached at 6 days as the cells reached confluence. In the presence of BEZ235, a dose-dependent decrease in cell proliferation was observed, with a significant decrease in cell proliferation observed at concentrations of 25nM and higher (Figure 5.3A, right panel, $p < 0.001$; one-way ANOVA). The IC_{50} for BEZ235-mediated inhibition of mBMSC growth was found to be 38nM (Figure 5.3C). As shown in Figure 5.3B, mBMSCs cultured in the presence of BKM120 exhibited a dose-dependent decrease in cell proliferation compared to vehicle alone, with a significant decrease in cell proliferation observed at concentrations of 125nM and higher (Figure 5.3B, right panel, $p < 0.01$; one-way ANOVA). The IC_{50} for BKM120-mediated inhibition of mBMSC growth was found to be 859nM (Figure 5.3C).

Figure 5.3. BEZ235 and BKM120 inhibit the proliferation of mBMSCs *in vitro*. mBMSCs were cultured in the presence of **(A)** BEZ235 (0-100nM) or **(B)** BKM120 (0-2000nM) for 6 days. At day 0, 2, 4, and 6 time points, the number of viable, proliferating cells was assessed using WST-1, and cumulative data were plotted as shown (left panels). Data are expressed as the mean ± SEM from replicate samples and are representative of three independent experiments using different mBMSC donors. The significance of the inhibition of mBMSC growth was determined from day 6 results (right panels). **p<0.01 and ***p<0.001, compared to vehicle, one-way ANOVA. **(C)** The IC_{50} for inhibition of mBMSC growth was determined from day 6 results using GraphPad Prism (right panels).

A

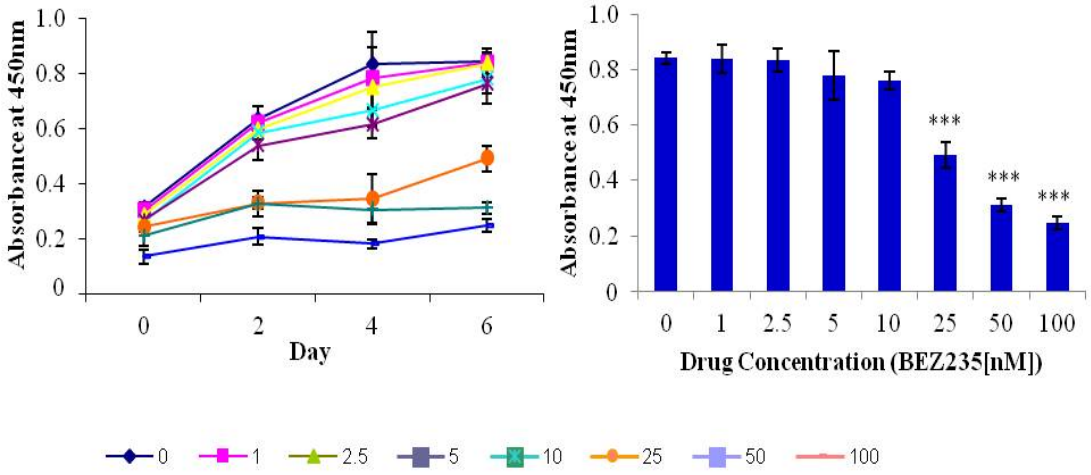

B

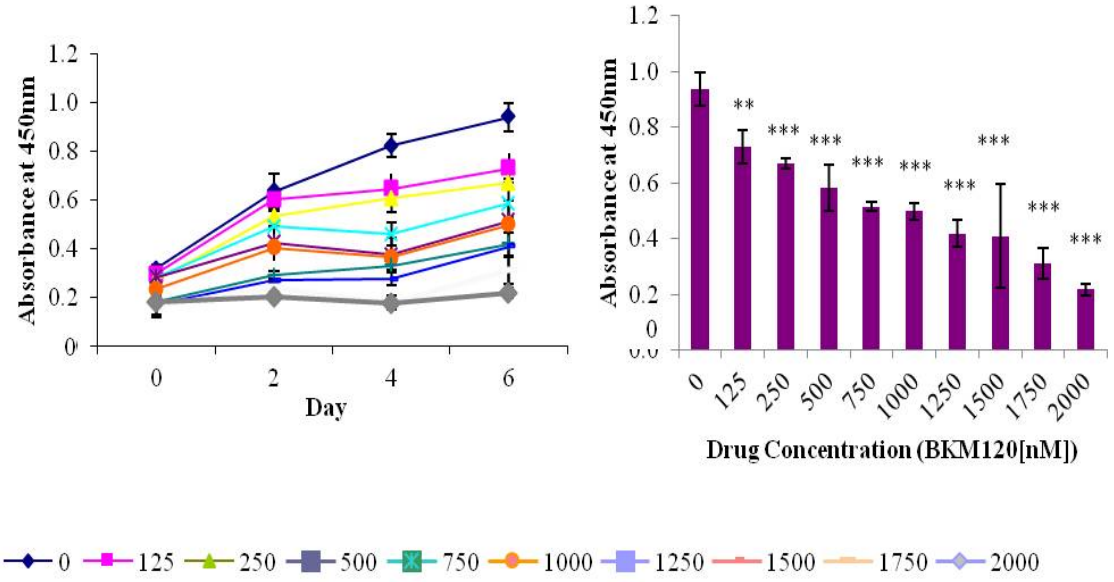

C

BEZ	38nM
BKM	859nM

5.2.1.3 BEZ235 and BKM120 do not induce apoptosis in mBMSCs

To examine the effect of BEZ235 and BKM120 on mBMSC apoptosis, mBMSCs were treated with ½ IC_{50}, IC_{50} and 2x IC_{50} BEZ235 (see IC_{50} in Figure 5.3C), ½ IC_{50}, IC_{50} and 2x IC_{50} BKM120 (see IC_{50} in Figure 5.3C), or vehicle alone (0.1% DMSO) for 2 days. Following the next day, the cells were stained with Ann V (marker for early apoptosis) and 7AAD (marker for late apoptosis) and analysed immediately by flow cytometry.

As shown in Figure 5.4, treatment of mBMSCs with BEZ235 did not induce a dose-dependent increase in the percentage of AnnV/7AAD+ cells (top right quadrant) when compared to the percentage of viable cells (bottom left quadrant). Similarly, treatment of mBMSCs with BKM120 did not induce a dose-dependent increase in the percentage of AnnV/7AAD+ cells when compared to the percentage of viable cells (bottom left quadrant) (Figure 5.5).

5.2.1.4 BEZ235 and BKM120 stimulate the osteogenic differentiation of mBMSCs in vitro

To examine the effect of BEZ235 and BKM120 on osteoblast activity, the ability of these drugs to drive osteogenic MSC differentiation and mineral formation was examined. mBMSCs were cultured under osteoinductive conditions in the presence of BEZ235 (1-100nM), BKM120 (125-2000nM) or vehicle alone (0.1% DMSO) for 2 weeks under hypoxic conditions. After 2 weeks, the amount of acid-solubilised calcium was measured using the Calcium Arsenazo assay and the data corrected for differences in cell numbers between treatments by determining total DNA content per well using Pico Green.

As shown in Figure 5.6A, treatment of mBMSCs with BEZ235 induced a dose-dependent increase in mineral production, with a significant (5-fold) increase in mineral production, on a per cell basis, in cultures treated with 100nM BEZ235 ($p < 0.01$; one-way ANOVA). Similarly, treatment of mBMSCs with BKM120 induced a dose-dependent increase in mineral production, with a significant (1 to 3-fold) increase observed in cultures treated with 750nM-2000nM ($p < 0.05$, one-way ANOVA; Figure 5.6B). Although, a significant increase in mineral production was observed in

Figure 5.4. BEZ235 does not induce apoptosis in mBMSCs. mBMSCs were treated with BEZ235 (½IC_{50}, 1x IC_{50} and 2x IC_{50}) and 0.1% DMSO for 2 days. Cells were then stained with Annexin V and 7-AAD for 15 minutes and analysed by flow cytometry.

UT BEZ235

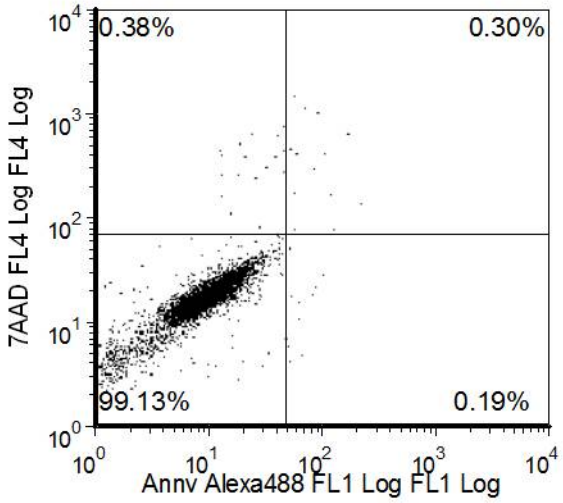

1/2x IC_{50} BEZ235

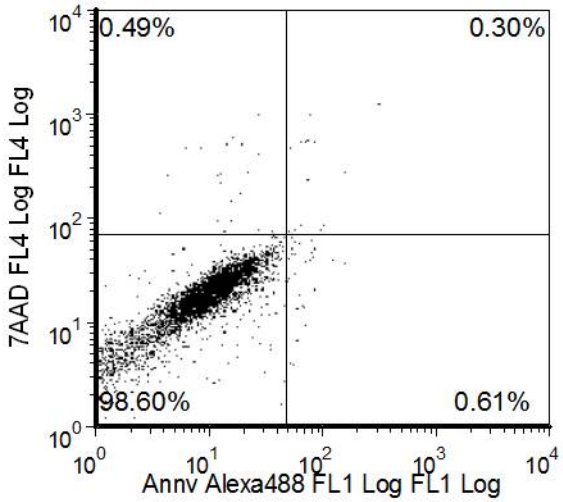

1x IC_{50} BEZ235

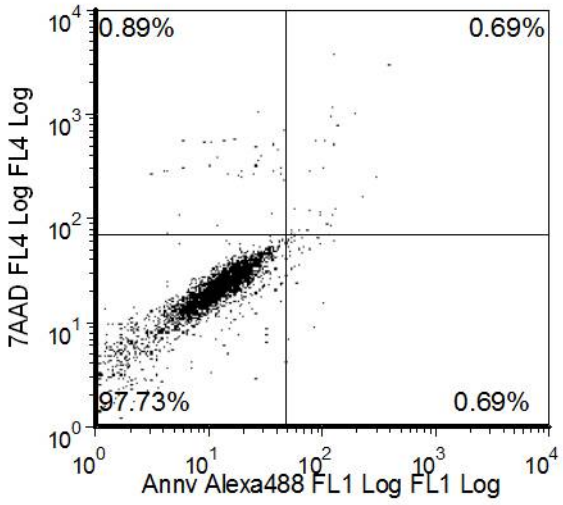

2x IC_{50} BEZ235

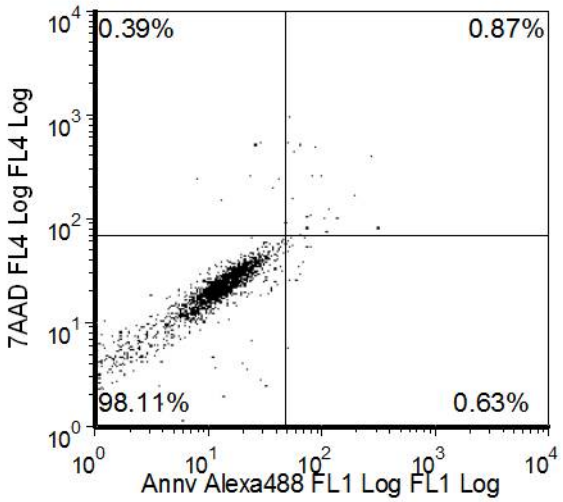

Figure 5.5. BKM120 does not induce apoptosis in mBMSCs. mBMSCs were treated with BKM120 (½IC_{50}, 1x IC_{50} and 2x IC_{50}) and 0.1% DMSO for 2 days. Cells were then stained with Annexin V and 7-AAD for 15 minutes and analysed by flow cytometry.

UT BKM120

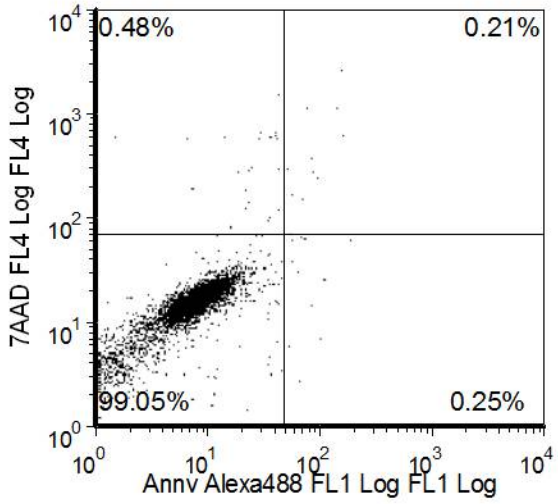

1/2x IC_{50} BKM120

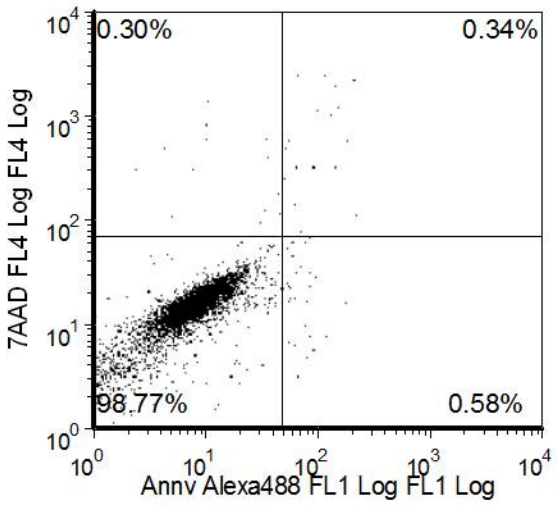

1x IC_{50} BKM120

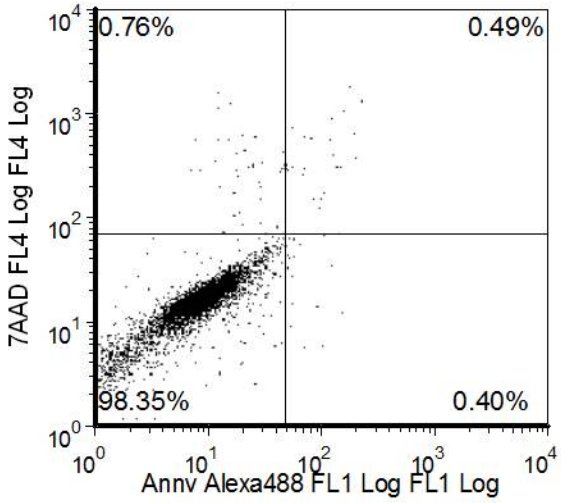

2x IC_{50} BKM120

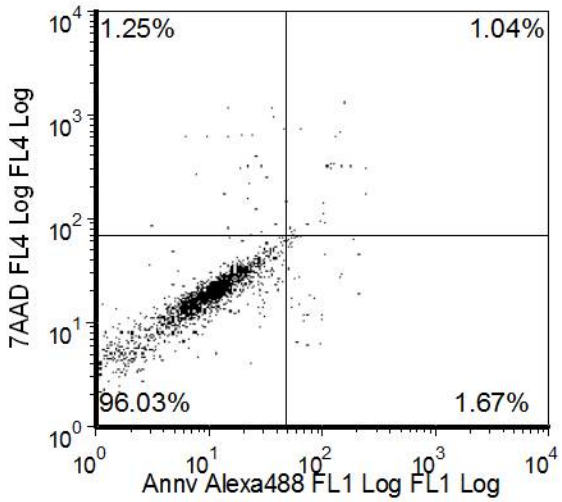

Figure 5.6. BEZ235 and BKM120 promote osteogenesis in mBMSCs *in vitro*. mBMSCs were cultured in osteogenic media supplemented with **(A)** BEZ235 (0-100nM) or **(B)** BKM120 (0-2000nM). After 2 weeks, mineral was dissolved with HCl and calcium content was quantitated using the Calcium Arsenazo assay. Calcium produced per well was corrected for relative cell numbers by normalizing to total DNA content per well. Data are expressed as the mean ± SEM from replicate samples, and are representative of three independent experiments using different mBMSC donors. *$p<0.05$, **$p<0.01$ and ***$p<0.001$, compared to vehicle, one-way ANOVA.

A

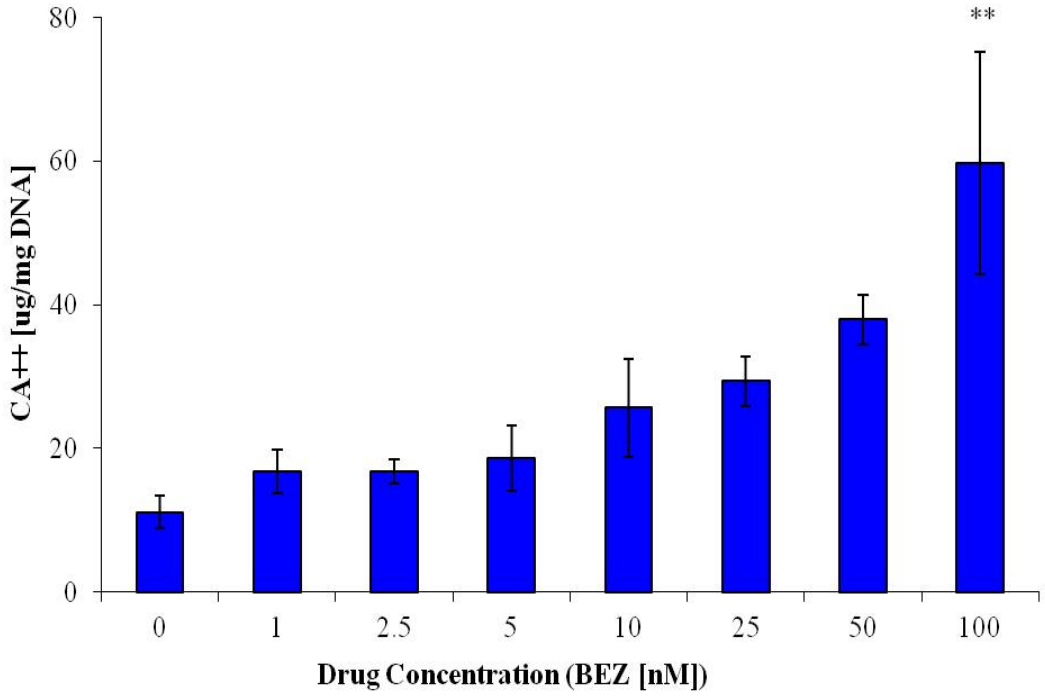
80
60
40
20
0
CA++ [ug/mg DNA]
**
0
1
2.5
5
10
25
50
100
Drug Concentration (BEZ [nM])

B

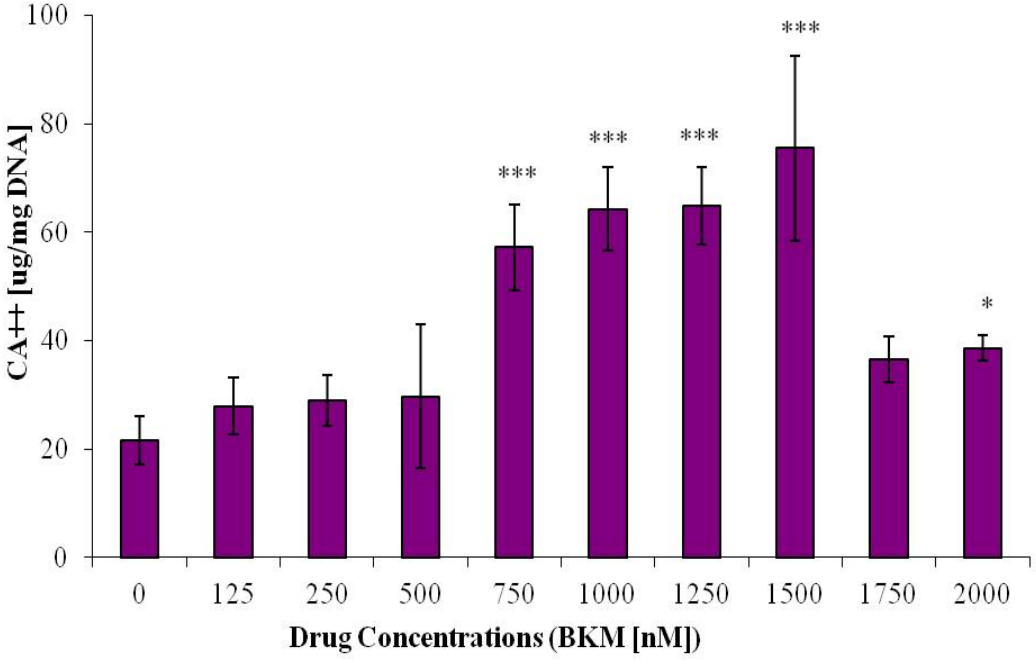
100
80
60
40
20
0
CA++ [ug/mg DNA]
***
***
***
***
*
0
125
250
500
750
1000
1250
1500
1750
2000
Drug Concentrations (BKM [nM])

mBMSCs treated with 2000nM BKM120, the ability of BKM120 to induce mineral formation was reduced at concentrations in excess of 1500nM.

5.2.2 The effect of BEZ235 and BKM120 on osteoclastogenesis *in vitro*

5.2.2.1 BEZ235 and BKM120 inhibit osteoclastogenesis and osteoclast activity in mBM cells *in vitro*

To determine the effect on BEZ235 and BKM120 on murine osteoclast formation, mBM cells, isolated from C57BL6/KaLwRij mice, were cultured with M-CSF and RANKL in the presence of BEZ235 (1-100nM), BKM120 (125-2000nM) or vehicle alone (0.05% DMSO) for 6 days. After the treatment period, cells were fixed and stained for the osteoclast marker TRAP, and the number of osteoclasts per well enumerated. As shown in Figure 5.7A, the addition of M-CSF and RANKL to mBM cells induced the formation of TRAP-positive, multinucleated osteoclasts in the vehicle-treated cultures. The addition of BEZ235 mediated a dose-dependent inhibition of osteoclast formation, with a complete inhibition of osteoclast formation observed at 25nM BEZ235 and above (Figure 5.7B, $p < 0.05$; one-way ANOVA). Similarly, a significant reduction in osteoclast formation was observed in response to BKM120 treatment at concentrations of 125nM and above (Figure 5.8, $p < 0.001$; one-way ANOVA), with a complete inhibition of osteoclast formation observed at 1250nM and higher.

To investigate the effect of BEZ235 and BKM120 on the ability of osteoclasts to resorb bone *in vitro*, mBM cells were cultured under osteoclastogenic conditions on calcium phosphate-coated slides for 9 days. Following treatment, mineral was stained with von Kossa silver stain and the area of resorption (clearing in the mineral substrate) was calculated using Image J software. A significant, dose-dependent decrease in the area of resorption pits was observed at all concentrations of BEZ235 (Figure 5.9, $p<0.01$; one-way ANOVA) and BKM120 (Figure 5.10, $p < 0.001$; one-way-ANOVA) examined. No resorption was observed between 25-100nM BEZ235 (Figure 5.9) and 1250-2000nM BKM120 (Figure 5.10) as no osteoclasts were formed (Figures 5.7 and 5.8).

Figure 5.7. BEZ235 inhibits osteoclast formation in mBM cultures *in vitro*. mBM cells were cultured under osteoclastogenic conditions in the presence of BEZ235 (0-100nM). Following 6 days of culture, cells were stained for TRAP. **(A)** A representative photograph of each well was taken at 20x magnification. Images are representative of three independent experiments using different mBM donors. Scale bars: 200µm. **(B)** The number of TRAP-positive cells with 3 or more nuclei were counted. Data are expressed as the mean ± SEM of replicate wells and are representative of three independent experiments using different mBM donors. *$p<0.05$ and ***$p<0.001$, compared to vehicle, one-way ANOVA.

A

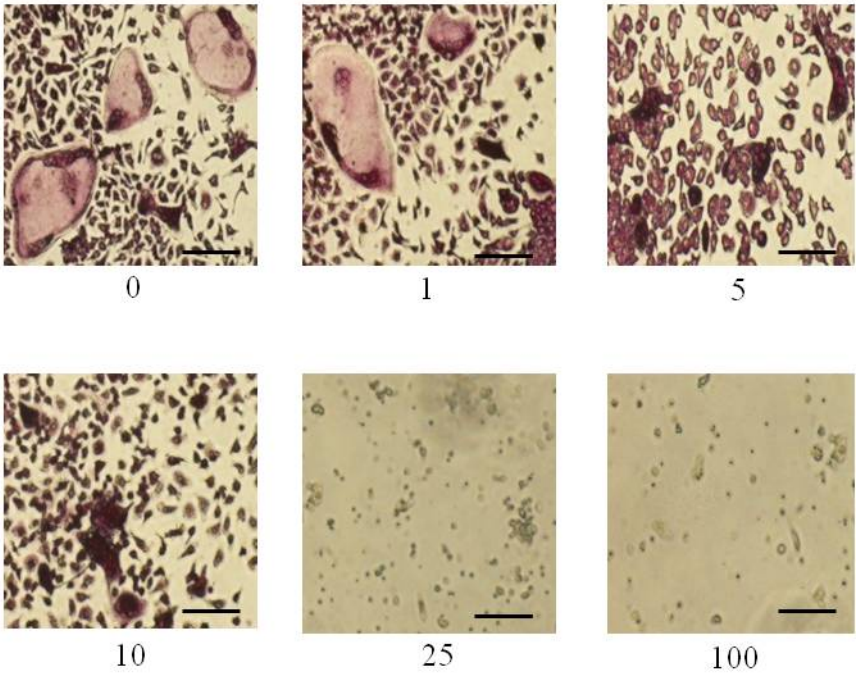
0
1
5
10
25
100

B

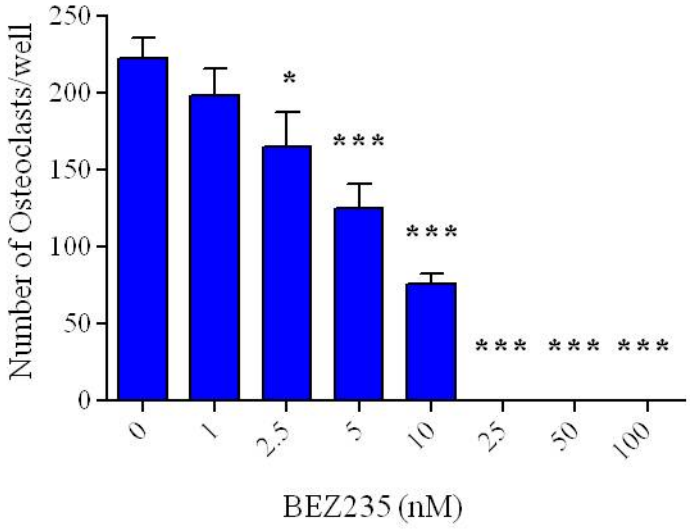
Number of Osteoclasts/well
250
200
150
100
50
0
*
***
***
***
***
***
0
1
2.5
5
10
25
50
100
BEZ235 (nM)

Figure 5.8. . BKM120 inhibits osteoclast formation in mBM cultures *in vitro*. mBM cells were cultured under osteoclastogenic conditions in the presence of BKM120 (0-2000nM). Following 6 days of culture, cells were stained for TRAP. **(A)** A representative photograph of each well was taken at 20x magnification. Images are representative of three independent experiments using different mBM donors. Scale bars: 200µm. **(B)** The number of TRAP-positive cells with 3 or more nuclei were counted. Data are expressed as the mean ± SEM of replicate wells and are representative of three independent experiments using different mBM donors. ***p<0.001, compared to vehicle, one-way ANOVA.

A

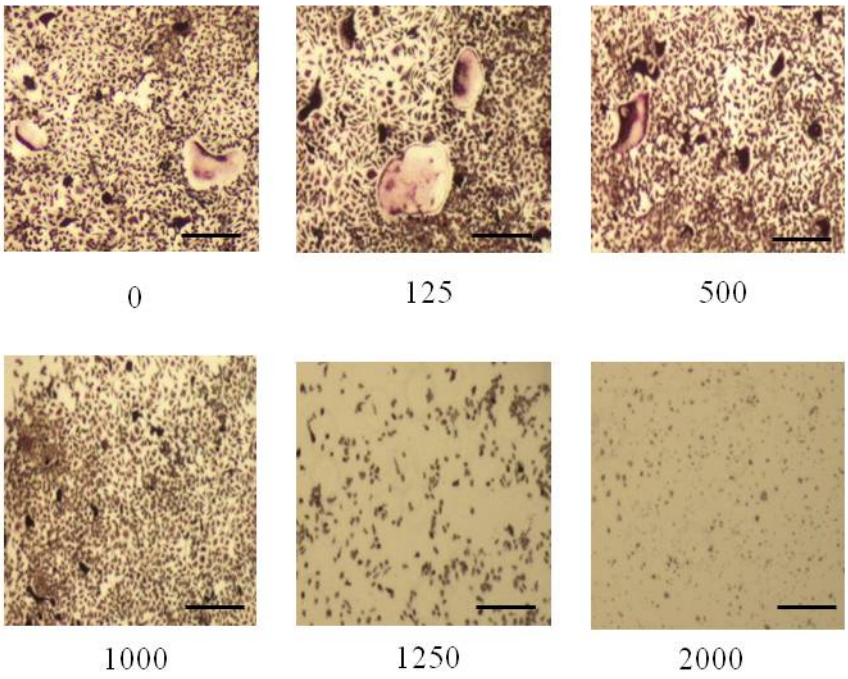
0
125
500
1000
1250
2000

B

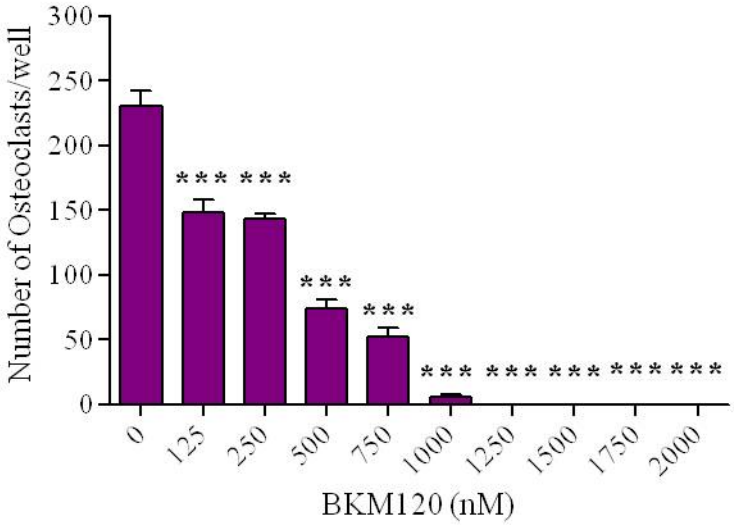
Number of Osteoclasts/well
300
250
200
150
100
50
0
*** *** *** *** *** *** *** *** *** ***
0
125
250
500
750
1000
1250
1500
1750
2000
BKM120 (nM)

Figure 5.9. BEZ235 inhibits the ability of murine osteoclasts to resorb mineral *in vitro*. mBM cells were cultured under osteoclastogenic conditions in the presence of BEZ235 (0-100nM) on calcium phosphate-coated slides for 9 days and mineral was stained with silver stain. **(A)** Silver-stained slides were photographed at 0.8x magnification. Images are representative of three independent experiments using different mBM donors. Scare bar: 2.5mm. **(B)** The area of substrate resorbed on the silver-stained slides (lacunae area) was calculated using Image J software. Data are expressed as the mean ± SEM of replicate wells and are representative of three independent experiments using different mBM donors. ** $p<0.01$ and ***$p<0.001$, compared to vehicle, one-way ANOVA.

A

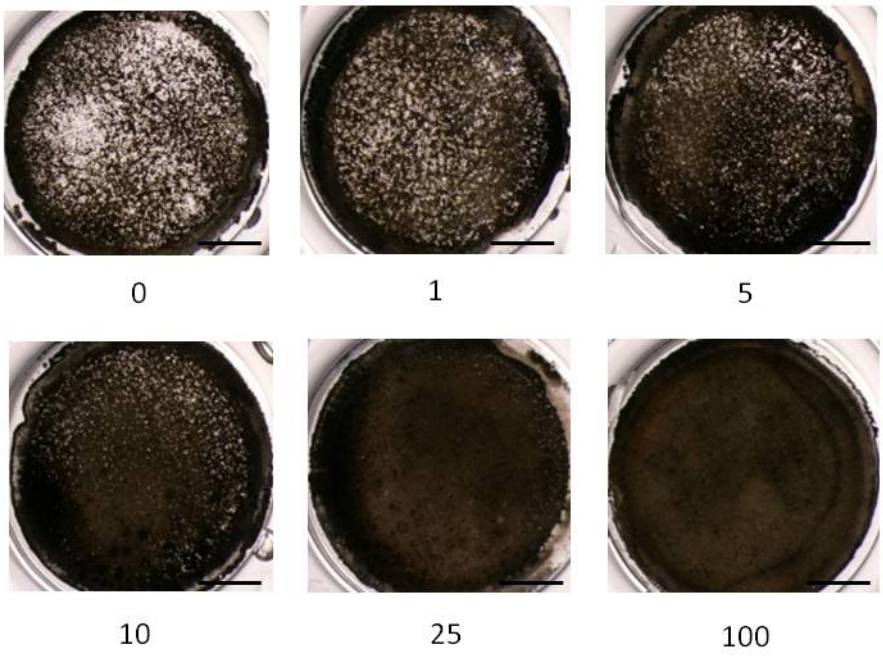
0
1
5
10
25
100

B

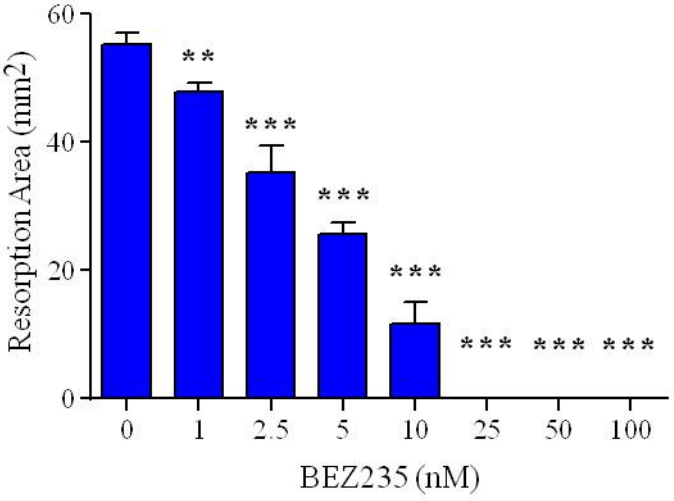
Resorption Area (mm2)
60
40
20
0
**
***
***
***
***
***
***
0
1
2.5
5
10
25
50
100
BEZ235 (nM)

Figure 5.10. BKM120 inhibits the ability of murine osteoclasts to resorb mineral *in vitro*. mBM cells were cultured under osteoclastogenic conditions in the presence of BKM120 (0-2000nM) on calcium phosphate-coated slides for 9 days and mineral was stained with silver stain. **(A)** Silver-stained slides were photographed at 0.8x magnification. Images are representative of three independent experiments using different mBM donors. Scare bar: 2.5mm. **(B)** The area of substrate resorbed on the silver-stained slides (lacunae area) was calculated using Image J software. Data are expressed as the mean ± SEM of replicate wells and are representative of three independent experiments using different mBM donors. ***$p<0.001$, compared to vehicle, one-way ANOVA.

A

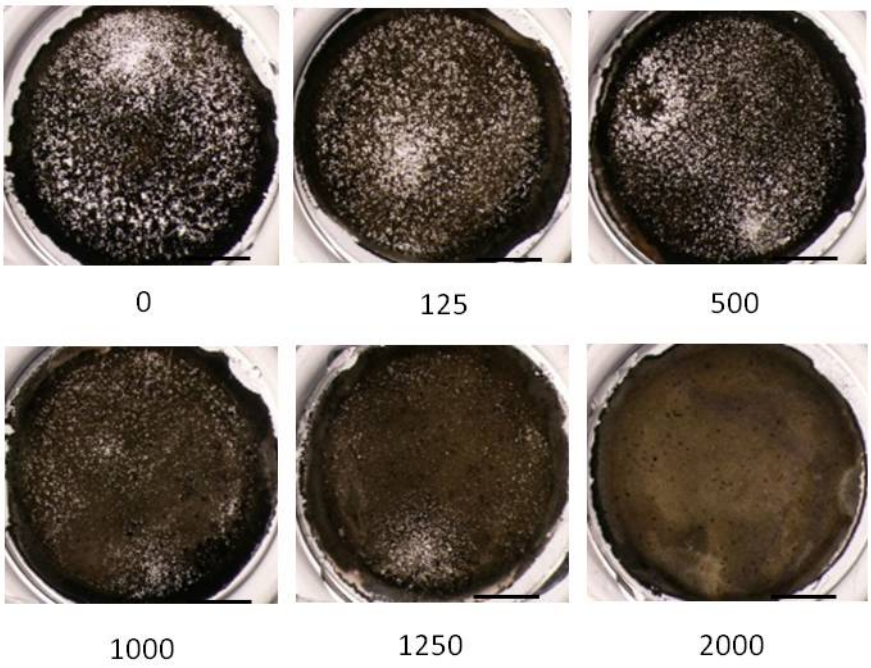
0
125
500
1000
1250
2000

B

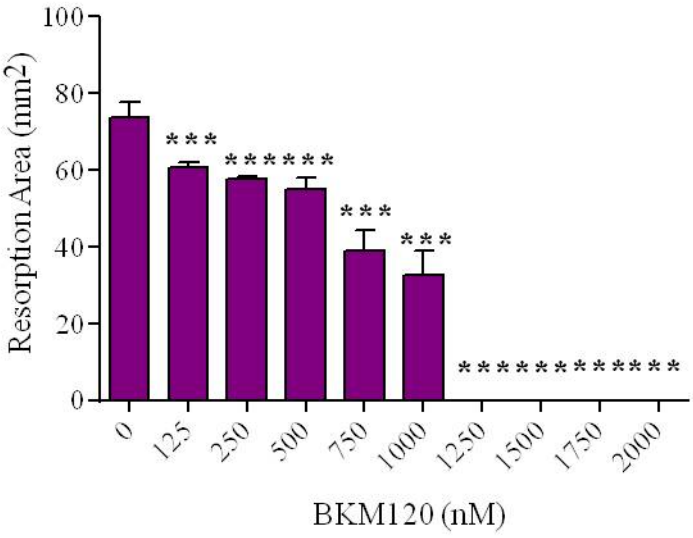
Resorption Area (mm2)
100
80
60
40
20
0
***
******
***
***
****
0
125
250
500
750
1000
1250
1500
1750
2000
BKM120 (nM)

5.2.2.2 BEZ235 and BKM120 inhibit the phosphorylation of Akt but not $p70^{S6K}$ in RAW264.7 cells

Due to the limited number of mBM cells that can be isolated from mice and the large number of cells required for the following studies, the murine monocyte/macrophage-like cell line, RAW264.7, was used to examine the effects of BEZ235 and BKM120 on the phosphorylation of Akt and $p70^{S6k}$, osteoclast cell proliferation and apoptosis induction.

To investigate the effect of BEZ235 and BKM120 on PI3K and mTOR signalling in RAW264.7 cells, RAW264.7 cells were serum-starved and the phosphorylation status of downstream effector molecules assessed by immunoblotting. Briefly, RAW264.7 cells were serum-starved overnight and treated with BEZ235 (1-100nM), BKM120 (125-2000nM) or vehicle alone (0.1% DMSO) in serum-free media for 2 hours before the preparation of cell lysates. The cell lysates were examined by Western immunoblot to determine the effect of BEZ235 and BKM120 on phosphorylation of Akt and $p70^{S6K}$. As shown in Figure 5.11A, a strong induction of phosphorylation of Akt_{Ser473} and Akt_{Thr308} was observed in the presence of vehicle alone. In the presence of BEZ235, a dose-dependent inhibition of the phosphorylation of Akt_{Ser473} and Akt_{Thr308} was observed from concentrations of 2.5nM and 1nM respectively. In contrast, the phosphorylation of $p70^{S6k}$ was not observed in the presence of vehicle alone or treatment. As shown in Figure 5.12A, BKM120 mediated a dose-dependent inhibition of Akt_{Ser473} and Akt_{Thr308} phosphorylation, at concentrations from 1000nM and 125nM respectively. Similar to BEZ235, phosphorylation of $p70^{S6k}$ was not observed in the presence of vehicle alone or BKM120 treatment.

Quantitation of the intensity of the phosphorylated Akt_{Ser473} and Akt_{Thr308} bands, normalised to the intensity of the total Akt bands, enabled the determination of the IC_{50} for inhibition of phosphorylation of Akt_{Ser473} and Akt_{Thr308} for each drug. As shown in Figure 5.11B, the IC_{50} for BEZ235-mediated inhibition of Akt_{Ser473} and Akt_{Thr308} phosphorylation was 12nM and 6.5nM respectively, whereas for BKM120, the IC_{50} was 1156nM and 556nM respectively (Figure 5.12B).

Figure 5.11. BEZ235 mediates a dose-dependent inhibition of Akt phosphorylation in RAW264.7 cells. (A) Serum-starved RAW264.7 cells were treated with BEZ235 (0-100nM) for 2 hours and lysates prepared for immunoblotting. An RCDC protein assay was performed to ensure equal amounts of protein were loaded in each lane, and proteins (50μg/lane) were resolved on 10% SDS-PAGE gels. Levels of phosphorylated Akt_{Ser473}, Akt_{Thr308}, and $p70^{S6k}$ and total Akt and $p70^{S6k}$ protein expression were detected using Western immunoblotting. **(B)** The IC_{50} for BEZ235-mediated inhibition of Akt_{Ser473}, Akt_{Thr308} and $p70^{S6K}$ phosphorylation was determined using Graphpad Prism software.

A

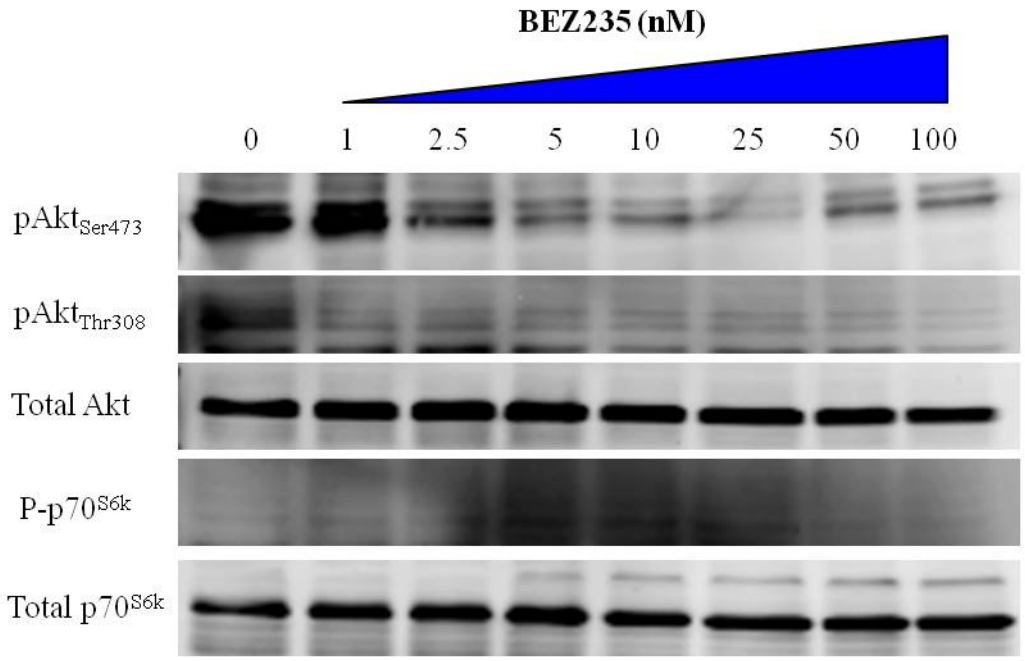

B

pAkt^{Ser473} IC$_{50}$	pAkt^{Thr308} IC$_{50}$	P-p70^{S6k} IC$_{50}$
12nM 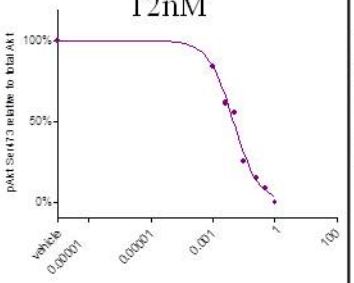	6.5nM 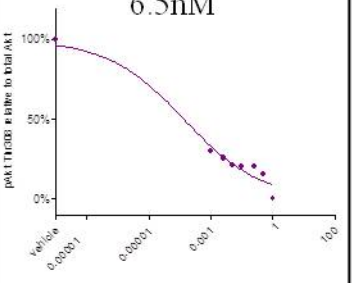	N/A

Figure 5.12. BKM120 mediates a dose-dependent inhibition of Akt phosphorylation in RAW264.7 cells. (A) Serum-starved RAW264.7 cells were treated with BKM120 (0-2000nM) for 2hours and lysates prepared for immunoblotting. An RCDC protein assay was performed to ensure equal amounts of protein were loaded in each lane, and proteins (50μg/lane) were resolved on 10% SDS-PAGE gels. Levels of phosphorylated Akt_{Ser473}, Akt_{Thr308}, and $p70^{S6k}$ and total Akt and $p70^{S6k}$ protein expression were detected using Western immunoblotting. **(B)** The IC_{50} for BKM120-mediated inhibition of Akt_{Ser473}, Akt_{Thr308} and $p70^{S6K}$ phosphorylation was determined using Graphpad Prism software.

A

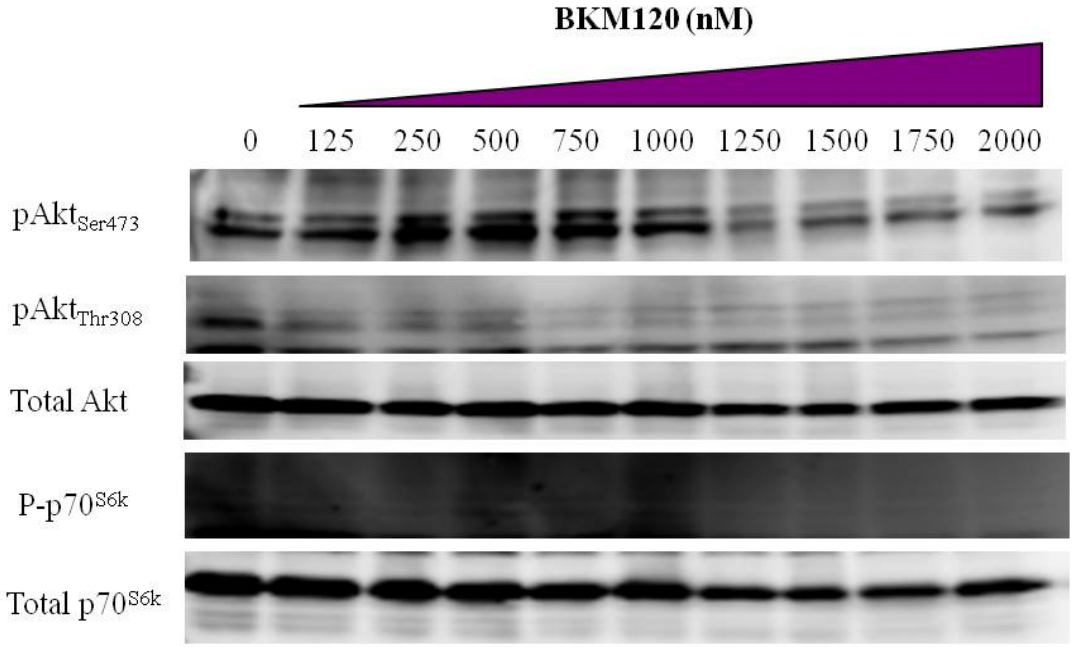

B

pAkt^{Ser473}IC$_{50}$	pAkt^{Thr308}IC$_{50}$	P-p70^{S6k} IC$_{50}$
1156nM 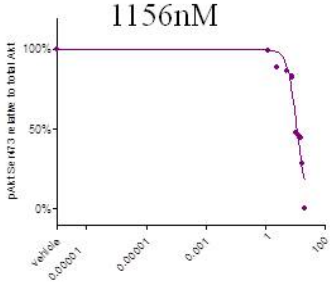	556nM 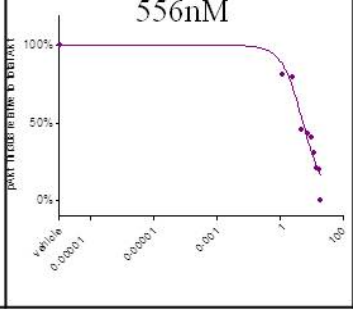	N/A

5.2.2.3 BEZ235 and BKM120 inhibit RAW264.7 cell proliferation

To examine whether BEZ235 and BKM120 affect RAW264.7 cell growth, RAW264.7 cells were seeded in 96 well plates and allowed to adhere overnight before being treated with BEZ235 (1-100nM), BKM120 (125-2000nM) or vehicle alone (0.1% DMSO) for 1, 3, and 5 days. At each of these time points, the number of cells per well was determined using the WST-1 assay. As shown in left panel of Figure 5.13A, RAW264.7 cells cultured in the presence of the vehicle alone displayed a progressive increase in cell number over the 5 days of culture, with a plateau reached at 5 days as the cells reached confluence. In the presence of BEZ235, a dose-dependent decrease in cell proliferation was observed, with a significant decrease in cell proliferation observed at concentrations of 1nM and higher (Figure 5.13A, right panel, $p < 0.05$; one-way ANOVA). The IC_{50} for BEZ235-mediated inhibition of RAW264.7 cell growth was 6nM (Figure 5.13C). As shown in Figure 5.13B, RAW264.7 cells cultured in the presence of BKM120 exhibited a dose-dependent decrease in cell proliferation compared to vehicle alone, with a significant decrease in cell proliferation observed at concentrations of 125nM and higher (Figure 5.13B, right panel, $p < 0.05$; one-way ANOVA). The IC_{50} for BKM120-mediated inhibition of RAW264.7 cell growth was 948nM (Figure 5.13C).

5.2.2.4 BEZ235 and BKM120 do not induce apoptosis in RAW264.7 cells

To examine the effect of BEZ235 and BKM120 on RAW264.7 cells apoptosis, RAW264.7 cells were treated with ½ IC_{50}, IC_{50} and 2x IC_{50} BEZ235 (see IC_{50} in Figure 5.12C), ½ IC_{50}, IC_{50} and 2x IC_{50} BKM120 (see IC_{50} in Figure 5.12C), or vehicle alone (0.1% DMSO) for 24 hours. The cells were then stained with Ann V (marker for early apoptosis) and 7AAD (marker for late apoptosis) and analysed immediately by flow cytometry.

As shown in Figure 5.14 treatment of RAW264.7 cells with BEZ235 did not induce a dose-dependent increase in the percentage of AnnV/7AAD+ cells (as shown in the top right quadrant) when compared to the percentage of viable cells (as shown in the bottom left quadrant). Similarly, treatment of RAW264.7 cells with BKM120 did not induce a dose-dependent increase in the percentage of AnnV/7AAD+ cells when compared to the percentage of viable cells (Figure 5.15).

Figure 5.13. BEZ235 and BKM120 inhibit the proliferation of RAW264.7 cells *in vitro*. RAW264.7 cells were cultured in the presence of **(A)** BEZ235 (1-100nM) or **(B)** BKM120 (0-2000nM) for 5 days. At day 0, 1, 3, and 5 time points, the number of viable, proliferating cells was assessed using WST-1, and cumulative data were plotted as shown (left panels). Data are expressed as the mean ± SEM from replicate samples and are representative of three independent experiments. The significance of the inhibition of RAW264.7 cell growth was determined from day 5 results (right panel). * $p<0.5$, ** $p<0.01$ and *** $p<0.001$, compared to vehicle, one-way ANOVA. **(C)** The IC_{50} for inhibition of RAW264.7 cell growth was determined from day 5 results using GraphPad Prism.

A

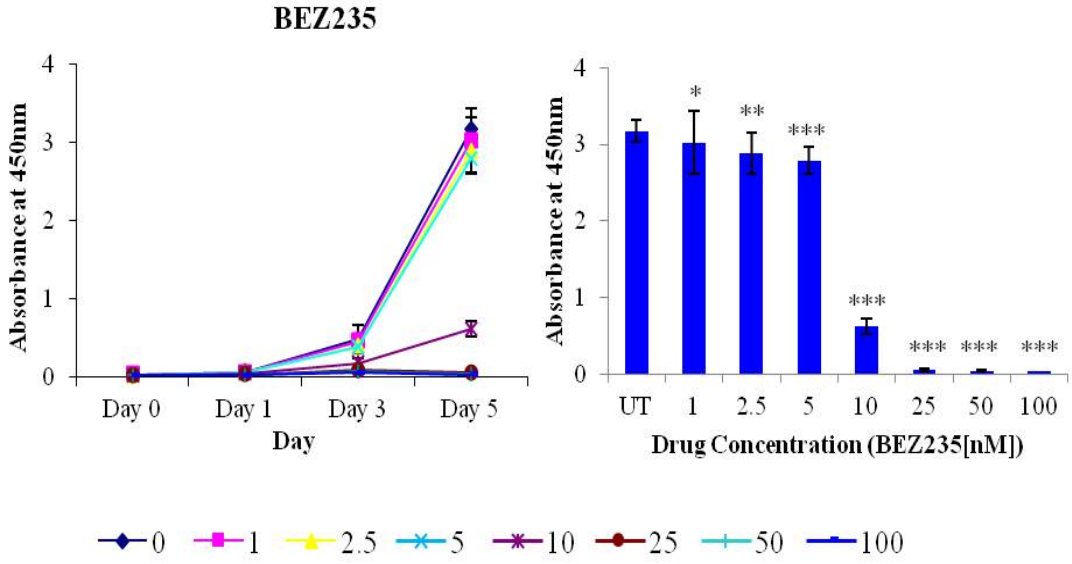

B

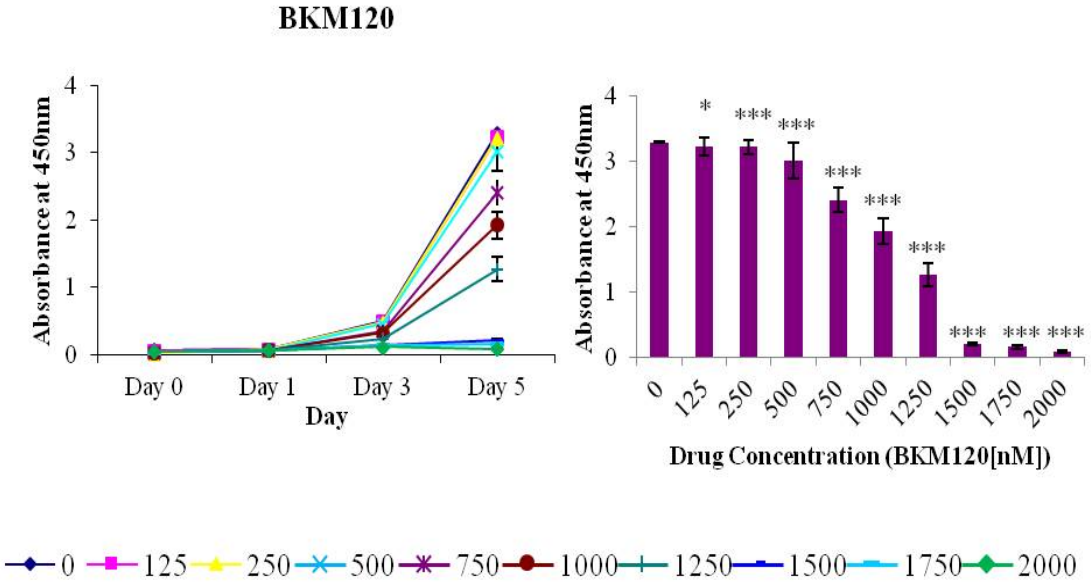

C

BEZ	6nM
BKM	948nM

Figure 5.14. BEZ235 does not induce apoptosis in RAW264.7 cells. RAW264.7 cells were treated with BEZ235 (½IC_{50}, 1x IC_{50} and 2x IC_{50}) and 0.1% DMSO for 24hours. Cells were then stained with Annexin V and 7-AAD for 15 minutes and analysed by flow cytometry.

UT BEZ235

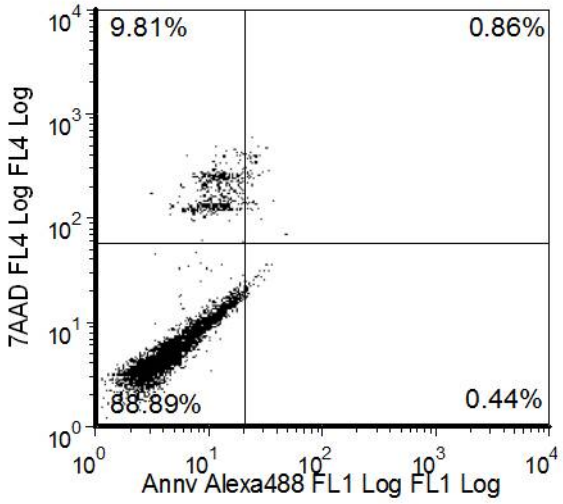

1/2x IC_{50} BEZ235

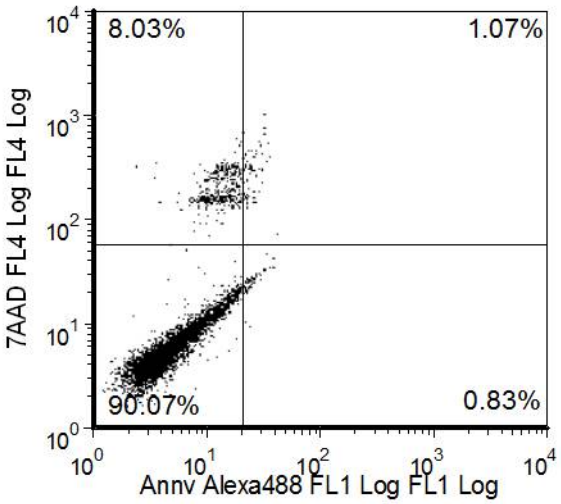

1x IC_{50} BEZ235

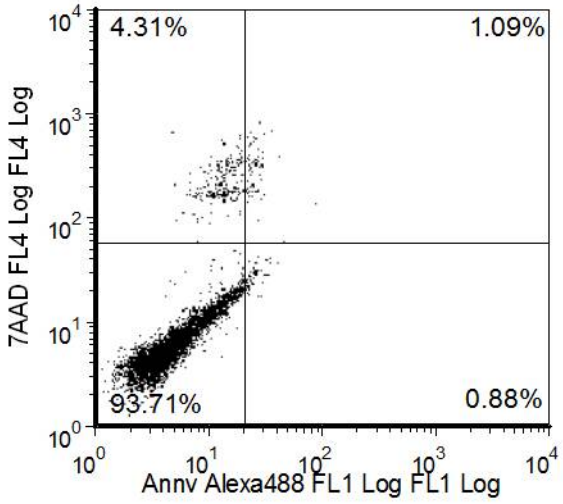

2x IC_{50} BEZ235

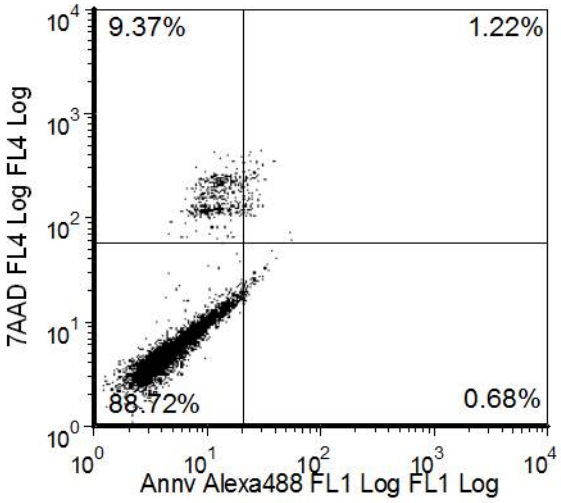

Figure 5.15. BKM120 does not induce apoptosis in RAW264.7 cells. RAW264.7 cells were treated with BKM120 (½IC_{50}, 1x IC_{50} and 2x IC_{50}) and 0.1% DMSO for 24hours. Cells were then stained with Annexin V and 7-AAD for 15 minutes and analysed by flow cytometry.

UT BKM120

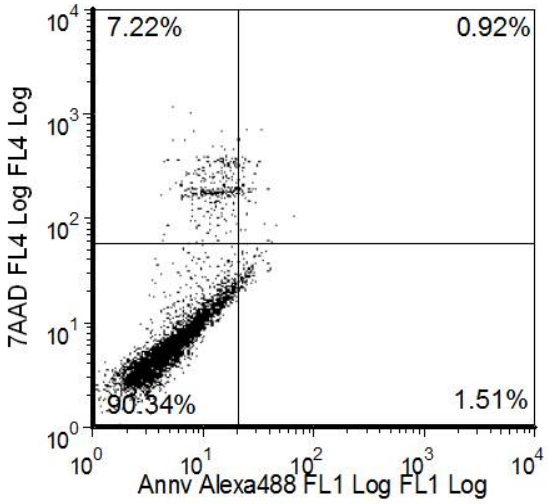

1/2x IC_{50} BKM120

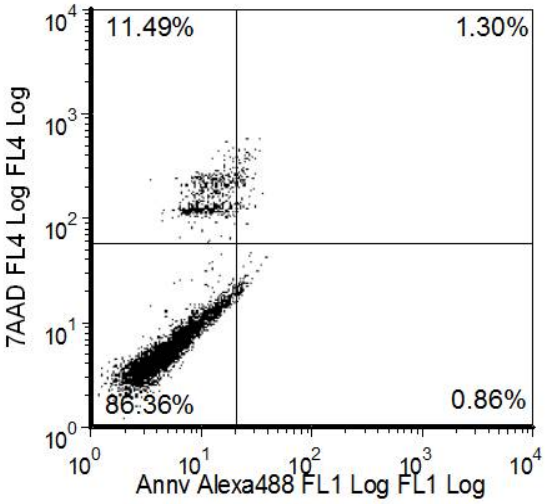

1x IC_{50} BKM120

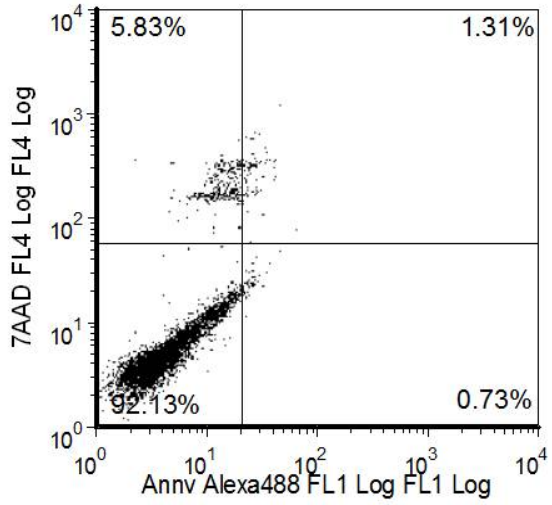

2x IC_{50} BKM120

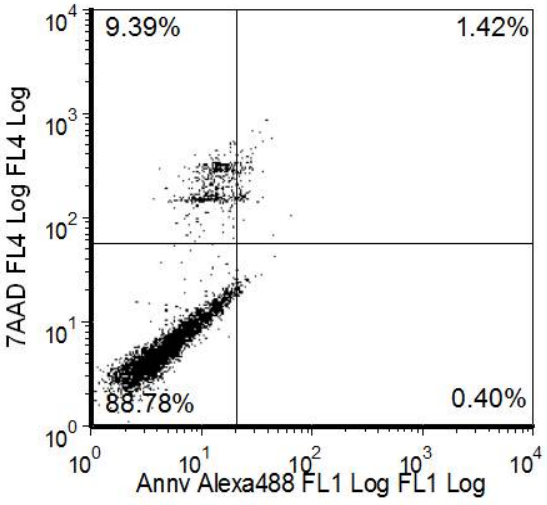

5.2.2.5 BEZ235 and BKM120 inhibit osteoclastogenesis and osteoclast activity in RAW264.7 cells *in vitro*

To examine the effect of BEZ235 and BKM120 on osteoclast formation in RAW264.7 cultures, cells were cultured with RANKL in the presence of BEZ235 (1-100nM), BKM120 (125-2000nM) or vehicle alone (0.05% DMSO) for 3 days. After the treatment period, cells were fixed and stained for TRAP and the number of osteoclast-like cells per well were enumerated. As shown in Figure 5.16A, RAW264.7 formed osteoclast-like cells in the presence of RANKL and in the presence of BEZ235, a significant decrease in the number of TRAP positive, multinucleated osteoclasts was observed at concentrations of 1nM BEZ235 and above (Figure 5.16B, $p < 0.001$; one-way ANOVA). A complete inhibition of osteoclast formation was observed at concentrations of 25nM BEZ235 and higher. In the BKM120-treated cultures, a significant decrease in the number of osteoclasts formed at concentrations of 125nM and above (Figure 5.17, $p < 0.001$; one-way ANOVA), with a complete inhibition of osteoclast formation observed at concentrations of 1250nM and higher.

To examine the effect of BEZ235 and BKM120 on osteoclast function in these cells, RAW264.7 cells were cultured under osteoclastogenic conditions on calcium phosphate-coated slides for 5 days and the area of resorption was calculated using Image J software. A significant decrease in the area of resorption was observed at all concentrations of BEZ235 (Figure 5.18, $p < 0.05$; one-way ANOVA) and BKM120 (Figure 5.19, $p < 0.001$; one-way ANOVA) examined.

5.3 *Discussion*

The balance between bone-forming osteoblasts and bone-resorbing osteoclasts is vital in maintaining the strength and integrity of the skeleton, and is markedly perturbed in MM patients[31]. While MM cells are not directly responsible for inducing bone loss in patients[31], they secrete factors and promote osteoclastogenesis and promote osteoclast survival, as well as inhibit osteoblast formation and activity[32].

As described in Section 5.1, inhibition of the PI3k and mTOR pathways have shown to promote osteoblastogenesis and inhibit osteoclastogenesis[17; 18; 19; 26]. Furthermore, previous studies from our laboratory have shown that BEZ235 stimulates osteogenic

Figure 5.16. BEZ235 inhibits the formation of osteoclast-like cells in RAW264.7 cultures *in vitro*. RAW264.7 cells were cultured under osteoclastogenic conditions in the presence of BEZ235 (0-100nM). Following 3 days of treatment, cells were stained for TRAP. **(A)** A representative photograph of each well was taken at 20x magnification. Images are representative of three independent experiments. Scale bars: 200µm. **(B)** The number of TRAP-positive cells with 3 or more nuclei were counted. Data are expressed as the mean ± SEM of replicate wells and are representative of three independent experiments. ***$p<0.001$, compared to vehicle, one-way ANOVA.

A

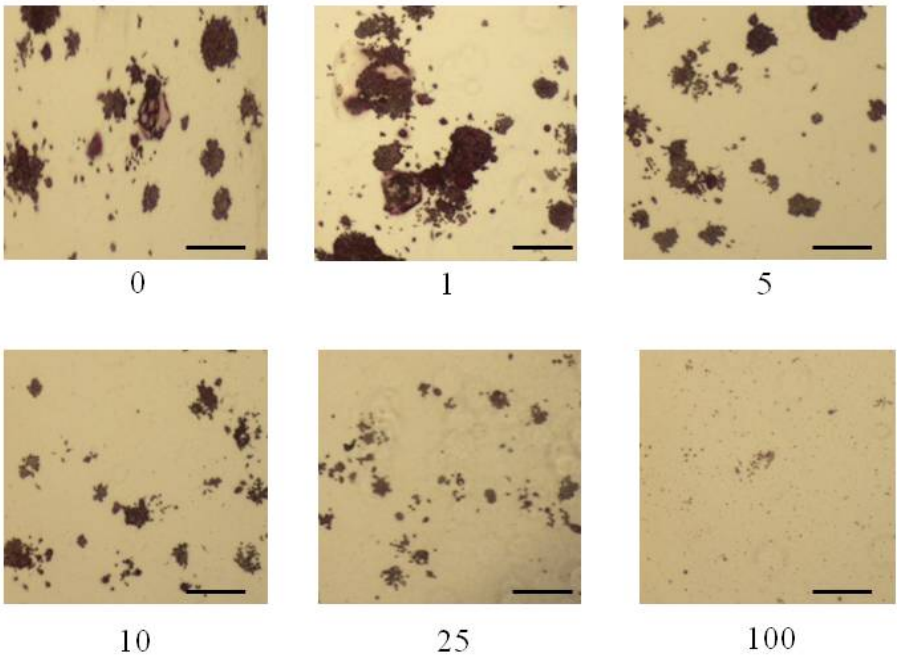
0
1
5
10
25
100

B

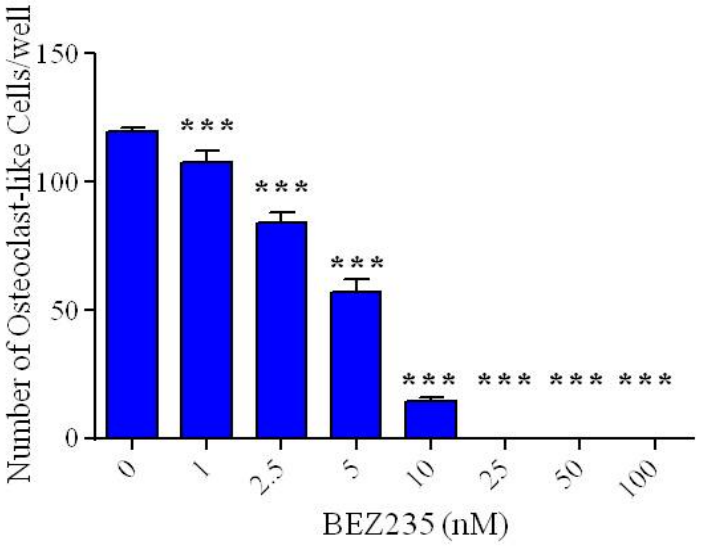
Number of Osteoclast-like Cells/well
150
100
50
0
***
***
***
***
***
***
***
0
1
2.5
5
10
25
50
100
BEZ235 (nM)

Figure 5.17. BKM120 inhibits the formation of osteoclast-like cells in RAW264.7 cultures *in vitro*. RAW264.7 cells were cultured under osteoclastogenic conditions in the presence of BKM120 (0-2000nM). Following 3 days of treatment, cells were stained for TRAP. **(A)** A representative photograph of each well was taken at 20x magnification. Images are representative of three independent experiments. Scale bars: 200µm. **(B)** The number of TRAP-positive cells with 3 or more nuclei were counted. Data are expressed as the mean ± SEM of replicate wells and are representative of three independent experiments. ***$p<0.001$, compared to vehicle, one-way ANOVA.

A

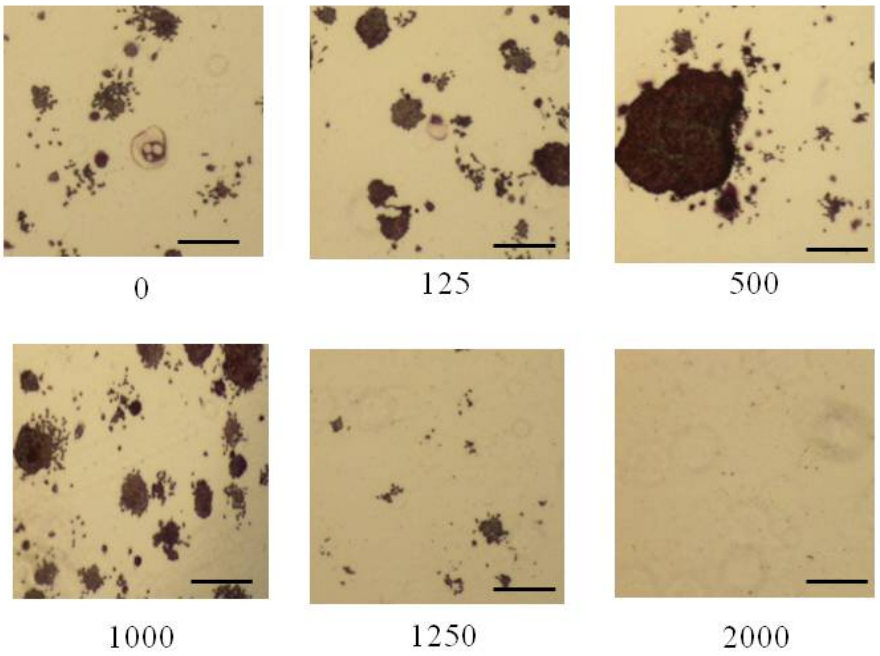
0
125
500
1000
1250
2000

B

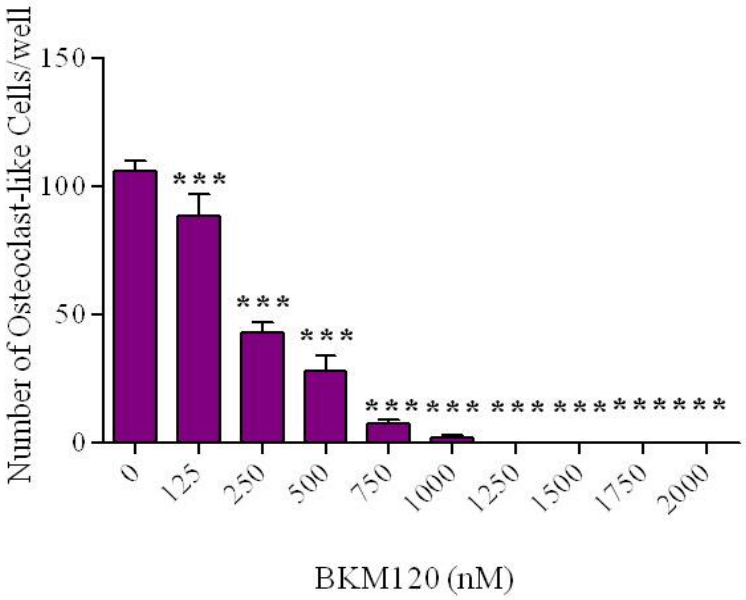
Number of Osteoclast-like Cells/well
150
100
50
0
***
***
***
0
125
250
500
750
1000
1250
1500
1750
2000
BKM120 (nM)

Figure 5.18. BEZ235 inhibits osteoclastic resorption in RAW264.7 cultures *in vitro*. RAW264.7 cells were cultured under osteoclastogenic conditions in the presence of BEZ235 (0-100nM) on calcium phosphate-coated slides for 5 days. Mineral was stained with von Kossa silver stain. **(A)** Silver-stained slides were photographed at 0.8x magnification. Images are representative of three independent experiments. Scare bar: 2.5mm. **(B)** The area of substrate resorbed on the silver-stained slides (lacunae area) was calculated using Image J software. Data are expressed as the mean ± SEM of replicate wells and are representative of three independent experiments. *$p<0.05$ and ***$p<0.001$, compared to vehicle, one-way ANOVA.

A

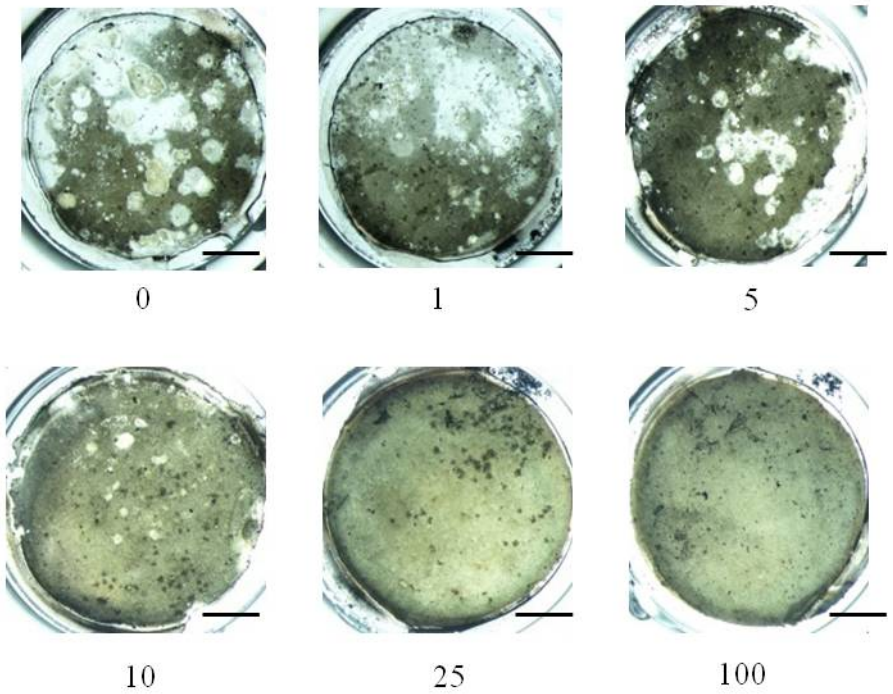
0
1
5
10
25
100

B

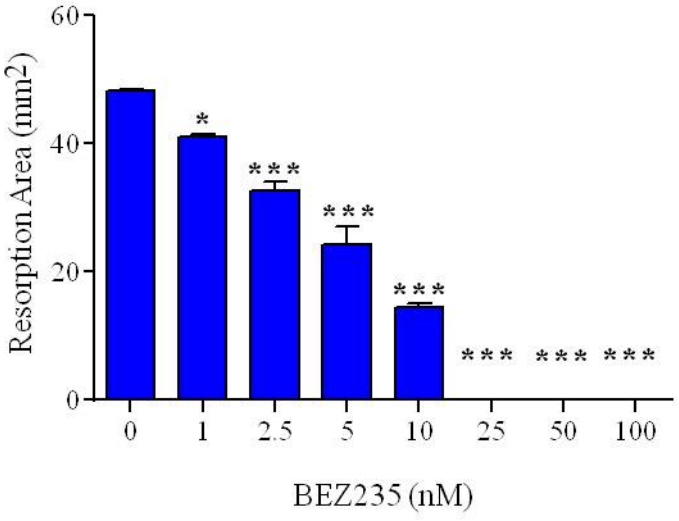
Resorption Area (mm2)
60
40
20
0
*
***
***
***
***
***
***
0
1
2.5
5
10
25
50
100
BEZ235 (nM)

Figure 5.19. BKM120 inhibits osteoclastic resorption in RAW264.7 cultures *in vitro*. RAW264.7 cells were cultured under osteoclastogenic conditions in the presence of BKM120 (0-2000nM) on calcium phosphate-coated slides for 5 days. Mineral was stained with von Kossa silver stain. **(A)** Silver-stained slides were photographed at 0.8x magnification. Images are representative of three independent experiments. Scare bar: 2.5mm. **(B)** The area of substrate resorbed on the silver-stained slides (lacunae area) was calculated using Image J software. Data are expressed as the mean ± SEM of replicate wells and are representative of three independent experiments. ***$p<0.001$, compared to vehicle, one-way ANOVA.

A

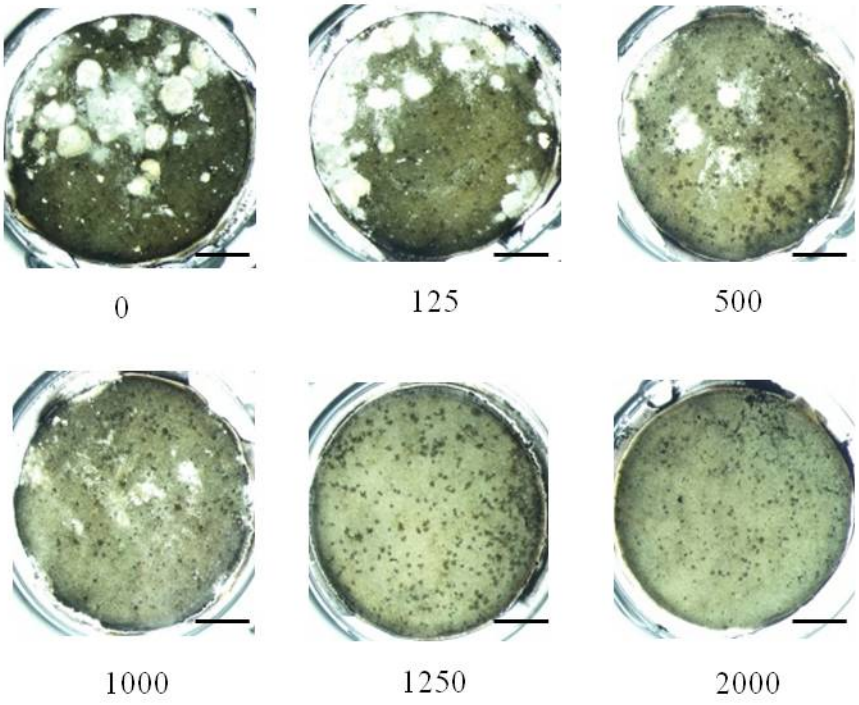
0
125
500
1000
1250
2000

B

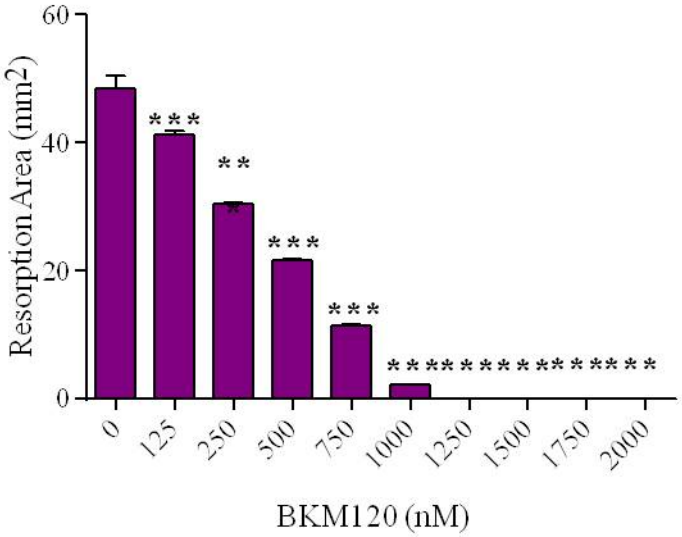
Resorption Area (mm2)
60
40
20
0
***
**
***
***
0
125
250
500
750
1000
1250
1500
1750
2000
BKM120 (nM)

differentiation and mineral formation *in vitro* in human MSCs and *de novo* bone growth in organotypic calvarial cultures[24]. To date, the effect of BEZ235 on osteoclasts, and the effect of BKM120 on osteoblasts and osteoclasts has not been examined. Having shown a preservation of bone volume, an increase in serum P1NP levels and a decrease in serum TRAcP5 levels in BEZ235 and BKM120 treated animals in Chapter 4, it was hypothesised that the inhibition of the PI3k and mTOR pathways with BEZ235 and BKM120 could induce osteogenesis and inhibit osteoclastogenesis.

As anticipated, BEZ235 inhibited the phosphorylation of Akt_{Ser473}, which is phosphorylated by mTORC2[33], and $p70^{S6k}$ in mBMSCs in a dose-dependent manner. Similarly BKM120 inhibited the phosphorylation of Akt_{Ser473}. However phosphorylation of Akt_{Thr308}, by PDK1 stimulating the catalytic activity of Akt[33], was not affected by either BEZ235 or BKM120. Studies have shown that phosphorylation of Akt_{Thr308} is inhibited by at least 100nM BEZ235 in human MM cell lines, breast cancer cell lines and acute myeloid leukaemia cell lines[33; 34; 35] and inhibited by 2000nM BKM120 in Rat1-myr-p110α, β, and δ cell lines and in human diffuse large B cell lymphoma cell lines,[36; 37] suggesting that high doses of BEZ235 and BKM120 are required to inhibit the phosphorylation of Akt .

Interestingly, BKM120 inhibited the phosphorylation of $p70^{S6k}$ in mBMSCs in a dose-dependent manner. A number of studies have demonstrated that $p70^{S6k}$ phosphorylation is inhibited by BKM120 at concentrations of more than 1000nM in human gastrointestinal cancer cells, glioblastoma cells and myeloma cell lines[37; 38; 39]. However, our data shows that the phosphorylation of $p70^{S6k}$ is inhibited from 500nM BKM120 with an IC_{50} of 794nM (Figure 5.2). This could be due to differences in seeding density and cell type as these factors can alter the response of the cells towards the drug[40].

Both drugs in inhibited phosphorylation of both AktThr308 and AktSer473 in the RAW264.7 cell line,, however interestingly; $p70^{S6k}$ phosphorylation was not detected under basal conditions in the presence of the vehicle alone. This was surprising, as it is known that the mTOR pathway is important for cell growth. A study by Lim and colleagues demonstrated that RAW264.7 requires the addition of exogenous phosphatidic acid, a cellular inflammation messenger mainly found in brain cell membrane, to activate $p70^{S6k}$ phosphorylation[41]. The absence of $p70^{S6k}$ phosphorylation and the need for exogenous phosphatidic acid to phosphorylate $p70^{S6k}$ suggest that

RAW264.7 cells heavily rely on the PI3k pathway for its ability to survive, grow and proliferate.

BEZ235 and BKM120 inhibit mBMSC proliferation (Figure 5.3) and RAW264.7 proliferation (Figure 5.13) *in vitro*. Using LY294002 and Rapamycin, previous studies have shown that inhibition of the PI3K and mTOR pathways inhibits MSC proliferation[42; 43; 44]. Our data support these findings and the findings of Martin and colleagues who demonstrated that BEZ235 inhibits hBMSC proliferation[24]. While BEZ235 and BKM120 were able to inhibit mBMSC and RAW264.7 proliferation, BEZ235 and BKM120 were not able to induce mBMSC and RAW264.7 cell apoptosis as shown in Figures 5.4, 5.5, 5.14 and 5.15. These findings are consistent with those described in Chapter 3, which showed that BEZ235 and BKM120 did not induce \ MM cell line apoptosis. Furthermore, our findings were in line with Martin and colleagues' who showed that BEZ235 was cytostatic towards human MSC when cultured with 10-250nM of BEZ235 for 14 days.

Having shown that BEZ235 and BKM120 inhibit the downstream phosphorylation of the PI3k and mTOR pathways and cell proliferation in murine-derived MSCs, the ability of these drugs to induce osteogenesis *in vitro* were investigated. A 5-fold increase and 2-3-fold increase in mineral formation was observed when the mBMSCs were cultured under osteogenic conditions with BEZ235 and BKM120, respectively (Figure 5.6). This is the first evidence to demonstrate that BKM120 induces mineral formation *in vitro*. This finding supports previous studies that have demonstrated that LY294002 and PI3k-specific inhibitors promote osteogenesis and mineral formation [18; 24]. As discussed in Section 5.1, a number of publications present contradicting evidence on the role of mTOR plays in osteogenesis[18; 19; 20; 21]. Studies by Vinals *et al* and Ogawa *et al* showed the inhibition of the mTOR pathway by Rapamycin increased Runx2 expression, early marker of osteoblastic differentiation and ALP and osteocalcin mRNA expression, late-stage markers of osteoblastic differentiation[18; 19]. In contrast, Isomoto *et al* and Singha *et al* demonstrated a decrease in ALP and osteocalcin mRNA expression in Rapamycin-treated mBMSCs that were cultured under osteogenic conditions[20; 21]. Recently, Martin and colleagues showed that knocking down mTOR using shRNA in SAOS-2 osteoblast-like cells increase mineral formation[24]. Using BEZ235, the studies presented here show that inhibiting both PI3k and mTOR pathway in mBMSCs induces osteogenesis, supporting the findings by Martin and colleagues[24].

In this chapter, the effects of BEZ235 and BKM120 on osteoclast formation and function *in vitro* were examined. While we only showed a significant reduction in osteolytic lesions present on the tibial cortical bone, and not the trabecular bone, of BEZ235- and BKM120-treated animals, it is likely that this can be attributed, in part, the inhibition of osteoclast formation and function as described in this chapter. A dose dependent decrease in TRAP-positive multinucleated osteoclasts was observed when mBM cells were cultured with BEZ235 or BKM120 under osteoclastogenic conditions (Figure 5.7 and 5.8). Similarly, BEZ235 and BKM120 were able to inhibit the formation and the resorptive function of the osteoclast-like cell line, RAW264.7. The inhibition of osteoclast and RAW264.7 osteoclast-like formation and resorption by both BEZ235 and BKM120 support the findings of several studies implicating the importance of the PI3k and mTOR pathways in stimulating osteoclast formation and function[14; 15; 17; 25; 26; 27].

As the PI3k and mTOR pathways play a vital role in cell survival, growth and proliferation, it is not surprising that the inhibition of these pathways by both BEZ235 and BKM120 led to inhibition of murine BM and RAW264.7 cell proliferation. McMillin and colleagues previously showed that BEZ235 is able to overcome the protection given by osteoclast-derived cytokines to MM cells *in vitro*[34]. This could be due to BEZ235 being able to inhibit osteoclast formation resulting in reduced MM cell protection. Other studies have shown that LY294002 and Rapamycin inhibit osteoclast activity[14; 15; 17; 25; 26; 27]. The data presented in this chapter support previous findings which showed that inhibition of the PI3k and mTOR pathways inhibit osteoclastogenesis. To our knowledge, the studies presented here are the first to show that BKM120 inhibits osteoclast formation and function, and that BEZ235 and BKM120 inhibit RAW264.7 osteoclast-like formation and function.

In conclusion, the data presented in this chapter showed that BKM120, a PI3k inhibitor, is as effective as BEZ235, a PI3k/mTOR inhibitor, in inducing osteoblastogenesis and inhibiting osteoclastogenesis *in vitro*. These data support the *in vivo* data presented in Chapter 4 where an increase in bone volume, serum P1NP levels and a decrease in TRAcP5 serum levels and the number of osteolytic lesions which perforate the cortices was observed in drug treated animals. Furthermore, these effective concentrations are achievable and well within the therapeutic concentrations of 100nM BEZ235 and 10μM BKM120 found in the plasma 16 hours post-administration of 50mg/kg BEZ235

and 60mg/kg BKM120 once daily[37; 45]. While concentrations of more than 1750nM BKM decrease osteogenesis (Figure 5.6), future studies would need to evaluate the osteogenic effects of BKM at concentrations greater than 2000nM.

Reference:

1. Pittenger, M. F., Mackay, A. M., Beck, S. C., Jaiswal, R. K., Douglas, R., Mosca, J. D., Moorman, M. A., Simonetti, D. W., Craig, S. & Marshak, D. R. (1999). Multilineage potential of adult human mesenchymal stem cells. *Science* **284**, 143-7.
2. Komori, T., Yagi, H., Nomura, S., Yamaguchi, A., Sasaki, K., Deguchi, K., Shimizu, Y., Bronson, R. T., Gao, Y. H., Inada, M., Sato, M., Okamoto, R., Kitamura, Y., Yoshiki, S. & Kishimoto, T. (1997). Targeted disruption of Cbfa1 results in a complete lack of bone formation owing to maturational arrest of osteoblasts. *Cell* **89**, 755-64.
3. Otto, F., Thornell, A. P., Crompton, T., Denzel, A., Gilmour, K. C., Rosewell, I. R., Stamp, G. W., Beddington, R. S., Mundlos, S., Olsen, B. R., Selby, P. B. & Owen, M. J. (1997). Cbfa1, a candidate gene for cleidocranial dysplasia syndrome, is essential for osteoblast differentiation and bone development. *Cell* **89**, 765-71.
4. Pinson, K. I., Brennan, J., Monkley, S., Avery, B. J. & Skarnes, W. C. (2000). An LDL-receptor-related protein mediates Wnt signalling in mice. *Nature* **407**, 535-8.
5. Brault, V., Moore, R., Kutsch, S., Ishibashi, M., Rowitch, D. H., McMahon, A. P., Sommer, L., Boussadia, O. & Kemler, R. (2001). Inactivation of the beta-catenin gene by Wnt1-Cre-mediated deletion results in dramatic brain malformation and failure of craniofacial development. *Development* **128**, 1253-64.
6. Nakashima, K., Zhou, X., Kunkel, G., Zhang, Z., Deng, J. M., Behringer, R. R. & de Crombrugghe, B. (2002). The novel zinc finger-containing transcription factor osterix is required for osteoblast differentiation and bone formation. *Cell* **108**, 17-29.
7. Day, T. F., Guo, X., Garrett-Beal, L. & Yang, Y. (2005). Wnt/beta-catenin signaling in mesenchymal progenitors controls osteoblast and chondrocyte differentiation during vertebrate skeletogenesis. *Developmental cell* **8**, 739-50.
8. Kawamura, N., Kugimiya, F., Oshima, Y., Ohba, S., Ikeda, T., Saito, T., Shinoda, Y., Kawasaki, Y., Ogata, N., Hoshi, K., Akiyama, T., Chen, W. S., Hay, N., Tobe, K., Kadowaki, T., Azuma, Y., Tanaka, S., Nakamura, K., Chung, U. I. & Kawaguchi, H. (2007). Akt1 in osteoblasts and osteoclasts controls bone remodeling. *PloS one* **2**, e1058.

9. Fischman, D. A. & Hay, E. D. (1962). Origin of osteoclasts from mononuclear leucocytes in regenerating newt limbs. *The Anatomical record* **143**, 329-37.
10. Tinkler, S. M., Linder, J. E., Williams, D. M. & Johnson, N. W. (1981). Formation of osteoclasts from blood monocytes during 1 alpha-OH Vit D-stimulated bone resorption in mice. *Journal of anatomy* **133**, 389-96.
11. Scheven, B. A., Visser, J. W. & Nijweide, P. J. (1986). In vitro osteoclast generation from different bone marrow fractions, including a highly enriched haematopoietic stem cell population. *Nature* **321**, 79-81.
12. Yasuda, H., Shima, N., Nakagawa, N., Yamaguchi, K., Kinosaki, M., Mochizuki, S., Tomoyasu, A., Yano, K., Goto, M., Murakami, A., Tsuda, E., Morinaga, T., Higashio, K., Udagawa, N., Takahashi, N. & Suda, T. (1998). Osteoclast differentiation factor is a ligand for osteoprotegerin/osteoclastogenesis-inhibitory factor and is identical to TRANCE/RANKL. *Proceedings of the National Academy of Sciences of the United States of America* **95**, 3597-602.
13. Lacey, D. L., Timms, E., Tan, H. L., Kelley, M. J., Dunstan, C. R., Burgess, T., Elliott, R., Colombero, A., Elliott, G., Scully, S., Hsu, H., Sullivan, J., Hawkins, N., Davy, E., Capparelli, C., Eli, A., Qian, Y. X., Kaufman, S., Sarosi, I., Shalhoub, V., Senaldi, G., Guo, J., Delaney, J. & Boyle, W. J. (1998). Osteoprotegerin ligand is a cytokine that regulates osteoclast differentiation and activation. *Cell* **93**, 165-76.
14. Gingery, A., Bradley, E., Shaw, A. & Oursler, M. J. (2003). Phosphatidylinositol 3-kinase coordinately activates the MEK/ERK and AKT/NFkappaB pathways to maintain osteoclast survival. *Journal of cellular biochemistry* **89**, 165-79.
15. Lee, S. E., Woo, K. M., Kim, S. Y., Kim, H. M., Kwack, K., Lee, Z. H. & Kim, H. H. (2002). The phosphatidylinositol 3-kinase, p38, and extracellular signal-regulated kinase pathways are involved in osteoclast differentiation. *Bone* **30**, 71-7.
16. Glantschnig, H., Fisher, J. E., Wesolowski, G., Rodan, G. A. & Reszka, A. A. (2003). M-CSF, TNFalpha and RANK ligand promote osteoclast survival by signaling through mTOR/S6 kinase. *Cell death and differentiation* **10**, 1165-77.
17. Mogi, M. & Kondo, A. (2009). Down-regulation of mTOR leads to up-regulation of osteoprotegerin in bone marrow cells. *Biochemical and biophysical research communications* **384**, 82-6.

18. Vinals, F., Lopez-Rovira, T., Rosa, J. L. & Ventura, F. (2002). Inhibition of PI3K/p70 S6K and p38 MAPK cascades increases osteoblastic differentiation induced by BMP-2. *FEBS letters* **510**, 99-104.
19. Ogawa, T., Tokuda, M., Tomizawa, K., Matsui, H., Itano, T., Konishi, R., Nagahata, S. & Hatase, O. (1998). Osteoblastic differentiation is enhanced by rapamycin in rat osteoblast-like osteosarcoma (ROS 17/2.8) cells. *Biochemical and biophysical research communications* **249**, 226-30.
20. Isomoto, S., Hattori, K., Ohgushi, H., Nakajima, H., Tanaka, Y. & Takakura, Y. (2007). Rapamycin as an inhibitor of osteogenic differentiation in bone marrow-derived mesenchymal stem cells. *Journal of orthopaedic science : official journal of the Japanese Orthopaedic Association* **12**, 83-8.
21. Singha, U. K., Jiang, Y., Yu, S., Luo, M., Lu, Y., Zhang, J. & Xiao, G. (2008). Rapamycin inhibits osteoblast proliferation and differentiation in MC3T3-E1 cells and primary mouse bone marrow stromal cells. *Journal of cellular biochemistry* **103**, 434-46.
22. Carracedo, A., Ma, L., Teruya-Feldstein, J., Rojo, F., Salmena, L., Alimonti, A., Egia, A., Sasaki, A. T., Thomas, G., Kozma, S. C., Papa, A., Nardella, C., Cantley, L. C., Baselga, J. & Pandolfi, P. P. (2008). Inhibition of mTORC1 leads to MAPK pathway activation through a PI3K-dependent feedback loop in human cancer. *The Journal of clinical investigation* **118**, 3065-74.
23. Tamburini, J., Chapuis, N., Bardet, V., Park, S., Sujobert, P., Willems, L., Ifrah, N., Dreyfus, F., Mayeux, P., Lacombe, C. & Bouscary, D. (2008). Mammalian target of rapamycin (mTOR) inhibition activates phosphatidylinositol 3-kinase/Akt by up-regulating insulin-like growth factor-1 receptor signaling in acute myeloid leukemia: rationale for therapeutic inhibition of both pathways. *Blood* **111**, 379-82.
24. Martin, S. K., Fitter, S., Bong, L. F., Drew, J. J., Gronthos, S., Shepherd, P. R. & Zannettino, A. C. (2010). NVP-BEZ235, a dual pan class I PI3 kinase and mTOR inhibitor, promotes osteogenic differentiation in human mesenchymal stromal cells. *Journal of bone and mineral research : the official journal of the American Society for Bone and Mineral Research* **25**, 2126-37.
25. Bradley, E. W., Ruan, M. M., Vrable, A. & Oursler, M. J. (2008). Pathway crosstalk between Ras/Raf and PI3K in promotion of M-CSF-induced MEK/ERK-mediated osteoclast survival. *Journal of cellular biochemistry* **104**, 1439-51.

26. Sugatani, T., Alvarez, U. & Hruska, K. A. (2003). PTEN regulates RANKL- and osteopontin-stimulated signal transduction during osteoclast differentiation and cell motility. *The Journal of biological chemistry* **278**, 5001-8.
27. Sugatani, T. & Hruska, K. A. (2005). Akt1/Akt2 and mammalian target of rapamycin/Bim play critical roles in osteoclast differentiation and survival, respectively, whereas Akt is dispensable for cell survival in isolated osteoclast precursors. *The Journal of biological chemistry* **280**, 3583-9.
28. Hock, J. M. & Canalis, E. (1994). Platelet-derived growth factor enhances bone cell replication, but not differentiated function of osteoblasts. *Endocrinology* **134**, 1423-8.
29. Gruber, R., Karreth, F., Kandler, B., Fuerst, G., Rot, A., Fischer, M. B. & Watzek, G. (2004). Platelet-released supernatants increase migration and proliferation, and decrease osteogenic differentiation of bone marrow-derived mesenchymal progenitor cells under in vitro conditions. *Platelets* **15**, 29-35.
30. Fitter, S., Dewar, A. L., Kostakis, P., To, L. B., Hughes, T. P., Roberts, M. M., Lynch, K., Vernon-Roberts, B. & Zannettino, A. C. (2008). Long-term imatinib therapy promotes bone formation in CML patients. *Blood* **111**, 2538-47.
31. Christoulas, D., Terpos, E. & Dimopoulos, M. A. (2009). Pathogenesis and management of myeloma bone disease. *Expert review of hematology* **2**, 385-98.
32. Dib, I. E., Gressier, M., Salle, V., Mentaverri, R., Brazier, M. & Kamel, S. (2008). Multiple myeloma cells directly stimulate bone resorption in vitro by down-regulating mature osteoclast apoptosis. *Leukemia research* **32**, 1279-87.
33. Serra, V., Markman, B., Scaltriti, M., Eichhorn, P. J., Valero, V., Guzman, M., Botero, M. L., Llonch, E., Atzori, F., Di Cosimo, S., Maira, M., Garcia-Echeverria, C., Parra, J. L., Arribas, J. & Baselga, J. (2008). NVP-BEZ235, a dual PI3K/mTOR inhibitor, prevents PI3K signaling and inhibits the growth of cancer cells with activating PI3K mutations. *Cancer research* **68**, 8022-30.
34. McMillin, D. W., Ooi, M., Delmore, J., Negri, J., Hayden, P., Mitsiades, N., Jakubikova, J., Maira, S. M., Garcia-Echeverria, C., Schlossman, R., Munshi, N. C., Richardson, P. G., Anderson, K. C. & Mitsiades, C. S. (2009). Antimyeloma activity of the orally bioavailable dual phosphatidylinositol 3-kinase/mammalian target of rapamycin inhibitor NVP-BEZ235. *Cancer research* **69**, 5835-42.
35. Chapuis, N., Tamburini, J., Green, A. S., Vignon, C., Bardet, V., Neyret, A., Pannetier, M., Willems, L., Park, S., Macone, A., Maira, S. M., Ifrah, N., Dreyfus,

F., Herault, O., Lacombe, C., Mayeux, P. & Bouscary, D. (2010). Dual inhibition of PI3K and mTORC1/2 signaling by NVP-BEZ235 as a new therapeutic strategy for acute myeloid leukemia. *Clinical cancer research : an official journal of the American Association for Cancer Research* **16**, 5424-35.

36. Zang, C., Eucker, J., Liu, H., Coordes, A., Lenarz, M., Possinger, K. & Scholz, C. W. (2013). Inhibition of pan-class I PI3 kinase by NVP-BKM120 effectively blocks proliferation and induces cell death in diffuse large B cell lymphoma. *Leukemia & lymphoma*.
37. Maira, S. M., Pecchi, S., Huang, A., Burger, M., Knapp, M., Sterker, D., Schnell, C., Guthy, D., Nagel, T., Wiesmann, M., Brachmann, S., Fritsch, C., Dorsch, M., Chene, P., Shoemaker, K., De Pover, A., Menezes, D., Martiny-Baron, G., Fabbro, D., Wilson, C. J., Schlegel, R., Hofmann, F., Garcia-Echeverria, C., Sellers, W. R. & Voliva, C. F. (2012). Identification and characterization of NVP-BKM120, an orally available pan-class I PI3-kinase inhibitor. *Molecular cancer therapeutics* **11**, 317-28.
38. Mueller, A., Bachmann, E., Linnig, M., Khillimberger, K., Schimanski, C. C., Galle, P. R. & Moehler, M. (2012). Selective PI3K inhibition by BKM120 and BEZ235 alone or in combination with chemotherapy in wild-type and mutated human gastrointestinal cancer cell lines. *Cancer chemotherapy and pharmacology* **69**, 1601-15.
39. Zheng, Y., Yang, J., Qian, J., Zhang, L., Lu, Y., Li, H., Lin, H., Lan, Y., Liu, Z., He, J., Hong, S., Thomas, S., Shah, J., Baladandayuthapani, V., Kwak, L. W. & Yi, Q. (2012). Novel phosphatidylinositol 3-kinase inhibitor NVP-BKM120 induces apoptosis in myeloma cells and shows synergistic anti-myeloma activity with dexamethasone. *Journal of molecular medicine* **90**, 695-706.
40. Kobayashi, H., Takemura, Y. & Ohnuma, T. (1992). Relationship between tumor cell density and drug concentration and the cytotoxic effects of doxorubicin or vincristine: mechanism of inoculum effects. *Cancer chemotherapy and pharmacology* **31**, 6-10.
41. Lim, H. K., Choi, Y. A., Park, W., Lee, T., Ryu, S. H., Kim, S. Y., Kim, J. R., Kim, J. H. & Baek, S. H. (2003). Phosphatidic acid regulates systemic inflammatory responses by modulating the Akt-mammalian target of rapamycin-p70 S6 kinase 1 pathway. *The Journal of biological chemistry* **278**, 45117-27.

42. Yan, X. L., Fu, C. J., Chen, L., Qin, J. H., Zeng, Q., Yuan, H. F., Nan, X., Chen, H. X., Zhou, J. N., Lin, Y. L., Zhang, X. M., Yu, C. Z., Yue, W. & Pei, X. T. (2012). Mesenchymal stem cells from primary breast cancer tissue promote cancer proliferation and enhance mammosphere formation partially via EGF/EGFR/Akt pathway. *Breast cancer research and treatment* **132**, 153-64.
43. Liu, X. B., Chen, H., Chen, H. Q., Zhu, M. F., Hu, X. Y., Wang, Y. P., Jiang, Z., Xu, Y. C., Xiang, M. X. & Wang, J. A. (2012). Angiopoietin-1 preconditioning enhances survival and functional recovery of mesenchymal stem cell transplantation. *Journal of Zhejiang University. Science. B* **13**, 616-23.
44. Hoogduijn, M. J., Crop, M. J., Korevaar, S. S., Peeters, A. M., Eijken, M., Maat, L. P., Balk, A. H., Weimar, W. & Baan, C. C. (2008). Susceptibility of human mesenchymal stem cells to tacrolimus, mycophenolic acid, and rapamycin. *Transplantation* **86**, 1283-91.
45. Maira, S. M., Stauffer, F., Brueggen, J., Furet, P., Schnell, C., Fritsch, C., Brachmann, S., Chene, P., De Pover, A., Schoemaker, K., Fabbro, D., Gabriel, D., Simonen, M., Murphy, L., Finan, P., Sellers, W. & Garcia-Echeverria, C. (2008). Identification and characterization of NVP-BEZ235, a new orally available dual phosphatidylinositol 3-kinase/mammalian target of rapamycin inhibitor with potent in vivo antitumor activity. *Molecular cancer therapeutics* **7**, 1851-63.

Chapter 6

Discussion

6.1 *Summary and General Discussion*

To date, MM is still an incurable haematological malignancy that accounts for approximately 15% of all haematological cancers[1; 2]. Approximately 80% of MM patients suffer from debilitating osteolytic bone lesions of the axial and apendicular skeleton, hypercalcaemia, increased plasma volume, renal failure and immunosuppression[1]. While the cause of MM is yet to be fully elucidated, environmental and genetic factors have been shown to be involved. With respect to genetic factors, numerous chromosomal mutations including chromosomal translocations such as 11q13, 4p16.3, 16q32 and 6p25 have been identified. Translocations involving the PI3k pathway have been identified in approximately 10-15% of MM patients while mutations of the RAS oncogenes, small GTPases which are able to activate the PI3k pathway[5], have been found in 30-50% of MM patients at diagnosis and 81% of patients at disease relapse[3; 4; 6; 7; 8; 9; 10; 11; 12; 13; 14; 15].

MM cell survival and proliferation is dependent on a number of pathways such as the PI3k and mTOR pathways[16; 17; 18; 19]. Studies using PI3k inhibitors such as BAY80- 6946 and mTOR inhibitors such as CCI-779, have highlighted the importance of the PI3k and mTOR pathways in maintaining MM cell survival both *in vitro* and in *in vivo* subcutaneous animal models[20; 21]. In line with the studies presented in this thesis, McMillin *et al* and Zheng *et al* have shown that BEZ235 and BKM120 can inhibit human MM cell proliferation *in vitro*[18; 19]. Furthermore, their studies showed increased oxidative stress, as evidenced by increased uptake of Foxo3a, and apoptosis, in the human myeloma cell line, MM.1S[18; 19], in response to BEZ235 or BKM120, suggesting that these drugs possess anti-MM properties. In studies outlined in this thesis, no significant induction of apoptosis was observed in response to BEZ235 or BKM120 treatment in human and murine MM cell lines. The sensitivity of the MM cell lines to the treatment of BEZ235 and BKM120 could be attributed to the cell lines used and the duration of the drug treatment *in vitro*.

The subcutaneous MM xenograft studies in NOD-SCID mice have demonstrated the ability of BEZ235 and BKM120 to significantly reduce MM tumour growth *in vivo*[18; 19]. This subcutaneous model only measures MM cell growth *in vivo* and does not mimic many of the hallmarks of human MM disease. Using the 5TGM1/KaLwRij systemic mouse model, which closely mimics the human MM disease, the studies presented in

this thesis show that two weeks of BEZ235 and BKM120 treatment resulted in a significant reduction in tumour growth, as measured by bioluminescence intensity and serum paraprotein levels, in established tumours.

In addition to regulating tumour cell growth and survival, the PI3k and mTOR pathways have also been implicated as important regulators of bone formation and bone resorption. Studies have shown that PI3k inhibitors, such as Wortmannin and LY294002, and mTOR inhibitors, such as Rapamycin, possess both pro-osteoblastic and anti-osteoclastic properties[22; 23]. Our laboratory has previously demonstrated that BEZ235 promotes osteogenesis in human MSCs and in an *in vitro* organotypic calvarial model[24]. In keeping with the finding of Martin *et al*, studies presented in this thesis show that BEZ235 and BKM120 promote osteogenesis in mBMSCs *in vitro*. In line with this, bone volume analyses performed on tibiae collected from both BEZ235-, BKM120- and vehicle-treated animals revealed an increase in a number of bone morphometric parameters (Figure 4.4 and 4.12) and a significant increase in serum P1NP levels in drug-treated animals compared to vehicle-alone. To our knowledge, this is the first study to demonstrate the pro-osteoblastic effects of BEZ235 and BKM120 in a systemic animal model of MM.

Akt1, the downstream effector of the PI3k pathway is highly expressed in bone cells and is necessary for the function of osteoclasts as Akt1 regulates RANKL expression, thereby stimulating osteoclastogenesis[25]. In contrast, the mTOR pathway has been shown to inhibit osteoprotegerin, an inhibitor of RANKL, and promote osteoclast formation and proliferation[26]. Inhibition of the PI3k pathway has been shown to inhibit RANKL- and Osteopontin-activated pathways and inhibit osteoclast differentiation, survival and migration[27]. Notably, the mTOR inhibitor Rapamycin was shown to increase osteoprotegerin expression, thus reducing osteoclast formation[26]. In the current study, we have demonstrated that both BEZ235 and BKM120 inhibit osteoclast formation and function in primary murine BM cells *in vitro,* in line with a number of studies which showed that osteoclastogenesis was inhibited when primary murine BMSCs and BMSC cell lines were cultured with LY294002, Wortmannin or Rapamycin [26; 27; 28; 29].

Previous subcutaneous xenograft studies of breast cancer and oral squamous cell carcinoma found that Rapamycin significantly reduced osteolytic bone loss *in vivo*[30; 31],

and increased serum OPG levels and bone thickness in neuroblastoma bone metastases xenograft models[32]. These findings are in line with our *in vivo* studies where a decrease in serum TRAcP5 levels and osteolytic lesions were observed in both BEZ235- and BKM120-treated animals. Our *in vivo* studies reflect our *in vitro* results, clearly indicating the anti-osteoclastic properties these drugs possess.

Of note, recent studies have also been performed to examine the effect of BEZ235 on normal bone remodelling. In one study, 21 days of BEZ235 treatment (45mg/kg/day *p.o.*) was shown to *increase* the number of osteoclasts in healthy C57BL/6J mice and *reduce* the number of osteoblasts. In another study, 22 days of BEZ235 treatment (10mg/kg/day, *i.p*) significantly reduced bone volume, bone density and fracture load in healthy C57Bl/6 mice[33]. The apparent discordance between our findings and the findings of presented in these studies could be due to the duration BEZ235 treatment and the health condition of the animals.

A unique aspect of our study was to compare the effectiveness of a dual PI3k/mTOR inhibitor and a single PI3k inhibitor. Our *in vitro* and *in vivo* studies show that BKM120, a single PI3k inhibitor, is as effective as BEZ235, a dual PI3k/mTOR inhibitor, at inhibiting MM cell proliferation and osteoclastogenesis and stimulating osteogenesis. This is in line with previous studies comparing the efficacy of LY294002 with the dual PI3k/mTOR inhibitor, PI-103 against tumour cell lines *in vitro* as the LY294002- or PI-103-treatment of primary acute myeloid leukaemia (AML) cells, glioblastoma cell lines and colorectal adenocarcinoma cell lines with either LY294002 or PI-103 induced tumour cell apoptosis[34; 35; 36]. Since mTOR is downstream of the PI3k pathway, we believe that mTOR can be inhibited directly by a PI3k inhibitor. In our study, we found that BKM120 inhibited the phosphorylation of $p70^{S6k}$, a downstream effector of the mTOR pathway in all the human and murine MM cell lines examined. This has been previously reported in studies using rat fibroblast, HeLa cells and rat cytotoxic T cells using LY294002 and Wortmannin[37; 38; 39]. While LY294002 and Wortmannin are PI3k-specific inhibitors, the PI3k and mTOR kinase domains have similar ATP binding sites that may allow these inhibitors to bind to the mTOR kinase domain[40]. BKM120-mediated inhibition of $p70^{S6k}$ phosphorylation was also seen in mBMSC and RAW264.7, which is in line with a study by Yu *et al.* who showed LY294002-mediated inhibition of $p70^{s6K}$ phosphorylation in human umbilical cord blood-derived stromal cells[41]. Although BKM120 was able to inhibit the

phosphorylation of $p70^{S6k}$, a dose of 1000nM BKM120 was required in order to see an effect on $p70^{S6k}$ phosphorylation. Overall, our *in vitro* findings suggest that BKM120 is as effective as BEZ235 in inhibiting the mTOR pathway.

Given that these pathways are vital for the maintenance of tumour cell survival and proliferation, phase I/II clinical trials have been carried out in patients with solid tumours such as breast cancer [42; 43]. These studies showed that these compounds are effective in reducing tumour size and are well tolerated with minimal adverse reactions such as lethargy, nausea and weight loss[42; 43; 44; 45]. While human clinical trials have yet to be been carried out on MM patients, the data from our *in vivo* studies suggest that these drugs could benefit MM patients.

To our knowledge, no *in vivo* studies investigating the efficacy of the PI3k inhibitors, LY294002 and Wortmannin, in cancer-induced osteolysis have been carried out. Studies have shown that these drugs were not well tolerated with animals displaying respiratory difficulty and lethargy after the administration of these drugs[46]. In contrast, *in vivo* xenograft models of breast cancer and oral squamous cell carcinoma have shown that inhibition of the mTOR pathway by Rapamycin significantly reduced osteolytic activity[30; 31]. The efficacy of Rapamycin in inhibiting osteolysis was also demonstrated by Hartwich *et al.* who found reported increased serum OPG levels and bone thickness in neuroblastoma bone metastases xenograft models[32]. These findings were reflected in a phase 3 clinical trials in hormone-receptor positive breast cancer patients. In these studies, the addition of Rapamycin to Exemestane (a drug used to treat breast cancer, treatment), resulted in a reduced incidence of breast cancer associated bone resorption[47; 48]. Like Rapamycin, the studies presented here, suggest that BEZ235 and BKM120 would display positive outcomes in the treatment of cancer-related bone metastases and MM-induced osteolysis. As MM remains an incurable disease, patients rely on the latest research to improve their lives. Hence, further research on the development of these novel therapies could not only prove to improve patient outcomes but one day MM could be a curable disease.

6.2 *Future Directions*

This thesis demonstrates that both BEZ235 and BKM120 are able to inhibit MM cell proliferation *in vitro* and slow the progression of MM *in vivo*. Whilst we observed no strong evidence to suggest that either drug induced MM cell apoptosis, previous studies

have shown that the combination of BEZ235 or BKM120 with Thalidomide, Bortezomib and Dexamethasone does induce MM cell apoptosis *in vitro*[18; 19]. As this has yet to be examined *in vivo,* future studies using the KaLwRij systemic model of MM to test these drug combinations are warranted.

To examine the effect of BEZ235 and BKM120 on bone remodelling in humans, future studies using bone trephines from human patients undertaking BEZ235 and BKM120 clinical trials would be useful. Furthermore, given the anabolic effects of these inhibitors on bone, future studies could examine their therapeutic efficacy in other bone-loss disorders such as osteoporosis, which affects 3.4% of the Australian population aged 55 and beyond[49]. These future studies would determine whether these drugs could be used as a treatment for other PI3k/mTOR related bone diseases besides cancer.

Reference:

1. MMRF. (2013). Multiple Myeloma: A Disease Overview (ed. Patient Handbook).
2. AIHW. (2012). Cancer in Australia: An Overview.
3. Bergsagel, P. L., Chesi, M., Nardini, E., Brents, L. A., Kirby, S. L. & Kuehl, W. M. (1996). Promiscuous translocations into immunoglobulin heavy chain switch regions in multiple myeloma. *Proceedings of the National Academy of Sciences of the United States of America* **93**, 13931-6.
4. Kuehl, W. M. & Bergsagel, P. L. (2002). Multiple myeloma: evolving genetic events and host interactions. *Nature reviews. Cancer* **2**, 175-87.
5. Castellano, E. & Downward, J. (2011). RAS Interaction with PI3K: More Than Just Another Effector Pathway. *Genes & cancer* **2**, 261-74.
6. Malgeri, U., Baldini, L., Perfetti, V., Fabris, S., Vignarelli, M. C., Colombo, G., Lotti, V., Compasso, S., Bogni, S., Lombardi, L., Maiolo, A. T. & Neri, A. (2000). Detection of t(4;14)(p16.3;q32) chromosomal translocation in multiple myeloma by reverse transcription-polymerase chain reaction analysis of IGH-MMSET fusion transcripts. *Cancer research* **60**, 4058-61.
7. Chesi, M., Nardini, E., Brents, L. A., Schrock, E., Ried, T., Kuehl, W. M. & Bergsagel, P. L. (1997). Frequent translocation t(4;14)(p16.3;q32.3) in multiple myeloma is associated with increased expression and activating mutations of fibroblast growth factor receptor 3. *Nature genetics* **16**, 260-4.
8. Chesi, M., Nardini, E., Lim, R. S., Smith, K. D., Kuehl, W. M. & Bergsagel, P. L. (1998). The t(4;14) translocation in myeloma dysregulates both FGFR3 and a novel gene, MMSET, resulting in IgH/MMSET hybrid transcripts. *Blood* **92**, 3025-34.
9. Ronchetti, D., Greco, A., Compasso, S., Colombo, G., Dell'Era, P., Otsuki, T., Lombardi, L. & Neri, A. (2001). Deregulated FGFR3 mutants in multiple myeloma cell lines with t(4;14): comparative analysis of Y373C, K650E and the novel G384D mutations. *Oncogene* **20**, 3553-62.
10. Lauring, J., Abukhdeir, A. M., Konishi, H., Garay, J. P., Gustin, J. P., Wang, Q., Arceci, R. J., Matsui, W. & Park, B. H. (2008). The multiple myeloma associated MMSET gene contributes to cellular adhesion, clonogenic growth, and tumorigenicity. *Blood* **111**, 856-64.
11. Soverini, S., Cavo, M., Cellini, C., Terragna, C., Zamagni, E., Ruggeri, D., Testoni, N., Tosi, P., De Vivo, A., Amabile, M., Grafone, T., Ottaviani, E., Giannini, B.,

Cangini, D., Bonifazi, F., Neri, A., Fabris, S., Tura, S., Baccarani, M. & Martinelli, G. (2003). Cyclin D1 overexpression is a favorable prognostic variable for newly diagnosed multiple myeloma patients treated with high-dose chemotherapy and single or double autologous transplantation. *Blood* **102**, 1588-94.

12. Santra, M., Zhan, F., Tian, E., Barlogie, B. & Shaughnessy, J., Jr. (2003). A subset of multiple myeloma harboring the t(4;14)(p16;q32) translocation lacks FGFR3 expression but maintains an IGH/MMSET fusion transcript. *Blood* **101**, 2374-6.
13. Neri, A., Murphy, J. P., Cro, L., Ferrero, D., Tarella, C., Baldini, L. & Dalla-Favera, R. (1989). Ras oncogene mutation in multiple myeloma. *The Journal of experimental medicine* **170**, 1715-25.
14. Neri, A., Baldini, L., Trecca, D., Cro, L., Polli, E. & Maiolo, A. T. (1993). p53 gene mutations in multiple myeloma are associated with advanced forms of malignancy. *Blood* **81**, 128-35.
15. Bezieau, S., Devilder, M. C., Avet-Loiseau, H., Mellerin, M. P., Puthier, D., Pennarun, E., Rapp, M. J., Harousseau, J. L., Moisan, J. P. & Bataille, R. (2001). High incidence of N and K-Ras activating mutations in multiple myeloma and primary plasma cell leukemia at diagnosis. *Human mutation* **18**, 212-24.
16. Hideshima, T., Nakamura, N., Chauhan, D. & Anderson, K. C. (2001). Biologic sequelae of interleukin-6 induced PI3-K/Akt signaling in multiple myeloma. *Oncogene* **20**, 5991-6000.
17. Hoang, B., Frost, P., Shi, Y., Belanger, E., Benavides, A., Pezeshkpour, G., Cappia, S., Guglielmelli, T., Gera, J. & Lichtenstein, A. Targeting TORC2 in multiple myeloma with a new mTOR kinase inhibitor. *Blood* **116**, 4560-8.
18. McMillin, D. W., Ooi, M., Delmore, J., Negri, J., Hayden, P., Mitsiades, N., Jakubikova, J., Maira, S. M., Garcia-Echeverria, C., Schlossman, R., Munshi, N. C., Richardson, P. G., Anderson, K. C. & Mitsiades, C. S. (2009). Antimyeloma activity of the orally bioavailable dual phosphatidylinositol 3-kinase/mammalian target of rapamycin inhibitor NVP-BEZ235. *Cancer research* **69**, 5835-42.
19. Zheng, Y., Yang, J., Qian, J., Zhang, L., Lu, Y., Li, H., Lin, H., Lan, Y., Liu, Z., He, J., Hong, S., Thomas, S., Shah, J., Baladandayuthapani, V., Kwak, L. W. & Yi, Q. (2012). Novel phosphatidylinositol 3-kinase inhibitor NVP-BKM120 induces apoptosis in myeloma cells and shows synergistic anti-myeloma activity with dexamethasone. *Journal of molecular medicine* **90**, 695-706.

20. Frost, P., Moatamed, F., Hoang, B., Shi, Y., Gera, J., Yan, H., Gibbons, J. & Lichtenstein, A. (2004). In vivo antitumor effects of the mTOR inhibitor CCI-779 against human multiple myeloma cells in a xenograft model. *Blood* **104**, 4181-7.
21. Glauer, J., Pletz, N., Schon, M., Schneider, P., Liu, N., Ziegelbauer, K., Emmert, S., Wulf, G. G. & Schon, M. P. (2013). A novel selective small-molecule PI3K inhibitor is effective against human multiple myeloma in vitro and in vivo. *Blood cancer journal* **3**, e141.
22. Vinals, F., Lopez-Rovira, T., Rosa, J. L. & Ventura, F. (2002). Inhibition of PI3K/p70 S6K and p38 MAPK cascades increases osteoblastic differentiation induced by BMP-2. *FEBS letters* **510**, 99-104.
23. Ogawa, T., Tokuda, M., Tomizawa, K., Matsui, H., Itano, T., Konishi, R., Nagahata, S. & Hatase, O. (1998). Osteoblastic differentiation is enhanced by rapamycin in rat osteoblast-like osteosarcoma (ROS 17/2.8) cells. *Biochemical and biophysical research communications* **249**, 226-30.
24. Martin, S. K., Fitter, S., Bong, L. F., Drew, J. J., Gronthos, S., Shepherd, P. R. & Zannettino, A. C. (2010). NVP-BEZ235, a dual pan class I PI3 kinase and mTOR inhibitor, promotes osteogenic differentiation in human mesenchymal stromal cells. *Journal of bone and mineral research : the official journal of the American Society for Bone and Mineral Research* **25**, 2126-37.
25. Kawamura, N., Kugimiya, F., Oshima, Y., Ohba, S., Ikeda, T., Saito, T., Shinoda, Y., Kawasaki, Y., Ogata, N., Hoshi, K., Akiyama, T., Chen, W. S., Hay, N., Tobe, K., Kadowaki, T., Azuma, Y., Tanaka, S., Nakamura, K., Chung, U. I. & Kawaguchi, H. (2007). Akt1 in osteoblasts and osteoclasts controls bone remodeling. *PloS one* **2**, e1058.
26. Mogi, M. & Kondo, A. (2009). Down-regulation of mTOR leads to up-regulation of osteoprotegerin in bone marrow cells. *Biochemical and biophysical research communications* **384**, 82-6.
27. Sugatani, T. & Hruska, K. A. (2005). Akt1/Akt2 and mammalian target of rapamycin/Bim play critical roles in osteoclast differentiation and survival, respectively, whereas Akt is dispensable for cell survival in isolated osteoclast precursors. *The Journal of biological chemistry* **280**, 3583-9.
28. Glantschnig, H., Fisher, J. E., Wesolowski, G., Rodan, G. A. & Reszka, A. A. (2003). M-CSF, TNFalpha and RANK ligand promote osteoclast survival by signaling through mTOR/S6 kinase. *Cell death and differentiation* **10**, 1165-77.

29. Saito, K., Ohara, N., Hotokezaka, H., Fukumoto, S., Yuasa, K., Naito, M., Fujiwara, T. & Nakayama, K. (2004). Infection-induced up-regulation of the costimulatory molecule 4-1BB in osteoblastic cells and its inhibitory effect on M-CSF/RANKL-induced in vitro osteoclastogenesis. *The Journal of biological chemistry* **279**, 13555-63.
30. Hussein, O., Tiedemann, K., Murshed, M. & Komarova, S. V. (2012). Rapamycin inhibits osteolysis and improves survival in a model of experimental bone metastases. *Cancer letters* **314**, 176-84.
31. Okui, T., Shimo, T., Fukazawa, T., Kurio, N., Hassan, N. M., Honami, T., Takaoka, M., Naomoto, Y. & Sasaki, A. (2010). Antitumor effect of temsirolimus against oral squamous cell carcinoma associated with bone destruction. *Molecular cancer therapeutics* **9**, 2960-9.
32. Hartwich, J. E., Orr, W. S., Ng, C. Y., Spence, Y., McLaughlin, J. M., Furman, W. L., McGregor, L. M. & Davidoff, A. M. (2013). Rapamycin increases neuroblastoma xenograft and host stromal derived osteoprotegerin inhibiting osteolytic bone disease in a bone metastasis model. *Journal of pediatric surgery* **48**, 47-55.
33. Smith, G. C., Ong, W. K., Costa, J. L., Watson, M., Cornish, J., Grey, A., Gamble, G. D., Dickinson, M., Leung, S., Rewcastle, G. W., Han, W. & Shepherd, P. R. (2013). Extended treatment with selective phosphatidylinositol 3-kinase and mTOR inhibitors has effects on metabolism, growth, behaviour and bone strength. *The FEBS journal* **280**, 5337-49.
34. Park, S., Chapuis, N., Bardet, V., Tamburini, J., Gallay, N., Willems, L., Knight, Z. A., Shokat, K. M., Azar, N., Viguie, F., Ifrah, N., Dreyfus, F., Mayeux, P., Lacombe, C. & Bouscary, D. (2008). PI-103, a dual inhibitor of Class IA phosphatidylinositide 3-kinase and mTOR, has antileukemic activity in AML. *Leukemia : official journal of the Leukemia Society of America, Leukemia Research Fund, U.K* **22**, 1698-706.
35. Westhoff, M. A., Kandenwein, J. A., Karl, S., Vellanki, S. H., Braun, V., Eramo, A., Antoniadis, G., Debatin, K. M. & Fulda, S. (2009). The pyridinylfuranopyrimidine inhibitor, PI-103, chemosensitizes glioblastoma cells for apoptosis by inhibiting DNA repair. *Oncogene* **28**, 3586-96.
36. Prevo, R., Deutsch, E., Sampson, O., Diplexcito, J., Cengel, K., Harper, J., O'Neill, P., McKenna, W. G., Patel, S. & Bernhard, E. J. (2008). Class I PI3 kinase

inhibition by the pyridinylfuranopyrimidine inhibitor PI-103 enhances tumor radiosensitivity. *Cancer research* **68**, 5915-23.

37. Brunn, G. J., Williams, J., Sabers, C., Wiederrecht, G., Lawrence, J. C., Jr. & Abraham, R. T. (1996). Direct inhibition of the signaling functions of the mammalian target of rapamycin by the phosphoinositide 3-kinase inhibitors, wortmannin and LY294002. *The EMBO journal* **15**, 5256-67.
38. Ballou, L. M., Selinger, E. S., Choi, J. Y., Drueckhammer, D. G. & Lin, R. Z. (2007). Inhibition of mammalian target of rapamycin signaling by 2-(morpholin-1-yl)pyrimido[2,1-alpha]isoquinolin-4-one. *The Journal of biological chemistry* **282**, 24463-70.
39. Gharbi, S. I., Zvelebil, M. J., Shuttleworth, S. J., Hancox, T., Saghir, N., Timms, J. F. & Waterfield, M. D. (2007). Exploring the specificity of the PI3K family inhibitor LY294002. *The Biochemical journal* **404**, 15-21.
40. Feldman, M. E. & Shokat, K. M. (2010). New inhibitors of the PI3K-Akt-mTOR pathway: insights into mTOR signaling from a new generation of Tor Kinase Domain Inhibitors (TORKinibs). *Current topics in microbiology and immunology* **347**, 241-62.
41. Yu, K. R., Park, S. B., Jung, J. W., Seo, M. S., Hong, I. S., Kim, H. S., Seo, Y., Kang, T. W., Lee, J. Y., Kurtz, A. & Kang, K. S. (2013). HMGA2 regulates the in vitro aging and proliferation of human umbilical cord blood-derived stromal cells through the mTOR/p70S6K signaling pathway. *Stem cell research* **10**, 156-65.
42. Cramer, J., Capples, D., KHackl, W., Lorand, D., Maira, M. S., Martus, H., Mukhopadhyay, S. & Zehender, H. (2009). BEZ235 Investigator's Brochure.
43. Ru, Q. & Cosaert, J. (2010). BKM120 Investigator's Brochure.
44. Maira, S. M., Pecchi, S., Huang, A., Burger, M., Knapp, M., Sterker, D., Schnell, C., Guthy, D., Nagel, T., Wiesmann, M., Brachmann, S., Fritsch, C., Dorsch, M., Chene, P., Shoemaker, K., De Pover, A., Menezes, D., Martiny-Baron, G., Fabbro, D., Wilson, C. J., Schlegel, R., Hofmann, F., Garcia-Echeverria, C., Sellers, W. R. & Voliva, C. F. (2012). Identification and characterization of NVP-BKM120, an orally available pan-class I PI3-kinase inhibitor. *Molecular cancer therapeutics* **11**, 317-28.
45. Maira, S. M., Stauffer, F., Brueggen, J., Furet, P., Schnell, C., Fritsch, C., Brachmann, S., Chene, P., De Pover, A., Schoemaker, K., Fabbro, D., Gabriel, D., Simonen, M., Murphy, L., Finan, P., Sellers, W. & Garcia-Echeverria, C. (2008).

Identification and characterization of NVP-BEZ235, a new orally available dual phosphatidylinositol 3-kinase/mammalian target of rapamycin inhibitor with potent in vivo antitumor activity. *Molecular cancer therapeutics* **7**, 1851-63.

46. Gupta, A. K., Cerniglia, G. J., Mick, R., Ahmed, M. S., Bakanauskas, V. J., Muschel, R. J. & McKenna, W. G. (2003). Radiation sensitization of human cancer cells in vivo by inhibiting the activity of PI3K using LY294002. *International journal of radiation oncology, biology, physics* **56**, 846-53.
47. Baselga, J., Campone, M., Piccart, M., Burris, H. A., 3rd, Rugo, H. S., Sahmoud, T., Noguchi, S., Gnant, M., Pritchard, K. I., Lebrun, F., Beck, J. T., Ito, Y., Yardley, D., Deleu, I., Perez, A., Bachelot, T., Vittori, L., Xu, Z., Mukhopadhyay, P., Lebwohl, D. & Hortobagyi, G. N. (2012). Everolimus in postmenopausal hormone-receptor-positive advanced breast cancer. *The New England journal of medicine* **366**, 520-9.
48. Gnant, M., Baselga, J., Rugo, H. S., Noguchi, S., Burris, H. A., Piccart, M., Hortobagyi, G. N., Eakle, J., Mukai, H., Iwata, H., Geberth, M., Hart, L. L., Hadji, P., El-Hashimy, M., Rao, S., Taran, T., Sahmoud, T., Lebwohl, D., Campone, M. & Pritchard, K. I. (2013). Effect of everolimus on bone marker levels and progressive disease in bone in BOLERO-2. *Journal of the National Cancer Institute* **105**, 654-63.
49. AIHW. (2011). A Snapshot of Osteoporosis in Australia 2011.